THE UNIVERSITY OF
WARWICK

University of Warwick institutional repository: http://go.warwick.ac.uk/wrap

**A Thesis Submitted for the Degree of PhD at the University of Warwick**

http://go.warwick.ac.uk/wrap/71244

THE UNIVERSITY OF WARWICK


SOME STRUCTURAL STUDIES

BY DEUTERIUM MAGNETIC RESONANCE


by


MARIA DA GRAÇA FERNANDES CRAVEIRINHA DILLON


A thesis submitted in partial fulfilment of the

requirements of the degree of Doctor of Philosophy



School of Molecular Sciences

July 1972

TO MY PARENTS

## ACKNOWLEDGEMENTS

# SUMMARY

Single crystals of $ND_4DSO_4$ and $Sr(DCOO)_2.2D_2O$ have been studied by deuteron magnetic resonance spectroscopy;  the apparatus and techniques used are described in some detail.

$ND_4DSO_4$ has considerable interest because of its ferroelectric properties:  spectra were recorded at 300 K and 230 K, within the paraelectric and ferroelectric phases respectively.  Symmetry relationships were used in solving the structure, particularly for refining the orientation data.  At room temperature, the two sets of bisulphate deuterons were found to have (within experimental error) the same quadrupole coupling constants and asymmetry parameters:

$$\frac{e^2Qq}{h} = 191.9 \pm 3KHz, \quad \eta = 0.094 \pm 0.02;$$

$$\frac{e^2Qq}{h} = 193.2 \pm 3KHz, \quad \eta = 0.070 \pm 0.01.$$

The quadrupolar constants appear somewhat larger than expected from the known $O\cdots O$ distances.  No evidence of disorder is apparent from the room temperature data.  At 230 K, both groups of deuterons appear to have suffered small angular displacements, essentially planar and antisymmetric with relation to the room temperature positions.  One type of deuteron undergoes movements of larger amplitude in a plane more favourably oriented with respect to the polar axis, [C], which suggests a definite contribution from these deuterons to the appearance of ferroelectricity.  The Curie point has been determined independently by use of the radiofrequency spectrometer; a value of $266 \pm 2K$ was obtained, in reasonable agreement with the literature value from dielectric constant measurements.  The $ND_4^+$ group is reorienting

rapidly both at 230 K and 300 K. Little change seems to occur upon transition. Some distortion of the tetrahedral structure, a possible difference in the reorientation rate for the two kinds of $ND_4^+$ ions, and a slight difference in their respective environments could be the main causes for the fine structure observed in the ammonium resonance.

The study of $Sr(DCOO)_2 \cdot 2D_2O$ gave the following average values for the quadrupolar constants and asymmetry parameters at 300 K:

formate ion $[DC(1)O(1)O(2)]^-$  $\dfrac{e^2Qq}{h} = 167.6 \pm 3KHz$  $\eta = 0.043 \pm 0.01$,

formate ion $[DC(2)O(3)O(4)]^-$  $\dfrac{e^2Qq}{h} = 170.3 \pm 3KHz$  $\eta = 0.025 \pm 0.01$.

$D_2O(1)$  $D_{1,2}$  $\dfrac{e^2Qq}{h} = 242.8 \pm 3KHz$  $\eta = 0.100 \pm 0.005$

$D_{5,6}$  $\dfrac{e^2Qq}{h} = 216.8 \pm 3KHz$  $\eta = 0.113 \pm 0.005$

Both formate ions give e.f.g. tensors very close to axial symmetry. For $[DC(1)O(1)O(2)]^-$, the deuteron is approximately aligned with the

$$C(1) \underset{\diagdown O(2)}{\overset{\diagup O(1)}{\phantom{C}}}$$

bisectrix in an essentially planar arrangement. For $[DC(2)O(3)O(4)]^-$ the deuteron shows a surprising deviation of $22^\circ$ from the plane of the COO group, as determined from Osaki's X-ray data. A weak C-D---O bonding interaction is tentatively suggested to account for this anomaly. $D_2O(1)$ was easily localised in the surrounding structure as known from X-ray data; the electric field gradient constants indicate that this molecule is 'static' at room temperature.

A $\overset{D}{\underset{D}{\diagup}}\hspace{-4pt}\diagdown O$ angle of $107.8^\circ$ is in good agreement with the value for free $H_2O$.  $D_2O(2)$ gave rise to broad and rather weak resonances with marked fine structure: some poorly defined curves were

analysed only approximately. The high quadrupolar constants

(330 ± 30 KHz) and asymmetry parameters (0.2 ± 0.1) derived for one set

of the curves suggest that this $D_2O$ molecule is weakly hydrogen bonded

(if at all), and may have a rather high degree of motional freedom.

# CONTENTS

# CHAPTER I

## INTRODUCTION

R.f. spectroscopic methods capable of studying quadrupolar inter-
actions constitute an expanding field of research side by side with the
methods of high resolution n.m.r.  All use the nuclei as subatomic probes to
study the internal fields in molecules and crystals, and their structural
significance.  There is, however, a distinct difference between the
nuclear magnetic dipole and nuclear electric quadrupole moment effects on
which one and the other are based: while the magnetic dipole interacts
with a magnetic field (and in this connection, except in ferromagnetic
materials, the internal fields usually constitute only a small fraction of
the external applied magnetic field), the nuclear electric quadrupole
moment interacts with an electrostatic field gradient, wholly of internal
origin.  Such interactions, produced by the charge distribution external
to the nucleus, can be quite large and rather sensitive to structural
details.  Although the basic knowledge of both phenomena dates from about
the same time (1945-6 and 1950 (1-3)), the more complex and very often non-
standard instrumentation required has caused slower development of
quadrupolar techniques.

According to the relative magnitudes of the nuclear quadrupolar
interaction and the interaction of the nuclear magnetic moment with the
magnetic field, two main areas of study may be distinguished (4).  If we
denote the net Hamiltonian $(\mathcal{H})$ of the system as the sum of the two
contributions,

$$\mathcal{H} = \mathcal{H}_M + \mathcal{H}_Q$$

where $\mathcal{H}_M$ is the Hamiltonian of the system of magnetic dipoles in the constant magnetic field (vide Sec.II-1), and $\mathcal{H}_Q$ is the nuclear electric quadrupolar Hamiltonian, the two possibilities are:

(i) $\mathcal{H}_M \gg \mathcal{H}_Q$ - the 'high field' case, first studied by Pound (3), who treated the problem by first order perturbation theory, and later extended by other workers (5,6). As a consequence of the interaction, the resonance signal acquires a fine structure, splitting into 2I components whose frequency separation is dependent on the orientation of the crystal in the magnetic field. In addition, the quadrupolar effects provide an extra mechanism of relaxation, particularly important for solids, thus giving a further contribution to line broadening beyond those normally present. Deuterium magnetic resonance (d.m.r.) is a specific example of a high field experiment, where the resonant nuclei have a spin quantum number I of 1.

(ii) $\mathcal{H}_Q$ is very large, to the extent of becoming almost wholly responsible for the dependence of the energy of the nucleus on its spin orientation. Nuclear resonance at zero or very low external magnetic fields can thus take place - such are the 'low field' or pure quadrupole resonance (n.q.r.) experiments. Large non centrally symmetric electric fields, as generated by bonding p electrons in covalent molecules, are normally required for these effects to be observable.

Powdered samples often give observable $^2$D resonances, despite the smearing out of the lines caused by random orientations of the crystals; however, single crystal work undoubtedly yields more extensive and more reliable information. The large size of the specimens required and the fairly complex spectrometer assemblies, which must be specifically designed for the recovery of the rather weak deuterium signals, are perhaps

the main difficulties with d.m.r. methods.  Ideally the crystal should not have two complicated a structure, to avoid splitting the total absorption into a large number of weak lines.

From stereographic studies of the dependence of the quadrupolar splitting on crystal orientation (Chapt.II), the electric field gradient tensor (e.f.g.) and its eigen vectors with respect to a crystal or molecular-based frame of reference can be evaluated for each set  of magnetically independent deuterons present in the structure.  A wealth of structural information can be acquired from d.m.r. studies:

(i) it has been found that the eigen vector corresponding to the largest principal component ($\phi_{zz}$) of the e.f.g. tensor is very nearly aligned with the bonding A-D direction (7); the remaining components are (within somewhat wider limits) also geometrically related to the bonding system (vide Sec.V.5).

(ii) The asymmetry parameter, which reflects the departure of the tensor ellipsoid from axial symmetry, also supplies rather less distinct information on the close surroundings of the deuterium atoms.

(iii) The quadrupolar constant $\frac{e^2 Qq}{h}$ reflects in a very sensitive way the nature and electronic structure of the A-D bond.  For hydrogen bonded systems, a large potential area of study open to d.m.r., some empirical correlations have been found (7,8,9) between the magnitude of the quadrupolar constant and the length of the O-O bridge (or the D --- O distance).

(iv) Spin-lattice relaxation time studies can provide detailed information on the dynamics of tunnelling or reorientation motions, an important mechanism in order-disorder processes such as those observed in some hydrogen bonded ferroelectric materials.

(v) D.m.r. occupies a unique position among nuclear quadrupolar techniques since deuterium is at present the only nucleus for which a reliable estimate of the nuclear quadrupole moment is available ($Q = +2 \cdot 7965 \times 10^{27}$ $cm^2$ (10)). For this reason, from the measured value of the quadrupolar constant, $e^2qQ/h$, the absolute value of $\phi_{zz} = eq$ can be determined. Moreover, in some simple molecules the values of the quadrupolar constants can be predicted from trial wave functions; the experimental $e^2qQ/h$ thus provides a sensitive test for such functions (11).

Crystalline hydrates, hydroxides, carboxylic acids, aldehydes, ammonium compounds and hydrocarbons are among the types of compounds so far examined by d.m.r.

Due to its involvement in the present work, a short account of ferroelectricity in crystals is now given. Two examples relevant to $ND_4DSO_4$ are included. Ferroelectricity involves the existence of spontaneous polarisation in a crystal which can be reversed by the application of a suitable electric field (at least equal to the coercive field). Phenomenologically, ferroelectricity has definite similarities to ferromagnetism, (for example the existence of a dielectric hysteresis loop), from which its name is derived. The analogy should not be taken too far, however; the two are essentially different in the nature of the interactions involved (12). Sharp dielectric anomalies and specific heat changes accompany the onset of a ferroelectric phase from an initial (paraelectric) phase cooled down through the transition temperature (Curie point). Whatever the compound or the mechanism of ferroelectricity, the phenomenon is restricted to the polar symmetry classes, i.e. those where the dipole moment per unit cell has an overall resultant (13).

$$\int \rho(\bar{r})\bar{r}dV \neq 0$$

As often happens in pseudosymmetric structures, real ferroelectric crystals are not normally true monocrystals; stresses of all kinds can encourage repeated twinning and formation of multidomains of opposite polarisation. The atomic displacements involved are generally rather small and difficult to investigate by diffraction technqiues: to quote Blinc (13), the ferroelectric phase is only a slightly distorted non-polar structure in the paraelectric stage. However small the atomic changes, they should noticeably affect the very sensitive internal field gradients; also, alteration of the symmetry from one phase to another will most likely change the multiplicity of the spectra. D.m.r. can thus constitute a valuable tool of research in this field, complemented by the determination of spin lattice relaxation times.

Ferroelectric behaviour appears to be favoured by H-bonded systems, partly because the A-H bonds themselves are polar to some extent (so that their ordering can induce the appearance of overall polarisation), and partly because any breaking or distortion of H-bonds on reversal of polarisation is usually a fairly easy process energetically. Many ferroelectric substances are disordered in the paraelectric state. Such is the case of $KD_2PO_4$, (14,15), which is one of the best understood examples of a ferro-electric compound. The deuterium atoms play a major role in the mechanism of ferroelectricity, as shown by a remarkable isotope effect of $+100^o$ in the Curie point upon deuteration. The main ferroelectric dipoles are the $PO_4$ groups and their adjoining hydrogens. The transition to the polar state corresponds to the 'freezing' of deuterium atoms in one or other of the off-centre positions on the very short O ---- O bridge, along which they were initially 'hopping' between two equilibrium sites.

Reversal of polarisation implies a shift of the D towards the other oxygen, to which it then becomes attached.

Ammonium sulphate undergoes a ferroelectric transition at $223^{o}$K. In contrast with $KD_2PO_4$, the isotope effect is relatively small, which suggests the rearrangement and ordering of heavy ions as the most likely cause of the transition. Twisting of the somewhat distorted ammonium groups has been shown to occur at this temperature (16). From d.m.r. studies (17), a high degree of thermal reorientation is apparent in the paraelectric phase, but is slightly more hindered in the ferroelectric stage: the equilibrium sites where the ammonium ions are 'frozen' correspond to changes of $30^{o}$ in the principal axis of each of the two kinds of ammonium ions. Some disagreement still remains in the interpretation of the room temperature d.m.r. and neutron diffraction data.

## CHAPTER II


## THEORY


As indicated in Chapter I, d.m.r. constitutes a specialised branch of 'high field' quadrupolar studies, and was first reported by Ketudat and Pound in 1956 (1). The present chapter gives a short account of the main sections of the theory relevant to d.m.r. studies; extensive reference has been made to Pound (2), Slichter (3), Volkoff et al (4,5), Cohen and Reif (6), and to a lesser extent Das and Hahn (7). The theses of Dr J. Clifford (8) and Dr J. Royston (9) were also consulted.

1. **Basic Principles.**

   **Energy levels of a magnetic dipole in a magnetic field $\bar{H}$.**

   A simple quantum mechanical approach which follows closely Reference 3, §1.2 and 6.1, is now described. Many nuclei can be allocated a total angular momentum $\bar{J}$ and total magnetic moment $\bar{\mu}$, related to each other by a simple equation of collinearity:

$$\bar{\mu} = \gamma \bar{J} \tag{1}$$

(scalar $\gamma$ is the gyromagnetic ratio and has a sign).

   In quantum mechanics $\bar{\mu}$ and $\bar{J}$ become (vector) operators; in particular, the angular momentum operator I may be defined by the expression:

$$\bar{J} = \hbar \bar{I}. \tag{2}$$

Application of a magnetic field $\overline{H}$ produces an interaction energy of the nucleus $-\overline{\mu}\,\overline{H}$. The Hamiltonian is given by:

$$\mathcal{H} = -\overline{\mu}\,\overline{H} \tag{3}$$

or, taking a field of intensity $H_o$ along a direction Z,

$$\mathcal{H} = -\gamma \hbar \, H_o \, I_z. \tag{4}$$

Eigen values for this Hamiltonian are multiples $(\gamma \hbar H_o)$ of the eigen values of $I_z$; the allowed energies are therefore:

$$E = -\gamma \hbar H_o m, \text{ where } m = I, I-1, \cdots\cdots\cdots, -I.$$

To detect the presence of a set of such energy levels, a time dependent interaction (angular frequency $\omega$) is necessary, such that transitions between the nuclear Zeeman levels are promoted, i.e.

$$\hbar \omega = \Delta E. \tag{5}$$

An alternating magnetic field perpendicular to the static field is normally the way of inducing such transitions. A perturbing term is introduced into the Hamiltonian which in first order restricts the allowed transitions to those between adjacent energy levels, giving

$$\hbar \omega = \Delta E = \gamma \hbar H_o, \text{ or} \tag{6}$$

$$\omega = \gamma H_o.$$

$\omega$ is the resonance frequency which corresponds to the classical (Larmor) frequency of gyroscopic precession of the magnetic moment in an external static magnetic field.

The nuclear electric quadrupole Hamiltonian. Application of a strong magnetic field.

Electric quadrupole effects arise primarily from the non sphericity of charge distribution for nuclei of spin greater than $\frac{1}{2}$. Such nuclei interact with electrostatic potentials of less than cubic symmetry, the energy of interaction being a function of the orientation of the nucleus with respect to its electrostatic environment. If this environment (or at least, its time average) is static, as in a crystal, the interaction perturbs unequally the magnetic sublevels of energy and the nuclear magnetic resonance line is split into several components. Quantitatively, the interaction energy of a nuclear charge distribution of density $\rho(r)$ with a potential V due to external charges is

$$E = \int \rho(r) V(r) d_T. \tag{7}$$

If this expression is expanded in a Taylor series about the origin, then

$$V(r) = V(o) + \sum_i x_i \left. \frac{\partial V}{\partial x_i} \right)_{r=o} + \frac{1}{2!} \sum_{i,j} x_i x_j \left. \frac{\partial^2 V}{\partial x_i \partial x_j} \right)_{r=o} + \ldots, \tag{8}$$

$$E = V(o) \int \rho d_T + \sum_i V_i \int x_i \rho d_T + \frac{1}{2!} \sum_{i,j} V_{i,j} \int x_i x_j \, \rho d_T \ldots \tag{9}$$

$$i,j = 1,2,3$$

($V_i$ and $V_{i,j}$ represent the first and second derivatives of V respectively).

If the mass centre of the nucleus is chosen as origin, the first term represents the electrostatic energy of the nucleus taken as a point charge, and is independent of orientation; the second, which involves

the electrical dipole moment of the nucleus, vanishes since the centre

of mass and the centre of gravity coincide and there is no induced

moment; the third is then the electric quadrupole term.

$-V_{ij} = -\dfrac{\partial^2 V}{\partial x_i \partial x_j}$ are the nine components (in Cartesian coordinates)

of the electric field gradient tensor (e.f.g.) at the site of the nucleus:

$$\nabla \bar{E} = -\nabla^2 V \tag{10}$$

where V is the electrostatic potential at the nucleus due to the

surrounding charges.   Furthermore, if Laplace's equation is evaluated

at the origin,

$$(\nabla^2 V)_0 = \sum_i V_{ii} = \frac{\partial^2 V}{\partial x^2} + \frac{\partial^2 V}{\partial y^2} + \frac{\partial^2 V}{\partial z^2} = 0 \tag{11}$$

(meaning that the electric field at the nucleus is due solely to

external charges),  it can be immediately inferred that $\overline{\nabla E}$ is traceless,

besides being symmetric.   It is always possible to find a set of

principal axes of the potential V for which the tensor takes a diagonal

form, i.e.

$$V_{ik} = 0 \qquad (i \neq k). \tag{12}$$

Normally the principal axes are so labelled that $V_{zz} = \phi_{zz} = eq$  has

the largest and $V_{xx} = \phi_{xx} = -eq(1 - \eta)/2$ has the smallest magnitude;

$\eta$ is the asymmetry parameter, defined by

$$\eta = \frac{V_{xx} - V_{yy}}{V_{zz}} \qquad (0 \leq \eta \leq 1). \tag{13}$$

In the case of axial symmetry, often a good approximation, the axis is taken as the Z direction, giving $\eta = 0$. As discussed in the article by Cohen and Reif (6), the Hamiltonian for the interaction of the quadrupole moment of a nucleus with the field gradient $\overline{\nabla E}$ at the nuclear site is given by

$$\mathcal{H}_Q = Q \nabla \overline{E} \tag{14}$$

where Q is the tensor defining the quadrupole charge distribution in the nucleus. The quadrupolar Hamiltonian $\mathcal{H}_Q$ can be expressed as a function of the principal components of the e.f.g., as follows:

$$\mathcal{H}_Q = \frac{eQ}{4I(2I-1)} [V_{zz}(3I_z^2 - I^2) + (V_{xx} - V_{yy})(I_x^2 - I_y^2)] \tag{15}$$

eQ - quadrupole moment of the nucleus,

I - total angular momentum of the system, and

$I_x, I_y, I_z$ are angular momentum operators in the principal axis frame of reference.

If the particular nucleus is introduced into a constant magnetic field, the net Hamiltonian is given by

$$\mathcal{H} = \mathcal{H}_Q + \mathcal{H}_M \tag{16}$$

where $\mathcal{H}_M$ may take a form virtually similar to (4). If the magnetic field is very strong (i.e. $\gamma h H_o \gg e^2qQ$) - the usual conditions for a d.m.r. experiment - $\mathcal{H}_Q$ may be regarded as a perturbation of $\mathcal{H}_M$.

Further development yields the following expressions for the energy

(up to second order) of the perturbed Zeeman levels (m) and the

frequencies of the allowed transitions for a nucleus of spin quantum

number I = 1:-

$$E_m = -m\gamma\hbar H_o + \frac{eQ}{4}(3m^2-2)V_o - \frac{m}{2\gamma\hbar H_o}\left(\frac{eQ}{4}\right)^2 x \left[(7-8m^2)V_{+1}V_{-1}+(3-2m^2)V_{+2}V_{-2}\right].$$

(17)

$$\left.\begin{array}{c}\nu_{01}=\nu_{10}\\ \nu_{-10}=\nu_{0-1}\end{array}\right\} = \frac{\gamma H_o}{2\pi} - \frac{3eQV_o}{2h} + \frac{3}{\gamma\hbar H_o h}\left(\frac{eQ}{2}\right)^2\left(-V_{+1}V_{-1}+V_{+2}V_{-2}\right)$$

(18)

(top signs for transition 0 ⟷ 1).

$V_o$, $V_{\pm 1}$, $V_{\pm 2}$ are the five irreducible e.f.g. components in a general

(non principal) set of axes, specifically the coordinate system in which

the spin angular momentum is quantised. The small quadrupole interaction

thus shifts the magnetic energy levels, originally equispaced, splitting

the magnetic resonance line into its 2I components (2 for deuterium nuclei).

(i) If first order terms only in the expressions above are considered,

the two new lines appear symmetrically disposed about the unperturbed

Larmor frequency $\nu_L$ (corresponding to transitions -1→0 and 0→1 for deuterons).

It should be noted that for nuclei of half integral I the resonance line

has a central component and $I-\frac{1}{2}$ pairs of satellites m ⟷ m-1 and

-(m-1) ⟷ -m.

(ii) Second order effects displace the centre of gravity of the two

lines (for $^2D$) with respect to $\nu_L$. This subject has been extensively

treated by Volkoff (5). Second order terms can be made to vanish by

measuring directly the frequency difference for the two satellite

lines:

$$2\Delta\nu \;=\; \nu_{10} - \nu_{01} \;=\; 3e\mathbf{Q}V_0/2h \tag{19}$$

In the present work, second order contributions have been ignored;
for the high field strengths at which the spectrometer was operated, it
is unlikely that the effect (inversely proportional to $H_0$) would be
large.

(iii) Expressions (17) and (18) also illustrate the orientation
dependence of the splittings, since they depend (through $V_0$, $V_{\pm1}$ and $V_{\pm2}$)
on the crystal orientation with respect to $\overline{H}$. (For a 'high field'
experiment, the magnetic field direction is the axis of quantisation.) By
transforming the tensor in the magnetic system of reference to a set
of axes fixed relative to the crystal, the expressions for the variation
of splitting with orientation can be derived. The problem has been
analysed by Volkoff et al (4) (first order) and Volkoff (5) (second order).
A 'stereographic' study of this orientation dependence by means of a
number of rotation patterns can lead finally to the e.f.g. tensor
components for the crystal axes, and from these the eigen vectors and
eigen values can be found, together with the asymmetry parameter and
quadrupolar constant, $e^2qQ/h \;=\; \emptyset_{zz} x \frac{2}{3} K \frac{I(2I-1)}{2m-1}$.

The sign of $\frac{e^2qQ}{h}$ cannot usually be inferred from solid state methods,
including d.m.r. (a change of sign would merely invert the order of the
energy levels involved (10), and introduce no observable difference in the
spectrum). Throughout this work the sign of $\emptyset_{zz} = eq = -\frac{\partial E_z}{\partial z}$ has been
assumed to be positive, i.e. determined by the nuclear contribution.
Since eQ is known to be positive for the deuteron (11), the quadrupolar
constant may thus be assumed to be positive.

## 2.  Calculation of the Components of the e.f.g. Tensor.

The deduction of the general expressions for the constants A, B and C, eqs. (24)(25)(26) followed the procedure of Volkoff et al (4) in a slightly modified form (9), to suit a completely general crystal position.  The main steps were:

(i)  A consideration of the interaction tensor $\phi_{iK}$ for each deuteron: it is a symmetrical, traceless tensor whose components in an orthogonal set of axes fixed in the crystal, $(\underset{\sim}{a}, \underset{\sim}{b}, \underset{\sim}{c})$ can be expressed as follows:

$$\phi_{iK} = \begin{bmatrix} \phi_{11} & \phi_{12} & \phi_{13} \\ \phi_{21} & \phi_{22} & \phi_{23} \\ \phi_{31} & \phi_{32} & \phi_{33} \end{bmatrix}$$

$$\phi_{iK} = \phi_{Ki}; \quad \phi_{11} + \phi_{22} + \phi_{33} = 0$$

$(\underset{\sim}{a}, \underset{\sim}{b}, \underset{\sim}{c})$ can conveniently be chosen to coincide with the set of crystallographic axes, or, where that is not possible (monoclinic and triclinic systems) with any Cartesian set easily related to it.

(ii) It is known (2,12) that the magnitude of the quadrupolar splitting when the magnetic field $\overline{H}$ is along a certain crystal direction is proportional to the component of the e.f.g. along $\overline{H}$.  If the direction of the (rotating) magnetic field is called z' and T is the matrix which converts from (a, b, c) to $(x'\ y'\ z')_{rot.}$, the $\phi_{z'z'}$ component of the interaction tensor in the rotating set of axes can be expressed as a linear function of $\phi_{ik}$ (tensor transformation (12)).  An intermediate, fixed laboratory set of axes is defined (Table II.1 and Fig. II-1).

TABLE II-1

| Axes | $(a\ b\ c)\ \xrightarrow{T_1}\ (x\ y\ z)\ \xrightarrow{T_2}\ (x'\ y'\ z')$ |
|---|---|
| | (fixed crystal set)    (fixed lab. system)    (rotated magn. syst.) |
| Tensor | $\emptyset$         $\emptyset_1$         $\emptyset_2\ =\ \emptyset'$ |
| Axes trans. matrix | $T_1 = \begin{bmatrix} a_{11} & a_{12} & a_{13} \\ & \ddots & \\ & & a_{33} \end{bmatrix}$     $T_2 = \begin{bmatrix} \sin\theta & \cos\theta & 0 \\ 0 & 0 & 1 \\ \cos\theta & -\sin\theta & 0 \end{bmatrix}$ |



OX – towards $90°$ on the magnet scale

OY – towards $0°$ on the magnet scale

OZ – vertically upwards

$OZ'_0$– origin for $\theta$

Fig II-1
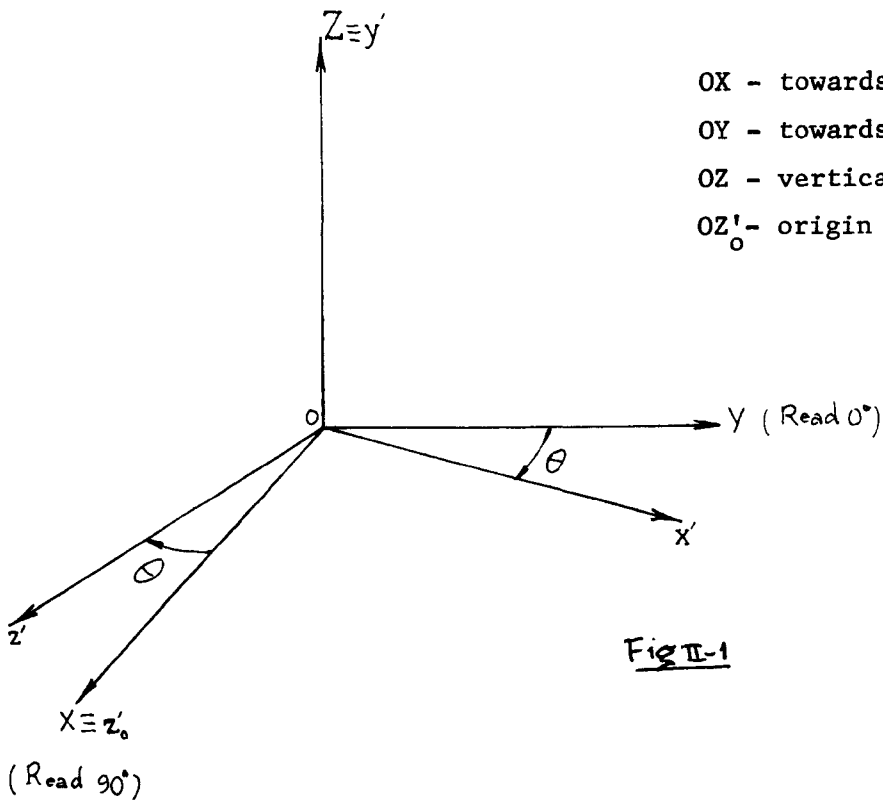
Although this choice of axes is counter to the clockwise direction for θ, it has two main advantages, since

i) it respects the direction of increasing θ on the magnet scale, which is also clockwise,

ii) it avoids the necessity of a systematic $90^o$ correction for all θ readings (true magnetic field direction perpendicular to reading direction).

From the general matrix equation for the transformation of a $2^{nd}$ rank tensor

$$\emptyset' = T \emptyset \tilde{T} \quad (\sim \text{ transpose}), \tag{20}$$

the expression for $\emptyset'_{33}$ can be derived:

$$\emptyset'_{33} = \alpha_{3K} \, \alpha_{31} \, \emptyset_{K1} \; ; \qquad \emptyset_{K1} = \emptyset_{1K} \tag{21}$$

$$= \alpha_{31}^2 \, \emptyset_{11} + \alpha_{32}^2 \, \emptyset_{22} + \alpha_{33}^2 \, \emptyset_{33} + 2\alpha_{31}\alpha_{32}\emptyset_{12} + 2\alpha_{31}\alpha_{33}\emptyset_{13}$$

$$+ 2\alpha_{32}\alpha_{33}\emptyset_{33}$$

This expression can be further developed, since

$$T = \{\alpha_{iK}\} = T_2 \times T_1 \tag{22}$$

By considering the rules of matrix multiplication, extracting the relevant matrix element from Table II-1, and finally combining the terms with the same trigonometric coefficients (diagonal and off diagonal $\emptyset_{iK}$ components taken separately), we find

p. 16 and 17. In equ. (21), (22) and (23) the index capital "K" should

be replaced by lower case "k" to avoid confusion with the constant K in

equations (24) to (26).

$$\phi'_{33} = \cos^2\theta \, [a_{1i}^2\phi_{ii} + 2a_{1j}a_{1K}\phi_{jK}] + \sin^2\theta[a_{2i}^2\phi_{ii} + 2a_{2j}a_{2K}\phi_{jK}]$$

$$j<K \qquad\qquad\qquad j<K$$

$$- 2\sin\theta\cos\theta \, [a_{1i}a_{2i}\phi_{ii} + (a_{1j}a_{2K} + a_{2j}a_{1K})\phi_{jK}]$$

$$j<K$$

$$j, \; K = 1,2,3 \qquad\qquad\qquad\qquad (23)$$

Since $\cos^2\theta$, $\sin^2\theta$ and $\sin\theta \times \cos\theta$ can easily be converted into linear functions of $\sin 2\theta$ and $\cos 2\theta$, the final expression for the splitting becomes:

$$2\Delta\nu = K\phi'_{33} = A + B \cos 2\theta + C \sin 2\theta, \text{ with} \qquad (24)$$

$$\begin{matrix} A \\ B \end{matrix} = \frac{K}{2} \left[ (a_{11}^2 \pm a_{21}^2)\phi_{11} + (a_{12}^2 \pm a_{22}^2)\phi_{22} + (a_{13}^2 \pm a_{23}^2)\phi_{33} + \right. \qquad (25)$$

$$\left. + 2(a_{11}a_{12}\pm a_{21}a_{22})\phi_{12} + 2(a_{11}a_{13} \pm a_{21}a_{23})\phi_{23} + 2(a_{12}a_{13}\pm a_{22}a_{23})\phi_{23} \right]$$

(top signs for A), and

$$C = -K\left[ a_{11}a_{21}\phi_{11} + a_{12}a_{22}\phi_{22} + a_{13}a_{23}\phi_{33} + (a_{11}a_{22} + a_{21}a_{12})\phi_{12} + \right.$$

$$\left. +(a_{11}a_{23} + a_{21}a_{13})\phi_{13} + (a_{12}a_{23} + a_{22}a_{13})\phi_{23} \right], \qquad (26)$$

where

$$K = \frac{3eQ(2m-1)}{2I(2I-1)h}$$

$I$ = nuclear spin quantum number,

$eQ$ = electric quadrupole moment,

$m$ = nuclear magnetic quantum number

and $h$ = Planck's constant.

It can be deduced immediately from expressions (25) and (26) that

substitution of all $a_{iK}$ by $-a_{iK}$ induces no change in the values of the

A, B, C constants, i.e. the d.m.r. experiment does not distinguish between

directions related by a centre of inversion. Some other simplifying steps

are possible for planes and symmetry axes.

### Determination of the $K\emptyset_{iK}$ components from experimental data.

i)   Evaluation of constants A, B, C.

Rotation patterns for at least two general crystal positions or

preferably for 3 mutually perpendicular orientations were constructed

from the measured splittings, recorded at regular angular intervals of $\overline{H}$

(and some intermediate positions). A least squares fit provides the

best way of minimising error in the calculation of the constants A, B, C

for each of the magnetically distinct deuterons. Since the general matrix

expression for least squares (12). becomes quite impracticable to use directly

on a desk calculator, the very much simplified equations for A, B and C

given by Pedersen (13) can be used as long as the readings are taken at

regular intervals on the angular scale. Although some loss of

experimental data (intermediate positions) results, and interpolation in

positions where spectra are not available or individual data are

inaccessible (superposition of signals) is necessary, these expressions are

of great practical use

$$A = \frac{1}{n} \sum_{i=1}^{n} \Delta H_i, \tag{27}$$

$$B = \frac{\sum\limits_{i=1}^{n} \Delta H_i \cos 2\theta_i}{\sum\limits_{i=1}^{n} \cos^2 2\theta_i}, \qquad (28)$$

$$C = \frac{\sum\limits_{i=1}^{n} \Delta H_i \sin 2\theta_i}{\sum\limits_{i=1}^{n} \sin^2 2\theta_i}; \qquad (29)$$

n is the number of angular readings for each curve, and $\Delta H_i$ is the magnitude of the splitting measured at $i\delta$, where $\delta$ is the (constant) angular separation between consecutive readings.

ii) For the crystal in two general positions, the following system of 6 linear equations with 6 unknowns (3 equations from each pattern) can be established for each deuteron line.

$$2A^I = (a_{11}^2 + a_{21}^2)K\phi_{11} + (a_{12}^2 + a_{22}^2)K\phi_{22} + (a_{13}^2 + a_{23}^2)K\phi_{33}$$
$$+ 2(a_{11}a_{12} + a_{21}a_{22})K\phi_{12} + 2(a_{11}a_{13} + a_{21}a_{23})K\phi_{13} + 2(a_{12}a_{13} + a_{22}a_{23})K\phi_{23}$$

$$2B^I = (a_{11}^2 - a_{21}^2)K\phi_{11} + (a_{12}^2 - a_{22}^2)K\phi_{22} + (a_{13}^2 - a_{23}^2)K\phi_{33}$$
$$+ 2(a_{11}a_{12} - a_{21}a_{22})K\phi_{12} + 2(a_{11}a_{13} - a_{21}a_{23})K\phi_{13} + 2(a_{12}a_{13} - a_{22}a_{23})K\phi_{23}$$

$$-C^I = a_{11}a_{21}K\phi_{11} + a_{12}a_{22}K\phi_{22} + a_{13}a_{23}K\phi_{33} + (a_{11}a_{22} + a_{21}a_{12})K\phi_{12} \qquad (30)$$
$$+ (a_{11}a_{23} + a_{21}a_{13})K\phi_{13} + (a_{12}a_{23} + a_{22}a_{13})K\phi_{23}$$

$$2A^{II} = (a_{11}'^2 + a_{21}'^2)K\phi_{11} + (a_{12}'^2 + a_{22}'^2)K\phi_{22} + (a_{13}'^2 + a_{23}'^2)K\phi_{33}$$
$$+ 2(a_{11}'a_{12}' + a_{21}'a_{22}')K\phi_{12} + 2(a_{11}'a_{13}' + a_{21}'a_{23}')K\phi_{13} + 2(a_{12}'a_{13}' + a_{22}'a_{23}')K\phi_{23}$$

$$2B^{II} = (a_{11}'^2 - a_{21}'^2)K\phi_{11} + (a_{12}'^2 - a_{22}'^2)K\phi_{22} + (a_{13}'^2 + a_{23}'^2)K\phi_{33}$$

$$+2(a_{11}'a'_{12}-a_{21}'a_{22}')K\phi_{12}+2(a_{11}'a_{13}'-a_{21}'a_{23}')K\phi_{13} + 2(a_{12}'a_{13}'-a_{22}'a_{23}')K\phi_{23}$$

$$-C^{II} = a_{11}'a_{21}'K\phi_{11}+ a_{12}'a_{22}'K\phi_{22} + a_{13}'a_{23}'K\phi_{33} + (a_{11}'a_{22}' + a_{21}'a'_{12})K\phi_{12}$$

$$+ 2(a_{11}'a_{23}' + a_{21}'a_{13}')K\phi_{13} + (a_{12}'a_{23}' + a_{22}'a_{13}')K\phi_{23}.$$

The coefficients of each variable can be extracted from the transformation matrix $T_1$(abc) → (xyz) for patterns I and II; x-ray methods provide, wherever possible, the classical way of determining the crystal orientation data. The system of equations above can be given in a more compact form:

$$T \times \phi = A, \text{ where} \tag{31}$$

$T(6x6)$ is the matrix of the coefficients of $K\phi_{iK}$ in the linear system (30),

$$\phi = \begin{bmatrix} K\phi_{11} \\ K\phi_{22} \\ K\phi_{33} \\ K\phi_{12} \\ K\phi_{13} \\ K\phi_{23} \end{bmatrix} \qquad\qquad A = \begin{bmatrix} 2A^I \\ 2B^I \\ -C^I \\ 2A^{II} \\ 2B^{II} \\ -C^{II} \end{bmatrix}$$

and $(T^{-1}T) \phi = T^{-1}A \rightarrow \phi = T^{-1}A.$

Inversion of T can be carried out by computer, or by an electronic calculator if a procedure such as the pivoting method (14) is followed.

(iii) Diagonalization of the interaction tensor as obtained in the previous section. A number of references (e.g. (12) and (14)) pays detailed attention to the subject. For the present work, the largest eigen value and respective eigen vector were found by successive approximations

(power iteration method).  The remaining eigen values were calculated

from the characteristic equation after 'extracting' the largest root

(the latter calculated to 5 or 6 significant figures to reduce

consequent errors).

Chapter III

The Spectrometer


III.A.  Spectrometer Assembly

1. General

The spectrometer was basically a laboratory-assembled bridge-type

n.m.r. instrument, as shown diagrammatically in Fig.III.1.  The specimen

coil formed the inductive part of a twin-T bridge circuit which, while

balancing out most of the R.F. carrier level in the absence of n.m.r.

absorption, responded sharply to any changes in the coil characteristics.

Such changes were caused by the absorption or dispersion of R.F. energy

by the nuclear spin system, when the magnetic field was swept slowly

through resonance.  The signal was then recovered from the demodulated

output of the receiver by a phase sensitive detector, using the same

audio source as the field modulation and with the modulation depth much

less than the line-width.  The first derivative of the absorption spectrum

was recorded.

This basic instrument was adapted to overcome the particular

problems of deuterium n.m.r., namely its inherent low sensitivity for

detection (of the order of $10^{-2}$:1 compared with protons at constant field)

and the broadness of the signals, often 3-5 KHz wide because of dipolar

effects.  It was therefore necessary to maximise as far as possible the

factors on which the signal to noise ratio S/N explicitly depends (1).

Particular attention was thus paid to the magnet-probe and signal

recovery stages.  Some of the important points to be considered were:

# FIG. III-1  Block Diagram of the Spectrometer



FIG. III-1  Block Diagram of the Spectrometer

# FIG. III-2    1 2 V.  Power  Supply
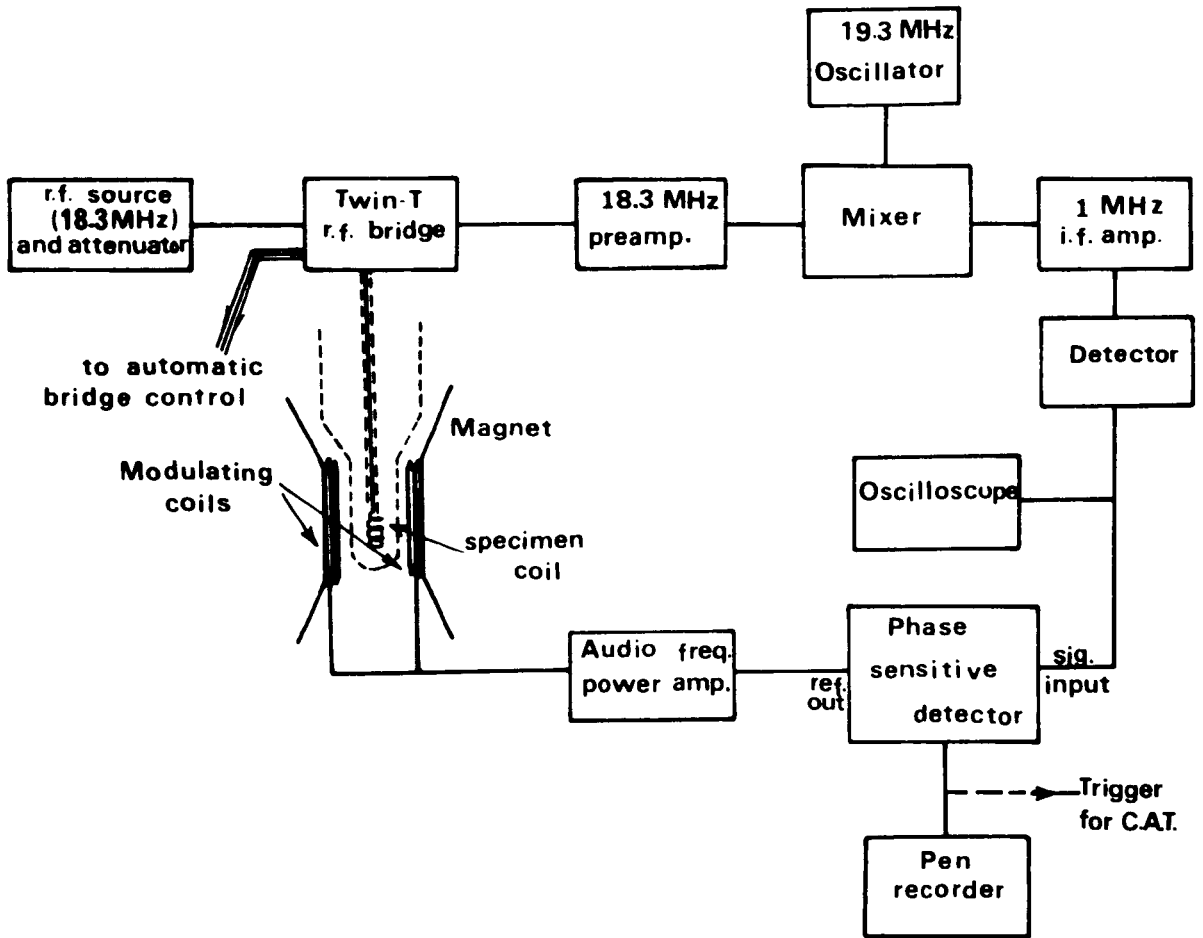


FIG. III-2    1 2 V.  Power  Supply
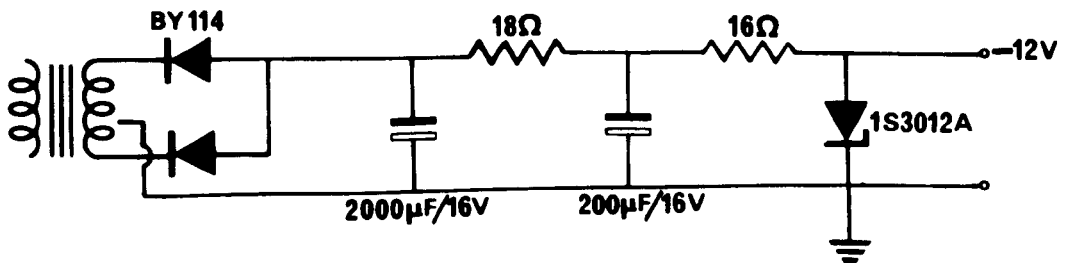
(a) frequency $\nu_o$ - and magnetic field accordingly - should be as high as feasible, since S/N depends on $\nu_o^{3/2}$. A powerful electromagnet was employed, enabling a working field of 28 kilogauss to be attained.

(b) the probe was specially designed to hold relatively large single crystals (about 1 $cm^3$), and had the highest practicable global Q factor

(c) the preamplifier and receiver had low noise characteristics, high amplification and narrow bandwidth. For signal recovery, phase sensitive detection with a long time constant was used as a means of drastically reducing the noise bandwidth of the system

(d) a computer of average transients (C.A.T.) was also used for further signal enhancement in the case of $ND_4DSO_4$.

As a special feature of this spectrometer, a very effective automatic control system (2,3) was added to the bridge circuit, to compensate for its oversensitive response to temperature changes or mechanical disturbances, and to dispense with intermediate readjustments in long (100 min.) runs. A considerable improvement in baseline stability was thereby achieved, at the cost of some extra noise from the diodes. A somewhat more detailed account of the spectrometer components follows.

## 2. The Magnet

The magnet used was a 15" Varian 3800 electromagnet, with a VFR2703 solid state power supply and control unit. The maximum attainable field was about 29000 gauss in a $1\frac{1}{4}$" gap at 142 amp. The working field range was 27993 $\pm$ 300 gauss, well within the region where the magnet had

been designed to achieve maximum homogeneity.  The latter depended very

sharply on the field setting, being at its poorest from 24000 to 26000

gauss.  Within the gap itself, homogeneity also varied markedly with

location.  The field homogeneity had been checked previously with a $D_2O$

sample (4): in the best position the linewidth was about 260 milligauss

at 28 KG.  At all field strengths the linewidth increased noticeably even

if the sample was moved as little as 1 mm from the ideal position.  There

was also a field difference of roughly 8 gauss for a displacement of 15 mm

from the best location.  For these reasons, positioning of the sample

could be critical, particularly for low temperature spectra.

Regulation of the field strength was based on a small Hall probe

attached to one of the pole pieces.  This was part of a negative feedback

control loop: the sensor response to short term variations of magnetic

field produced the necessary correction from the current-controlling

circuit.  Long term stability depended ultimately on the constancy of

room temperature.  Neither the laboratory room nor the field control panel

was thermostated; daytime temperature fluctuations and the warming-up of

the magnet itself had a very marked effect on field drift rate.  It took

about 3 h. after switching on for the field to stabilise.  When fairly

steady conditions were reached, e.g. no more than about 3 gauss/h drift,

spectrum recording was normally possible for long periods.  The drift

rate was evaluated for each spectrum so that corrections could be applied.

For setting the value of the field, there was a main field control,

and a fine incremental one of up to 100 gauss; both were set manually.

Field sweep facilities were provided by a potentiometer driven by a

synchronous motor, which rotated the sweep dial between -50% and +50% of

the selected field range.  The latter gave a selection of 17 ranges, from

250 milligauss up to 40 kilogauss.  Sweep times from 0•5 min. to 100 min.
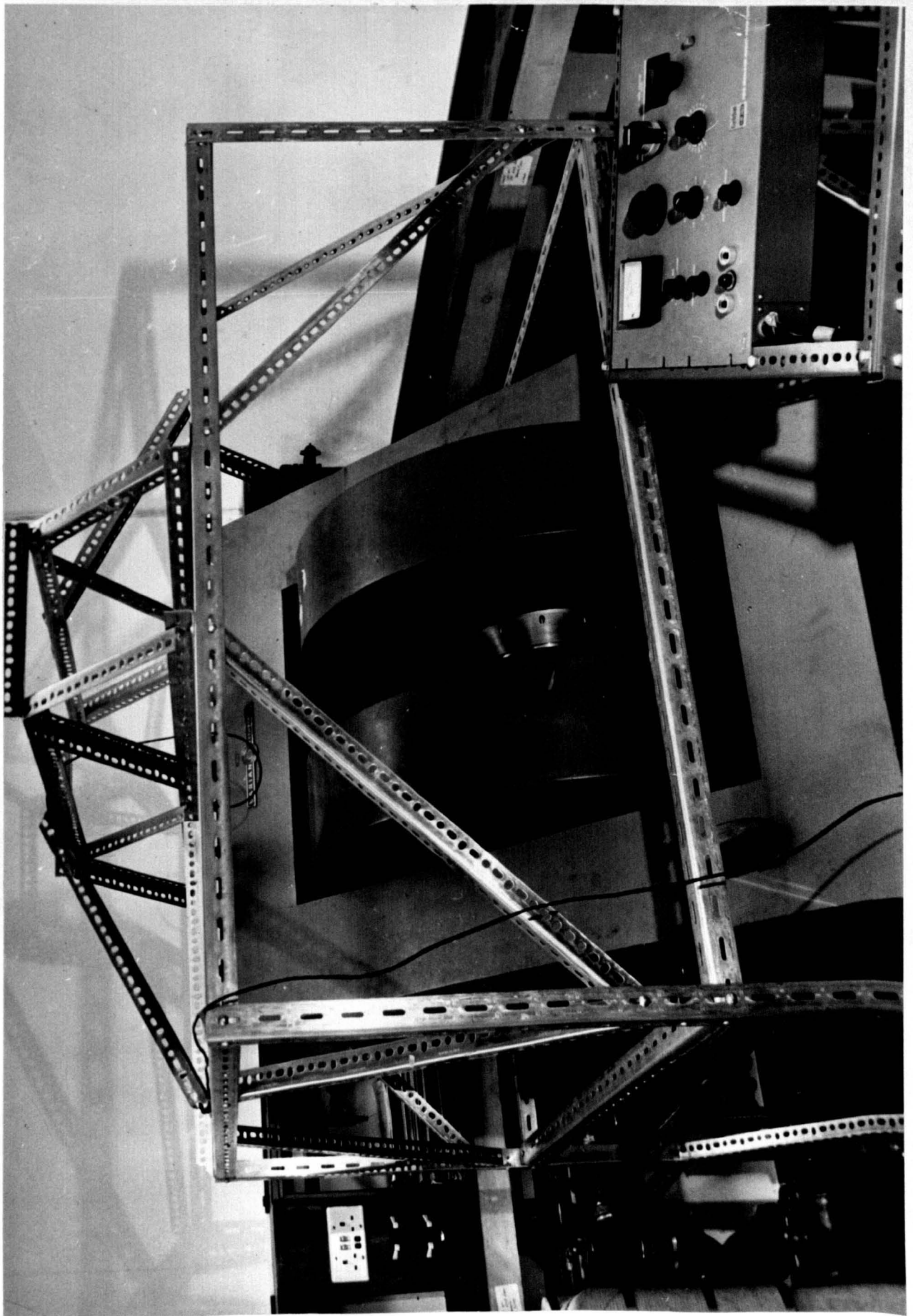
could also be chosen.  Field sweep calibration studies had shown (4) that the sweep could depart from linearity by up to 0·15% of the whole (-50% +50%) sweep range.  A significant improvement (~50%) resulted, however, if the range was taken between shorter limits (± 49·79% or less).  The field sweep potentiometer was the most likely cause of the observed non-linearity.

Cooling of the main magnet coils was provided by circulation of distilled water, which also flowed through the cold plate of the power supply.  A heat exchanging unit enabled heat transfer from the "core" water to the water of the external circulation system, which was connected to a large cooling tower outside the building.  Even this was occasionally insufficient in warm weather.  Efficient operation of the magnet was improved by careful cleaning every 2-3 months, using hot "Oakite" (Oakite Products Inc., New York) solution.  Afterwards the system was rinsed and finally refilled with distilled water and a few drops of "Panacide", to cut down the growth of bacteria or algae.

As the photograph shows, an aluminium dexion frame was firmly built round the magnet and the probe support was fixed to it.

### 3. Modulating Coils

As is common in fixed frequency n.m.r. spectrometers, the magnetic field was modulated for signal detection, at the same audiofrequency (37·3 Hz) as used for the signal recovery system.  The reference source output on the phase sensitive detector (p.s.d.) was amplified and then fed to the coils.  A modulating unit was built which consisted of a 12 volt supply (Fig.III.2) connected to a commercial (Newmarket) audio power amplifier.  Each of the Helmholtz modulating coils consisted of 200 turns of 22 s.w.g. enamelled copper wire wound round a perspex former

and mounted on the pole pieces. They were connected in parallel. Depths of modulation of up to 2•5 gauss could be achieved. The operating values depended on the strength of the absorption; for the very strong ammonium signal, about 0•2 gauss was sufficient, while weak signals normally required 0•6 to 1 gauss and occasionally more ($\leq$ 2 gauss).

### 4. The R.F. Bridge

Bridge systems, as null-methods, have the great advantage of reducing the carrier level enough to permit considerable amplification before rectification, besides cancelling out noise due to spurious modulation. The R.F. bridge used was basically an asymmetrical twin T Anderson bridge (5) as shown in Fig.III.3. The character of the residual unbalance in the bridge must be controlled, since this determines the nature of the signal observed (1). In an Anderson bridge, phase and amplitude can be balanced independently, by adjusting the appropriate capacitors. The absorption mode is achieved with complete phase balance and slight detuning of the amplitude; dispersion mode results if the settings are reversed.

One difficulty with R.F. bridges is their high sensitivity to external disturbances, such as temperature changes, vibration, etc. This problem is accentuated by the stringent conditions required for observation of weak and broad deuterium resonances. The bridge was therefore constructed as solidly as possible, and high quality electrical components were used throughout. For better insulation it was surrounded by styrofoam.

An early attempt to thermostat its immediate surroundings, by means of a thick polythene bag, hair dryer, contact thermometer and relay failed because large electrical disturbances were induced in the spectrometer

FIG.III-3 Twin-T r.f. Bridge
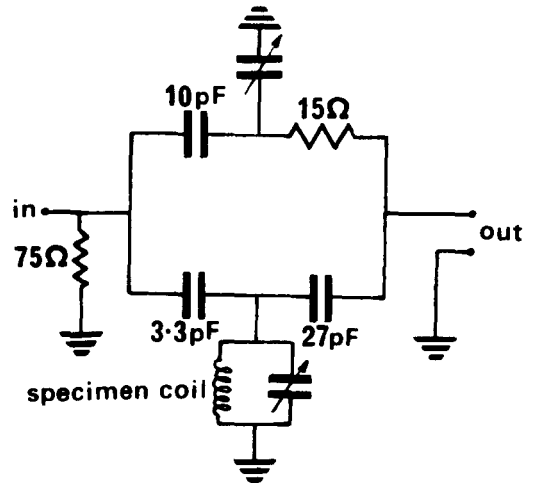


FIG.III-4 Remote Balancing Circuit

A fine phase control
B fine amplitude control
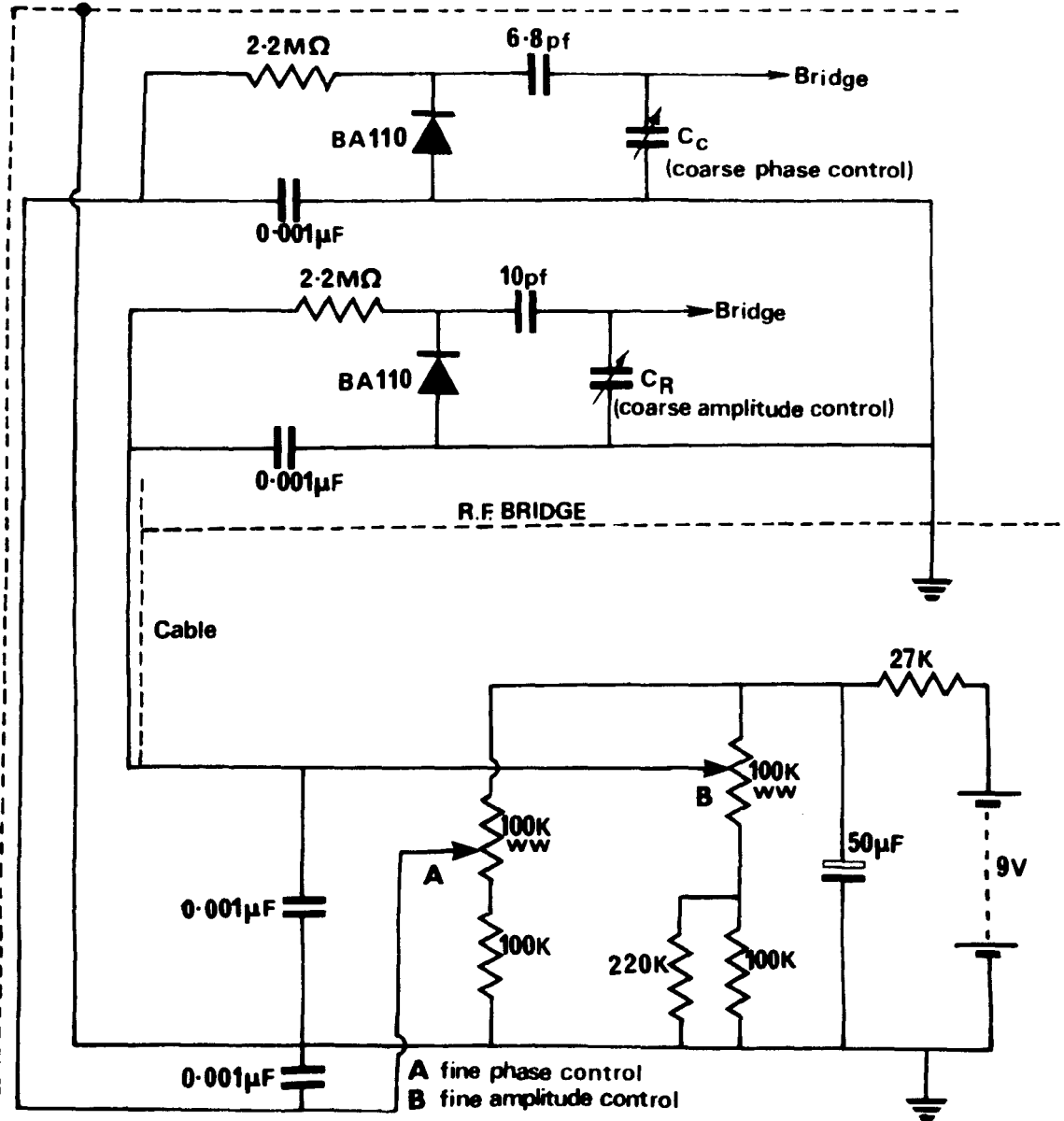
when the relay and heater were operating.

A further, more successful improvement was introduced by building a manual remote control to the bridge. Varactor diodes were coupled to each of the main tuning capacitors, for which they acted as additional fine adjustments. The capacitance of such diodes depends on their reverse potential bias, which was set with a potentiometer on the "remote" part of the control circuit (Fig.III.4). This manual control system proved reasonably satisfactory, and was used in the first patterns obtained from $ND_4DSO_4$. A few adjustments were necessary during a run, so the constant presence of the operator was required.

A decisive improvement came finally when both bridge controls were made automatic, by deriving the potential for biassing the diodes electronically. The system was designed and built by Fryer (3), who modified the control loop discussed by Mehring and Kanert (2). The automatic phase control was designed to maintain a precise phase balance, while the amplitude control aimed at keeping constant a preset amplitude detuning. To increase the effectiveness of the controls, the bridge sensitivity was increased by making $C_1$ and $C_2$ 3·3 and 27 pF respectively (Fig.III.5A).

(a) <u>Amplitude Control</u> (Fig.III.5B).

This system was based directly on the work of Mehring and Kanert (2). Deviations of the bridge output voltage $V_T$ from the preset value were compensated by a change of the capacitance $C_a$ or, to be more precise, of the capacitance of its complementary varactor diode. For this purpose, $V_T$ was amplified and detected in the receiver. Its direct voltage $V_D$ is compared to the reference voltage $V_S$ selected by a 100K helipot in the differential amplifier, the output of which gives the voltage

FIG.III-5   Automatic  Bridge  Control

(A) Bridge  Circuit
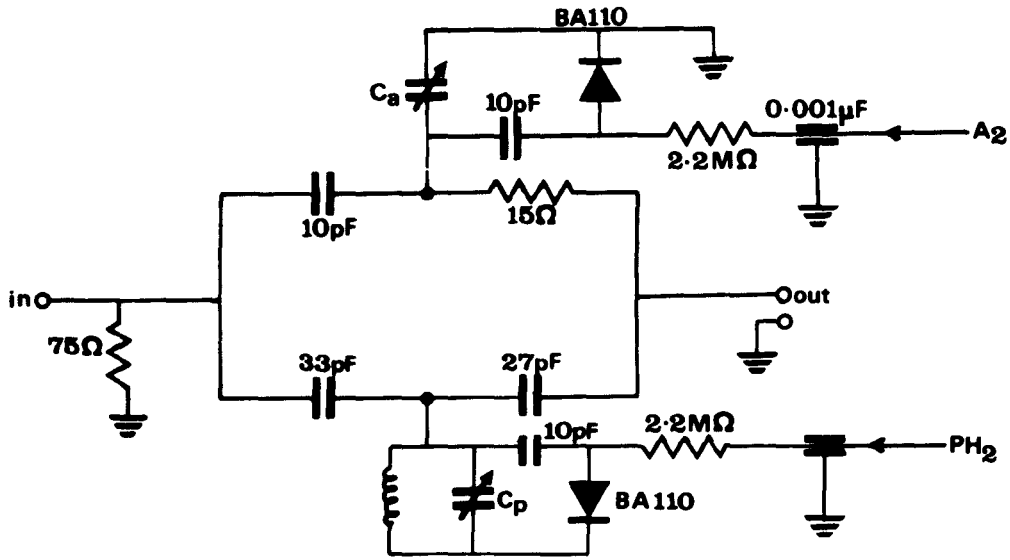
(B) Amplitude  Control
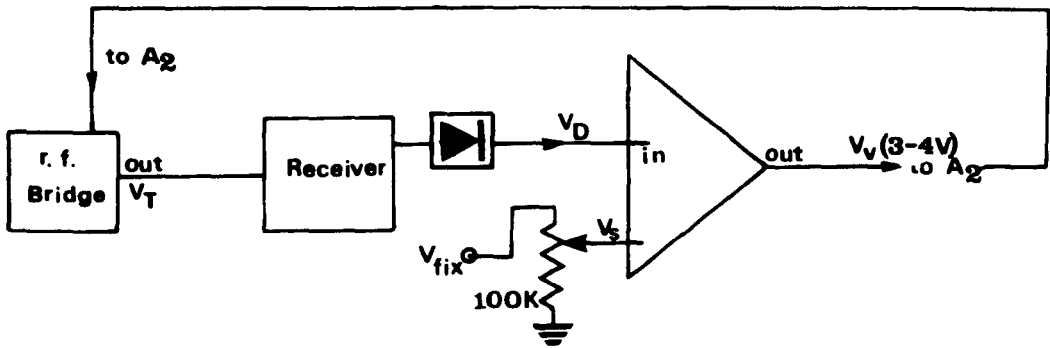
(C) Phase  Control
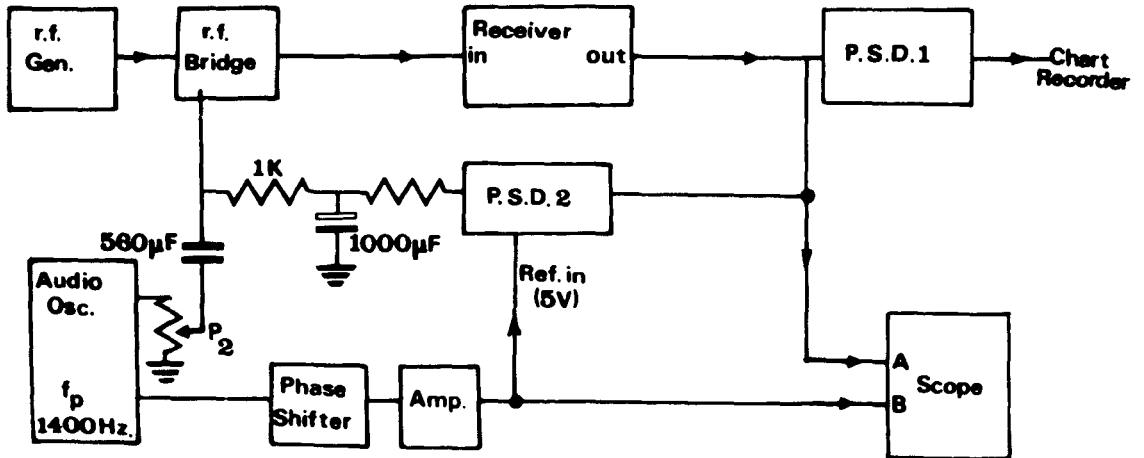
$$V_V = \text{const.} \times (V_D - V_S)$$

This control voltage $V_V$, after amplification, is fed into the input $A_2$ of the bridge with such a polarity as to obtain negative feedback.

(b) <u>Phase control</u> (Fig.III.5C)

An alternating voltage of audiofrequency $f_p$ was applied to the varactor diode associated to tuning capacitor $C_p$. The demodulated output of the receiver contained a signal $f_p$, except when the phase was perfectly balanced. This signal was rectified by a phase sensitive detector operating at frequency $f_p$, the resultant d.c. voltage being fed back to bias the varactor. As long as feedback was negative, the $f_p$ signal from the receiver was reduced to zero, and the bridge was kept in phase balance. To reduce any possibilities of degradation of the n.m.r. signals by the unwanted control frequency $f_p$, the latter was made much higher (1400 Hz) than the magnetic field modulation frequency; $f_p$ was then easily filtered out.

In practice the bridge was first tuned roughly with the coarse manual controls, and the receiver set at low gain. This was then increased slowly up to the working level; if the initial tuning had brought the bridge close enough to the automatic control working range, the latter locked in and took over. Otherwise, a few more repetitions eventually achieved this result. The oscilloscope (triggered at $f_p$) should then display a small stationary waveform at frequency $2f_p$, its amplitude easily adjusted with $P_2$. By comparing $2f_p$ and $f_p$ waveforms directly on the screen, it was easy to adjust the phase shifter to an optimum setting. After it was set, the automatic control did not need readjusting for several hours. Often it locked immediately after the spectrometer was switched on, in spite of large temperature changes while the magnet was warming up.

The working voltages at the bridge can be summarised as follows:

R.F. voltage (r.m.s.) applied to bridge, $e_s$, between 180 mV

and 380 mV, depending on the crystal being studied and its

conditions (particularly temperature),

R.F. voltage across sample coil, $e_c$, between 65 mV and 135 mV,

R.F. field thus generated, $H_1 = 0 \cdot 0145$ gauss (estimated for

100 mV across coil).

The values of $e_c$ and $H_1$ were calculated from the formulae given by

Anderson (5), including the balance conditions for a twin T R.F. bridge,

the ratio $|e_c|/|e_s|$, and an approximate expression for $H_1$.

### 5. The Coil

The construction of a coil with a high Q factor was based partly

on trial-and-error and partly on data from the Radio Engineer's Handbook

(6). The diameter was chosen so as to balance the conflicting

requirements of a large sample volume and of a reasonable distance between

the coil and the surrounding copper tube, (used as both screen and heat

leak), to reduce inductance losses. A diameter of 8 mm was adopted;

inductance losses should then be no higher than 40%. From the tables

of maximum Q at different frequencies and coil former diameters, best

results were predicted for windings of either

8 turns/cm, 22 s.w.g. copper wire

9 turns/cm, 24 s.w.g. copper wire

A 1 cm. long coil of nine turns in 24 s.w.g. enamelled copper wire was

wound round a perspex rod surrounded by P.T.F.E. ("teflon"). After

the cement (polystyrene or araldite) set, the coil was very easily

slipped out. The Q of such a coil was found to be 163 at $18 \cdot 3$ Mc/s.

This value fell appreciably to around 90 when it was mounted inside its tightly-fitting perspex holder in the large probe (Fig.III.7). To prevent further losses, coaxial cable was not used to connect the bridge and probe; instead they were joined directly by a BNC coupler. The final Q factor of the probe plus connector was 86.

## 6. The Probe

Four main requirements determined the design of the probe:

1. Provision for low temperature studies, with the ability to keep the temperature steady to within $\pm 1 \cdot 5^{\circ}C$ for several hours.

2. Reliable electrical performance.

3. Inclusion of a specimen holder, relative to which the position of the crystal could be fixed accurately from X-ray or optical goniometer data. Furthermore, it should enable crystal location with respect to a fixed laboratory system of axes, once the probe is transferred to the magnet.

4. The possibility of removing the probe from the magnet frame and replacing it in a rapid and reproducible way.

Some drawings of the probe are shown in Figs. III.6, 7 and 8, most of them self-explanatory.

### (a) Low temperature arrangements

Heat conduction through an appropriate heat-leak was chosen as an easier and more reliable system of sample cooling, in preference to a permanent stream of cold air or nitrogen. The probe was constructed largely of copper, with short lengths of German silver on both inner and outer conductors to reduce heat conduction. As the figure shows, the

# FIG.III-6 Probe Assembly



aluminium platform

magnet coil

styrofoam lid

copper basket

copper can

Dewar

pole piece

sample zone

0          5        10cm
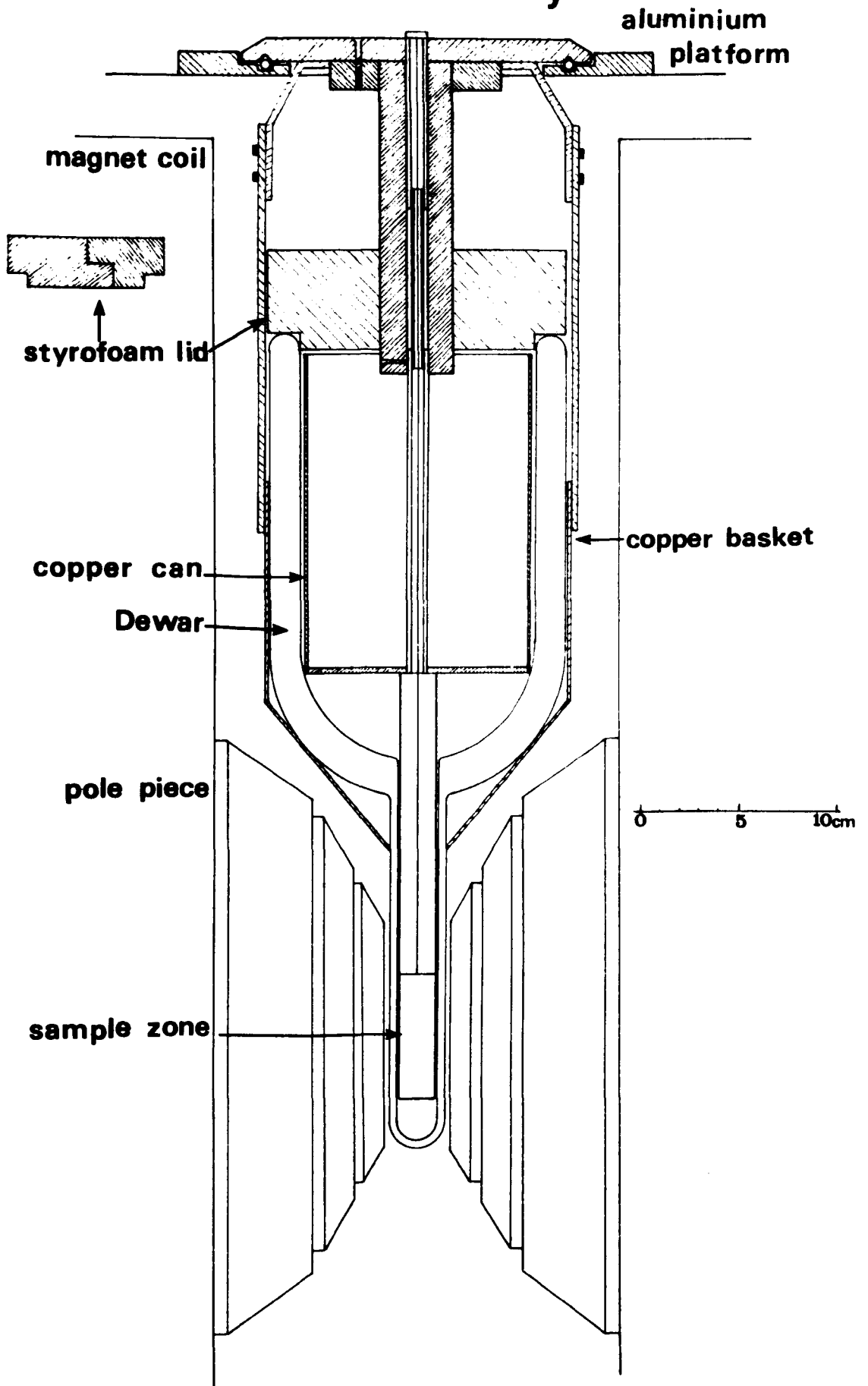
coolant was placed fairly high in the probe, in a thick walled copper container. Cardice could be used quite satisfactorily, provided the reservoir was refilled before each run. To help in establishing a better thermal contact, methylated spirits was added successfully for the later low temperature patterns. Access of damp air or coolant to the coil zone was effectively prevented by filling the gap between the dewar walls and the probe with plasticine. A special styrofoam lid (Fig.III.6), detail) was assembled above the coolant.

Extensive preliminary temperature checks were carried out in the probe by inserting the junction of a copper-constantan thermocouple in the centre of the coil. The results are summarised in Table III.1. All the above tests were carried out on the isolated probe. The heat generated by the magnet raised the temperature at the coil location by up to $3^{\circ}C$, however, while reducing appreciably the temperature stability. In a typical test, the temperature of the probe with cardice as coolant rose by $3 \cdot 5^{\circ}$ in 90 minutes. The main cause for this behaviour was the poor insulation provided by the non-silvered sections of the dewar (section III.5c). For the actual spectrometer runs, a small thermocouple was fixed to the outside of the copper tube at the height of the sample. The cold junction was an ice-distilled water mixture; a digital voltmeter (Solartron "LM 1420") monitored accurately the voltage from the thermo-couple. Recharging followed any excessive temperature rise.

(b) Earthing (electrical behaviour)

Wherever possible, metal joints were hard soldered for better thermoelectrical contact. The end of the coil was soldered to a small brass nut embedded in perspex piece A (Fig.III.7) and joined to the copper can via a screw.

## Table III.1

### Temperature Tests on Probe

| Coolant | Average temp. at centre of coil ($^{o}$C) | Temp. gradient across coil ($^{o}$C/cm) | Temperature Stability | |
|---|---|---|---|---|
| | | | temp. variation ($^{o}$C) | time |
| ice | 9·0 | negligible | +0·4 | 12 h |
| cardice | -52·3 | 0·6 | +1·3 | 4 h |
| cardice-methylated spirits 'slush' | -57·5 -46·5 (Probe II*) | 0·8 | +0·6 +0·5 | 6 h 10 h |
| liquid nitrogen | -165·5 | 2·8 | +0·5 | 3 h |

\* Probe II - specially adapted probe used for the second crystal position of $ND_4DSO_4$.

(c) <u>Crystal holder arrangement</u>

The crystal was oriented in the magnetic field by an adaptation of a method used by Dr. J. Royston (4). In this technique, the normal to a small mirror fixed to the crystal support acts as reference. This surface-aluminised mirror was carefully glued with araldite to a flat m accurately machined on the crystal holder, and parallel to its axis (Fig.III.8). A slot in the surrounding perspex piece and copper tube, and a non-silvered zone on both dewar walls, allowed a beam of light to pass through to the mirror. A second flat n formed the plane of attachment to a small perspex locking piece fixed to an X-ray goniometer. The latter (a Unicam S25) had a Webski slit facility, which was used for optical determination of the mirror azimuth in the X-ray camera. For optical goniometry, (using a 'Techne' two circle goniometer), a slightly different design of the crystal holder included two mirrors $90^{\circ}$ apart (section V.2). Some variation was also introduced for the second crystal position of $ND_4DSO_4$ (Section IV.3a).

(d) <u>Probe support</u>

A small dexion cage was fixed solidly to two bars of the magnet frame. A sketch is shown in Fig.III.9. Provision was made for three kinds of orthogonal movements of the probe:

1. Vertical – metal piece A rested on three levelling
   screws fixed to the bottom of this cage.

2. Back-to-front – piece A was firmly wedged against
   the sides of the cage by means of 1/8" teflon strips.
   A second set of adjusting screws, fixed to the front of
   the cage, enabled the probe to slide smoothly and
   reproducibly against the teflon 'runners'.

3. Sideways - the frame dexion bars themselves could be given

slight lateral movements. One adjustment only was

necessary, at the very start,to centre the probe support.

Small angular movements could also be given with the

levelling screws.

(e) <u>Dewar support</u>

Two thick copper handles (Fig .III.9) hold the copper piece

which supported the dewar. The whole probe was eased into place

through the narrow gap, rather like a basket, with its handles back

to front. It was then rotated into the operating position.

(f) The possibility of having to rotate the crystel instead of

the magnet had to be anticipated, since the magnet had been known to

jam on its bearings. Mobile piece B thus had a $360^{\circ}$ scale which, with

a complementing set of verniers on piece A, would permit accurate

reading of the crystal angular position. A teflon O-ring eased the

movement and insulated electrically the probe from the magnet frame.

7. <u>R.F. source, receiver and phase sensitive detector.</u>

The radiofrequency source was a 'home-built' crystal oscillator

already available, operating at a fixed frequency of 18.2963 MHz. A

built-in attenuator, with 1 dB steps,reduced the output from 4.28V to

the operating level (180-380 mV). The instrument was characterized

by very low noise, and a high frequency stability. Frequency variations

were generally below 0.04 KHz ($<$ 0.1 gauss) during a working day, so

that frequency drift was a negligible source of error compared with

other factors.

The receiver was a specially designed superhet. (Decca Instruments),

with low noise characteristics and variable gain control; it provided

high amplification before detection (80-127 dB). The first stage of

the receiver system was a low noise preamplifier tuned to 18.3 MHz,

followed by a mixer to give an intermediate frequency of 1 MHz, which

was further amplified before diode detection (vide block diagram, Fig.III.1).

A noise figure of 2.6 dB was measured with a Marconi TF 1106 noise

generator.

Signal recovery detectors were either a Princeton Applied Research

(P.A.R.) model JB-4 or A.I.M. Electronics model 5-1. Both instruments

had output time constants of 1, 3, 5 and 10s. The P.A.R. also had provision

for an external time constant attachment. The sophisticated separate

unit system of the A.I.M. proved very versatile. Also, in contrast with

the P.A.R. unit, its single-ended output (i.e., with zero D.C. offset)

proved better for working in conjunction with a computer of average transients.

### 8. The Computer of average transients.

The signal to noise ratio for $ND_4DSO_4$ at low temperature proved to be

very poor, with signals barely detectable. An attempt was made to overcome

this problem by recording the spectra several times and comparing the

"bumps", but it was difficult to obtain consistent results. A much longer

time constant of 30 sec. proved hardly effective, besides lengthening

considerably the spectra recording times.

These difficulties were overcome by the use of a computer of average

transients (C.A.T.), which, by scanning rapidly and repeatedly through the

spectra and accumulating the data in its memory, enhances the signal to

noise ratio by a factor equal to the square root of the number of scans.

The instrument used was a Biomac 1000 which contained 1000 addresses, each

of 16 bits. Crystal controlled sweep times through these locations from

5 msec. to 82 sec. were available. The sweep time could also be controlled

externally via an external advance input (0.5V to 5V level). Intersweep

delays were given in binary increments to crystal accuracy. Averaging

could be performed through 1, 2 or 4 channel inputs ($\pm$ 3V).

The resolution in amplitude was 1:64.

In the first attempts to use this instrument with the spectrometer, a triggering pulse was taken from the field dial retransmitting potentiometer which was coupled to the field sweep potentiometer. This signal was used to trigger a monostable multivibrator which gave a 9V pulse lasting 0.3 ms at the external trigger input of the C.A.T.

Since the position of the trigger point was time dependent, rather than field dependent, serious broadening of the signals occurred after a few scans. For a reasonable signal enhancement, spectrum searches normally took 50 to 100 min., during which the magnetic field could differ by as much as 4 to 6 gauss. Such long accummulation periods were necessary, since a full 250 gauss range had to be covered in each sweep, and also because relaxation times impose a practical limitation on the speed of scanning with solid samples.

An internal triggering signal is ideal for compensating field drift, but is not normally possible from a solid sample. Ammonium bisulphate, however, so difficult to handle in other ways, showed the redeeming feature of a very strong narrow central signal from the rotating ammonium ions, which could be used for this purpose.

In practice, the P.S.D. output was passed through a X20 amplifier built by J. Royston (Fig.III.10), and thence to a Schmidt trigger (Fig.III-11). This unit acted as a kind of voltage sensitive switch when the positive going side of the signal rose above the triggering threshold of the circuit. The actual trigger point was set at about 0.4 gauss after the centre of the main signal, and approximately +3V above the noise level (Fig.III-13, detail);

## FIG.III-10  X20 Amplifier



FIG.III-10  X20 Amplifier

## FIG.III-11 Schmidt Trigger
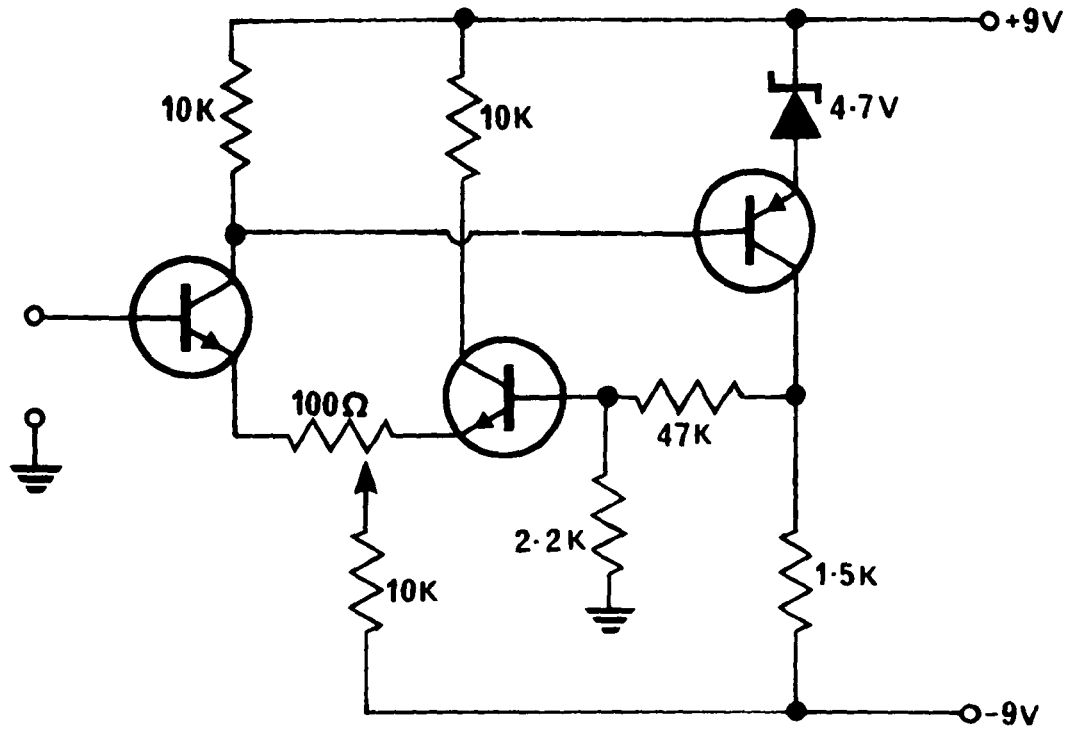


FIG.III-11 Schmidt Trigger
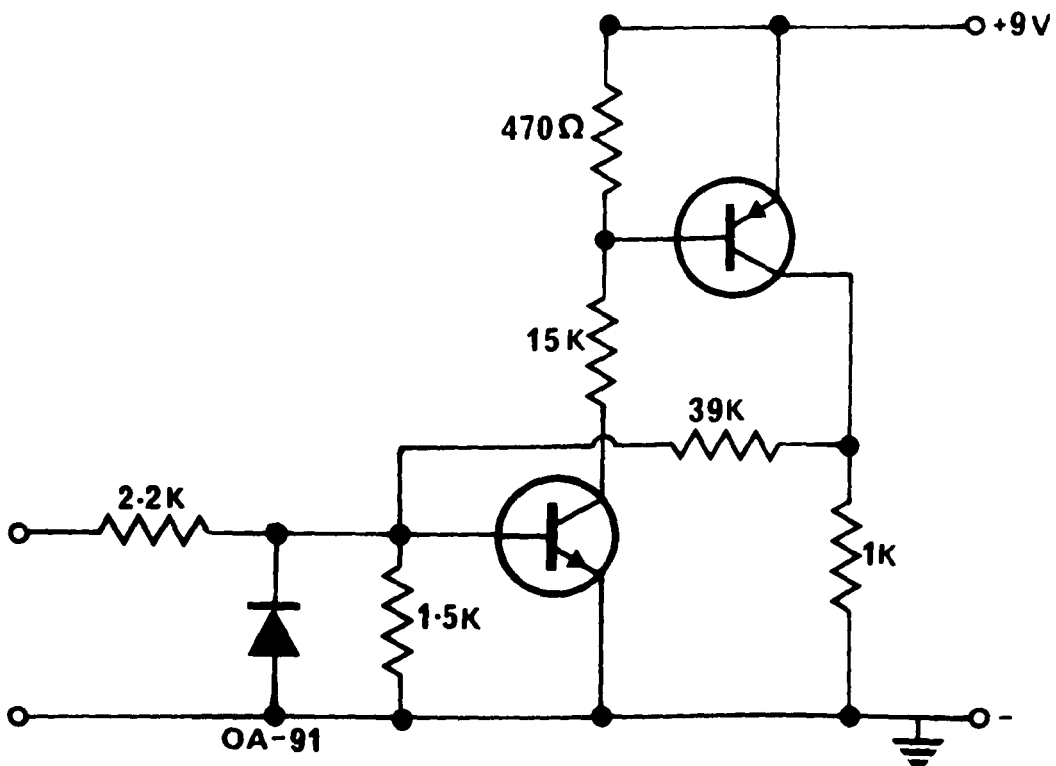
the zero shift control on the P.S.D. was used for this purpose. Fig.III-12 shows the additions to the spectrometer to allow C.A.T. running.

The C.A.T. did not have long enough scanning times in its internal mode to work in conjunction with a field sweep rate of 250 gauss/5 min. A small, very stable audio oscillator (Farnell) generated the necessary low frequency square wave (3.5 Hz. or 7.4 Hz) to be fed through the external advance facility of the C.A.T. To prevent overloading of the instrument, scanning through the central signal was avoided; a small delay was introduced on both sides of the triggering point. Conveniently, the memory contents were automatically displayed during part of the delay, enabling the progress of the accummulation to be followed closely. Fig.III-13 shows schematically the time distribution during one scanning period. To obtain the correct location of the recorded signals, field sweep calibration data were available from J. Royston; data from Fig.III-13 were also taken into consideration. Small errors introduced through time-base fluctuations or drift effects in individual scans were ignored: frequency stability on the audio oscillator was better than 1 in $10^4$, and drift would not affect the field by more than 0.2 gauss at any point in the spectrum. The effect of small variations in the triggering point has also been neglected.

Typical conditions for a C.A.T. spectrum were:-

       delay before = 5.12s

       delay after  = 5.12s

       sweep time (external advance) = 284.99s (start)
                                        = 285.01s (finish)

       no. of scans = 16

       Total time  = 90 min.

       (time constant in P.S.D. output = 1s)

FIG.III-12  Block Diagram for C.A.T. Attachment
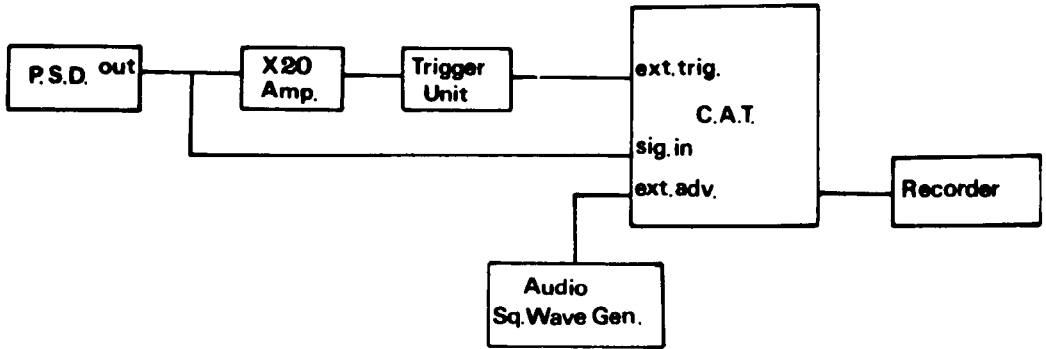


FIG.III-13  Time Distribution in C.A.T. Long Runs
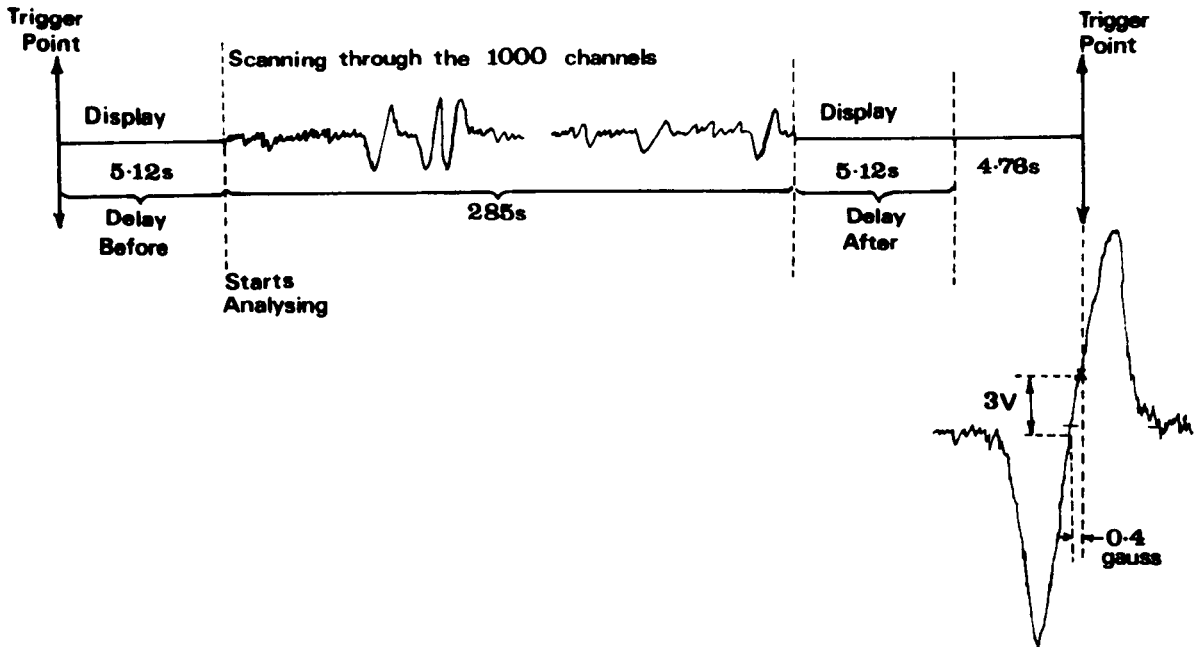


FIG.III-14  Alignment of Probe in the Magnet Gap
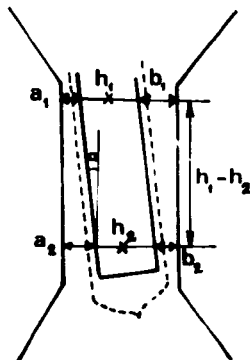
Before each spectrum, the frequency of the square wave generator was accurately adjusted to 1 part in 3000 by using a Hewlett-Packard frequency counter, model 5428L. Provision was also made for shorter (100 gauss) spectra or portions of larger spectra.


III.B. Determination of Rotation Patterns

The full experimental procedure involved in the determination of one rotation pattern is now described. The probe was located on its support on the magnet frame, and then centred and set as vertically as possible. The magnet was rotated to check whether the fragile dewar walls had a good clearance all round. The spectrometer was switched on and a reasonably strong signal was recorded and optimised, by careful adjustment of the controls. Small vertical movements and minimal angular adjustments were then given to the probe by means of the levelling screws, until maximum height and minimum distortion of this signal were achieved, indicating that the sample was then in a position of maximum field homogeneity (generally 1 in $10^5$ gauss). Before normal spectrum routine was started, a preliminary determination of the probe position and mirror azimuth ensured that any subsequent disturbance of the probe could easily be checked. Basically, the azimuth (relative to the scale on the base of the magnet) was found by comparing the reflection from the probe reference mirror with the reflection from a second, magnet-bound mirror, and rotating the magnet until the centres of both reflections were aligned vertically (4). The magnet scale was then read. This second mirror was fixed to an accurately machined aluminium block, which could be tightly wedged against the pole pieces. Due to the weakness and dispersion of the reflection from the probe mirror, the whole determination was carried out in the darkened room. A collimator and lamp were used as source of a

strong, parallel, light beam; a piece of greased semitransparent graph paper acted as a screen, its grid being useful for aligning the reflections. Some practical details had been solved by previous workers, such as the ingenious use of a divergent lens to attenuate the large divergence of the light beam, after it had passed through two thicknesses of dewar wall (4).

As many data as possible were obtained concerning the position of the probe, so that it could be replaced as reproducibly as possible. A clinometer, read at two positions $90^{\circ}$ apart, gave an accurate set of spatial angular co-ordinates for platform B (Fig.III.9) at the top of the probe; a reading was also taken on the angular scale engraved on B. Spectra were then recorded at $5^{\circ}$ or $10^{\circ}$ intervals and, whenever necessary, in intermediate positions. Because of the natural periodicity of all patterns, only a $180^{\circ}$ range had to be covered. No detectable centre of gravity shift was observed with either crystal, as would be expected at these high field strengths, so that half spectra only were recorded.

Recording conditions for an ordinary spectrum were:

(a) Magnetic field sweep rate: 5 gauss/min. (range 100, 250 or 500 gauss, according to the crystal involved and the magnitude of the splitting.)

(b) Depth of modulation in modulating coils: 0·6 to 1·0 gauss (also crystal dependent). Modulation frequency 37·3 Hz.

(c) R.F. level: 180 to 380 mV

(d) Time constant at P.S.D. output: 10s

(e) Recorder range 1V, occasionally 0·5V

Chart speed 60 cm/h.

(f) Frequency (constant) 18296·30 $\pm$ 0·05 KHz

To attenuate non linearity effects caused by the field sweep
potentiometer (4),care was taken not to use the magnetic field sweep
outside a -48% - +48% range on the sweep dial.

Field drift corrections could be very important, so that
determination of the magnetic field was essential at both the start and
finish of each spectrum. This was done either by using a strong central
signal from the actual crystal or by means of an externally added
reference. For the first compound (ammonium bisulphate) the process was
very much simplified. The field sweep dial was set at a fixed value,
normally +48% of the sweep range. For a more sensitive determination,
the recorder sensitivity was increased to 1V and the time constant
lowered to 1s. The centre of the signal was then easily located on the
pen recorder by moving the incremental control through the resonance
position, and the reading noted. The process was repeated after the
whole spectrum was finished, and the new reading on the incremental
control registered. The difference in the two readings gave the field
drift. The time between the first and last determinations was read from
a stop clock or simply deduced from the length of chart paper consumed
during the run. Spectra where drift was serious, say more than 1 gauss/
10 min., were rejected for measurement purposes.

For the strontium formate crystal, which does not show a constant,
strong central signal, a small capillary of hexadeuteroacetone was used as
external reference. The extra peak thus produced was comparatively weak,
so that the technique used previously could not be applied. The
alternative procedure was then to record it and measure its distance
against one or more calibration points, taken from the field sweep dial.
These references marks were made manually, by moving rapidly the Y control

on the pen recorder, at the precise instant when a certain division was passed on the dial.

An emergency method had to be adopted in one case, when the acetone in a badly sealed capillary finally evaporated. It involved rotating the magnet each time to a particular position where a strong central signal occured (vide Chapter V pattern III, $\theta = 172^{o}$), and proceeding as above.

Apart from a very real advantage in the measurements, it was not essential for the signal used in drift calculations to be central. Any prominent resonance in the particular spectrum, preferably near to its start, could be used. Centering was more difficult, since much more than half a spectrum had to be recorded; the central line was then inter-polated between two symmetrical signals, after drift corrections had been applied. This procedure was only occasionally necessary, when the reference peak became obscured by other signals.

After all the spectra for one rotation pattern had been completed, the mirror azimuth was redetermined and the probe alignment with respect to the pole pieces was checked and measured. A travelling microscope was used for this purpose. A small perspex piece was designed which enabled back to front angular movements of the collimator in an accurately vertical plane to be made. This feature made measurements possible at two different horizontal (marked) levels $h_1$ and $h_2$ (Fig.III.14) without intermediate readjustments. In each determination, the pole pieces and the edges of the copper tube were focussed successively. The distance $h_2 - h_1$ was also measured with the microscope set vertically. Two angles of tilt $\alpha$ and $\beta$ were thus determined for values of $0^{o}$ and $90^{o}$ respectively, on the magnet scale. These were enough to define any necessary correction to be introduced in the calculation of the crystal transformation matrix.

# CHAPTER IV

## $\underline{ND_4DSO_4}$.

## 1. Introduction

Ammonium bisulphate is ferroelectric in the range between $-3^\circ$ and $-119^\circ$C, and as such its structure offers particular interest. Moreover, the coexistence in the same molecule of an ammonium group and an acid hydrogen from the bisulphate ion provides an excellent opportunity for distinguishing between the two alternative explanations of the mechanism of ferroelectricity. This may proceed either by hydrogen ordering in a hydrogen-bonded lattice, or by an organisation of larger structural groupings, namely $NH_4^+$ or $HSO_4^-$ itself. $(NH_4)_2SO_4$, for example, is known to be ferroelectric, with an ordering of the $NH_4^+$ ions occuring at the Curie point (1,2). Some controversy has arisen on this subject, however (3).

From studies of the dielectric constant (4) it is known that ferroelectric behaviour also takes place in the deuterated form; the transition temperature is slightly lowered, from $-3^\circ$ (5) to $-10.9^\circ$ (4). Some of the main characteristics of the ferroelectric and non-ferroelectric forms may be summarised as follows (5,6):-

### TABLE IV-1

| Crystal form | Temp. limits, $^\circ$C | Space Group Z | Cell dimensions $^*$ |
|---|---|---|---|
| non ferroel. | $> -3^\circ$ $(-10.9^\circ)$ | $P2_1/c$, Z = 8 or *$B2_1/a$ Z = 16 (monocl.) | a = 24.66 Å b = 4.60  $\beta$ = 89.87$^\circ$ c = 14.82 |
| ferroelectric | $-3^\circ$ to $-119^\circ$ $(-10.9$ to $-115^\circ)$ | $Pc$ or *$Ba$ (monocl.) | a = 24.37 Å b = 4.62 $\beta \simeq 90^\circ$ c = 14.80 |
| ·non ferroel. | $< -119^\circ$ $(-115^\circ)$ | P1 or * B1 (tricl). | a = 24.43 Å $\alpha \simeq 90^\circ$ b = 4.56   $\beta$ = 91$^\circ$12' c = 15.15   $\gamma \simeq 90^\circ$ |

(in brackets, temperatures for the deuterated compound)

\* pseudoorthorhombic

An extremely low coercive field and a rather high degree of disorder along [c] in the room temperature form are two features worth mentioning. There is evidence that the low temperature transition is of first order while the other is possibly of second order (5).

The study of the structure by means of X-ray and neutron diffraction techniques is in progress (6,7,8). Room temperature data have recently been published (6). Relatively high thermal parameters for one of the two types of $HSO_4^-$ $(S_1)$ ion in the room temperature structure, a feature also found in the isomorphous rubidium salt (9), are compatible with a disordered behaviour for this kind of ion (7). According to this model, an essentially rigid, though somewhat distorted bisulphate ion is disordered $(S_D)$ between two equally probable sites, symmetrically displaced from the coordinates of the ordered model. The maximum amplitude of the movement would be of the order of 0.55 Å. In the ferroelectric phase, these $S_D$ groups order themselves antisymmetrically with respect to the room temperature centre of symmetry.

The small effect of deuteration upon the Curie temperature has so far been interpreted as meaning no major involvement of the hydrogen atoms in the mechanism of ferroelectricity. On the other hand, studies by inelastic neutron scattering (10) do not detect any very significant change in the torsional state of the $NH_4^+$ ions. Below the higher Curie temperature, a suggestion of a shoulder becomes barely noticeable after the sharp peak at 260 $cm^{-1}$ from the room temperature form, which is mainly due to the torsional motions of the ammonium ions. A clear peak doubling appears, however, below $-119°C$, at $\sim 290$ and 190 $cm^{-1}$. A detailed study of the Raman spectrum has also been carried out recently (11).

The object of the present work was to study the room temperature and ferroelectric phases in an attempt to throw some light on the way the

transition at the upper Curie point affects the hydrogen atoms, particularly those integrated in the $S_D$ ions. The low temperature transition was not studied. Thermal and electrical data suggest a much more drastic transformation (first order) at the lower Curie point, presumably involving the $NH_4^+$ ions (5,10). The already proven possibility of shattering the crystal at this transition point, together with a many-fold increase in the number of signals (lower symmetry, and 'freezing' of $NH_4^+$), which are thus predicted to be very weak, were some of the reasons for not attempting such a lengthy task.

Single crystals were quite difficult to grow and knowledge of the orientation was hard to acquire. The way of achieving it was a mixed technique of d.m.r. and X-ray Laüegrams. Since the crystals showed a preferential tendency in their direction of growth, two rotation patterns were obtained from the same original specimen which was set at orientations $30^o$ apart. A degree of error in the determination of the matrix transformation from the crystal axes to the laboratory set had to be reduced by devising a method of refining the data.

## 2. Crystal growth.

Two crystals of the fully deuterated compound were grown from the melt, by using a modification of the Bridgman-Stockbarger method (12). The crystal developed from a seeded zone in the molten material enclosed in a special container, as it was lowered very slowly ($\sim$ 1.33 mm/h) across a steady downward temperature gradient. Deuteration of the compound was the initial step, however.

(i) The deuterated compound.

The deuteration process consisted basically of repeated isotopic exchanges between the protonated salt and $D_2O$(99.7 atom %D). The compound

was reagent grade;recrystallisation from ordinary $H_2O$ was not

considered necessary.   Moreover, crystal growth itself tended to

segregate impurities to the last stages of crystallisation, in a kind of

zone refinement.  The whole procedure was carried out in an enclosed

container.   Early attempts at using a conventional vacuum line failed;

the high water-retaining capacity of the salt made it practically impossible

to evaporate the last fractions of syrupy solution, trapped under a

hard crust of dry compound.  Much better results and close control of

the operating conditions were achieved with the specially devised apparatus

sketched in Fig. IV-1.   A large trap immersed in liquid nitrogen and

communicating with the evaporation compartment by a short, large bore tube

was the means of bringing the solution to complete dryness.  The degree of

vacuum had to be strictly controlled to avoid  tumultuous boiling;   the

pressure was lowered considerably in the final stages.   Successive portions

of $D_2O$ were allowed to drain on to the solid.  Five recrystallisations

were carried out; a good enrichment was assumed, for it is known that both

the bisulphate hydrogen and those of the $NH_4^+$ group are quite labile.

Care had to be taken in the fifth operation to keep the temperature in a

range of $35^o$ to $40^o$;   this was an essential condition since the general

phase diagram (13) indicates that below $\simeq 30^o$ a different salt separates

out.  A 'thermostated dry bag' as described in Sec. III-A4 was successfully

employed for this purpose;   on other batches of the compound a manually

controlled water bath was used instead.

(ii)  The crystal for d.m.r.

Ammonium bisulphate is extremely hygroscopic.  It also has the

unpleasant ability,when molten, to corrode ordinary soft glass.  Several

attempts at coating portions of the material with layers of 'styrofoam' in

$CCl_4$ proved unfruitful.  Equally unsuccessful was a specially machined thin

walled polystyrene container which proved permeable to moisture;   problems

FIG. IV-1 Deuterium Exchanging Unit

to pump

D$_2$O

Thermometer

Liq. N$_2$
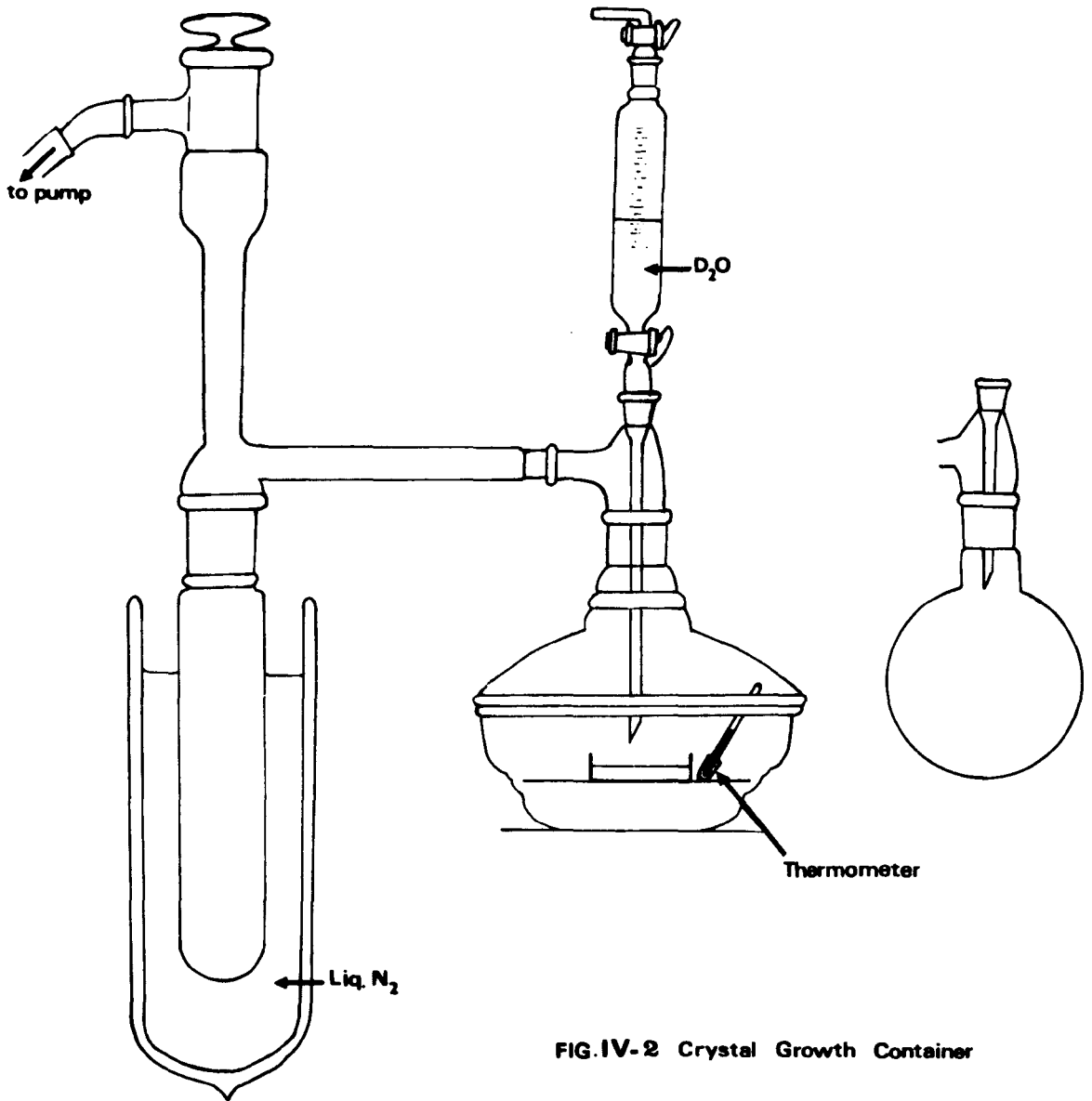
FIG. IV-2 Crystal Growth Container

of orientation and crystal transfer would also have presented difficulties.
The best solution, which avoided any crystal coating or transfer, consisted
of growing the specimen in an adequate permanent container, versatile
enough to enable X-ray work to be carried out, as shown in Fig. IV-2.
For this reason the end of the capillary had very thin walls.  Since
ordinary soda glass was not satisfactory (in a few trial runs the tube
walls were etched by the compound to the point of cracking or completely
breaking), medium walled pyrex tubing was employed.

Fig. IV-3A shows a sketch of the furnace used for crystal growth:
it is formed by two concentric glass tubes, the inner one with a length of
constantan wire wound round and kept in position with high temperature cement.
The base and top of the furnace were machined from $\frac{1}{8}"$ sindano board.  A
considerable amount of insulation was included throughout - asbestos tape
and cotton wool between the two tubes, more cotton wool and $\frac{3}{8}"$ styrofoam
on the outside.  To even out the temperature in the hottest part of the
oven ($148^{\circ} - 150^{\circ}$), a $\frac{1}{16}"$ concentric copper tube was added.

A slow descent of the specimen and a very steady temperature were
essential requirements, not only to improve the quality of the crystal
but equally to avoid spurious seeding.  The latter effect could easily
arise from temperature fluctuations since the crystal growing temperature
(m.p. zone) was normally located on a fairly steep section of the furnace
curve (Fig. IV-3B).  Fluctuations of the mains voltage and temperature
variations in the surroundings were the main sources of difficulty:  the
effect of the latter persisted whatever the amount of insulation.  (The
lid and its small aperture were the principal weak points).  To solve
both problems:-

(a)  the temperature of the immediate surroundings of the furnace was
rendered constant ($\pm 0.1^{\circ}$) by thermostating a cupboard in the laboratory.

## FIG. IV-3A Furnace



Heating Resistance

Copper Tube

Insulation

A,B,C Sindano Board
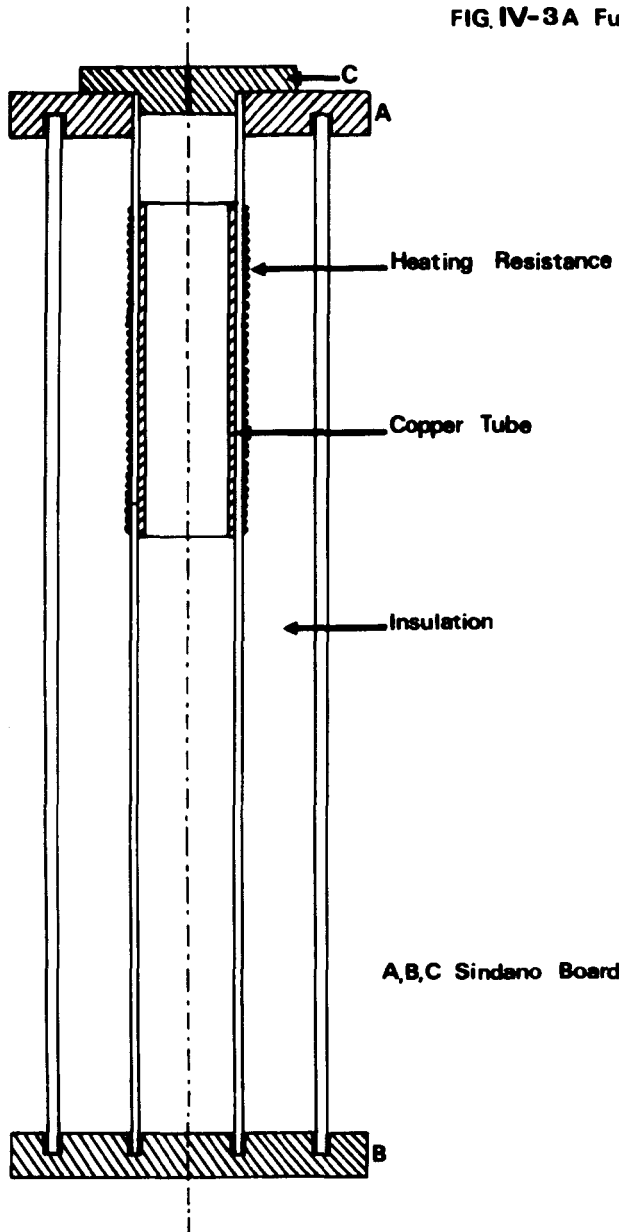
FIG. IV-3B Temperature Profile
of the Furnace



°C

150

m.p.

140

130

18    cm    13    8
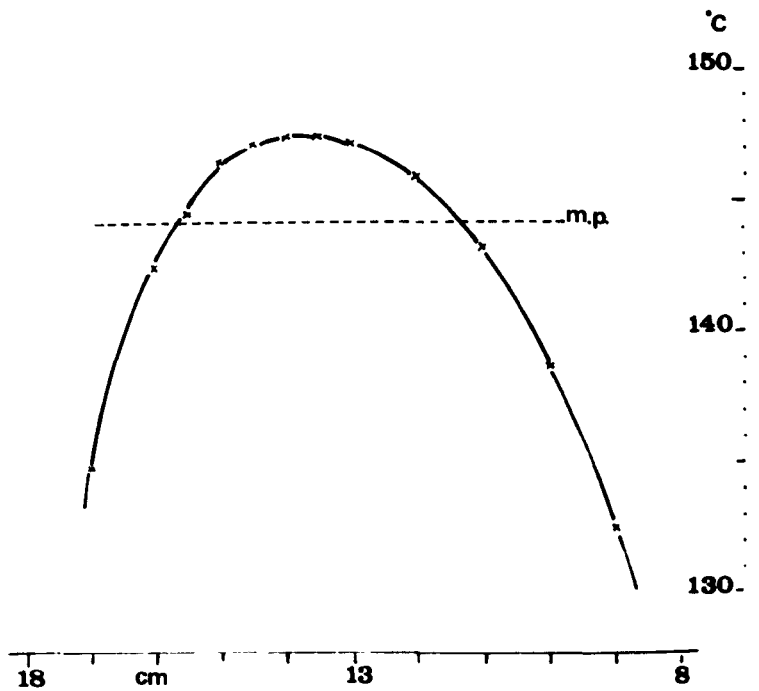
A 0.5 kw heater plus contact thermometer and relay were used for this purpose; a fan behind the heater controlled and homogenised the air flow. The temperature selected was $28.0^o$; it could be easily restored after opening and closing the door for any necessary checks.

(b)  a stabilised power supply (Kingshill) was employed instead of a mains operated transformer.

(iii)  Growing the specimen.

The main steps in crystal growth can be summarised as follows.

(a)  In a dry bag (with $P_2O_5$ as desiccant) the powdered compound was transferred to the container by means of a short wide-necked polythene funnel. A $P_2O_5$ U-tube was adapted to the open end and the constriction sealed rapidly.

(b)  In a paraffin, or preferably glycerol, bath the compound was slowly warmed until the melting point, which was read in the process by taking the capillary as reference. The outlet from the crystal growth container (Fig. IV-2) led via a 2-way tap either to a source of dry nitrogen or to a vacuum pump (with liquid nitrogen traps). By this means the molten compound could be degassed under controlled conditions. The deuterated salt is considerably more viscous than the protonated form, and the removal of the last air bubbles required fairly low pressures. The temperature had to be closely watched meanwhile, for fear of boiling the liquid, which was a rather sudden and tumultuous process. The pressure could then be restored and further attempts made. Often the amount of solid initially filling the crystal section of the tube was not sufficient, because of the loosely packed character of the material. In such cases the container was lowered further in the hot bath, so as to enable dry portions of the salt retained above the constriction to melt. Lowering the pressure led the melted

portions downwards. After degassing, the compound was allowed to solidify very slowly. The tube was then sealed under anhydrous conditions (U-tube with $P_2O_5$ adapted to the open end).

(c) The temperature profile of the furnace was determined by means of a long copper-constantan thermocouple placed at regular intervals along the axis of the stabilised oven. The container was then suspended from the shaft of the small synchronous motor used for driving the crystal; a counterweight balanced its weight. The specimen was carefully positioned at the exact height which would enable the whole compound to melt with the exception of a small (4-6 mm) section of the capillary. This small portion of polycrystalline solid acted as the source of random seeds from which crystal growth could progress - the length of capillary above this section was generally a good enough filter to allow only one specimen to develop until it reached the wide section of the container. Once thermal equilibrium had been reached (4h. to be safe) the motor was started. When the calculated time for growth had elapsed, the cotton thread was transferred to a wider shaft to let the crystal reach a cooler part ($40^o$ below m.pt.) of the oven more rapidly. The final stages of cooling were performed in a prewarmed Dewar. The crystals were extremely sensitive to thermal stress; a number of cracks sometimes appeared despite the precautions taken.

Two transparent protonated specimens were obtained by the technique described above; three deuterated samples were then grown, two of which were of reasonable quality. Examination between two large crossed polaroids confirmed that they were single crystals. Sharp extinctions over the whole specimen were much easier to detect when using sodium radiation in a dark room: general light diffusion and reflection from the glass were then minimised.

At a later stage of the work it was found by chance that the quality of the crystals could be improved by cooling them to cardice temperature, restoring them gradually to room temperature and repeating this annealing process a number of times.

Two rotation patterns for general positions of the crystal are the minimum requirements for complete solution of the e.f.g. tensor, provided that the orientation of the specimen can be determined by some auxiliary method, such as X-ray diffraction. It was hoped that at least two of the samples available would be in such conditions, since the criterion of seed selection was quite random. Experiment did not confirm this expectation, however; the room temperature patterns from two of the specimens showed obvious similarities. (At a later stage it was found that the axis of the container was at $\sim 15^{\circ}$ from [a] in one of them). To overcome this difficulty, an attempt was made to grow a crystal at an angle to the axis of the probe. The method consisted of enclosing the material in an almost spherical bulb, terminating in a tilted capillary. Since crystals do not turn corners, one could reasonably expect that it would grow along the capillary direction (set vertical in the furnace). Unfortunately the thinly blown walls did not stand the strain produced by the expansion of the solid when melting. A spherical shape is fundamentally unfavourable for this purpose.

3.   General spectrometer conditions.

(a)  Adapted holder for second crystal.

As already mentioned, instead of two independent crystals in general positions, one specimen in two different mountings was used for the two sets of rotation patterns. Figs. IV-4A, B and C show schematically the steps involved in converting the crystal from the first setting I to the second II.   Some relevant numerical data are included.

Fig IV-4   The crystal in positions (I) and (II)

(I)

(A)

coil former

(B)

copper shield

earth tag

30°

$m_3$

(C)

A

(II)
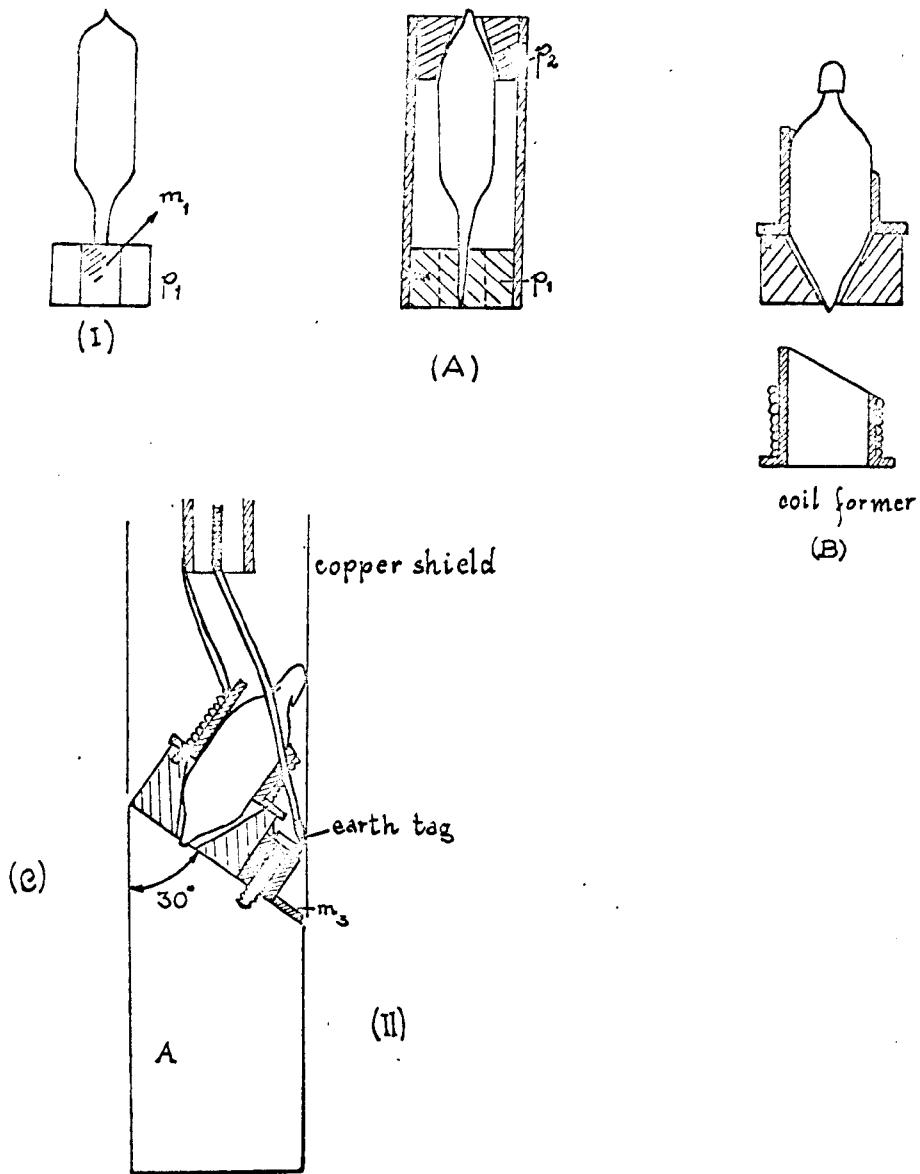
Fig. IV-5   Coolant Reservoir
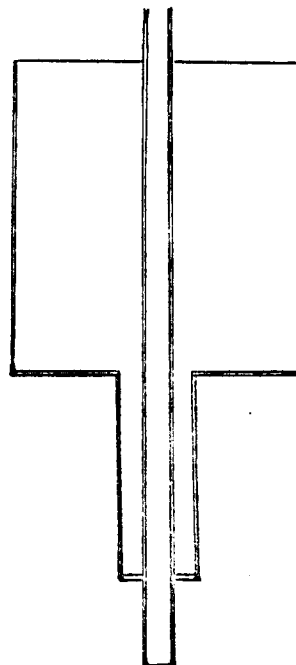
Stage (i)    A cylindrical perspex piece fitting tightly to pieces $p_1$ and $p_2$, and locked to them by a screw, kept the assembly accurately aligned while low temperature araldite set on join j.  Piece $p_2$ was an almost exact duplicate of $p_1$, except for the carved depression where the bulky top of the crystal was to be lodged.   Various small files were used to shape an originally conical section to the irregular shoulder contours of the crystal container.   A mirror $m_2$ on $p_2$ enabled goniometric determination of the angular deviation between the normals to $m_1$ and $m_2$, assumed to be in a plane perpendicular to the common cylinder axis.

Stage (ii)    In a dry bag ($P_2O_5$ desiccant), $p_1$ and part of the capillary section were carefully cut by means of a diamond pencil and the exposed section of the crystal rapidly covered with a new small glass cap filled with araldite.

Stage (iii)   The crystal was mounted on piece A which formed an accurately machined platform (at $30^o$) on a perspex cylinder fitting closely to the internal wall of the Dewar.  The very small gap between the cylinder and the glass was adequately sealed with thin P.T.F.E. sheet wound to the right thickness.   An auxiliary mirror $m_3$ was included for simplifying the determination of the orientation.   A small locking piece secured the crystal and its immediate holder to the main platform.  A 'portable' coil and former were fixed to the small ledge on $p_2$ (three 10 B.A. screws). The earth end was soldered directly to a short, thick section of enamelled copper wire (16 or 18 s.w.g.) which was hard soldered to the copper tube of the probe;   the inner was directed to a tag where it joined the other coil end.  To ensure sufficient and homogeneous cooling for the sample, a thin piece of copper sheeting was cut and soft soldered to the cooling tube, while enclosing the crystal mounting up to the platform height.  A small slot was cut to leave mirror $m_2$ visible.

Stage (iv)   Complementing this assembly, a new coolant reservoir
and copper-German silver coaxial cable had to be integrated in the probe.
Temperature tests proved that only with the coolant fairly close to the
sample location could the necessary temperature (-40 to $-50^{\circ}C$) be reached.
Fig. IV-5 shows part of the assembly, with a pocket of coolant ($CO_2$ +
methylated spirits) reaching low down in the probe ($\sim$ 7-9 cm from the
centre of the coil).

Stage (v)   To guarantee more adequate screening round the specimen coil,
a sheath of 32 s.w.g. copper sheeting was tailored to fit round the outside
tail end of the Dewar.  A number of screws secured it to the supporting
copper basket.  To avoid any direct contact of the metal with the pole pieces,
particularly at low temperatures where 'sweating' of the Dewar could
occur, an insulating layer of self-stick 'transpaseal' was tightly wrapped
round the earthing.  With not much space available, care had to be taken
in aligning the probe and checking that no knocks against the pole pieces
could take place.

(b)  Recording the spectra.

A number of initial spectrometer tests was carried out with a sample
of $D_2O$ 'doped' with iron(III) ions.:  a S/N ratio of 540:1 was achieved.
The general spectrometer conditions for both compounds  have already been
specified in Sec. III-B.  The S/N ratio was good at room temperature (3.5:1)
and at least two patterns have been run without C.A.T. enhancement.  For
reasons of simplicity (no drift corrections necessary), uniformity of
conditions with the low temperature patterns and time saving (not many scans
necessary for detectability), both the room temperature patterns shown
in the experimental results were obtained with the C.A.T. adapted to the

spectrometer. (The triggering procedure for the C.A.T. has been described in Sec. III-A7). Although within the general ranges given in Sec. III-B for r.f.,field modulation depth and sweep rate, the settings for this crystal may be further summarised:-

TABLE IV-2

| Spectrom. conditions | Room temp. patterns | | Cardice patt. (C.A.T.spect.) | Main signal studies |
|---|---|---|---|---|
| | Ordin.spectra | C.A.T.spectra | | |
| r.f. (mv) | 375 (sometimes 265) | 375 (sometimes 265) | 190 | 80-190 |
| depth of modulation | 1.0 g | 1.2 - 1.5g | 1.2 - 1.5g | 0.17-0.20g |
| time const. | 10s | 1s | 1s | 1s |
| field sweep rate | 5g/min | 50g/min | 50g/min | 10g/min |
| temp ($^{\circ}$C) | 31.5$\pm$ 2 | 31.5 $\pm$ 2 | -40$^{\circ}$ $\pm$ 2 | 31.5 $\pm$ 2 |

4. Experimental results.

(a) Room temperature: Patterns I and II.

Experimental results for these two patterns are shown in Figs. IV-6 and IV-7. Half-splittings (gauss) taken at regular intervals ($10^{\circ}$) are given in Appendix I, tables I and II. The same tables include values for A*, B* and C* constants for the four curves, as calculated by using the least squares expressions referred to by Pedersen (14). Pattern I has a number

FIG.IV-6 ND$_4$DSO$_4$ Pattern I (300 K)
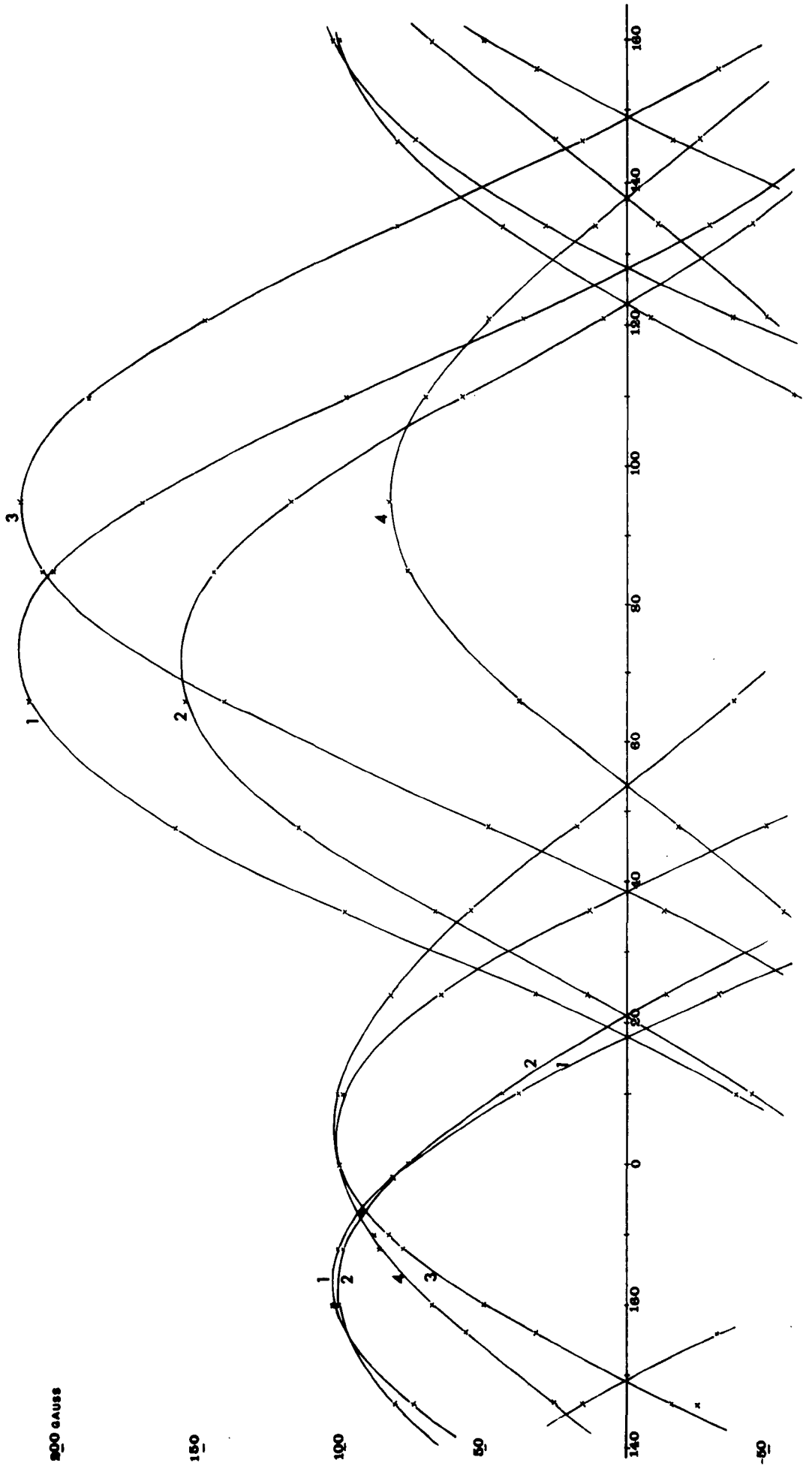
of points extrapolated from the experimental curves. In fact this
pattern was a repeat of a previous one, which had been completely assigned,
but which had to be abandoned due to a slight movement of the probe during
the measurements. To simplify matters, the pattern was re-checked by
taking C.A.T. spectra for a number of magnet positions where the curves
could be unambiguously resolved. By referring to the cancelled pattern
as a guide, positions in the vicinity of crossing points were avoided.

In addition to the central signal from the reorienting ammonium ions,
four signals are present in patterns I and II, a number which can easily be
predicted from the symmetry elements of the space (or point) group and
the number of symmetrically independent molecules (two) in the unit cell.
A stereographic projection shows readily that in general four signals are
to be expected from the bisulphate group, two from each kind of ion.



point group 2/m
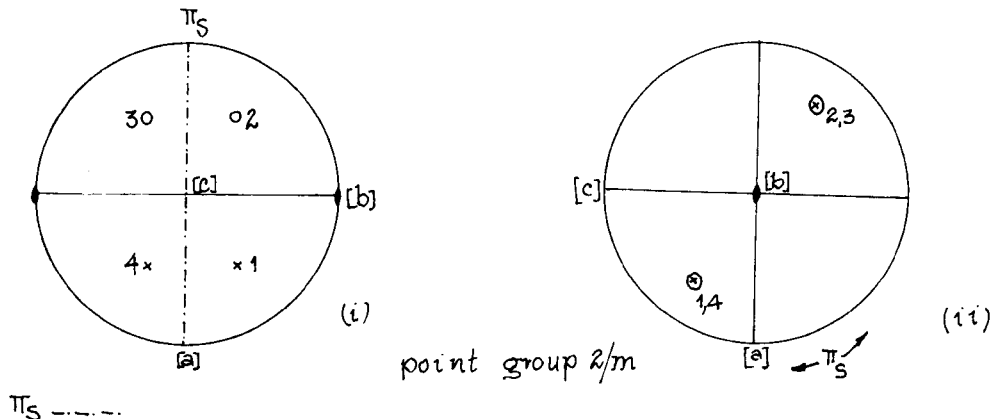
It is clear that deuterons 1 and 3, and likewise 2 and 4, would give no
independent signals, since they are related by a centre of symmetry. If
the crystal happened to be in the particular orientation indicated in fig.(ii)
above ([b] perpendicular to the magnetic field which thus moves in a plane
of symmetry), all four lines from each group should collapse to a singlet.
In the figures above and indeed throughout this work, a set of axes
corresponding to a pseudo-orthorhombic unit cell has been considered.

FIG.IV-7 ND$_4$DSO$_4$, PATTERN II (300K)
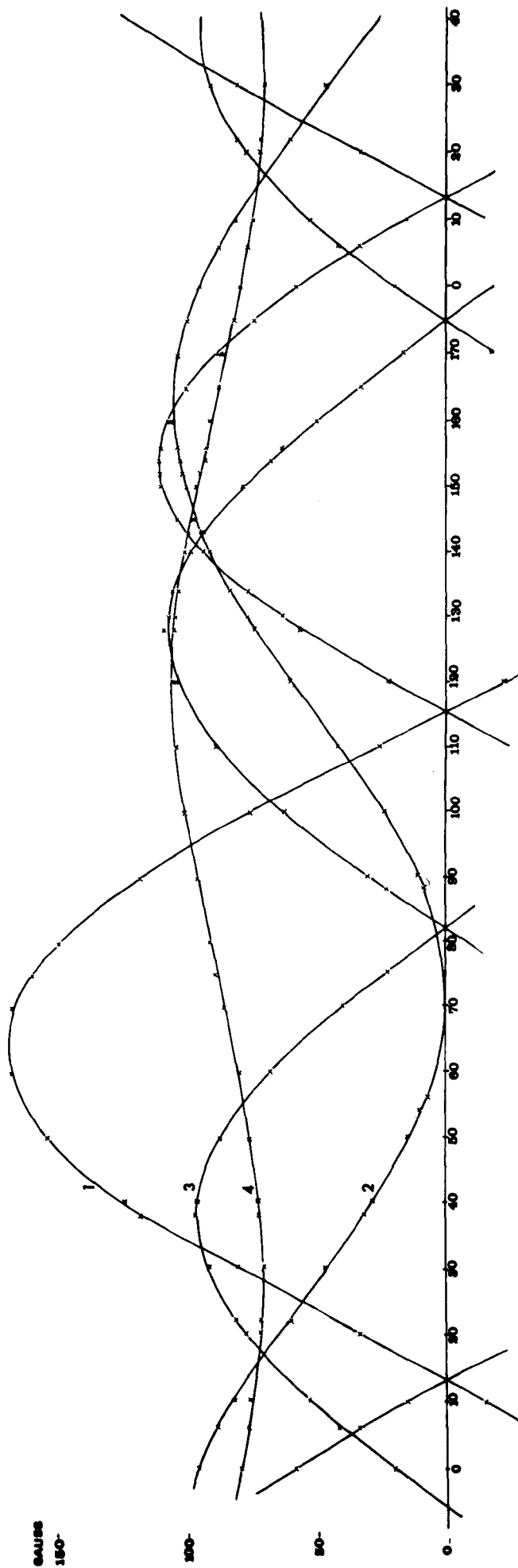
In complete contrast with pattern II, pattern I shows an overall regularity which immediately suggests that some symmetry element (possibly axis $\underset{\sim}{b}$) is not far from the plane of rotation of the magnetic field. This condition of near symmetry thus gives some indication concerning the crystal orientation. There is, however, in both patterns a feature with a far more specific meaning: for field positions $173.2^{\circ}$ and $142.6^{\circ}$ in I and II respectively, all the lines have crossing points in two groups of two. This special direction of complete equivalence for pairs of symmetrically related deuterons (1,4 and 2,3) clearly corresponds to the interaction of the plane of symmetry with the plane of the magnetic field. In pattern I, all four lines cluster together around the $173^{\circ}$ region, and careful resolution of the curves was necessary to decide which were the symmetrically related lines (confirmed by a mathematical analysis). Remarkably, this $173.2^{\circ}$ field position appeared to be close to a special direction (denoted as $\bar{r}_0$) of complete equivalence for all the bisulphate deuterons in the structure: if the probe had possessed a more versatile arrangement for crystal movements in the gap, it would have been interesting to locate such an orientation $\bar{r}_0$ and thus have direct proof that no centre of gravity shift was taking place (15). This conclusion was reached independently by recording both halves of a number of spectra and checking that they were symmetrical within experimental error. In any case, second-order shifts are not expected at these high field strengths.

(b) Low temperature patterns.

For both crystal positions the low temperature rotation patterns were determined; the results are shown graphically in Figs. IV-8 and IV-9. The number of signals doubled on passing through the ferroelectric transition point, an expected consequence of the loss of the screw axis

FIG. IV-8  ND$_2$DSO$_4$  PATTERN Γ'
230K
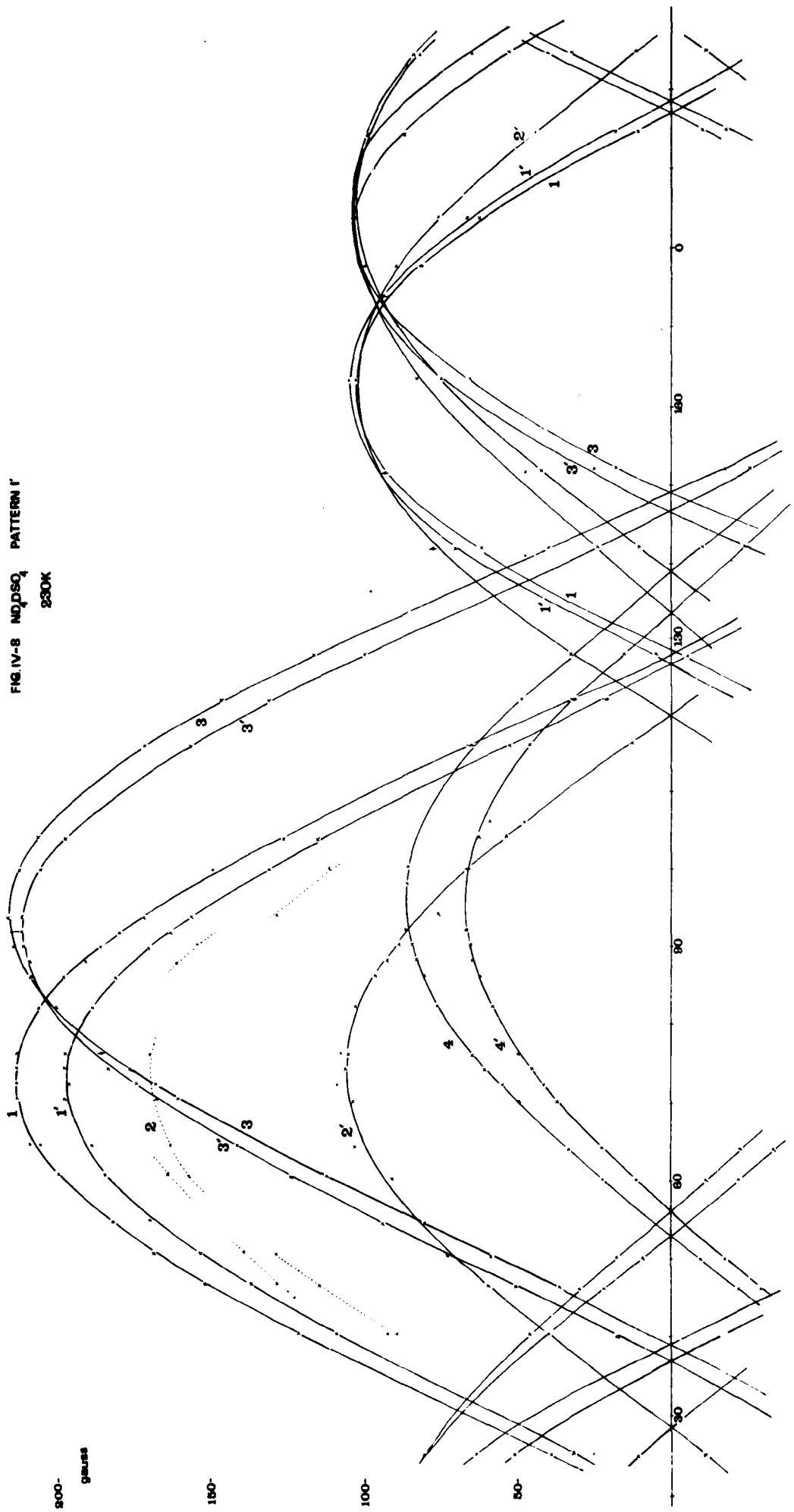
by a change of the crystal symmetry from space group $P2_{1/c}$ to $P_c$. Since very small atomic displacements occur at the Curie point, each of the newly formed pairs of lines has individual components very near to each other and to the original (room temperature) line. This close proximity of the signals and also their weakness (S/N ratio no more than half the value at room temperature) made the resolution of the patterns a very tedious and lengthy task.

The extensive use of tracing paper (semi-transparent graph paper) proved of great practical help for:-

(i) checking perfect symmetry of lines about the maximum,

(ii) locating the maximum and minimum, by folding the traced curve along its symmetry line,

(iii) checking that the minimum and maximum sections from the same curve were exactly equivalent in shape, and

(iv) deciding between two close alternative positions.

In a few instances, some simple relationships (tabulated below) have also been employed.

TABLE IV-3

| $\theta^{\circ} \rightarrow$ | $0^{\circ}$ | $90^{\circ}$ | $45^{\circ}$ | $135^{\circ}$ |
|---|---|---|---|---|
| $y(\theta)$ | A + B | A - B | A + C | A - C |

| $\theta \rightarrow$ | $\theta_o$max. | $\theta_o + 90^{\circ}$ | $\theta_o \pm 30^{\circ}$ | $\theta$min $\pm 30^{\circ}$ | $\theta_o \pm 45^{\circ}$ |
|---|---|---|---|---|---|
| $y(\theta)$ | A + D | A - D | A + D/2 | A - D/2 | A |

FIG.IV-9 ND$_2$DSO$_4$  PATTERN II'
230K

For example, by reading the splitting for two positions $90^{\circ}$ about the maximum (or minimum), the value of A can immediately be extracted. All expressions in Table IV-3 may readily be derived from the equation (Sec. II-2):-

$$y(\theta) = A + B \cos 2\theta + C \sin 2\theta$$

or its more compact version

$$y(\theta) = A + D \cos 2(\theta - \theta_o)$$

(preferably taking $\theta_o = \theta_{max.}$).

Observation of patterns I' and II' and comparison with their room temperature counterparts reveal that deuteron 2 undergoes a remarkable transformation; both low temperature lines 2' and 2" are fairly well separated (pattern II'): furthermore, one of these low temperature components can hardly be detected in pattern I'.


(c) The central signal.

The central $(ND_4^{+})$ signal, extensively saturated under normal recording conditions (too high r.f; too slow scans) was the subject of an independent study once the main patterns for each crystal position had been finished. By scanning rapidly through the ammonium resonance under low r.f. and small modulation depth (conditions in table IV-2), the recording was carried out (at every $5^{\circ}$ of the magnet scale) on a very much expanded time scale (6cm/min.). Despite a degree of distortion, due mainly to the poor homogeneity of the magnetic field, a definite fine structure on the signal became quite obvious at some field positions (Fig. IV-10). At low temperature, the S/N ratio was somewhat poorer but

the fine structure was still present, virtually unchanged except for an increase of about 20% in the separation of the outside branches of the signal. Some broadening of the lines (10-15%) also took place. Only exceptionally were the individual component resonance spaced enough to permit a reliable location of their respective centres - a partial collapse always occurred. An available computer program (Dr J. Royston, of the same laboratory), designed to simulate the superposition of several Gaussian resonances at different separations and linewidths, was used to try to reproduce one of the composite experimental spectra obtained. The latter was found to be compatible with the superposition of three signals of virtually the same linewidth (0.88 $\pm$ 0.10 gauss; 0.58 $\pm$ 0.06 KHz.), a central one of relative intensity 2 and two satellites, each of intensity 1, equally spaced about the centre.

To achieve a rough idea of the variations in the lineshape of the signal, the separation between the maxima of the two outside components was measured wherever possible and plotted against the respective field positions. The procedure was repeated for the low temperature results. Fig. IV-10 includes a comparison between room temperature and cardice spectra at some field positions. It should be noted that the data are from an early single crystal whose orientation could not be determined. This does not invalidate the general conclusions, however (Sec. IV-9).


(d) Transition temperature.

It was found by chance with an early bisulphate crystal that when the probe was allowed to warm up to room temperature from cardice temperature, the behaviour of the bridge underwent a sharp change close to $0^{\circ}C$, sometimes becoming completely detuned. The automatic control appeared to compensate the general probe changes accompanying the gradual rise of temperature until a sudden discontinuity completely upset the already
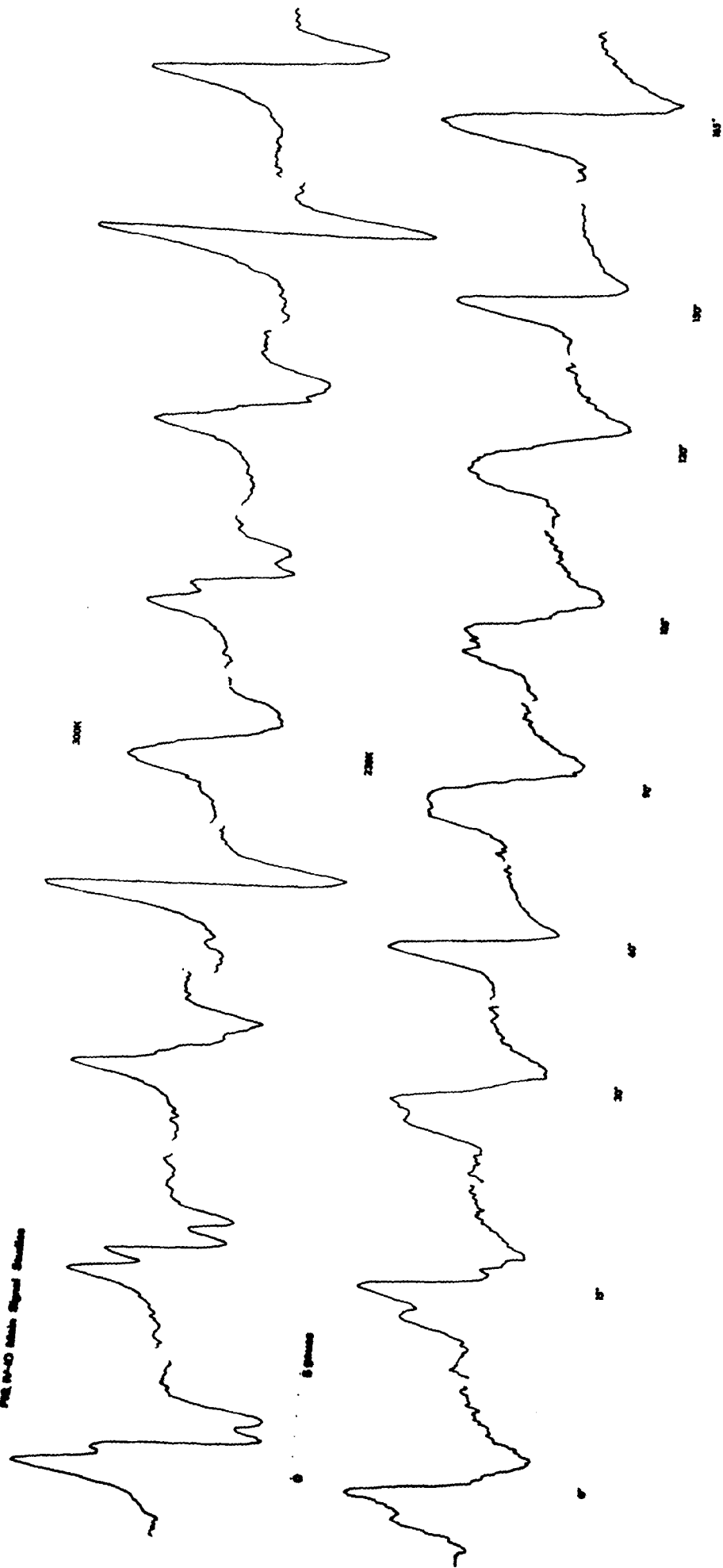
delicate balance. A similar effect, though somewhat less distinct

(probably because of the very steep temperature change), took place in

the reverse process of recharging the reservoir with cardice. The

reproducibility of the two related events and the short temperature range

over which they occurred, suggested as a possible cause an internal

temperature-dependent transformation in the crystal itself. The many-fold

increase of the dielectric constant in the material (4,5) on passing through

the upper Curie point and the consequent change in the bulk susceptibility

could well trigger the sudden change in the r.f. balance of the bridge.

By connecting the d.c. voltage output of the bridge on the automatic

amplitude control to the terminals of the pen recorder, the ensuing

voltage changes could easily be followed, temperature readings being taken

at close intervals in the neighbourhood of the suspected Curie point.

Fig. IV-11 shows the general shape of one of the resulting cooling curves:

against a background of fairly constant slope, a disturbance shows around

$-8^{\circ}C$. To try to compensate for the systematic error in the temperature

readings introduced by the location of the thermocouple some distance

away from the bulk of the crystal, a second recording was carried out when

warming up the probe. The overall average value (six readings) was found to

be $-7^{\circ}C$.

Other sources of error should also be considered, such as bad thermal

conduction by the crystal, which causes a delay in the response to

temperature variations and gives a finite interval for the transformation.

These somewhat uncontrollable sources of error are not expected to exceed

$2^{\circ}$. The most likely temperature for the Curie point can therefore be given

as $-7^{\circ} \pm 2^{\circ}C$, a result in reasonable agreement with the more accurate value

of $-10.9^{\circ}$ from dielectric constant measurements (4).

Fig.IV-11    Determination of the transition temperature
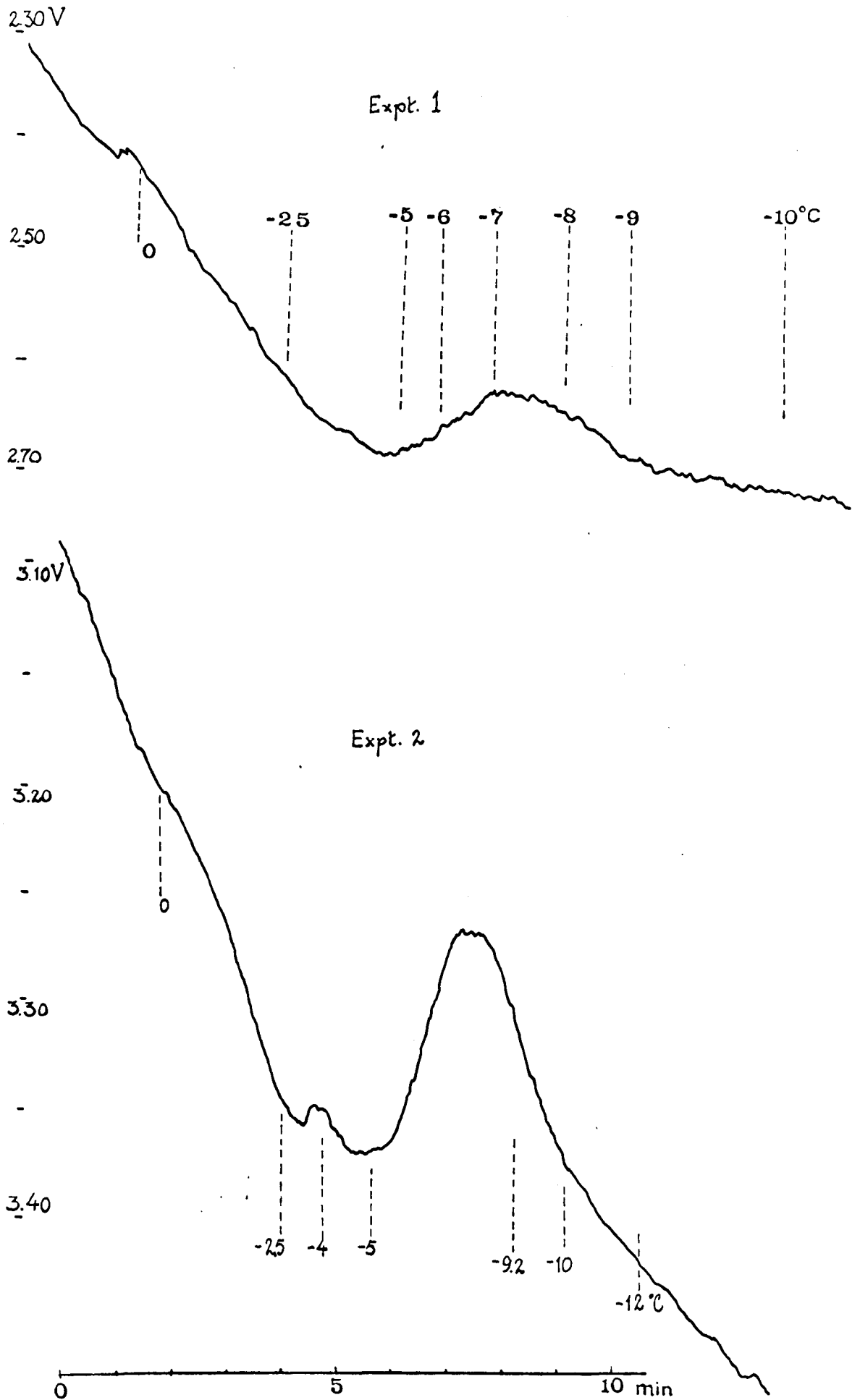
5. <u>The crystal orientation.</u>

The absence of natural faces was a great disadvantage in trying to determine the crystal orientation. Furthermore, the size of the specimen and the high absorbance of the pyrex walls caused some difficulty in the use of classical X-ray techniques for setting the crystal. The thin walled capillary section, intended for the X-ray work, was nevertheless far too opaque to ordinary Cu $K_\alpha$ radiation: the amount of background scattering was very serious in oscillation photographs. The crystal had also not grown close enough to a zone axis to give distinct layer lines with just a slight curvature. A harder radiation source (Mo) was tried, but the slight improvement effected in observing individual spots was marred by the overall scale contraction due to the use of radiation of shorter wavelength. The photographs became so densely crowded that any regularity could not be detected. Unexpectedly, some excellent Laüegrams were obtained, even with Cu $\alpha$ radiation (2.5 h. exposure; unfiltered radiation). The determination of the orientation of a low-symmetry crystal in a general position relying purely on Laüe exposures is a long and complicated task. The Laüe method is normally employed as a refinement to some previous, possibly rather inaccurate, data obtained by another technique. For the present crystal, the d.m.r. results themselves proved to be the most adequate way of arriving at this necessary preliminary knowledge. A d.m.r. rotation pattern is a faithful image of the crystal's inner structure and symmetry. Without auxiliary information from other sources, it is still possible to locate accurately the intersection of a plane (or an axis) of symmetry (previous section), to infer the proximity of an axis of symmetry, and even to have a rough idea of the distribution of the deuterium atoms

  (i) from the location of the maxima of the curves (Appendix II-3)

  (ii) from the general shape of the curves.

These are somewhat flattened if the A-D direction is near the axis of rotation, but rather sharp and steeply sloped if close to the plane of the magnetic field. Conclusions are more difficult to draw for the less usual case of a high asymmetry parameter ( $\eta > 0.2$ ), but a degree of motional averaging sometimes occurs (e.g. $D_2O$ in crystalline hydrates) and the individual, static deuterons cannot be 'seen'.

The orientation procedure for the present crystal involved two main stages:-

(i) the crystal was rotated about the intersection of the plane of symmetry $\pi_s$ with the plane of the magnetic field $\pi_H$, until simultaneous collapse of the two pairs of lines occurred. Either $\pi_s$ or the axis of binary symmetry $E_2$ was then set vertical (I and II respectively, in Fig. IV-12).

(ii) By maintaining the crystal in the gap at whatever angular position was reached in stage (i) and rotating the magnet, it was then possible to decide between hypotheses I and II, since the latter would entail complete collapse of both pairs of lines over the whole rotation range (Sec. IV-4a).

A complete experimental assembly had to be devised; the large probe with all its bulky low temperature equipment was not versatile enough to allow angular displacements greater than $1^\circ$ or $2^\circ$. Two main requirements had to be considered.

(a) The probe unit had to be as small as possible for maximum angular tilt within a $1\frac{1}{4}$" gap. A short ($\sim 5$ cm.) length of $\frac{1}{32}$" copper tubing consituted the r.f. screen, and supported the coil former. A slot through the copper and adjoining perspex left the necessary clearance for the reference mirror. A small copper lid was hard soldered to the top of the small probe, and had in turn the screw cap of a miniature B.N.C. plug

Fig IV-12   Crystal orientation



$\pi_S \perp \pi_{\bar{H}}$

(I)

$\pi_S \equiv \pi_{\bar{H}}$

(II)
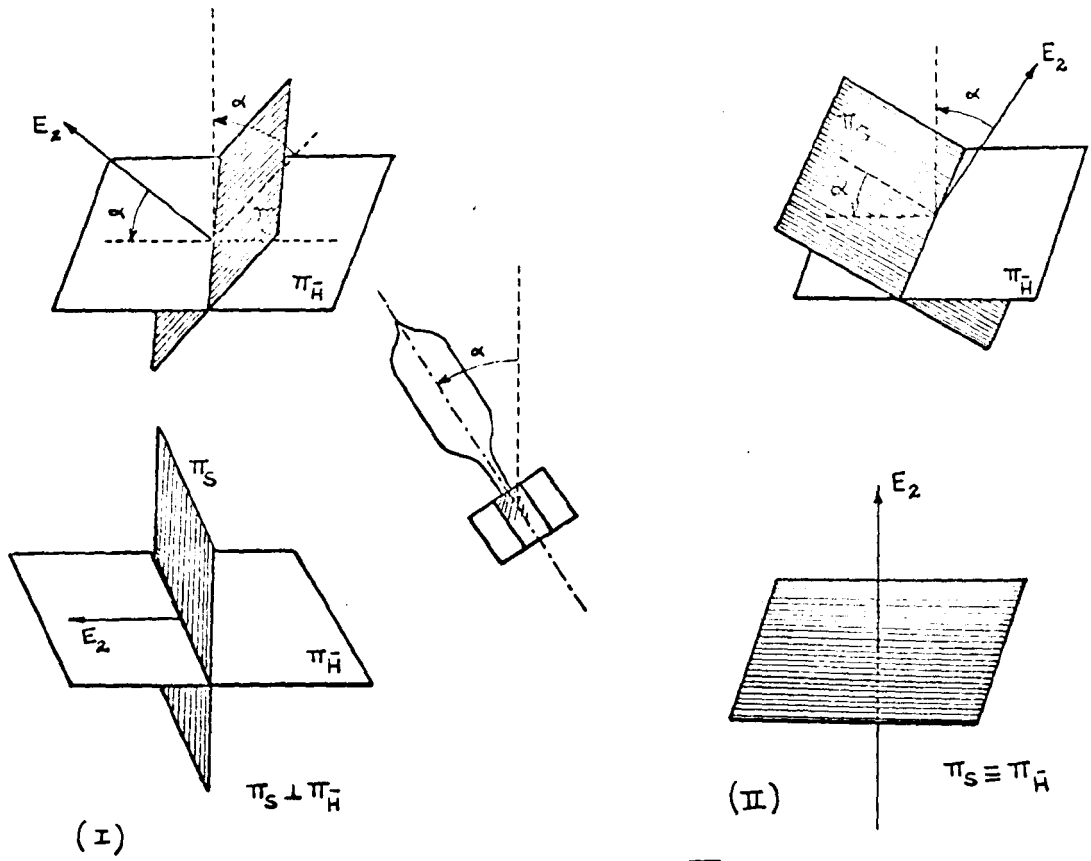
Fig. IV-13  Spectrometer adaptation for orientation of the crystal.



probe

locking screws

Lab. jack

$l_1, l_2, l_3$  locking and locating screws
1, 2, 3  levelling screws
1', 2', 3'  centring screws

Aluminium block
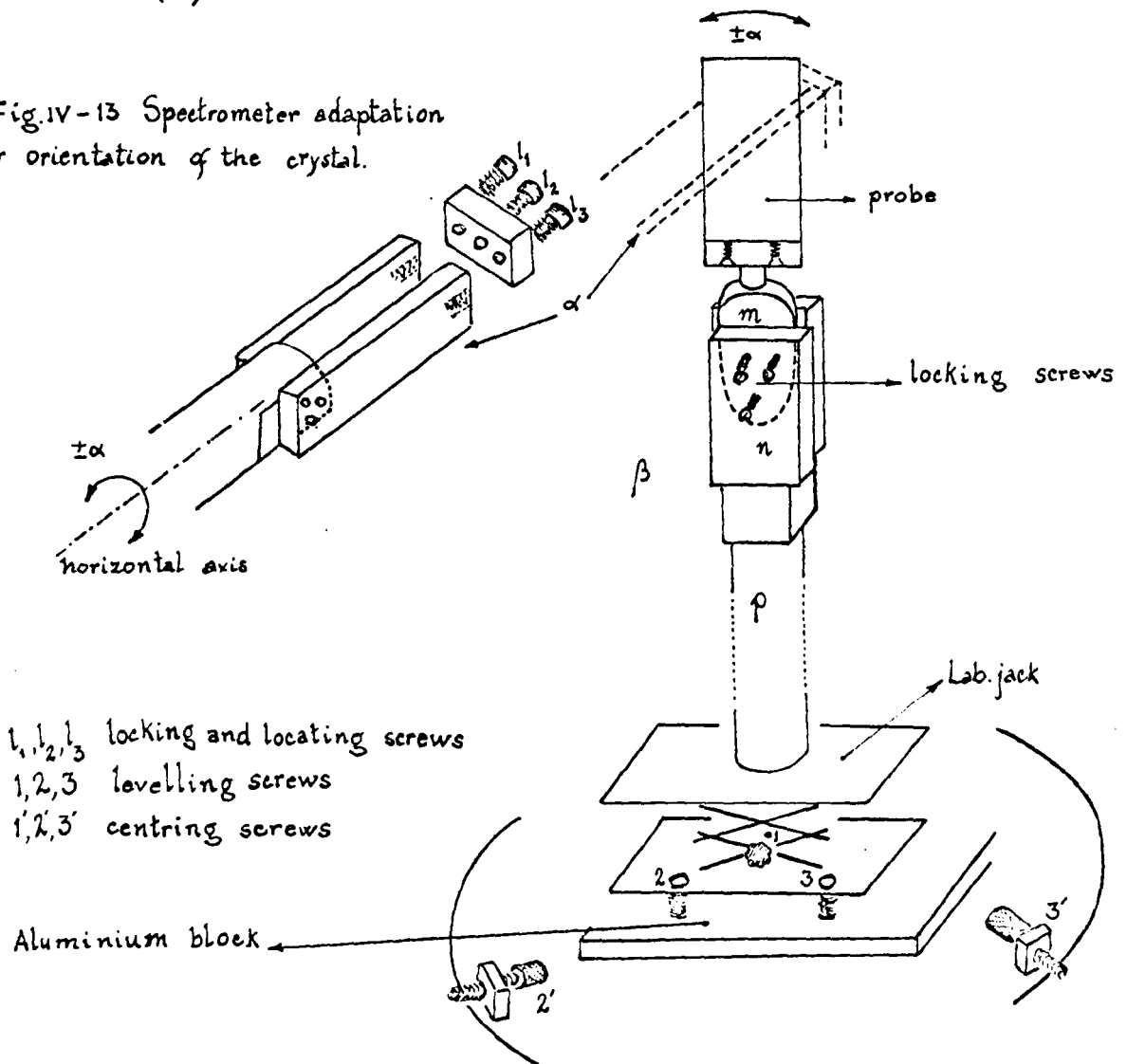
soft soldered to it. A miniature socket and miniature coaxial cable provided a flexible connection to the R.F. bridge.

(b) It was necessary to transfer the crystal holder from a magnet-bound rotating device ($\alpha$) to a second, magnet-independent, support ($\beta$) without loss of crystal angular position or mirror azimuth.

Already available from previous work, assembly $\alpha$ consisted essentially of an aluminium platform and a rotating plate with an engraved angular scale and auxiliary vernier. A hand-driven anti-backlash device and an excellent set of ball bearings provided a very reliable and quite reproducible rotation movement. A small adaptation was added: mounted along the axis, a 1" thick perspex rod terminated in a pair of flat perspex jaws (Fig. IV-13) extended until the central section in the gap. The platform and rotating plate were fixed to the magnet yoke and set vertically against the main coil: a spirit level on a 'flat' along the perspex arm helped to adjust the rotation axis close to the horizontal. Support $\beta$ was floor standing, and consisted of a similar flat-jawed clamp mounted on a perspex rod at right angles to the first, and capable of locking on to a small vertical parallel-faced perspex piece m attached to the base of the probe (Fig. IV-13). Additional facilities were included for:-

vertical movements - the rod was fixed to the top platform of a laboratory jack,

levelling - three equidistant screws (OBA) lifted the base of the jack above a section of $^3/8$" aluminium sheet,

centring - the aluminium piece rested on a circular wooden board which wedged against the fixed base of the magnet by means of three long brass screws.

The second requirement for the probe design was easily accomplished by a process of 'jaw to jaw transfer', by fixing the probe to new clamp Y and only then releasing the locking screws to the original clamp X.

The main experimental steps in the orientation procedure were:

(i) the probe was held in the fixed vertical support $\beta$, centred, aligned with the pole pieces and set vertical in the gap. A preliminary mirror azimuth reading $\theta_o$ was then taken.

(ii) The magnet was rotated until the magnetic field became perpendicular to the intersection of the symmetry plane $\pi_s$ with $\pi_H$ (Fig. IV-12) as deduced from examination of rotation pattern I (magnet scale reading $\sim 2^o$ from mirror reflection).

(iii) The probe was transferred carefully from $\beta$ to the horizontal support $\alpha$. The crystal was then rotated in the field and successive spectra recorded at $2^o$ intervals on either side of the initial position. A search was made for the crystal orientation at which both pairs of symmetrically related lines had their crossing points. Unfortunately this position was outside the $\pm 12^o$ rotation range of the probe in the gap. Nevertheless it could easily be extrapolated from the $24^o$ section of pattern recorded, Fig. IV-14-A. A rotation of $18 \pm 0.5^o$ counter-clockwise was found to be necessary to bring coincidence between the plane of the magnetic field and either $E_2$ or the symmetry plane itself.

(iv) Support $\alpha$ was raised and oriented so as to recover the now tilted probe with as little disturbance as possible. The rotating plate and platform were removed from their magnet perch. Since an $18^o$ rotation could not be achieved in the magnet, the probe and support had to be removed, after two preliminary clinometer readings ($90^o$ apart) on the top platform of the jack. The probe was given an additional inclination up to $18^o$ (using $\alpha$) and then remounted in the magnet along the gap, rather than

FIG. IV-14 A

200 — gauss

100—

-20
(ccw)          -10              0              10              20°
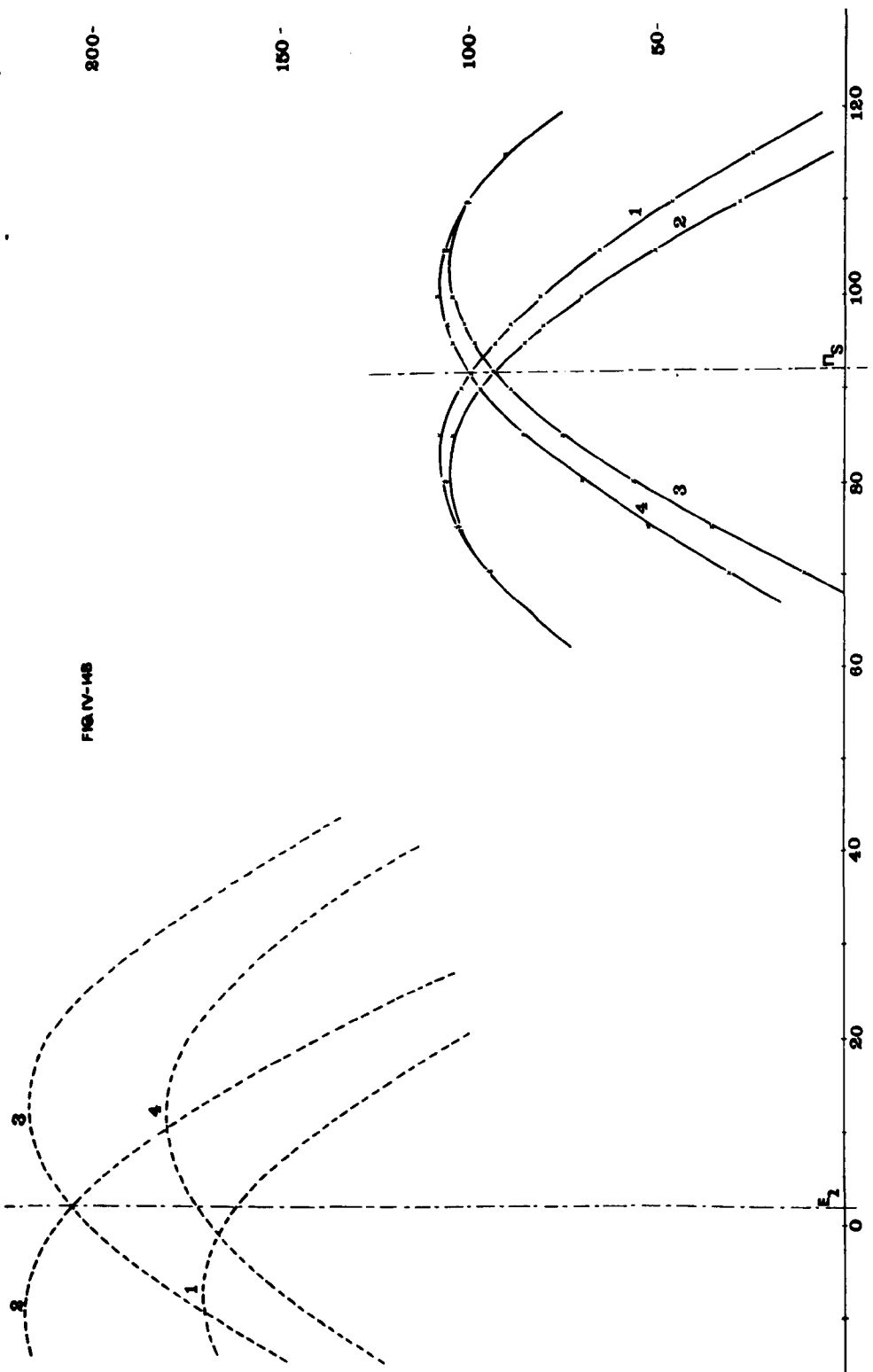
FIG IV-14B

across it.   Spectra were recorded at $5^O$ intervals or less for as wide a range as the probe permitted ($\sim 40^O$), Fig. IV-14-B.  The pairs of lines (1,4; 2,3) and their extrapolated sections were far from collapse; on the other hand, the pattern showed a very definite symmetry, compatible with the symmetry axis lying in the plane $\pi_H$.  The quasi-symmetry of pattern I is thus in good agreement with a symmetry axis $\sim 18^O$ from the horizontal.

Laüe photographs taken with the crystal set at an $18^O$ inclination in the direction calculated from the various patterns, and with the beam directed along [b], fully confirmed the above conclusions.

Finally, a search was made for the c- (and a-) axis position by purely crystallographic means; a rather obscured rotation photograph suggested a small ($5^O$ - $6^O$) inclination of [a] (pseudo-orthorhombic cell) from the vertical.  This indication, complemented by a number of Laüegrams along the b and c directions, led to a more accurate crystal setting (Figs. IV-15,16).  For identification purposes, the Laüegrams were compared with identified Laüe photographs of $NH_4HSO_4$ crystals along [b] and [c], kindly provided by Dr R.J. Nelmes of Edinburgh University.

If $\alpha$, $\beta$ and $\gamma$ are used to denote the angular readings from the top arc, lower arc and main circle respectively of the X-ray goniometer, the experimental values obtained were (regardless of sign):-

$$\alpha = 6^O$$
$$\beta = 16^O$$
$$\gamma = 1^O$$

Small corrections had to be applied, since the perspex base for the crystal rested on the arcs with a slight inclination.
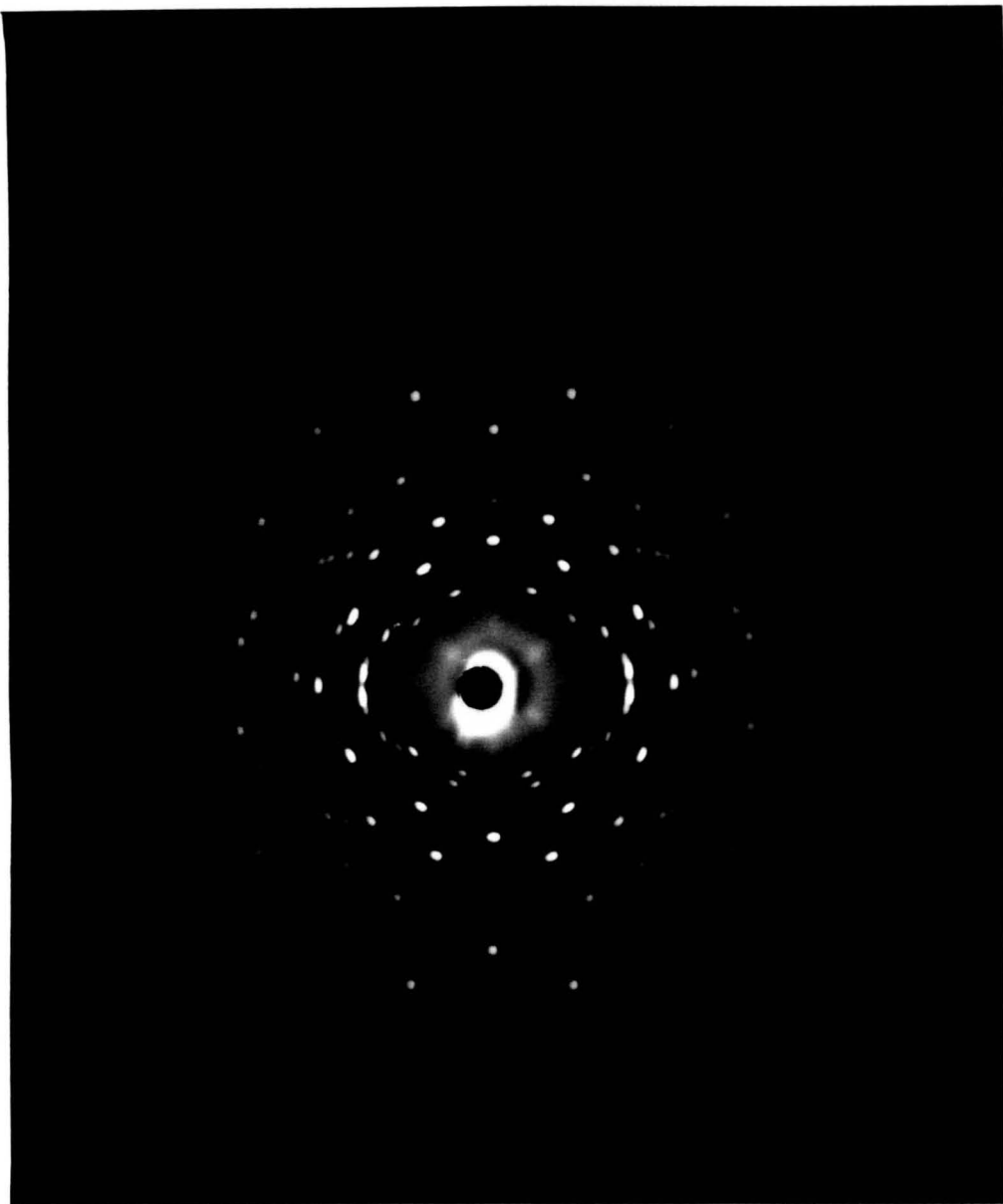
Fig.IV.15.  Laüe photograph along [c], with [a] vertical.
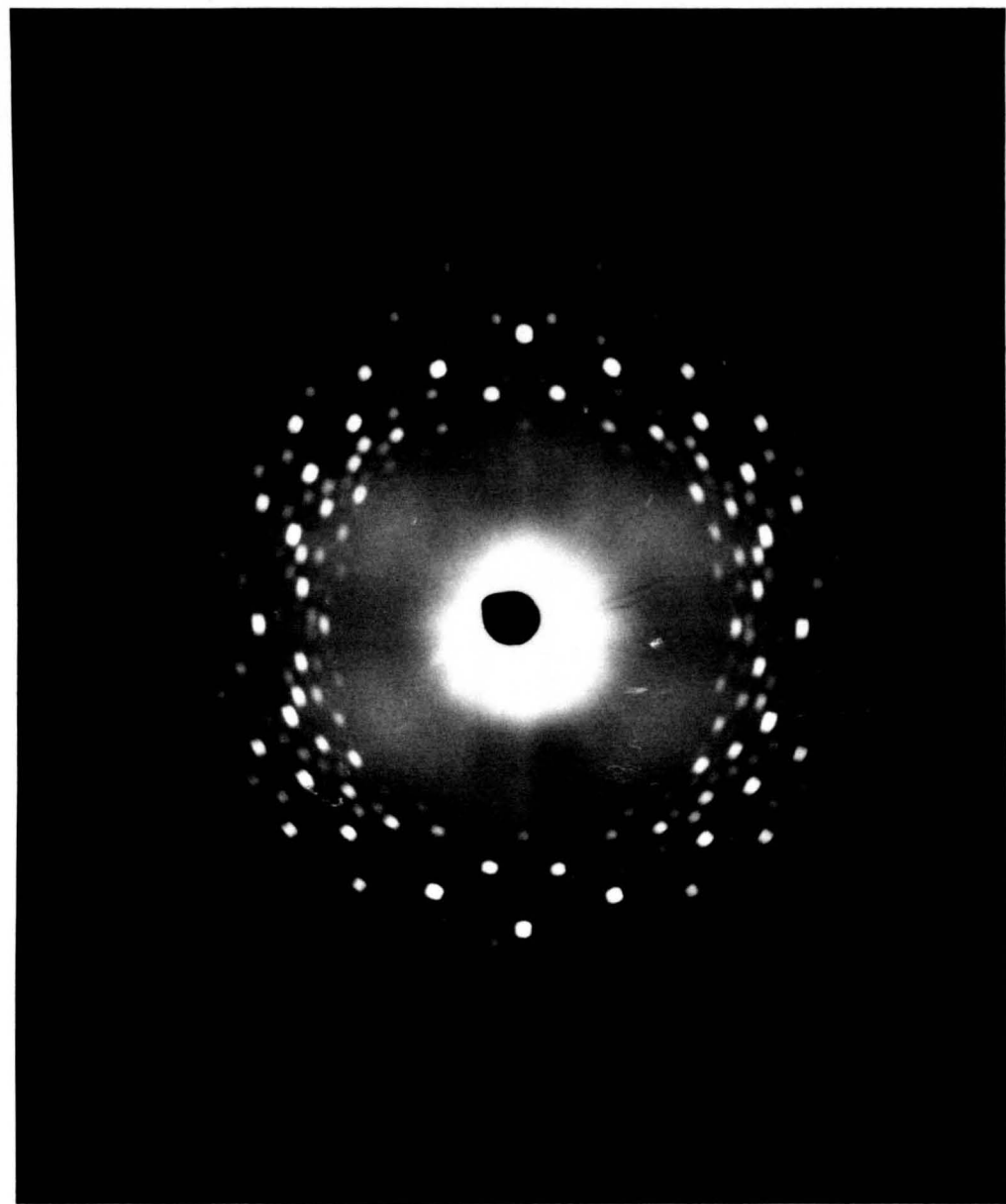
Fig.IV.16.  Laüe photograph along [b], with [a] vertical.

# 6. Calculations.

(a) Choice of axes: transformation matrix.

As mentioned in Sec. II-2, the transformation matrix $T_I$, which relates a crystal-based set of axes (taken as the pseudo-orthorhombic set) to the laboratory axes, has to be evaluated. For pattern I, only the three mutually perpendicular angular coordinates $\alpha$, $\beta$, $\gamma$ had to be taken into account, since the corrections for misalignment of the probe were found to be negligible ( $< 0.2^{\circ}$ ). The general transformation $(a,b,c) \rightarrow (X, Y, Z)$ involved a number of intermediate steps, namely:

$$
\begin{array}{ccccccccc}
a & & X_c & & X_b & & X_p & & X \\
 & \xrightarrow{T_0} & & \xrightarrow{T_1} & & \xrightarrow{T_2} & & \xrightarrow{T_3} & \\
b & \longrightarrow & Y_c & \longrightarrow & Y_b & \longrightarrow & Y_p & \longrightarrow & Y \\
 & & & & & & & & \\
c & & Z_c & & Z_b & & Z_p & & Z
\end{array}
$$

where $(a,b,c)$ is the crystallographic set of axes;

$(X_c,Y_c,Z_c)$ is a second Cartesian set fixed in the crystal and easily related to it:
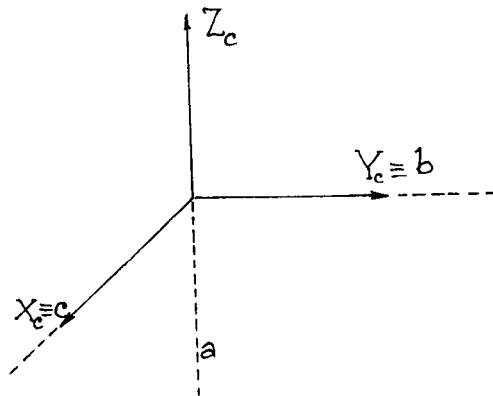


$(X_b,Y_b,Z_b)$ is a system of axes related to the goniometer head.
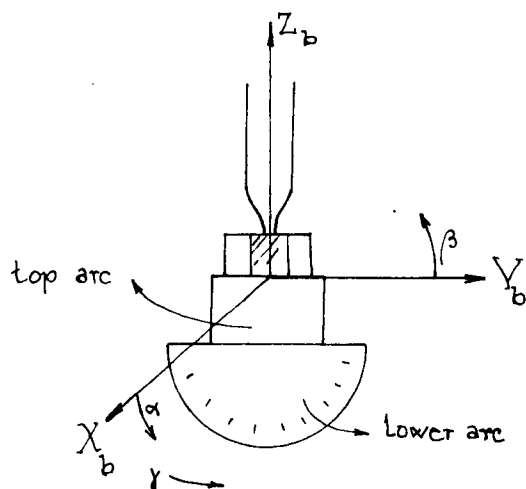
$\alpha$ = angular reading on top arc ($60^{\circ}$)

$\beta$ = angular reading on bottom arc ($16.0^{\circ}$)

$\gamma$ = angular reading on main circle ($1.0^{\circ}$)

$(X_p, Y_p, Z_p)$ are axes defined for the crystal support in the probe.
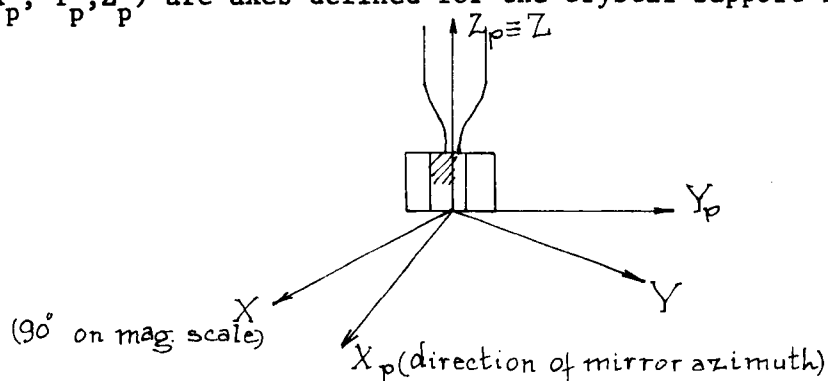


(X, Y, Z) are the fixed laboratory axes (defined in Chapter II).

From purely geometric considerations of sketches representing the axis changes upon successive $\alpha$, $\beta$ and $\gamma$ angular displacements, the general expression for $T_1$ could be deduced.

$$T_1 = \begin{bmatrix} \cos\alpha\cos\gamma + \sin\alpha\sin\beta\sin\gamma & \sin\alpha\sin\beta\cos\gamma - \cos\alpha\sin\gamma & -\sin\alpha\cos\beta \\ \cos\beta\sin\gamma & \cos\beta\cos\gamma & \sin\beta \\ * & * & \cos\alpha\cos\beta \end{bmatrix}$$

($\alpha_{31}$, $\alpha_{32}$ can be easily determined, since $T_1$ is a unitary matrix (16)).

Matrix $T_2$ introduced small corrections $\alpha^1 = -0.5^{\circ}$ and $\beta^1 = 1.0^{\circ}$ due to a slight offset of the crystal support when attached to the arcs (Sec. IV-5).

Rotation matrix $T_3$ was evaluated directly from the mirror azimuth readings. The calculated values for the main matrices are listed below:

$$T_0 = \begin{bmatrix} 0 & 0 & 1 \\ 0 & 1 & 0 \\ -1 & 0 & 0 \end{bmatrix}$$

$$T_2 \times T_1 \;=\; \begin{bmatrix} .9957 & .00904 & -.0921 \\ .01836 & .9562 & .2923 \\ .09074 & -.2927 & .9519 \end{bmatrix}$$

$$T_3 \;=\; \begin{bmatrix} .9966 & -.08194 & 0 \\ .08194 & .9966 & 0 \\ 0 & 0 & 1 \end{bmatrix}$$

$$T_I = T_3 \times \underbrace{T_2 \times T_1 \times T_0}_{T_1'} \begin{bmatrix} .1158 & -.0693 & .9909 \\ -.2838 & .9537 & .0999 \\ -.9519 & -.2927 & .0907 \end{bmatrix}$$

For low temperatures (pattern I'), the same experimental $T_1'$ was considered a justified assumption, since the changes in the crystallographic axes are rather small and quite impossible to assess under the present conditions.

For pattern II, the experimental $T_{II}$ matrix was calculated from $T_1$ by considering the successive changes in crystal orientation introduced by the different steps of the orientation procedure. Table IV-4 and Fig. IV-17 give all the partial matrices used and the choice of axes at each stage. In the last column, some remarks are added about the technique of obtaining the experimental data.

Fig. IV-17



| a | $X_1$ | $X_2$ | $X_3$ | $X_4$ | $X$ |
|---|---|---|---|---|---|
| b $\xrightarrow{T_1'}$ | $Y_1 \xrightarrow{T_\alpha}$ | $Y_2 \xrightarrow{T_\beta}$ | $Y_3 \xrightarrow{T_\gamma}$ | $Y_4 \xrightarrow{T_\delta}$ | $Y$ |
| c | $Z_1$ | $Z_2$ | $Z_3$ | $Z_4$ | $Z$ |
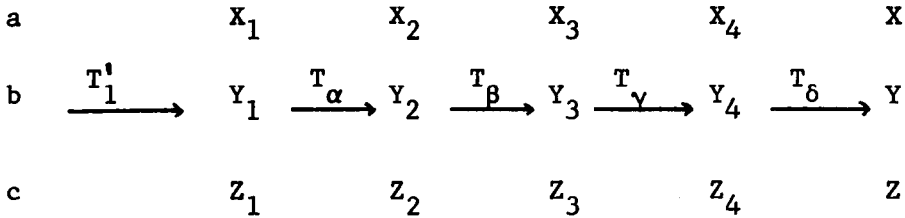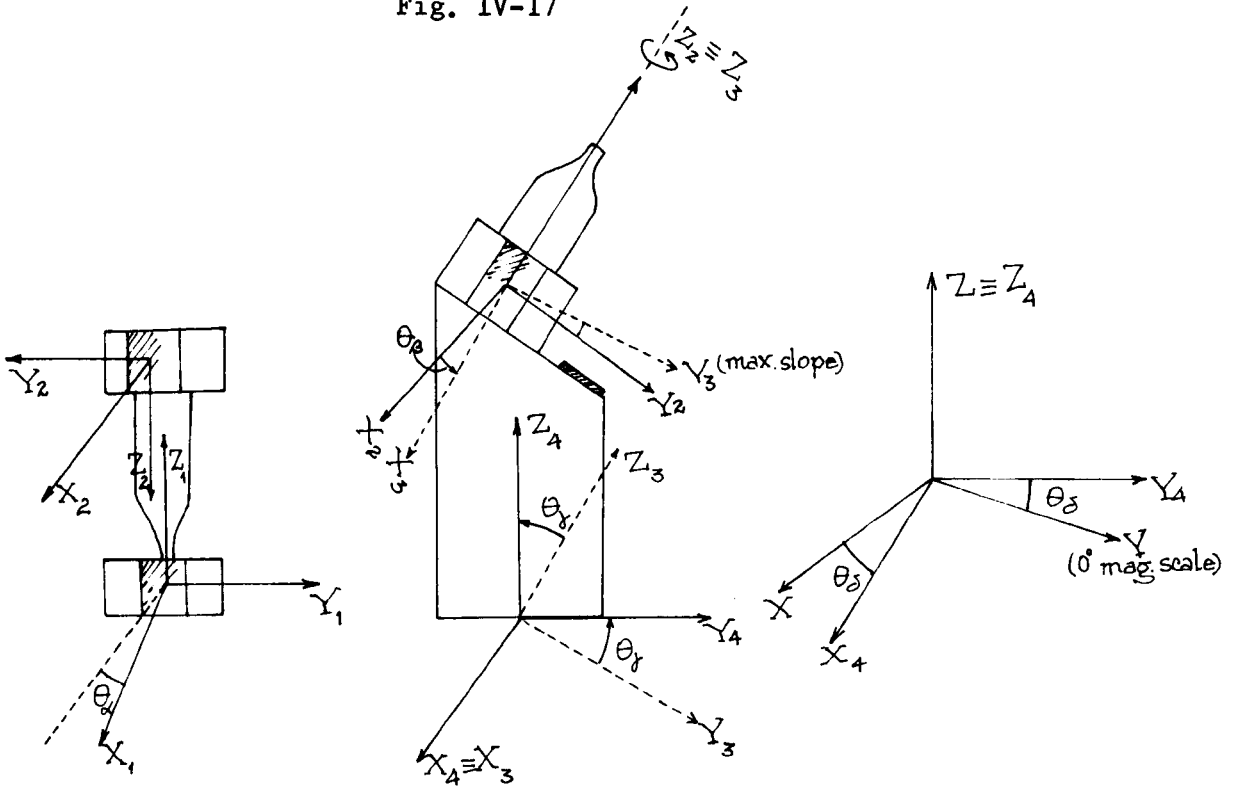
TABLE IV-4

| Matrix | Matrix elements | | | Exp. data and measurement technique |
|---|---|---|---|---|
| $T_\alpha$ | 0.9997 | 0.0256 | 0 | $\theta_\alpha$ = 1.5$^o$ |
| | 0.0256 | -0.9997 | 0 | optical goniometry * |
| | 0 | 0 | -1 | |
| $T_\gamma \times T_\beta$ | 0.9995 | -0.0314 | 0 | $\theta_\beta$ = -1.8$^o$ |
| | 0.0272 | 0.8668 | 0.4980 | $\theta_\gamma$ = 29$^o$ 52' |
| | | | | indirect calc. on optical |
| | -0.0156 | -0.4978 | 0.8672 | gon. data |
| $T_\delta$ | 0.8142 | -0.5806 | 0 | $\theta_\delta$ = 35.5$^o$ |
| | 0.5806 | 0.8142 | 0 | mirror azimuth reading and calc. on gon. data |
| | 0 | 0 | 1 | |

* an additional misalignment with relation to the cylinder axis (1.2$^o$)

also detected was later identified as due to one of the mirrors, offset

by about 1.1$^o$ when glued.

$T_{II}$ was then calculated from the matrices above:

$$T_{II} = T_\delta (T_\gamma \times T_\beta) T_\alpha T_1'$$

$$T_{II} = \begin{bmatrix} -0.3648 & 0.4489 & 0.8157 \\ 0.6386 & -0.5169 & 0.5700 \\ 0.6776 & 0.7289 & -0.0981 \end{bmatrix}$$

For further accuracy another matrix ought to have been included to allow for the inclination of the probe within the gap and the degree of alignment of the inner walls of the Dewar to which piece A was fitting. For a number of reasons, mainly possible irreversible changes in the position of the Dewar when removing the external earthing, and difficulty in observing the Dewar walls, a correct assessment of these errors was not practicable. Their existence was beyond question, however; a dark liquid viewed thragh the Dewar walls showed some misalignment, possibly higher than $1.5^\circ$.

(b)   Refinement of the transformation matrix.

A   6 x 6 matrix T corresponding to the equality

$$T\emptyset = A \quad (\text{Sec. II-2})$$

was evaluated from the elements of $T_I$ and $T_{II}$.

$$T = \begin{bmatrix} .0939 & .9143 & .9918 & -.5573 & .1727 & .0531 \\ -.0671 & -.9047 & .9718 & .5252 & .2861 & -.3279 \\ -.0329 & -.0661 & .0990 & .1301 & -.2696 & .9380 \\ .5409 & .4687 & .9904 & -.9878 & .1329 & .1430 \\ -.2748 & -.0657 & .3405 & .3328 & -1.3232 & 1.3217 \\ -.2330 & -.2321 & .4650 & .4753 & .3130 & -.1658 \end{bmatrix}$$

$$T^{-1} T\emptyset = T^{-1}A \quad \rightarrow \quad \emptyset = T^{-1} A$$

Inversion of T was carried out on an IME 26 calculator by following a pivoting method (17). The disproportionately large values of $T^{-1}$ matrix elements and the smallness of determinant $|T^{-1}|$ showed the unwelcome (and unsuspected) fact that the six equations in $\phi_{ik}$ were not linearly independent, and hence that positions 1 and 2 of the crystal could not have been completely general. It was realised that the intersection of the plane of symmetry was rather close to the direction of the mirror reflection which, as Fig. IV-17 shows, was in turn close to the axis of the $30^{\circ}$ rotation. This difficulty was bypassed by resorting to the symmetry relationships between the $\phi_{ik}$ tensor components of related deuterons. It can be shown that two deuterons related to each other by a binary symmetry axis b (and/or a plane of symmetry perpendicular to it) have $\phi_{ik}$ tensor components (in a rectangular set of axes a b c)

$$\phi_{11} = \phi'_{11}$$
$$\phi_{22} = \phi'_{22}$$
$$\phi_{33} = \phi'_{33}$$
$$\phi_{12} = -\phi'_{12}$$
$$\phi_{13} = \phi'_{13}$$
$$\phi_{23} = -\phi'_{23}$$

which only differ in the sign of $\phi_{12}$ and $\phi_{23}$.

T could thus be inverted in a slightly modified form, after some exchange of information between the deuterons of the symmetry pairs 1,4 and 2,3. It was found easier, because of the method of inversion used, to substitute the last line for a certain deuteron by the corresponding line from its symmetrical counterpart (i.e. $-\alpha_{64}$ instead of $\alpha_{64}$; $-\alpha_{66}$ instead of $\alpha_{66}$). At the same time the necessary correction in the last element of matrix A was made (e.g. $C_{II}^4$ instead of $C_{II}^1$ for

deuteron 1). Tensor components for deuterons 1, 2, 3 and 4 are now tabulated.

Table IV-5

| Deut. | 1 | 4 | 2 | 3 |
|---|---|---|---|---|
| $K\phi_{11}$ | - 70.71 | - 99.88 | -134.8 | -167.4 |
| $K\phi_{22}$ | 208.5 | 211.5 | 260.1 | 265.6 |
| $K\phi_{33}$ | -123.3 | -135.1 | -112.3 | -123.7 |
| $K\phi_{12}$ | -147.5 | 152.0 | 60.07 | - 68.59 |
| $K\phi_{13}$ | 37.91 | 37.80 | - 8.74 | - 11.95 |
| $K\phi_{23}$ | - 68.59 | 41.21 | - 89.90 | 67.98 |

The table shows large divergences in the numerical values, which were interpreted as arising mainly from unavoidable experimental errors in the data for $T_{II}$ and possibly $T_I$, particularly as $30^\circ$ represents a relatively small change from one crystal position to another. Even without a mathematical error analysis, a big influence of crystal setting errors for two patterns from crystals in closely similar orientations can be anticipated. The limiting case would be that of two almost coincident crystal positions, for which the slightest errors would bring a virtually complete lack of knowledge of the tensor components.

Further refinement of the tensor components was attempted, by trying to refine T. Symmetry considerations formed the basis of this approach, which involved three main steps.

(1)  All the curves were converted to a new origin, coincident

with the field reading $\theta_o$ at which the symmetry plane intercepts $\pi_{\overline{H}}$.



$$\theta = \theta' - \theta_o$$

$$y(\theta) = A + B \cos 2\theta + C \sin 2\theta$$

$$= A + B \cos 2(\theta'-\theta_o) + C \sin 2(\theta' - \theta_o)$$

$$= A + \underbrace{(B \cos 2\theta_o - C \sin 2\theta_o)}_{B'}\cos 2\theta' + \underbrace{(B \sin 2\theta_o + C \cos 2\theta_o)}_{C'} \sin 2\theta'$$
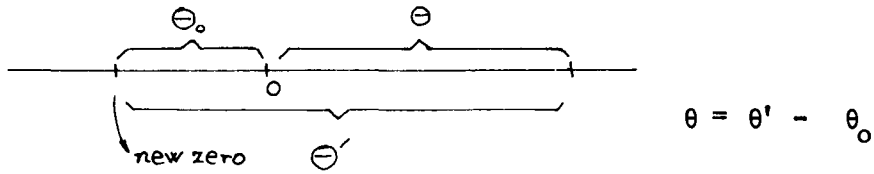
B', C' are the transformed constants, referred to the new origin

at $\theta_o$.   The same conclusions may be reached from the general expressions

for A, B and C (Sec. II-2).  It is interesting to note that A = A' is

quite insensitive to the change of axis, or rather, the reference azimuth.

By the procedure above, one angular variable was eliminated.  The crystal

position could then be fully defined by the parameters $\alpha$, $\beta$ as shown.

$\alpha$- rot. angle about $Y_{\alpha,\beta}$
$\beta$- rot. angle about $X_{\alpha,\beta}$

plane $(X,Y)_{\alpha,\beta} \equiv \pi_{\overline{H}}$



$X_{\alpha,\beta}$ = direction of intersection of $\pi_H$ with the symmetry plane (field reading $\theta_o$)
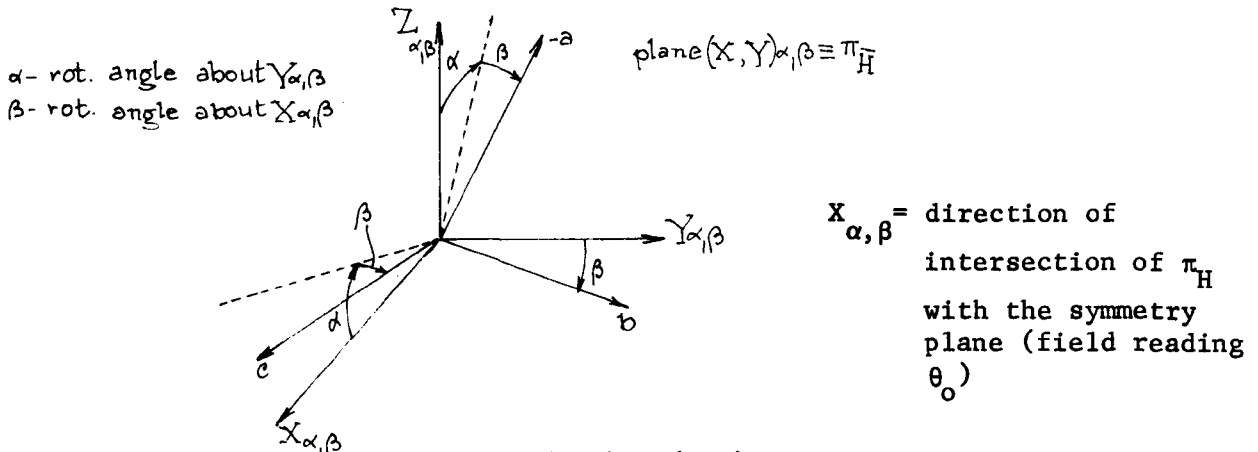
The general axis transformation (abc) → $(XYZ)_{\alpha,\beta}$ can be expressed by the

matrix

$$T_{(\alpha,\beta)} = \begin{array}{ccc} \sin\alpha & 0 & \cos\alpha \\ -\sin\beta\cos\alpha & \cos\beta & \sin\beta\sin\alpha \\ -\cos\beta\cos\alpha & -\sin\beta & \cos\beta\sin\alpha \end{array}$$

(2) The general expression for A, B and C take the following form:

$$\begin{matrix}A\\B\end{matrix} = \tfrac{1}{2}\{(\sin^2\alpha \pm \sin^2\beta\cos^2\beta)\phi_{11} \pm \cos^2\beta\phi_{22} + (\cos^2\alpha \pm \sin^2\beta\sin^2\alpha)\phi_{33}$$

$$\mp \sin2\beta\cos\alpha\phi_{12} + \sin2\alpha[1 \pm \sin^2\beta]\phi_{13} \pm \sin2\beta\sin\alpha\phi_{23}\}$$

(top signs for A)

$$C = \tfrac{1}{2}\sin2\alpha\sin\beta(\phi_{11}-\phi_{33}) - \sin\alpha\cos\beta\phi_{12} + \cos2\alpha\sin\beta\phi_{13} - \cos\alpha\cos\beta\phi_{23}$$

If the terms in $\phi_{11}$ $\phi_{22}$ $\phi_{33}$ $\phi_{13}$ are separated, i.e. the sections which are invariant from one deuteron to its symmetrically related counterpart

$$\begin{matrix}A\\B\end{matrix} = \tfrac{1}{2}[(\sin^2\alpha\phi_{11} + \cos^2\alpha\phi_{33}) + \sin2\alpha\phi_{13} \pm (\sin^2\beta\cos^2\alpha\phi_{11} + \cos^2\beta\phi_{22}$$

$$+ \sin^2\beta\sin^2\alpha\phi_{33}) \mp \sin2\beta\cos\alpha\phi_{12} \mp \sin2\alpha\sin^2\beta\phi_{13} \pm \sin2\beta\sin\alpha\phi_{23}]$$

(top signs for A)

$$C = \tfrac{1}{2}\sin2\alpha\sin\beta(\phi_{11}-\phi_{33}) + \cos2\alpha\sin\beta\phi_{13} - \cos\beta[\sin\alpha\phi_{12} + \cos\alpha\phi_{23}]$$

A number of simplifications may be made, and by combining these expressions, smaller 'blocks' of variables can easily be obtained,

e.g. $\quad A + B = \sin^2\alpha\phi_{11} + \cos^2\alpha\phi_{33} + \sin2\alpha\phi_{13}$ $\qquad\qquad$ (i)

If a pair of deuterons symmetrically related by the two-fold axis are denoted by 1 and 4,

$$A_1 - A_4 = -(B_1 - B_4) = \sin2\beta(\cos\alpha\phi_{12} - \sin\alpha\phi_{23}) \qquad\qquad (ii)$$

$$2(A_1 - B_4) + (A + B)_{1,4} = \cos2\beta[(A + B)_{1,4} + 2\phi_{22}] \qquad\qquad (iii)$$

$$C_1 + C_4 = 2\sin\beta[\tfrac{1}{2}\sin2\alpha(\phi_{11} - \phi_{33}) + \cos2\alpha\phi_{13}] \qquad\qquad (iv)$$

$$C_1 - C_4 = -2\cos\beta[\sin\alpha\phi_{12} + \cos\alpha\phi_{23}] \qquad\qquad (v)$$

As a consequence of (i),

$$(A + B)_1 = (A + B)_4 \qquad\qquad (vi)$$

a very useful expression which makes it possible to 'pair' symmetrically

related deuterons when the crossing points are not easy to sort out (as in

patterns I and I'). Expression (vi) and its (non-identical) twin

$$(A + B)_2 = (A + B)_3 \qquad\qquad (vii)$$

confirm mathematically the previous graphical finding that curves 1,4

and 2,3 cross at the same $\theta$ (Sec. IV-4A). (A + B is really the

splitting for $\theta = 0$, this origin deliberately chosen to coincide with

the intersection of the plane of symmetry with $\pi_H$). Equalities (vi)

and (vii) hold very closely in the room temperature form, as can be seen

in Table IV-6 below.

By means of equations (i) - (v), a number of practical steps can

be taken towards determining the tensor components together with the

orientation parameters $\alpha$, $\beta$:-

(i) By using four equations of type (iii) (deuterons 1,4 patterns I and II;

the same for deuterons 2,3), the four variables $\beta^I$, $\beta^{II}$, $\phi_{22}^{1,4}$, $\phi_{22}^{2,3}$ can

be calculated with an accuracy primarily dependent on the precision of

the pattern data. (Equation (iii) was used with some reserve for pattern II,

because it depends on cos $2\beta$ which happened to be close to zero.) The

calculations were carried out by successive approximations, taking as

starting data the values of $\beta^I$ and $\beta^{II}$ obtained from $T_I$ and $T_{II}$, by

considering that

$$T_{\alpha,\beta}^{I} = T_{\theta_o}^{I} \times T^{I}$$

$$T_{\alpha,\beta}^{II} = T_{\theta_o}^{II} \times T^{II}$$

where $T^I$, $T^{II}$ are the (a, b, c) → (X Y Z) transformation matrices, for

patterns I and II respectively (vide IV-6a). $T_{\theta_o}^{I}$ and $T_{\theta_o}^{II}$ are the transformation

matrices for the change of origin by rotation (X Y Z) → $(X, Y, Z)_{\alpha\beta}$, as

indicated in the figure above.
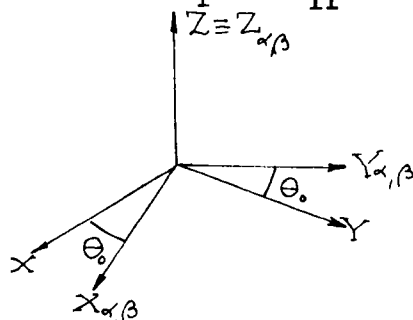
## TABLE IV-6

|  | 1 | 4 | 2 | 3 |
|---|---|---|---|---|
| $A'^{I} \cong A$ | 73.19 | -12.96 | 37.00 | 72.01 |
| $B'^{I}$ | -196.39 | -110.59 | -157.51 | -192.13 |
| $C'^{I}$ | 73.95 | - 51.15 | 65.49 | - 76.18 |
| $(A'_i+B'_i)^{I}$ | -123.20 | -123.55 | -120.53 | -120.12 |
| $A'^{II}$ | 39.03 | -113.97 | - 67.98 | - 6.72 |
| $B'^{II}$ | -167.41 | - 15.00 | - 53.86 | -114.46 |
| $C'^{II}$ | - 70.58 | 15.91 | - 41.29 | 64.97 |
| $(A'_i+B'_i)^{II}$ | - 28.38 | -128.96 | -121.85 | -121.18 |

(all values in KHz).

$A'$, $B'$, $C'$ are referred to the intersection of the symmetry plane
as origin.

The relative signs of the constants for deuterons 1,2, 3 and 4 in
pattern II have been deduced by extrapolation (to $30^{o}$) of the orientation
pattern (Fig. IV-14A).

(ii) To determine $\phi_{12}$ $\phi_{23}$, equations (ii) and (v) were combined:

$$\phi_{12} = \begin{vmatrix} \dfrac{A_1 - A_4}{-\sin 2\beta} & -\sin \alpha \\[2ex] \dfrac{C_1 - C_4}{-2 \cos \beta} & \cos \alpha \end{vmatrix} \quad ; \quad \phi_{23} = \begin{vmatrix} \cos \alpha & \dfrac{A_1 - A_4}{-\sin 2\beta} \\[2ex] \sin \alpha & \dfrac{C_1 - C_4}{- 2 \cos \beta} \end{vmatrix}$$

By rewriting (i) and (iv) as

$$(A + B) + \tfrac{1}{2}\phi_{22} = M_1 = -\tfrac{1}{2}\cos 2\alpha(\phi_{11}-\phi_{33}) + \sin 2\alpha\,\phi_{13}$$

$$\frac{C_1 + C_4}{\sin\beta} = M_2 = \sin 2\alpha(\phi_{11}-\phi_{33}) + \cos 2\alpha\,\phi_{13}$$

the system can be solved for $(\phi_{11}-\phi_{33})$ and $\phi_{13}$; again approximate values of $\alpha_I$ and $\alpha_{II}$ were used initially. Tensor components obtained from both patterns could be compared and averaged. In the course of the calculations, and could also be refined to some extent. Finally, component $\phi_{11}$ (or $\phi_{33}$) may be easily extracted from (i).

From a knowledge of $\alpha^I$, $\beta^I$, $\alpha^{II}$ and $\beta^{II}$, and of $\theta_o$, the experimental matrices $T^I$ and $T^{II}$ were reevaluated, as well as T. The three are listed below.

$$\begin{cases} \alpha_1 = 5.0^o \\ \beta_1 = 17.2^o \end{cases} \quad \begin{cases} \alpha_2 = 3.3^o \\ \beta_2 = 227.0^o \end{cases}$$

$$T^I = \begin{bmatrix} .12069 & -.11134 & .98643 \\ -.28245 & .94877 & .14165 \\ -.95166 & -.29571 & .08306 \end{bmatrix} \; ; \; T^{II} = \begin{bmatrix} -.39550 & .41205 & .82086 \\ .61668 & -.54319 & .56978 \\ .68066 & .73155 & -.03927 \end{bmatrix}$$

$$T^{cor.} = \begin{bmatrix} .09434 & .91256 & .99310 & -.56284 & .15809 & .04912 \\ -.06521 & -.88777 & .95297 & .50908 & .31812 & -.48845 \\ -.03409 & -.10564 & .13973 & .14596 & -.26152 & .92012 \\ .53671 & .46484 & .99845 & -.99588 & .05345 & .057464 \\ -.22387 & -.12527 & .34915 & .34402 & -1.3520 & 1.2955 \\ -.24390 & -.22382 & .46771 & -.46893 & .28086 & .21110 \end{bmatrix}$$

$T_I$ and $T_{II}$ do not differ appreciably from the original values; individual differences in direction cosines are no higher than $2.5^o$ (pattern I) or $3.4^o$ (pattern II). (These discrepancies are for element $\alpha_{33}$, which is far more affected than any other.) Inversion of T and evaluation of the $\emptyset_{ik}$ tensor components could fortunately be carried out on a small Varian 620L computer at Durham University.

(c) Calculated results.

The bisulphate ion - room temperature.

Recalculated tensor components from the room temperature data are tabulated below($IV$-7)The first two columns represent the joint 1,4 and 2,3 tensor components respectively, as calculated in the process of refining $\alpha$ and $\beta$; they are included for comparison. The frame of reference is again the pseudoorthorhombic set of axes a, b, c.

Diagonalisation was carried out manually on a Wang electronic desk calculator kindly lent by Professor T.C. Waddington. The largest eigenvalue (and eigenvector) were found by the power iteration (successive approximation) method as mentioned in references (16) and (17). Convergence was sometimes accelerated by averaging in intermediate stages. For symmetrically related deuterons, it was found that the whole process could be much abbreviated by taking as an initial approximation the eigenvector from the related deuteron (corrected for sign). The calculations were continued until convergence to five significant figures occurred; normalisation followed. The remaining latent roots $\lambda_2$ $\lambda_3$ were calculated from the characteristic equation (experimental) after division by $(\lambda - \lambda_1)$:

$$\begin{vmatrix} a_{11} - \lambda & a_{12} & a_{13} \\ a_{12} & a_{22} - \lambda & a_{23} \\ a_{13} & a_{23} & a_{33} - \lambda \end{vmatrix}_{\text{Experimental}} = 0. \qquad a_{ik} = \emptyset_{ik}$$

Table IV-7

The Interaction Tensor Components (300 K) (recalculated)
(all in KHz).

| Tensor comp. $K\emptyset_{ik}$ | joint calc. | | Calculated tensor components | | | |
|---|---|---|---|---|---|---|
| | 1,4* | 2,3* | 1 | 4 | 2 | 3 |
| $K\emptyset_{11}$ | −78.98 | −145.80 | −76.35 | −80.34 | −144.38 | −145.20 |
| $K\emptyset_{22}$ | 210.27 | 264.36 | 212.95 | 210.20 | 267.90 | 265.16 |
| $K\emptyset_{33}$ | −131.29 | −118.56 | −130.17 | −129.68 | −118.47 | −117.40 |
| $K\emptyset_{12}$ | −156.81 | 55.92 | −151.49 | 158.40 | 59.90 | − 54.95 |
| $K\emptyset_{13}$ | 34.61 | − 15.31 | 39.09 | 33.22 | − 10.74 | − 15.73 |
| $K\emptyset_{23}$ | − 53.28 | − 80.30 | − 51.07 | 51.42 | − 78.02 | 79.34 |
| Trace | − | − | 6.43 | .18 | 5.05 | 2.56 |

** signs taken as for deuterons 1 and 2 respectively

$$\lambda^3 - \lambda^2 (a_{11} + a_{22} + a_{33}) + \lambda(A_{11} + A_{22} + A_{33}) - \Delta = 0, \text{ where}$$

$a_{11} + a_{22} + a_{33}$ is the experimental trace E (invariant, and ideally = zero).

$A_{ik}$ is the cofactor of element $a_{ik}$, and $\Delta$ is the determinant of $\emptyset_{ik}$ matrix. Putting $-(A_{11} + A_{22} + A_{33}) = a$,

$$\lambda^3 - E\lambda^2 - a\lambda - b = 0 = (\lambda - \lambda_1) [\lambda^2 - (\lambda_1 - E)\lambda + \frac{b}{\lambda_1}]$$

$$\lambda_{2,3} = \tfrac{1}{2} [-(\lambda_1 - E) \pm \sqrt{(\lambda_1 - E)^2 - \frac{4b}{\lambda_1}}]$$

For evaluation of the corresponding principal directions ($\alpha'_j$ direction cosine), the equations of definition were used directly

$$\emptyset_{ij} \alpha'_j = \lambda' \alpha'_i \qquad j = 1,2,3; \; \lambda' = \lambda_2, \lambda_3$$

By arbitrarily putting $\alpha_1 = 1$, the homogeneous system in $\frac{\alpha'_2}{\alpha'_1}$, $\frac{\alpha'_3}{\alpha'_1}$ could easily be solved. Vectors ($1 \; \frac{\alpha'_2}{\alpha'_1} \quad \frac{\alpha'_3}{\alpha'_1}$) were afterwards normalised.

Table IV-8
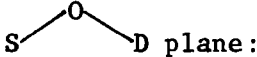
The Diagonalised Interaction Tensors (300 K).

| Deut. | | Eigenvectors qxx qyy qzz | | | Eigenvalues $K\phi_{xx}K\phi_{yy},K\phi_{zz}$ (KHz) | $e^2qQ/h$ KHz | as. param. $\eta$ |
|---|---|---|---|---|---|---|---|
| 1 | a | .5888 | .7058 | .3940 | -124.6 | 191.4 | .109 |
|   | b | .3727 | .1955 | -.9071 | -156.0 | | |
|   | c | .7173 | -.6809 | .1479 | 287.1 | | |
| 4 | a | .3995 | .8243 | .4013 | -133.0 | 192.4 | .078 |
|   | b | -.3135 | -.2886 | .9047 | -155.4 | | |
|   | c | .8615 | -.4871 | .1431 | 288.6 | | |
| 2 | a | .0448 | .9894 | .1382 | -133.6 | 194.4 | .066 |
|   | b | .1841 | -.1442 | .9723 | -152.9 | | |
|   | c | .9819 | -.0181 | -.1886 | 291.6 | | |
| 3 | a | .2189 | .9668 | .1303 | -132.1 | 192.3 | .075 |
|   | b | .2201 | .0809 | -.9721 | -153.7 | | |
|   | c | -.9506 | .2423 | -.1951 | 288.4 | | |
| 1,4$_*$ | a | .4830 | .7789 | .4001 | -133.4 | 192.2 | .075 |
|   | b | .3452 | .2506 | -.9045 | -155.0 | | |
|   | c | .8048 | -.5749 | .1478 | 288.3 | | |
| 2,3$_*$ | a | .1956 | .9720 | .1321 | -133.9 | 192.2 | .071 |
|   | b | -.2201 | -.0880 | .9715 | -154.3 | | |
|   | c | -.9557 | .2179 | -.1968 | 288.2 | | |

* signs taken as for 1 and 2

7.    Discussion of the room temperature results.

Examination of Table IV-8, particularly the $q_{zz}$ direction cosines

and quadrupolar constants, reveals that all the deuterons are roughly

aligned along [b], each of them presumably involved in a fairly strong

hydrogen bond.   The magnitude of the quadrupolar constants indicate that

the H-bonds are almost certainly shorter than 2.8Å (18).   Both conclusions

are in close agreement with the crystal data from X-ray and neutron

diffraction work (6).   A projection of the structure along (010)

(from reference (6)) is shown in Fig. IV-18.   In Table IV-9, the

geometrical relationships between the e.f.g. tensors for both kinds of

bisulphate deuterons and the surrounding structure are considered, including:

(i)    the direction cosines of O·····O and OD as derived from the

       crystallographic data compared with the $q_{zz}$ eigenvector;   angles $\varphi_z'$

       and $\varphi_z$ respectively are defined:

(ii)   the value of the O····O hydrogen bonded distance:

(iii)  the angle $\varphi_y'$ between the $q_{yy}$ direction and the normal to the

       S—O—D plane:

(iv)   the assignment of the atoms in the structure;   the nomenclature from

       reference 6 was followed:

(v)    the angle between the OH and O····O directions (in brackets), as

       given by Nelmes (6).

The evident smallness of $\varphi_z'$ and $\varphi_y'$ confirm the assignments above.   It

has been observed in other H-bonded systems that, within 10-15°, $q_{yy}$ is

normal to the plane defined by X-O-D, X being the next atom to which

oxygen is bound (vide also chapter V).   In the present case, the divergence

in the values of $\varphi_y'$ for deuterons 2 and 3 is possibly due to experimental

error, as is evident from the difference between the numerical values of the

off diagonal components of pairs of tensors 1,4 and 2,3 (Table IV- 7).
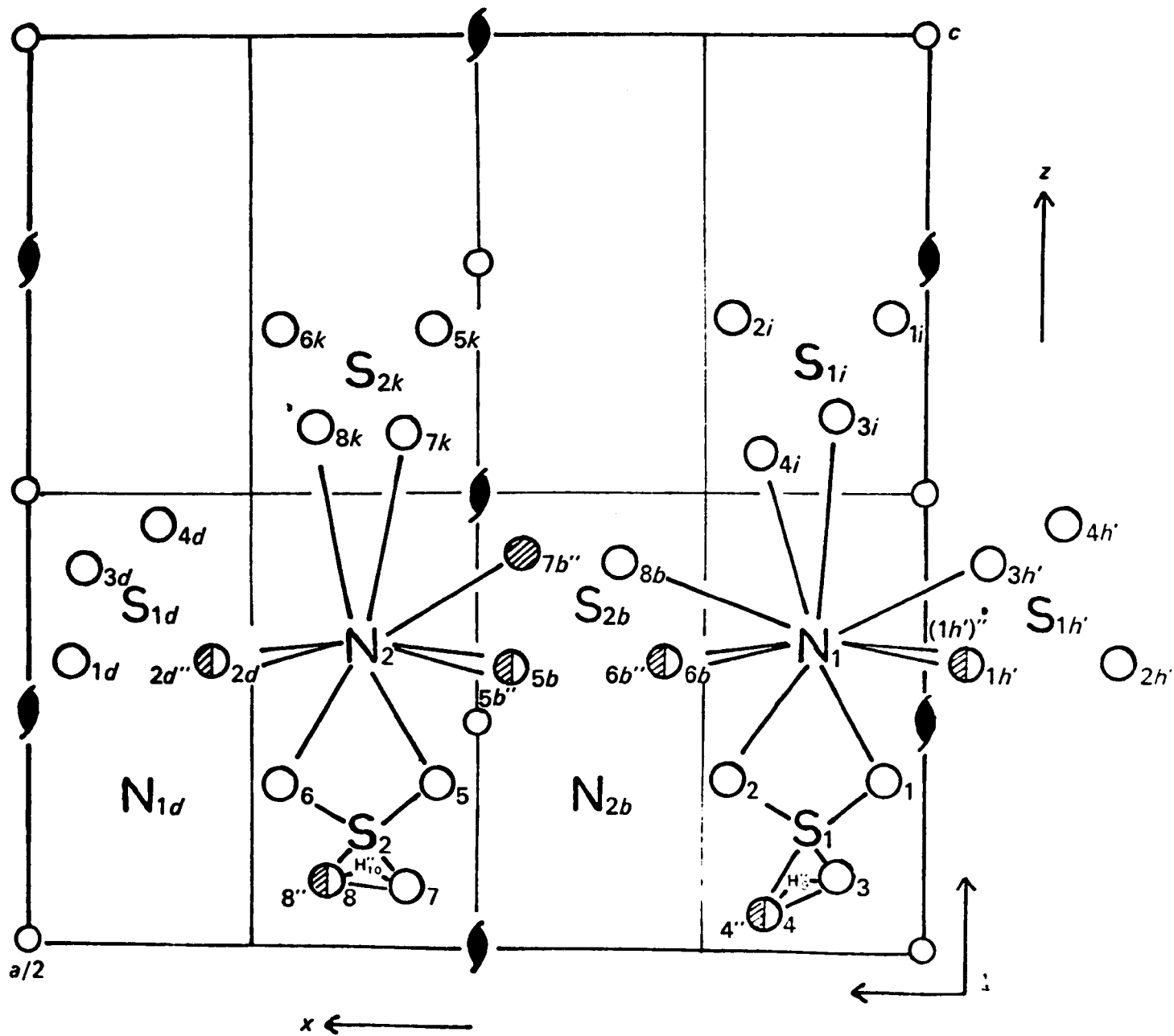
Fig.1V.18. The structure of $ND_4DSO_4$ viewed down [010]

Table IV-9

| Deut. | $q_{zz}$ | O····O | O-D | $\varphi'_z$ | $\varphi_z$ | $\varphi'_y$ | Assignment |
|---|---|---|---|---|---|---|---|
| 1 | -.3940<br>+.9071<br>-.1479 | -.3539<br>.9327<br>-.0710 | -.4094<br>.9006<br>-.1461 | 5.25°<br>(6±4°) | 1.0° | 5.9° | $H_{10}$<br>d0··0= 2.60Å |
| 4 | .4013<br>.9047<br>.1431 | .3539<br>.9327<br>.0701 | .4094<br>.9006<br>.1461 | 5.25°<br>(6±4°) | 0.6° | 8.3° | $H'_{10}$ |
| 2 | -.1382<br>-.9723<br>+.1886 | -.1807<br>-.9596<br>.2155 | -.0595<br>-.9080<br>.4148 | 2.9°<br>(14±3°) | 14.2° | 14.0° | $H_9$<br>d0··0= 2.51Å |
| 3 | .1303<br>-.9721<br>-.1951 | .1807<br>-.9596<br>-.2155 | .0595<br>-.9080<br>-.4148 | 3.2°<br>(14±3°) | 13.8° | 6.9° | $H'_9$ |

Note: dir. cos. of $q^1_{zz}$ and $q^2_{zz}$ have been multiplied by -1.

Such components (although numerically small for deuterons 2 and 3) play

a major role in the determination of the $q_{xx}$ and $q_{yy}$ directions.

The similarity of the quadrupolar constants for the two sets of

deuterons (1,4; 2,3) is somewhat unexpected, in view of the difference

in H-bond length and the proposed disordered behaviour for one kind of

bisulphate ion $(H_9S_1O_1O_2O_3O_4)^-$ in the room temperature form (7). If a

completely rigid $DSO_4^-$ ion is assumed, disordered between two sites

0.55 Å apart as suggested by Nelmes (7), the consequent motions of the D

atom about the equilibrium position could have a pronounced effect on the

number and linewidth of the signals, and on the value of the quadrupolar

constant. Such a mechanism would produce a decrease in the effective

value of the e.f.g. components. By similar reasoning, a slightly higher

asymmetry parameter could indicate a degree of anisotropy in this movement,

affecting the three components to different extents. Admittedly the

amplitude of the vibrations affecting D should be restricted by the second

oxygen atom $O_x$ to which it is hydrogen bonded, but, since $O_x$ belongs to

another disordered $SO_4D^-$ group (along [b]), a disordered condition should

persist. No noticeable effect is evident, however, all four signals at

room temperature looking very much alike. A possible explanation is that

the deuteron switches positions at a much higher rate than the quadrupolar

frequency (more precisely, the frequency difference $\nu_1 - \nu_2$ between the two

extremes in the vibration). If the exchange rate were very slow, two

separate signals would be observed. The amplitude of the movement about

the mean position was estimated not to exceed $7^{\circ} - 8^{\circ}$.

It should be stressed that in the process of refining $\alpha$ and $\beta$ some

'loss of detail' may have occurred, as a consequence of the systematic

averaging. The value of $\sim 192$ KHz for the quadrupolar constant of

deuterons 1,4 and 2,3 is slightly surprising, some 20 KHz. above that
predicted from the O···O bond length. The quadrupolar constant is very
useful as a structural tool because of its great sensitivity to changes in the
immediate surroundings of deuterons involved in hydrogen bonding, rather
like n.m.r. chemical shifts or i.r. frequency shifts. Some empirical
correlations have been given for H-bonded systems (18,19) between the O···O
or the H···O distances and the magnitude of the quadrupolar constant.
From the graph given by Blinc and Hadži (18) and the two known O···O
distances (table ), the predicted values would be

$$d^{1,4} = 2.60 \text{ Å} \quad ; \quad \frac{e^2 q Q}{h} = 160 \text{ KHz.}$$

$$d^{2,3} = 2.51 \text{ Å} \quad ; \quad \frac{e^2 q Q}{h} = 130 \text{ KHz.}$$

Although some error is expected in all the previous calculations, 30-70 KHz.
looks too large to be explained in this way. The maximum splittings found
from the rotation patterns were about 420 gauss ($\sim$ 274 KHz.). The
quadrupolar constant should therefore be no less than $\frac{2}{3}$ x 274 = 183 KHz.,
a lower limit well in excess of the values predicted above. The influence
of the central sulphur atom in the distorted tetrahedron should perhaps be
taken into account. Fig. IV-19 shows the configuration of the H-bonded
system in both cases, with angular values deduced from the d.m.r. results.

It is worth noting that the $q_{zz}$ values for deuterons 2 and 3 appear
to be very close to alignment along the O···O direction (Table IV-9),
in contrast with a deviation from linearity of $14 \pm 3^{\circ}$ found by neutron
diffraction. Curiously, the $q_{zz}$ direction from d.m.r. is very near to
the corresponding direction calculated for one of the two sites in the
disordered model, as the table shows.

## Fig. IV-19
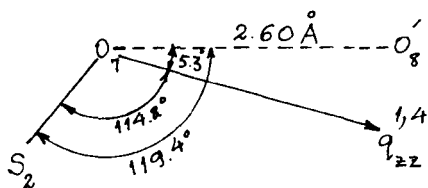


$D_{1,4} \equiv H_{10}$

$O_7, O_8'$ – oxygen atoms from successive $[S_2O_5O_6O_7O_8]$ groups along $[b]$
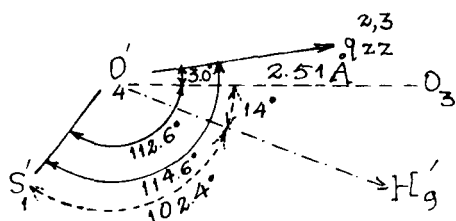
$D_{2,3}' \equiv H_9'$

$O_3, O_4'$ – oxygen atoms from successive $[S_1O_1O_2O_3O_4]$ groups along $[b]$

## Table IV-10

| $q_{zz}$ dir. cos. | | Calculated | |
|---|---|---|---|
| deut. 2 | deut. 3 | $O_{(4)}^+-H_{(9)}^+$ dir. cos. | $O_{(4)}^--H_{(9)}^-$ dir. cos. |
| -.1382 | .1303 | -.104 | -.232 |
| -.9723 | -.9721 | -.973 | -.878 |
| .1886 | -.1951 | .206 | .420 |

$(O_{(4)}^+-H_{(9)}^+$ and $O_{(4)}^--H_{(9)}^-$ refer to the alternative sites in the disordered model).

$\left\{ \begin{array}{l} \text{Angle between } q_{zz}(2) \text{ and } O_{(4)}^+H_{(9)}^+ = 2^\circ \\ \text{Angle between } q_{zz}(3) \text{ and } O_{(4)}'^+H_{(9)}'^+ = 1.6^\circ \end{array} \right.$

$\left\{ \begin{array}{l} \text{Angle between } q_{zz}(2) \text{ and } O_{(4)}^-H_{(9)}^- = 15.3^\circ \\ \text{Angle between } q_{zz}(3) \text{ and } O_{(4)}'^-H_{(9)}'^- = 15.2^\circ \end{array} \right.$

8. <u>The bisulphate ion at 230 K.</u>

(a) <u>General results.</u>

There were several reasons for the lesser reliability of the low temperature readings, the chief one being the poor S/N and consequent difficulty in locating the signals. Temperature fluctuation (mainly for pattern I') over a section of the polarisation curve (5) where the slope is still considerable was the most likely cause of the difficulty in observing some signals, and the large variations observed in their positions. Moreover, small angular or positional adjustments of the crystallographic axes during the transition (e.g. $\alpha$ may have varied by up to $1^{o}$) affected in a sensitive way the application of the same T transformation matrix to the low temperature data. To identify each of the newly split lines in the two patterns, it was considered that

(i) the curves which moved the least with relation to their room temperature counterparts should do so in both patterns, and

(ii) the symmetry relationships between values of A and B for pairs of related deuterons should hold at low temperature, despite the loss of the screw axis. The glide plane is retained, and a similar kind of direction cosine relationship should still be valid, except for sign, as shown below.

(a) Direction cosines ($\alpha_n$) for deuterons $D_{I-IV}$ at 300 K

(I $\cdots\cdot$ IV arbitrary indices)

| | $D_I$ | $D_{II}$ | $D_{III}$ | $D_{IV}$ |
|---|---|---|---|---|
| Point group | $\alpha_1$ | $-\alpha_1$ | $-\alpha_1$ | $\alpha_1$ |
| $2_1/m$ | $\alpha_2$ | $\alpha_2$ | $-\alpha_2$ | $-\alpha_2$ |
| | $\alpha_3$ | $-\alpha_3$ | $-\alpha_3$ | $\alpha_3$ |

I and III (and likewise II and IV) are related by a centre of inversion $\bar{1}$, and are therefore indistinguishable by d.m.r.

I and II are related by 2.

III and IV are related by 2.

(b)  230 K  $D_I$ `  $D_I'$

Point group m  $\alpha_1$  $\alpha_1$

$\alpha_2$  $-\alpha_2$

$\alpha_3$  $\alpha_3$

$D_I'$ is comparable to $D_{II}$, except for sign which does not affect the d.m.r. experiment, so the relationships still hold. Unfortunately considerations (i) and (ii) are not of much help for curves 2 and 2' in pattern II, Fig.IV-9: not only are they equally spaced about the room temperature form, but also the experimental error in the determination of A and B is such that the equations $(A + B)_i = (A + B)_k$ are equally satisfied with 2,3 or 2,3' as symmetrical pairs. Low temperature signals derived from pairs 1,4 and 2,3 are treated separately.

(i) Deuterons related to 1 and 4 in the room temperature form.

The four deuterons have been called, 1,1', 4 and 4', each pair having evolved from original line 1 or 4 respectively, by loss of the centre of inversion in the transition. For easier identification, the dashed symbols represent the two deuterons whose curves diverge most from their room temperature counterparts. Listed below are the relationships $A_i + B_i = A_k + B_k$ used in the identification of symmetrically related pairs, and the e.f.g. components as determined from successive products $T^{-1}$ x A (Sec. II.2).

Table IV-11

|  | Deut. | 1 | 4 | 1' | 4' |
|---|---|---|---|---|---|
| **PAT.I'** | A   KHz | 72.47 | -9.00 | 59.46 | -23.15 |
|  | B | -191.70 | -109.57 | -183.38 | -101 .10 |
|  | C | 75.26 | - 50.79 | 72.64 | - 42.45 |
|  | A + B | -119.23 | -118.57 | -123.92 | - 124.25 |
| **PAT.II'** | A | 39.54 | -114.90 | 49.78 | - 114.72 |
|  | B | -164.91 | - 9.88 | -183.62 | - 19.53 |
|  | C | - 77.93 | 19.04 | - 74.03 | 17.68 |
|  | A + B | -125.37 | -124.78 | - 133.84 | - 134.25 |
|  | $K\phi_{11}$ | - 75.9 | - 94.4 | - 10.7 | - 44.7 |
|  | $K\phi_{22}$ | 206.4 | 216.7 | 173.4 | 194.0 |
|  | $K\phi_{33}$ | -127.3 | -123.5 | -131.5 | - 127.9 |
|  | $K\phi_{12}$ | -152.1 | 161.4 | -157.3 | 171.7 |
|  | $K\phi_{13}$ | 44.2 | 27.4 | 38.4 | 17.4 |
|  | $K\phi_{23}$ | - 50.9 | 48.4 | - 47.6 | 37.2 |
|  | Trace | 3.2 | - 1.2 | 31.2 | 21.4 |

All A, B, C constants referred to $\theta = \theta$ (sym. plane) as origin.

The joint effect of experimental error, and slight changes of the crystal orientation during the transition, is evident from the divergence in the numerical values of corresponding tensor components for related deuterons, and is particularly serious for $\phi_{11}$. The orientation errors are systematic and can be reduced to some extent. Since a full scale orientation refinement would at this stage be a far too lengthy task for the eight lines of the low temperature form, the equations in Sec. IV-6b were used directly for the data from pattern I', which were expected to be more accurate, both for crystal orientation and for the constants A, B, C. The redetermined components and the results of diagonalisation are as follows:

|  | $K\phi_{11}$ | $K\phi_{22}$ | $K\phi_{33}$ | $K\phi_{12}$ | $K\phi_{13}$ | $K\phi_{23}$ |
|---|---|---|---|---|---|---|
| deut$^s$1,4 | -82.57 | 208.38 | -125.81 | -148.68 | 37.98 | -53.29 |
| deut$^s$ 1',4' | -49.37 | 181.74 | -132.37 | -150.17 | 44.23 | -47.39 |

Signs taken as for deuterons 1 and 1', respectively.

(ii) Deuterons 2,2,3,3'.

Given the difficulty in deciding which of the two deuterons was 2 or 2' in pattern II', the trial and error method had to be adopted, by associating 2' (pattern I') with each of the two choices at low temperature and checking by multiplication by $T^{-1}$ which alternative led to values of the $\phi_{ik}$ components in better agreement with each other, i.e. except for sign $\phi^{2'}_{ik} = \phi^{3'}_{ik}$. The most coincident results are in table IV-13, where deuteron 3 is also included.

## Table IV-12

### Diagonalised tensor components (230°K) for the (a, b, c) pseudo-orthorhombic crystal axes:

| Deut. | | Eigenvectors $q_{xx}$ $q_{yy}$ $q_{zz}$ | | | Eigenvalues (KHz) $K\phi_{xx}, K\phi_{yy}, K\phi_{zz}$ | quad.const. $\dfrac{e^2qQ}{h}$(KHz) | asym. par. $\eta$ |
|---|---|---|---|---|---|---|---|
| | a | .4910 | .7801 | .3878 | -125.6 | | |
| 1,4 | b | .3462 | .2338 | -.9086 | -155.4 | 187.3 | .106 |
| | c | .7994 | -.5804 | .1552 | 280.9(5) | | |
| | a | .7257 | .5264 | .4431 | -111.9 | | |
| 1',4' | b | .4545 | .1168 | -.8831 | -153.4 | 176.9 | .156 |
| | c | .5165 | -.8422 | .1545 | 265.4 | | |

## Table IV-13

| Deut. | 2' | 3' | 2 | 3 |
|---|---|---|---|---|
| $K\phi_{11}$ | -154.6 | -167.4 | | -109.2 |
| $K\phi_{22}$ | 216.0 | 250.2 | not | 273.6 |
| $K\phi_{33}$ | -120.2 | -122.1 | allocated on | -119.8 |
| $K\phi_{12}$ | 91.4 | - 85.7 | pat. I', | - 35.5 |
| $K\phi_{13}$ | - 26.7 | - 14.5 | except for a | - 14.0 |
| $K\phi_{23}$ | - 63.7 | 62.7 | few points | 80.4 |
| Trace | - 58.8 | - 39.3 | - | 44.6 |

The diagonalised tensor components are:

Table IV-14

| Deut. | | $q_{zz}$ | Eigenvalues(KHz) $K\phi_{xx}, K\phi_{yy}, K\phi_{zz}$ | quad.const. $\frac{e^2qQ(KHz)}{h}$ | asym.par. $\eta$ |
|---|---|---|---|---|---|
| | a | .2281 | -129.9 | | |
| 2' | b | .9566 | -178.7 | 166.6 | .195 |
| | c | -.1811 | 249.9 | | |
| | a | .1918 | -132.4 | | |
| 3' | b | -.9685 | -184.4 | 185.0 | .188 |
| | c | -.1589 | 277.5 | | |
| | a | .0930 | -110.8 | | |
| 3 | b | -.9767 | -137.5 | 195.3 | .091 |
| | c | -.1934 | 292.9 | | |

Not surprisingly, the degree of numerical agreement for pair 2' and 3' is poor: the very large value of the experimental trace in table IV-13 is evidence for the errors incurred. $q_{xx}$ and $q_{yy}$ direction cosines have not been included, for their values would be little more than meaningless; besides, the present incomplete knowledge of the low temperature coordinates of neighbouring heavy atoms precludes any comparison and determination of $\varphi'_z$, $\varphi_z$ or $\varphi'_y$.

In spite of the limitations imposed by experimental error, a number of general conclusions can be inferred from the data in tables IV-12 and IV-14.

(b) Deuterons 1,4,1', and 4'.

These deuterons suffer relatively small transformations upon

passage through the Curie point; the first pair moves only slightly $(0.8^{\circ})$

from the original position: 1' and 4' have slightly higher deviations.

For these atoms, not only the amplitude of the transformation is small

$(< 3^{\circ})$, but also there is almost no change $(< 0.5^{\circ})$ in the C components

of the OD vector. It can easily be shown that, within experimental error,

the slight displacements suffered by individual deuterons arise on a plane

almost at right angles $(81.0^{\circ})$ to [c].

$$(q_{zz}^{1,4} \wedge q_{zz}^{1',4'}) \text{ normalised} = \bar{n} \equiv [-.0538, .1458, .9878]$$

$$\bar{n}/(q_{zz}^{1,4}) \text{ RT} = -.0074 \quad (0.4^{\circ} \text{ off the plane})$$
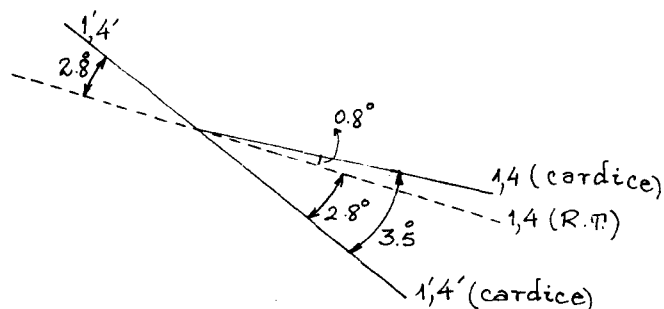


This conclusion remains valid despite the magnitude of our errors, since

by chance it could be checked independently. It is known from X-ray

data that [c] is no more than $5^{\circ}$ or $6^{\circ}$ from the horizontal plane, which is

also the plane of the magnetic field $\pi_H$. Also, $\phi_{zz}$ for deuteron 1

(and also 3) in the first pattern happens to be very close to the horizontal;

the magnitude of the highest splitting is about 98.2% of the theoretical

maximum:

the maximum possible splitting $= (\frac{3}{2} \frac{e^2 qQ}{h})$ is $\frac{3}{2} \times 192.2 = 288.33$ KHz.,

whereas that observed for deuteron 1 is 283.05 KHz. A deviation of $10^{\circ}-11^{\circ}$

from $\pi_H$ has been estimated: in these conditions the location of the maximum

of the curve should be very close indeed to the projection of the OD vector

on the horizontal plane (Appendix III). Given the proximity of [c] to

this same plane, the constancy of the components along this axis for

deuteron 1 (RT) and 1,1' can easily be checked from the invariance

of the location of the maxima for the respective curves. The numerical

data are given below.

| | 300 K | 230 K | |
|---|---|---|---|
| Deut. | 1 | 1 | 1' |
| $\tan 2\theta_{max}$ <br> $= C/B$ | -.377 | -.393 | -.396 |
| $\theta_{max}$ <br> ( $\theta_o$ at $173.2^{\circ}$) | $79.7^{\circ}$ | $79.3^{\circ}$ | $79.2^{\circ}$ |

These conclusions agree with the 'concentric' appearance of both curves

1,1' and 4,4': 1 and 4 maintain much the same position as at room

temperature, while 1' and 4' are lower by 15 to 20 gauss, indicating an

approach of OD towards the magnetic field rotation axis ($\sim 18^{\circ}$ from [a]).

The ferroelectric transition thus affects very little the original

deuterons 1 and 4: while half of the curves (1,4) are quite insensitive to

the transformation, the remainder suffer a deflection of $\sim 3^{\circ}$, mainly in the

($\underline{a}$, $\underline{b}$) components. Neither the order of magnitude nor the direction of the

angular changes would suggest that this set of deuterons plays a very

active role in the appearance of polarisation along [c]. Similar

conclusions have been reached independently from the available low

temperature X-ray data (8): the $SO_4$ group to which this deuteron is

attached undergoes no significant changes at the Curie point.

Strict comparison of numerical values must be treated with some reserve

without further refinement of the d.m.r. data. Since the $q_{zz}$ component is

the least affected by error of all the e.f.g. eigenvectors, however,

and the data for pattern I' are thought to be rather more reliable, the

following table has been organised to compare the d.m.r. and neutron

diffraction (at $203^{\circ}K$) results for these four deuterons. Since only the

b-axis projection is at present available from X-ray work, the $\frac{\Delta a}{\Delta c} = \frac{\cos \alpha_1}{\cos \alpha_3}$

ratio was considered throughout. (Some room temperature data are also

included).

Table IV-15    $\Delta a/\Delta c$ values

| temp $^{\circ}K$ | Deut. | OD(d.m.r.) | neut.dif. and X-ray data | |
|---|---|---|---|---|
| | | | O-D | O...O |
| $300^{\circ}K$ | 1,4 | 2.706 | 2.801 | 5.052 |
| $230^{\circ}K$ | 1,4 | 2.498 | - | 9.8 * |
| | 1',4' | 2.868 | - | 3.23* |

* tentative allocation

The better agreement between one of the $\frac{\Delta a}{\Delta c}$ ratios for O...O and the d.m.r.

O-D direction may mean that one of the two kinds of deuterons (possibly

1',4') is tending towards better alignment along the O...O direction, while

the other (1,4) maintains a similar relative position as before. This would

account for the smaller quadrupolar constant found for deuterons 1', 4'

relative to 1,4. Even if this difference is an accidental consequence of

experimental error, the observed general trend of a decrease in $e^2qQ/h$

seems to indicate at least some contraction in the bond upon cooling.


(c)  Deuterons 2,3, 2' and 3'.

An inspection of the patterns and table IV.14 shows that at least one

of these deuterons undergoes a noticeable change from the room temperature

form. Experimental error affects the results for these deuterons quite

severely. The $q_{zz}$ direction cosine still appears reasonable, however;  the

values for 2' and 3' agree within $2.5^{o}$. Comparison between the room

temperature and cardice results immediately shows that deuterons 3' and 3 (and

presumably 2 and 2' for which data are not so complete) are displaced in

opposing directions with relation to the original positions.

Fig. IV-20



$\begin{cases} 2,2 & \text{pairs of deuterons} \\ 3,3 & \text{related by a centre} \end{cases}$

of inversion $\bar{1}$, indisting-

uishable by d.m.r.
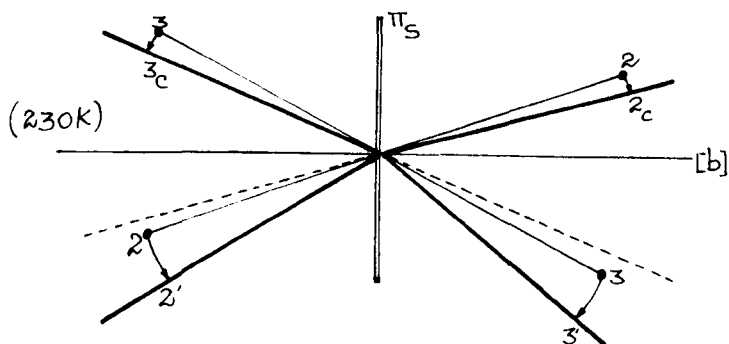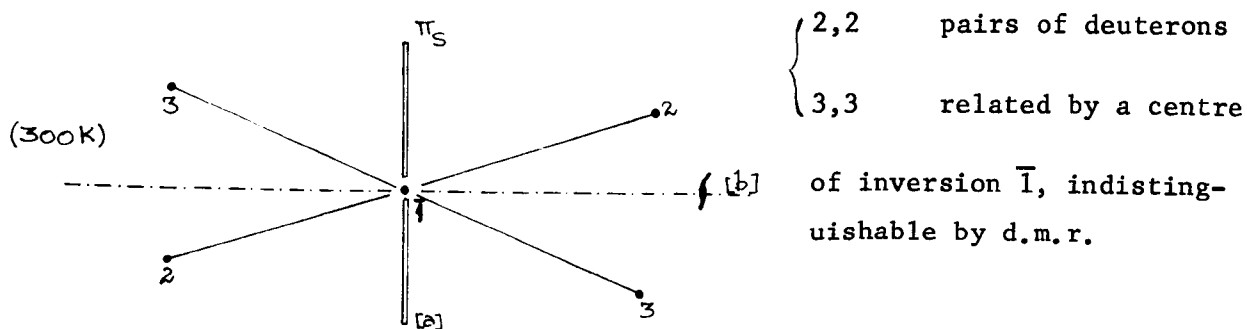

(angular values in fig. not

necessarily in accordance

with the real values)

From the figure (confirmed by a small spatial model) there seems to be
a net directional effect with relation to the ac plane. Examination of
table IV.14 and the large angular variations in the a components compared
with room temperature suggests [a] rather than [c] as the direction of
maximum change. A difference in behaviour between the two pairs of
deuterons 2,2' and 3,3' appears to take place from the patterns (especially
pattern II'); while the first pair shows lines almost equidistant from
the original room temperature line (the average of both sets of A, B, C
constants at low temperature being very close indeed to the RT values), the
second pair shows one line (3) hardly affected by the change, while the
maximum of the other (3') has clearly moved away from [c] by about $2.5^{\circ}$.
If this apparent disparity could be proved to have structural significance,
a number of possible causes could be advanced, such as intrinsic twinning
of the specimen (not apparent from room temperature data, however),
formation of domains of opposite polarisation, or, more likely still, the
breakdown of symmetry relationships in a somewhat disordered structure.
Unfortunately the location of line 2 was almost impossible in pattern I', so
that the data are incomplete, while experimental error does not improve
their reliability. Lines 2 and 2' are afterwards examined separately by
approximate methods. <u>Lines 3,3'</u> In the following table, direction cosines
for the $q_{zz}$ direction are compared with each other and with the room
temperature data; the direction cosine of the bisectrix of the 3,3' angle
is also included. Fig. IV-21 gives a very schematic representation of
the geometric relationship between (3,3') cardice and (3) RT.

<u>Fig. IV-21</u>
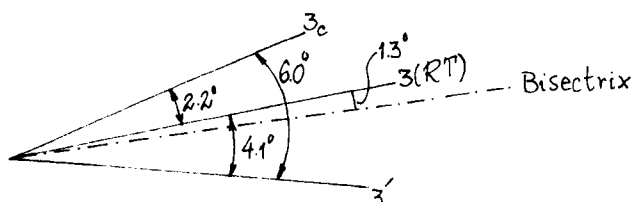
Table IV-16

| 300 K | 230 K | | |
|---|---|---|---|
| 3 | 3c | 3' | $q_{zz}^3 \bigwedge q_{zz}^{3'}$ bisector |
| .1303 | .0930 | .1918 | .1425 |
| -.9721 | -.9767 | -.9685 | -.9740 |
| -.1951 | -.1934 | -.1589 | -.1763 |

The empirical observation from the pattern that 3 moves much less than 3'
is confirmed. Once again the coplanarity of the transformation is evident.

$$(q_{zz}^{3c} \bigwedge q_{zz}^{3'}) \text{ normalised} = \bar{n} = [-.3062, -.2129, -9279]$$

$$\bar{n} / (q_{zz}^3)_{RT} = -.0140 \quad (0.8^{\circ})$$

This time, in contrast to deuterons 1 and 4, the plane of displacement is
considerably closer to [c] $(68^{\circ})$ and could thus be more extensively involved
in the polarisation along that direction. It is interesting to note that
the deviation of deuteron 3' from [c], evident in table IV-16, should be
independent of experimental error: a study of curve 3' (pattern I') on
a similar basis as for curves 1 and 1' (previas section)shows clearly a
displacement (away from [c])of the curve maximum which is of the expected
order of magnitude (Table IV-17).

Table IV-17

| temp (K) | deut | $\tan 2\theta_{max} = \dfrac{C}{B}$ | $\theta_{max}$ | $\theta_{max}^{RT} - \theta_{max}^{card}$ | $ang(q_{zz})_{[c]}^{RT} - ang.(q_{zz})_{[c]}^{card}$ |
|---|---|---|---|---|---|
| 300K (RT) | 3 | .1449 | 94.2° | - | - |
| 230 K | 3 | .1482 | 94.2° | 0° | 0.15° |
| (cardice) | 3' | .0551 | 91.6° | 2.6° | 2.2° |

|  |  | from direct observation of curves on the pattern | from diagonalised tensor (table IV-16) |

From the values above, the quasi-invariance of deuteron 3 is also clear.

Lines 2,2'

Since complete data were not available for these deuterons, a number of approximate calculations was carried out, mainly on data from pattern II'. A simplified method of calculation was used which fits to the experimental curve a series of theoretical curves evaluated for axially symmetric tensors with a convenient quadrupolar constant. The procedure was checked by comparison with the (solved) room temperature curves, their respective $q_{zz}$ eigenvectors, and their quadrupolar constants. A slight correction was introduced for constant C to reduce the error caused by the hypothesis of axial symmetry (which normally affects C mostly); once again the room temperature data were used as reference.

For easier handling of the equations, all these approximate calculations were carried out relative to a 'fixed' set of laboratory axes $(X_{\alpha\beta} Y_{\alpha\beta} Z_{\alpha\beta})$ (Sec. IV-6a). It is known (17) that the eigenvalues of the tensor (and

hence the quadrupolar constant and $\eta$ ) do not depend on the frame of

reference; as for the eigenvectors, a simple conversion $T(q_{zz})_{X_{\alpha\beta}Y_{\alpha\beta}Z_{\alpha\alpha}} = (q_{zz})_{abc}$ restores $q_{zz}$ to the crystallographic axes (abc).

$(T (X_{\alpha\beta}Y_{\alpha\beta}Z_{\alpha\beta} \longrightarrow abc)$ had been evaluated at an earlier stage of the

calculations - Sec. IV-6). The expressions employed for A, B, C

were (formally similar expressions are used in Chap. V):-

$$A \simeq K'(1 - 3\alpha_{33}^2) \longrightarrow \frac{A}{K'} = 1-3z^2,$$

where

$$K' = \frac{Keq}{4} = \frac{3}{8} \frac{e^2qQ}{h} .$$

$$B \simeq 3K' (\alpha_{13}^2 - \alpha_{23}^2) \longrightarrow \frac{B}{K'} = 3(x^2-y^2);$$

$$C \simeq -6K'\alpha_{13}\alpha_{23} \longrightarrow \frac{C}{K'} = -6xy.$$

$$q_{zz} = \begin{bmatrix} \alpha_{13} \\ \alpha_{23} \\ \alpha_{33} \end{bmatrix} = \begin{bmatrix} x \\ y \\ z \end{bmatrix} \qquad (\alpha_{13}, \alpha_{23}, \alpha_{33} \text{ are direction cosines of } q_{zz} \text{ in the 'fixed' laboratory axes}).$$

From these relationships, the following expressions may be deduced:

$$|x - y| = \sqrt{\frac{2 + A/K' + C^{corr.}/K'}{3}} = K_1,$$

$$|x + y| = \sqrt{\frac{2 + A/K' - C^{corr.}/K'}{3}} = K_2, \text{ and}$$

$$x^2 - y^2 = \frac{1}{3} \frac{B}{K'} = \pm K_1 K_2.$$

(A, B, C are referred to the intersection of $\pi_S$ with $\pi_{\overline{H}}$ as origin).

Systematic use of these relationships led by a process of successive

approximations to the following rough values for $q_{zz}$:-

|                          | a     | b     | c      |
|--------------------------|-------|-------|--------|
| Deuteron 2(pattern II')  | .040  | .978  | -.206  |
| Deuteron 2'(pattern II') | .313  | .939  | -.142  |
| Deuteron 2'(pattern I')  | .290  | .943  | -.166  |

The $q_{zz}$ directions as deduced from patterns I' and II' are in reasonable agreement with each other $(1.8^{\circ})$ but displaced by $4.5^{\circ}$ from the data in Table IV-14. If this value is taken tentatively as the limit of error in the approximate calculations, the relationships between the $q_{zz}$ directions at both temperatures may be schematically represented:
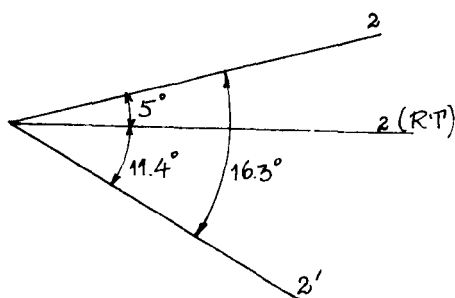


$(q_{zz}^{2} \wedge q_{zz}^{2'})$ normalised = $\bar{n}^{2,2'}$ = [.165, -.210, -.964].

$\bar{n}^{2,2'} / (q_{zz}^{2})_{RT}$ = .00(04)

Despite the obvious limitations of this approach, the qualitative conclusions may be compared with those for deuterons 3,3'; these are coplanarity of the three $q_{zz}$ vectors, antisymmetric displacements with relation to the room temperature centre of inversion, and unequal angular displacements (one about twice as big as the other).

Comparison of the d.m.r. results for deuterons 2,2' and 3,3' with the X-ray low temperature data so far available (8) is shown in table IV-18.

As in table IV-15, the $\frac{\Delta a}{\Delta c}$ values were calculated in each case.

<p style="text-align:center;">Table IV-18</p>

| Temp.(K) | Deut. | O–D (d.m.r.) | X-rays and neutron diffraction | |
| --- | --- | --- | --- | --- |
| | | | O...O | O–D |
| 300 (RT) | 2,3 | 0.70 | 0.84 | 0.14 |
| 230 (card.) | 2 | 0.20 (v.approx) | 0.01* | – |
| | 3 | 0.48 | | |
| | 2' | 1.26 2.0 (v.approx.) | 4.35* | – |
| | 3' | 1.21 | | |

* tentative allocation

while the antisymmetry of the transformation with relation to the form at 300 K is evident from both sets of results, it appears that the oxygen atoms (presumably the sulphate groups themselves) suffer larger directional changes than the hydrogen-bonded deuteriums. The poor accuracy of some of the d.m.r. results above ($\pm 4^\circ$) precludes any further consideration as to the linearity of the bonds.

I.R. data (20) confirm the existence of changes in the hydrogen-bonding frequency region: a 3165 cm$^{-1}$ band (at 20$^\circ$C) is replaced by a doublet (3100, 3190 cm$^{-1}$) at -96$^\circ$C. Similar doubling occurs in RbHSO$_4$ (3200 cm$^{-1}$ at 20$^\circ$C: 3200 and 3100 cm$^{-1}$ at -130$^\circ$C), which is known to be an isomorphous ferroelectric (9). Raman work (21) has also given evidence of changes in frequency (1033 cm$^{-1}$ at 313K; 1049 cm$^{-1}$ at 223K), and striking

variations of intensity for one of the $v_3$ bands of $SO_4^{2-}$, a feature

attributed to increasing distortion of the sulphate ions. More recent Raman

data (11) have led to similar conclusions; low frequency and polarisation

data were also reported. Prominent Rayleigh wings, somewhat temperature-

dependent, were observed in specific polarisations, which could be due to

rotatory motions of either the $SO_4^{2-}$ groups or a distorted ammonium ion.

The observed fine structure of the $ND_4^+$ d.m.r. signal proves that the

ammonium ion is not subject to isotropic free motion: deviations from

tetrahedral symmetry, together with crystal field effects and a possible

difference in the reorientation rates of the two types of non-equivalent

$NH_4^+$ ions are the most likely causes of the residual coupling (22). Distor-

tion of the $NH_4^+$ tetrahedra are not unusual in ammonium salts (23).


9. General conclusions.

Results on the room temperature form are generally in close

agreement with the X-ray and neutron diffraction data. No evidence was

found, however, for the disordered behaviour of one of the deuterons belonging

to the bisulphate group with abnormally high thermal parameters: both

linewidths and quadrupolar constants are virtually equivalent for all the

bisulphate deuterons in the structure. Any variation of the $e^2qQ/h$ values

may have been wiped out by experimental error: the predicted amplitude of

the 'disorder' about the mean position ($\pm 7^o$ to $8^o$) would not produce

variations higher than 4-5 KHz ($\leqslant 2.7\%$ of the value of the constant).

This very approximate calculation has been carried out on the simplifying

assumption that the $q_{zz}$ vector undergoes free rotation about an imaginary

stationary axis at $0^o$, rather like trans-1,2-dichloroethane around the

Cl-Cl axis (24). A variable temperature study between room temperature and

the ferroelectric transition point would perhaps throw more light on the behaviour of this bisulphate ion; broadening and eventually smearing out of this group of signals should arise when the frequency of the process slows down to a rate of the same order of magnitude as the quadrupolar frequency. However inconclusive the d.m.r. results may be concerning the motional state of the bisulphate ion, there are two points where they seem more definite; room temperature data show very clearly the existence of deuterium atoms closely attached to the nearest S-O group in a 'frozen' position (vide $q_{xx}$ and $q_{yy}$ geometric relationships with the neighbouring atoms in the structure): on the other hand, the general symmetry requirements for a 2/m point group seem to be closely followed.

The most striking features of the transformation suffered by the acid deuteriums at the Curie point are the anisotropic angular displacements in antisymmetric directions with relation to the room temperature centre of inversion. Within experimental error, such displacements occur in a common plane with the room temperature $q_{zz}$ vector. Individual movements do not seem to exceed $3^{\circ} -4^{\circ}$ (although a full assessment could not be made for deuterons 2 and 2', which may have displacements of larger amplitude); if that happens, it would be a consequence of some breakdown in the symmetry requirements. The evidence strongly suggests the group of deuterons 2,3,2' and 3' as the most favourable to induce the appearance of polarisation along [c]; not only are the atomic movements of larger amplitude, but also the plane in which they occur is at a closer angle to [c]. These findings are in full agreement with the low temperature X-ray results so far available; deuterons 2,3,2' and 3' belong to the 'disordered' bisulphate ion which at low temperature orders itself in an antisymmetric orientation with relation to the room temperature centre of inversion. On the evidence of d.m.r. experiments alone, deuterons 1 and 4 should not be completely excluded from

possible contribution to a general orientation of molecular dipoles; for $KD_2PO_4$, where a mechanism of order-disorder in the deuterium atoms is responsible for the appearance of ferroelectricity (25,26), the D freezing movements take place in a direction almost perpendicular to the polar axis: small displacements of the heavy atoms also occur. X-ray data so far indicate that the individual displacements of deuterons $D_1, D_4, D_1', D_4'$ in the adjoining bisulphate group are rather small.

Whether the D atoms are forced by the sulphate group into an essentially rigid formation, or whether a slight articulation of the O-D bond in the bisulphate group occurs at the transition, thus tending towards a closer alignment along the O···O direction (Sec. IV- 8b), cannot be resolved at the moment. Refinement of the orientation data and redetermination of the quadrupolar constants for each D atom is an obvious further step towards elucidating the mechanism of ferroelectricity in this salt.

## CHAPTER V

## STRONTIUM FORMATE DIHYDRATE

### 1. Introduction

This compound is of particular interest since two independent determinations of its structure by X-ray diffraction have been published (1,2), but do not agree with each other. The structure given by Galigné and Falgueirettes (2) in their preliminary report has been severely criticised by Clark (3), however, and the results of Osaki have been taken as more reliable.

Besides extending the structural information, d.m.r. studies may also be of value for:

i) establishing the degree of involvement of the formate ions in hydrogen bonding with neighbouring water molecules;

ii) studying the lone deuteron attached to the carbon atom, which gives formic acid a special place in the carboxylic acid series; and

iii) investigating the reorientation motion of the water molecules.

Comparison with related compounds follows as a natural consequence; d.m.r. studies have been carried out on another formate, $Cu(DCOO)_2 \cdot 4D_2O$ (4,5). The structure of formic acid is also known from both X-ray (6) and d.m.r. (7) techniques.

Strontium formate dihydrate is an orthorhombic crystal; Nitta (8) determined its space group $(2_1 2_1 2_1)$ and unit cell parameters (a = 7·30Å; b = 11·99Å; c = 7·12Å; Z = 4). The crystals are piezoelectric (9) and optically negative; morphologically the principal forms are domes parallel to $\alpha$ and $\gamma$, and a pinacoid perpendicular to $\beta$ (10). ($\alpha$, $\beta$ and $\gamma$ are optical directions which for an orthorhombic space group should

coincide with the crystallographic axes). Elastic and thermoelastic

constants have been studied by Haussuehl (11) (Sec. V.5).

2. Experimental details

    (a) Crystal growth

        Strontium formate dihydrate grows easily in large, beautiful,

single crystals, perfectly transparent. Reasonably large specimens can

even be grown from seeds under conditions as crude as a beaker of

saturated solution on a hot plate; gentle stirring helps to avoid

spurious seeding. Single crystals of strontium formate dihydrate and

velocity of crystal growth have been extensively studied (11,12,13).

The deuterated compound was first prepared directly from formic acid-$d_2$.

The most convenient way of growing a single crystal was by introducing a

seed into a suitably concentrated solution of the salt (in $D_2O$), and

slowly cooling it from an initial temperature slightly higher than the

saturation point. This temperature had to be below $72^o$, above which the

anhydrous form separates out. The whole process was carried out in closed

containers wherever possible, to prevent exchange of $D_2O$ with

atmospheric moisture. Transfer of the compound and crystal handling were

also performed under an inert atmosphere for the same reason.

        The principal steps in the preparation of the fully deuterated single

crystal of $Sr(DCOO)_2,2D_2O$ are now described.

    (i) Preparation of the deuterated compound

        Some preliminary trial runs were carried out with protonated

samples at several dilutions, starting with the conditions and

concentrations given by Holden and Singer (14), until the ideal temperature-

concentration conditions were found for the initial solution. Best results

were obtained for solutions slightly over-saturated at room temperature,
which not only enabled a slow enough process of growth to take place
close to room temperature (30-40°C range), but also involved much smaller
quantities of the deuterated materials.

The salt was prepared by slowly adding strontium carbonate (4·3 g.) to
a slight excess (3·0 g.) of formic acid-d$_2$ (Koch-Light ≥ 98 atom% D) in
28·4 ml. D$_2$O (≥ 99·7 atom % D). The solution was then warmed up to
60-70°, and rapidly filtered in a dry bag.

(ii) <u>Growth and selection of a suitable seed</u>

The previously prepared solution was introduced into a very
simple crystal growth container (Fig.V.1), specially designed for this
purpose. It consisted of a narrow, flat-bottomed long-necked flask with
a thermometer pocket adapted to it. The lower part of this pocket had
its walls blown very thin; this feature and a drop of mercury inside
ensured a much better thermal contact and quicker equilibrium with the
solution. Ground glass joints with teflon sleeving were used throughout
to prevent contamination of the solution by grease.

The best way of obtaining seeds was by suspending a fragment of
human hair in the hot (< 72°) concentrated solution, which was then
allowed to cool overnight, preferably inside a large, prewarmed Dewar.
Next day a fine, sparkling selection of small crystals covered the whole
length of hair. A good specimen was then selected and left to grow
'in situ' without further disturbance, while all the remaining unwanted
seeds were easily removed by guiding them gently along the hair.

(iii) <u>Growth of the crystal for d.m.r.</u>

The saturation temperature was carefully checked by warming the

Fig. V-1  Crystal growth device

thermometer pocket

seed
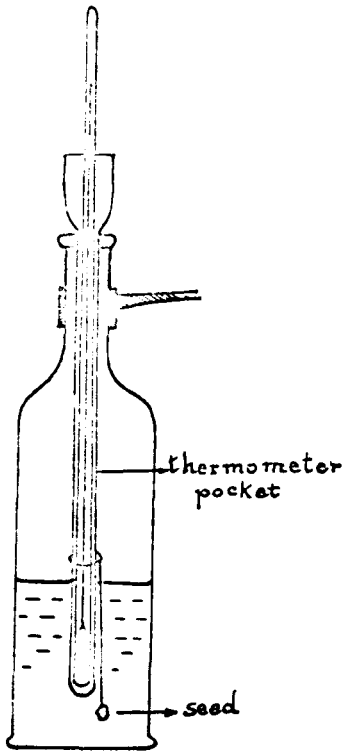
Fig. V-2  The crystal

Fig. V-3  Crystal holder

(I)

(II)          (III)

A

B          C

B

A

D

$h_1$   $h_2$

locking screw          D

2

3

1
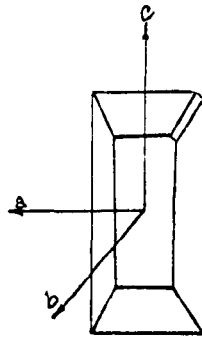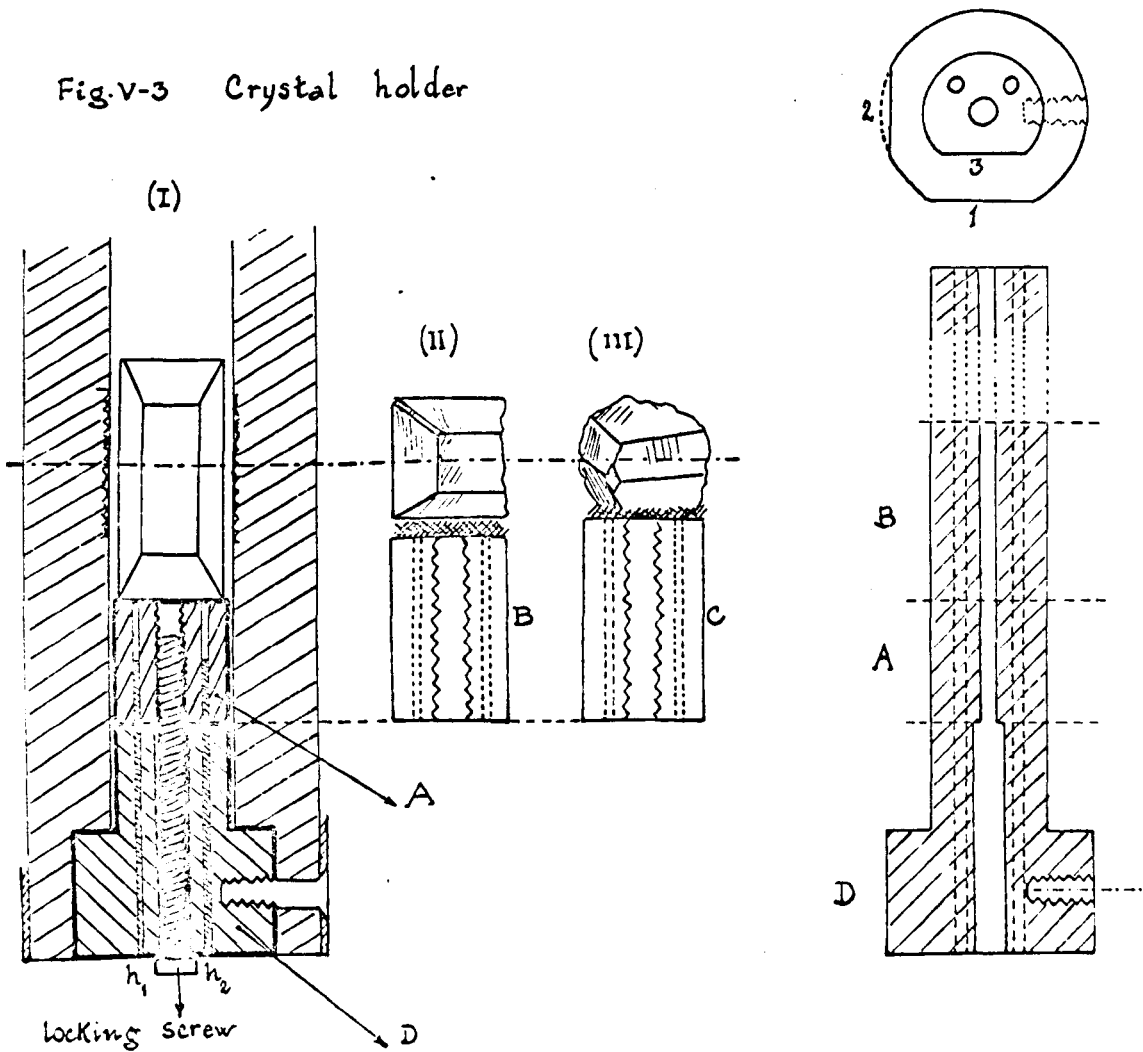
deuterated solution slowly on a magnetic stirrer-hot plate. A previously calibrated thermostat bath was then set to about $0 \cdot 3^{o}$ above this value, and the solution and container allowed to equilibrate therein. The hair and seed were attached to the thermometer shaft, and rapidly immersed in the solution, once equilibrium had been attained. Spurious seeding was avoided by allowing the outer layers of the crystal seed to dissolve. The main stage of growth was then initiated by lowering slightly the temperature setting on the thermostat bath. A fairly large crystal $(16 \cdot 5 \times 8 \cdot 5 \times 6 \cdot 7 \text{ mm})$ grew over a period of just under two days, rather more quickly than expected.

The specimen was given a protective coating by immersing it in a solution of foamed polystyrene in dry carbon tetrachloride. The supporting hair was easily removed.

### (b) Goniometry

The crystal is roughly sketched in Fig.V.2. Forms {110} and {010} were very well developed, giving an elongated, prismatic habit to the crystal. Slight irregularities on its surface gave the faces a step-like structure, not unusual in large specimens. As a result, diffuse and in some cases rather weak reflections were produced.

Sets of goniometer readings were recorded on a Techne two-circle instrument both for the crystal in its original form, and for each of the subsequent mountings, in order to identify the crystallographic axes and determine their positions relative to the crystal holder. Two mirrors 1 & 2 (Fig.V.3) approximately at right angles to one another defined a 'zone' parallel to the axis of the crystal support. The normal to mirror 1 constituted the angular reference for the crystal

setting on the optical goniometer and afterwards on the probe in the magnet.

### Identification of crystallographic axes

The pinacoid form was easily identifiable as being $\{010\}$, a fact confirmed from other sources (2,11,12).

The closeness of values for the $\underset{\sim}{a}$ and $\underset{\sim}{c}$ axes in this crystal (7•332Å and 7•144Å respectively (1)) pose a particular problem for their identification. The Barker index (15) was no real help, since its data concern a non-specified system of co-ordinates.

$$\text{Angles between } (010)\widehat{\phantom{.}}(110) \;=\; \alpha_1 \;=\; 58^{\circ}\ 42'$$
$$(010)\widehat{\phantom{.}}(011) \;=\; \alpha_2 \;=\; 59^{\circ}\ 18'$$

can easily be calculated from cell dimensions. The differences between $\alpha_1$ and $\alpha_2$ was certainly within the experimental error of the goniometer readings, in view of the poor quality of some of the reflections. For many faces the cross wires were tentatively centred on a fairly broad patch of light. To reduce experimental error, a large $(5 \leq n \leq 17)$ number of readings was taken for each face. Angular measurements from stereographic projections (15) gave in most cases values which, although numerically unreliable, had nevertheless the correct relative magnitude consistent with the assignment of axes given in Fig.V.2.

Some of the experimental values were found to be:

$$\alpha_1 \;=\; 58^{\circ}\ 16';\quad 58^{\circ}\ 2';\quad 57^{\circ}\ 3'$$
$$\alpha_2 \;=\; 58^{\circ}\ 46';\quad 58^{\circ}30';\quad 58^{\circ}\ 43'$$

An X-ray oscillation photograph $(15^{\circ})$ was taken with the transverse axis in Fig.V.2 set vertical; the value of 7•31Å found for the layer spacing confirms the choice indicated, inasmuch as one can trust the results

obtained from such a large specimen by X-ray methods (16). The morphology of this crystal has been extensively studied, however, and on the assumption that deuteration introduces no major changes, the elongated direction may safely be taken as the c-axis. It is also noteworthy that complex chains are found within the crystal parallel to this axis (1).

A degree of malformation in the crystal itself produced noticeable deviations from Euler's law, according to which dihedral angles between faces should be constant if the same crystallographic forms are involved. Two other sources of error were purely instrumental. The first of these comprised the equivalent to a zero reading correction on the horizontal circle, but this could be eliminated. By means of a slip gauge (which serves as a set of two accurately parallel reflecting surfaces), the exact position was found where the plane containing the axis of the vertical circle was normal to the plane defined by the telescope and collimator ($90^{o}$ 46'). Secondly, a constructional inaccuracy caused a 15' offset on the vertical circle axis, so that during a rotation it really precessed by that angle about the correct position. No facility was available on the instrument to correct this effect.

All of the above considerations show that there were unavoidable limitations on the accuracy with which the position of the crystallographic axes relative to the axis of the crystal holder could be determined. This inherent inaccuracy provided one of the justifications for the use of an approximation method to solve the crystal structure (Sec. V.4a).

Crystal handling for each rotation pattern is described in some detail in section V.2d.

## (c) Crystal Holder

A holder was specially designed for this crystal, versatile enough to accomplish three main purposes:

(i) Support of three specimens of different dimensions at the same height in the probe. A variable height assembly, with small detachable pieces A, B and C (Fig.V.3), where the crystal was mounted in turn, was adopted.

(ii) Optical goniometry requirements. Since the instrument available (Techne) did not possess the usual type of head with graduated arcs for holding the crystal, a more complete definition of the position of the crystal support was required. Two auxiliary mirrors at $90^{\circ}$ were therefore used, instead of one; they were glued against two flats 1 and 2, accurately machined parallel to the holder axis.

(iii) X-ray goniometry requirements. Some difficulty arose from the fact that the X-ray beam could not reach any higher than 16·5 mm. above the top of the goniometer head. As Fig.V.3 shows, the crystal was located in the probe support at a much higher level. The sectional character of the crystal holder made it possible to use the crystal plus its immediate joining piece for X-ray goniometry, and afterwards to reassemble the whole unit reproducibly. On each of pieces A, B and C, an additional mirror could be attached to flat 3 for azimuth reference in the X-ray camera.

In practice pieces A, B, C and D were machined together, as well as three locating holes, one of them partially tapped for a fixing screw. Flats 1 and 3 were milled in succession to be exactly parallel. Only then was the original perspex piece separated into transverse sections A, B, C, and D, and flat 2 machined on section D. Two tight-fitting brass

rods ($h_1$ and $h_2$) gave the correct alignment to each assembly (Fig.V.3). The accuracy of the settings of mirrors 1 and 2 was checked at a later stage; the reflection from each mirror was compared with a 'standard' reflection of the same object, obtained from a slip gauge used as reference mirror.

### (d) Preparation of the specimen for each rotation pattern

Three rotation patterns were obtained by rotation of the crystal about the principal directions of a triorthogonal set of axes. For a rhombic crystal these were conveniently chosen to coincide with the three main crystallographic directions [a], [b], [c]. The specimn was therefore mounted as closely as possible (within $3^\circ$) so that each of these directions in turn was perpendicular to the magnetic field. Fig.V.9 in sec.V4-b shows the position of the crystal for each pattern.

### (i) Crystal for pattern I ([c])

For the first pattern, the original specimen was mounted along its direction of natural elongation, [c]. Given the crystal dimensions, however, several edges and one of the pinacoid faces had to be slightly filed to fit the coil. A powdered sapphire nail file (Henckels) was used successfully for this purpose. Since fairly large surfaces of the material became exposed, the whole procedure was performed under a strong stream of dry nitrogen; the crystal was rapidly re-coated afterwards.

The top of the perspex support was filed down in the form of a V, as similar as possible to the shape of the terminal part of the crystal. A layer of plasticine was added before the specimen was wedged into place. Minimal movements of the sample by lightly adjusting the plasticine base (with the tip of a very small screwdriver) gave an approximate, purely

visual setting. Prominent faces and vertical edges constituted the main references. Further adjustments were carried out on the goniometer head, followed by checks on whether or not the main prismatic faces were in 'zone adjustment'.

The crystal was then fixed more permanently to the support with a special kind of araldite (100 parts by weight CY208 + 100 parts MY750 + 16 parts HY951) adequate for room temperature and low temperature purposes. Since this was a very fluid, slow-setting mixture (2 days), the crystal with the fresh adhesive was located in position inside the probe and allowed to set. Two days later, it was removed and the final readings recorded. Unfortunately, either because of subsidence while the araldite was hardening, or more likely, because of slight movement of the sample when introduced into the close fitting coil, a small tilt ($\sim 3^{o}$) was detected from the goniometer readings. This is apparent also from observation of pattern I. Close to $\theta = 0^{o}$, general doubling of the lines is a very obvious feature. A good filling factor was achieved with this crystal (c.75%). Before the specimen was re-positioned in the probe, the small capillary of deuterated acetone (Sec.III.B) was lightly attached to the crystal support by means of plasticine and a touch of polystyrene cement.

(ii) Crystal for pattern II ([a])

This specimen was prepared by halving the previous crystal and mounting one of the fragments along [a]. A thin, strong nylon thread was used for the long and delicate sawing operation: now and again it was moistened with $D_2O$ to help local dissolution of the material. The file and a sharp scalpel helped to enlarge and deepen the fine groove thus obtained. The cut surface was further filed and rounded for a better fit

to the coil. The same general technique (with plasticine etc.) was followed as for crystal I. Goniometric readings were taken and the capillary of hexadeuteroacetone added in the same way. The setting for this crystal was quite satisfactory, as pattern II shows; pairs of lines are almost completely collapsed over the full range.

(iii) Crystal for pattern III ([b])

For this pattern, a smaller fraction of the crystal was filed down to fit the coil with the pinacoid face at the top, as close as possible to the horizontal (a small spirit level proved helpful for this purpose). Not many reflections were available for optical goniometry, and the crucial reflection off the top face was of poor quality. A slight tilt was therefore unavoidable.

(e) Recording the Spectra

The working conditions were substantially the same as given in Sec.III.B. A lower r.f. level was necessary than for $ND_4DSO_4$ at room temperature.

$$r.f. = 330 \text{ mV} \quad (r.f. \text{ at coil} = 118 \text{ mV})$$

Depth of modulation $\simeq 1$ gauss

The r.f. frequency was read at the start and end of the day. The temperature was also checked with a thermometer inside the large copper can; its value remained fairly constant for the same day ($\pm 0 \cdot 5^o$C), once the magnet had stabilised. Day to day variations did not influence the average value for room temperature spectra ($29 \cdot 5^o$C) by more than $\pm 1 \cdot 2^o$. The low temperature spectra were obtained under virtually the same operating conditions.

FIG V-4   Sr(DCOO)$_2$ 2D$_2$O   PATTERN I   c AXIS

300K
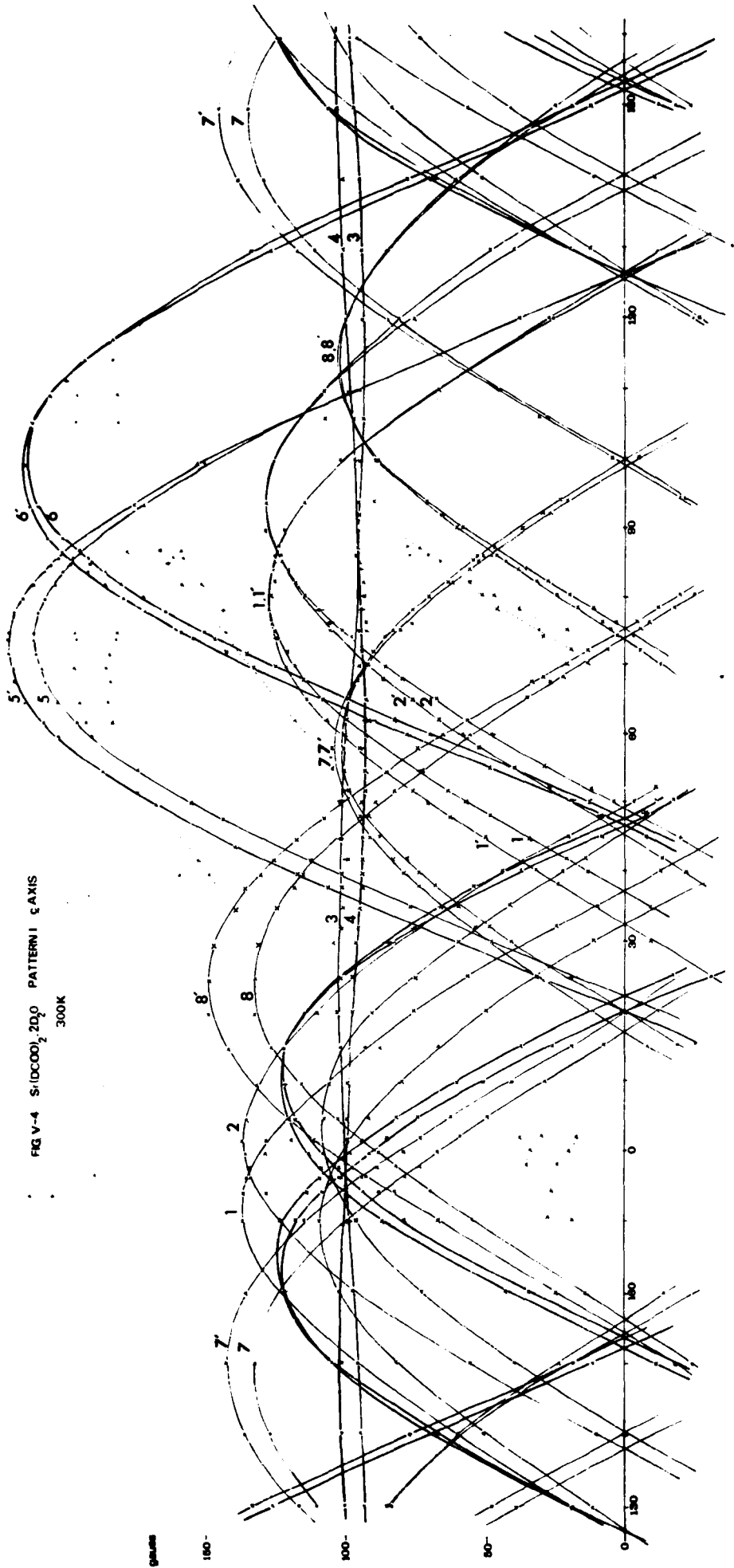
The fourteen main signals were readily observable ($\frac{S}{N} \geq 3$); no C.A.T.

enhancement was found necessary. Some other signals, weak ($\frac{S}{N} \simeq 2$) and

fairly broad ($\sim 7$ g.), were detectable in certain field positions,

especially near to axis crossing points and where superposition of

neighbouring signals and/or their own fine structure permitted. Parts of

the corresponding curves are marked in dashed lines on some of the

patterns (Sec.V.3a). The number of these lines was difficult to establish,

given the weakness of the resonances; from pattern II (for which the crystal

was better set) as reference, twelve such lines were fairly conclusively

established. These have all been assigned to the same $D_2O$ molecule,

and are considered separately in Sec.V.5c.


3. Results

    (a) Patterns I, II and III

       All of the experimental results for $Sr(DCOO)_2 \cdot 2D_2O$ are given in

Patterns I, II and III (Figs. V.4, V.5 and V.6), and the corresponding

tables for regular angular intervals in Appendix II. For all rotation

patterns, half splittings (in gauss), as measured from the reference

signal and corrected for drift, are plotted against magnet angular

positions. Spectra were normally recorded every $5^{\circ}$ or $10^{\circ}$; a number of

additional intermediate positions were also found necessary.

    Some curves proved fairly difficult to sort out, particularly in

zones very overcrowded with signals (especially in pattern I). The use of

tracing paper, and the mathematical relationships given in Sec.IV.4, again

proved helpful. The most striking regularity of all the patterns is an

almost perfect symmetry about two field positions $90^{\circ}$ apart. This

feature also assisted in the solution of the pattern, one half of which

FIG.V-5 Sr(DCOO)₂2D₂O Pattern # g Axis 300K

FIG V-6  SrHDCOO₂ 2D₂O  PATTERN III  b AXIS
300K
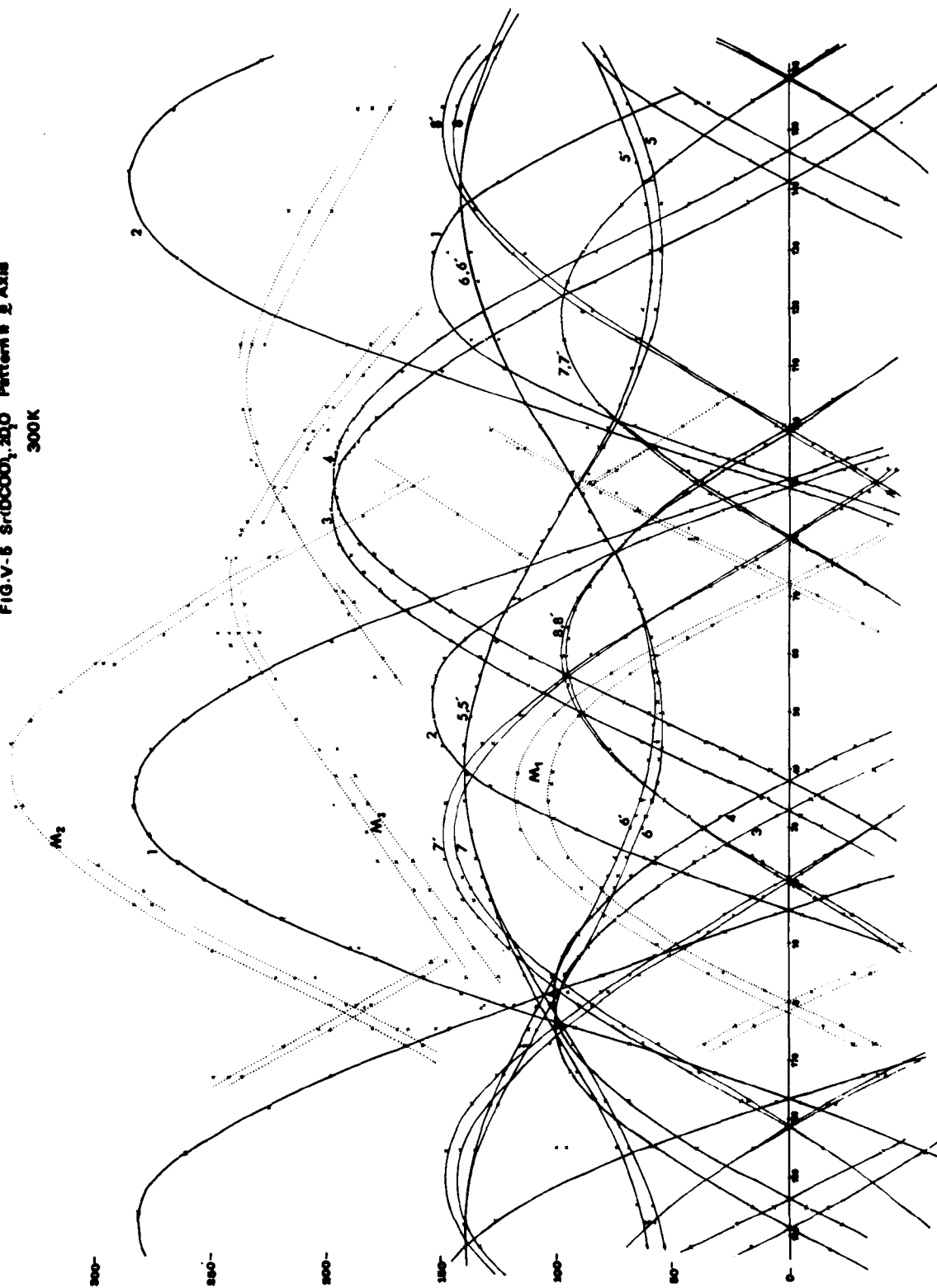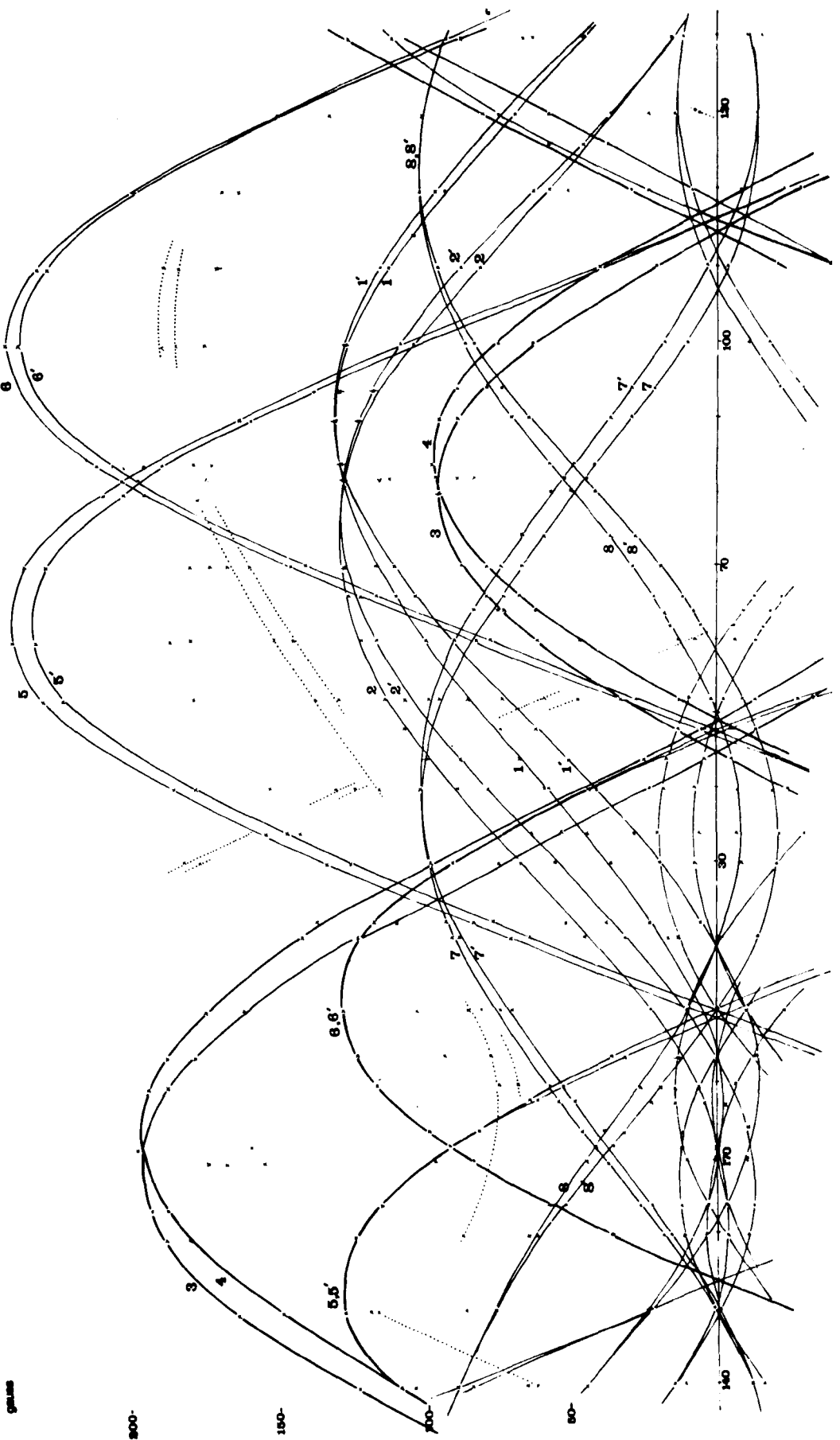
was investigated in considerably more detail. The 'reflected' half

received somewhat sparser attention; a number of supporting spectra at

regular intervals ($10^{\circ}$) was usually sufficient.

The d.m.r. experiment 'sees' a crystal point-symmetry of 222. This

automatically generates a set of three symmetry planes each perpendicular

to one of the two-fold axes. The normals to such planes, and also the

direction of their intersections with the plane $\pi_H$ in which the magnetic

field rotates will necessarily be directions of exact equivalence for

symmetrically related deuterons, regardless of crystal misalignment.

Consequently, these particular orientations of the magnetic field $\overline{H}_{\alpha}$, $\overline{H}_{\beta}$,

$\overline{H}_{\gamma}$ must correspond to a crossing point for all the pairs of deuterons

related to one another by each of the additional symmetry planes. For a

crystal aligned with the rotation axis exactly coincident with a symmetry

axis, only two crossing points for symmetry-related lines would occur,

exactly at $90^{\circ}$ from each other. Complete collapse of pairs of lines

would then occur over the whole range, with considerable simplification

of the rotation patterns. Fig.V.7 gives a pictorial representation of

the form of the patterns for two related deuterons; the three inter-

ception points with the symmetry planes are indicated. Pattern I shows

several clear examples, sometimes rather entangled with each other.

This double character for the lines other than 3 and 4 (Sec.V.5) repeats

throughout all of the patterns, and is particularly serious in pattern I.

For some crystal orientations (particularly in zones of high

splitting), a characteristic fine structure was observed for the signals

of lines 1, 1', 5, 5', 6 and 6'. Each resonance was split into three

components, whose separation and intensity ratio could not be

established with certainty, partly because of interference from the

Fig. V-7 Rotation Pattern for two pairs of
symmetrically related deuterons in a slightly offset crystal
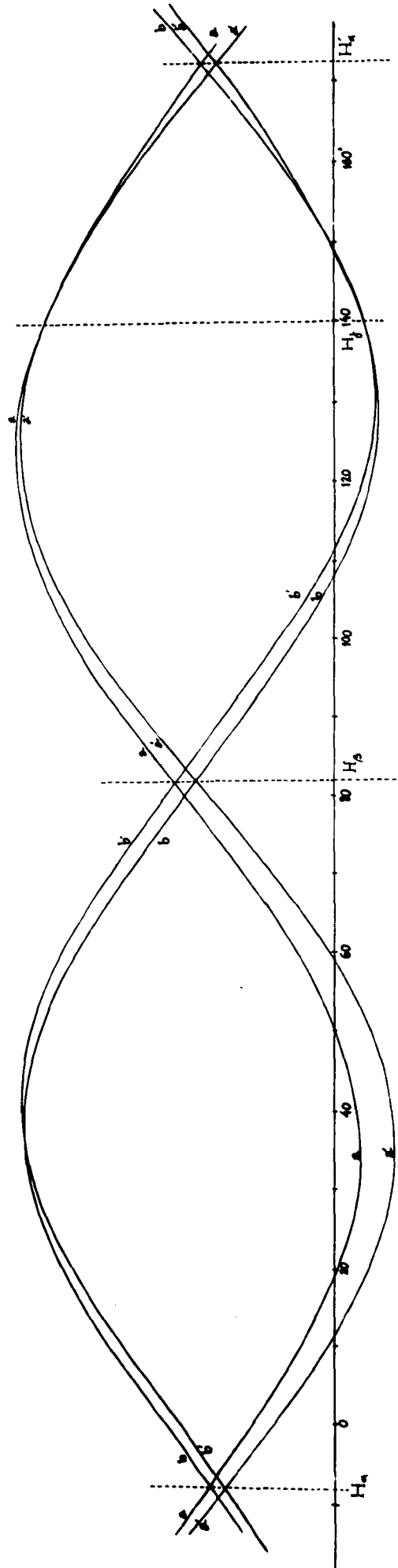
neighbouring signal. Dipole-dipole coupling between the two deuterons

in $D_2O$ is responsible for the line structure. A 1:3:2 intensity ratio

and asymmetrical spacings are predicted for a reorienting $D_2O$ molecule,

while three equally-spaced, equally intense lines should occur for a

stationary molecule (17). The separation of the components depends on

orientation; the maximum spread is about 4KHz. for a flipping molecule,

and 2/3 of this value for a stationary one (18). Deuterons 1, 5 and 6

(and also 2) were therefore allocated to $D_2O$ molecules. Subsequent

determination of the e.f.g. constants confirmed this provisional

assignment.

(b) Low temperature spectra

At a stage when neither the number of signals, nor their

assignments, was clear, it was decided to run some spectra at low

temperature and look for any changes. Crystals I and II were thus

examined under cardice conditions ($\sim$-45°C). The weakness of many of the

resonances, and the increased complexity of the spectra, rendered worse

by the overall doubling of signals due to crystal offset, made comparison

of the spectra difficult for any field position other than the crossing

points, where natural signal reinforcement makes observation more

favourable. As Fig.V.8 shows, the fourteen stronger signals studied at

room temperature (seven at the crossing points) maintain very

approximately their locations. A slight scale expansion is to be expected,

however, due to some increase of the quadrupolar constants (18). New

sets of signals are clearly apparent in zones A and B where at room

temperature a rather poorly-defined disturbance was observed.

Any variations in the number and location of signals will certainly

be caused by a change of motional behaviour of the crystalline $D_2O$

FIGV-6 Pattern B 8Z
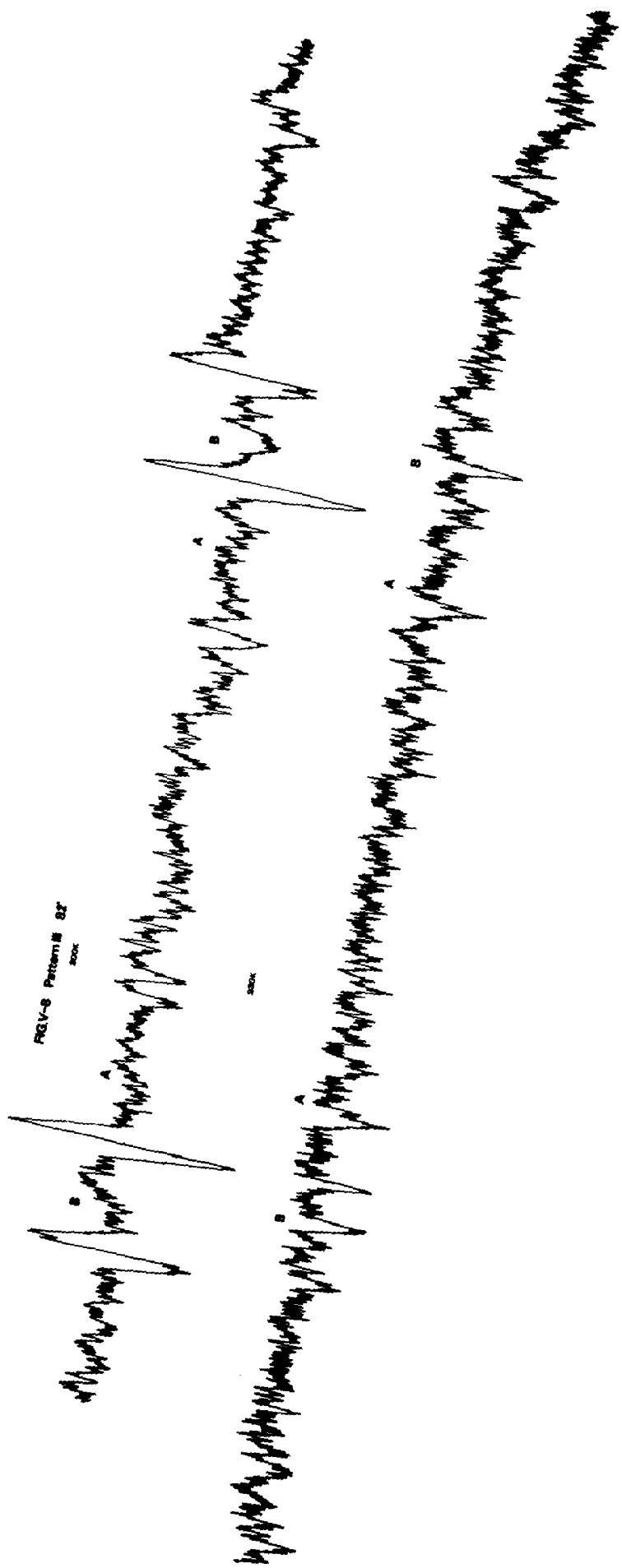
molecules. An ordinary 'static' water molecule will produce in principle

two deuterium resonances, each of these showing a degree of multiplicity

dependent on the symmetry of the crystal. If the intermolecular forces

affecting such a molecule are weak enough to permit a high degree of

freedom, the two deuterons can rapidly switch positions by 'flipping'

about the molecular symmetry axis. A motionally averaged signal will then

result, provided that the frequency of the reorienting movement is higher

than the quadrupolar interaction frequency $e^2qQ/h$. A lowering of

temperature can 'freeze' a flipping molecule in a static position. The

averaged signal should then broaden, fade out completely around the

transition temperature, and finally reappear at two new positions

corresponding to the new quadrupole coupling tensors.

For strontium formate dihydrate there are four molecules per unit

cell in two groups of two crystallographically equivalent entities, yet

all are magnetically independent because of the low crystal symmetry.

A maximum multiplicity of four is to be expected for a particular kind

of deuteron, assuming the crystal is in a general orientation. As already

explained, a perfect alignment of the crystal was not achieved, and for

this reason the anticipated collapse to half the number of lines did not

occur. Table V.1 shows the maximum number of signals predicted and

observed for possible combinations of rotating and stationary water

molecules. The notation for the two kinds of independent molecules

follows Osaki's work (1). The d.m.r. lines have been allocated after

determination of the e.f.g. constants (following section).

The number of signals from $D_2O(II)$ at either temperature is not

clear. As already mentioned, this molecule was the subject of a separate

study (Sec.V.5c). Apart from eliminating possibility (2) from the various

Table V.1

| Deuteron | All $D_2O$ static | All $D_2O$ flipping | 1 $D_2O$ static 1 $D_2O$ flipping | Observed | |
|---|---|---|---|---|---|
| | | | | $303^\circ$K | $230^\circ$K |
| $[DCOO^-]_1$ | 4 | 4 | 4 | $2^*$ | $2^*$ |
| $[DCOO^-]_2$ | 4 | 4 | 4 | 4 | 4 |
| $[D_2O]_1$ | 8 | 4 | $\left\{ \begin{array}{l} 8 \\ \\ 4 \end{array} \right.$ | 8 | 8 |
| $[D_2O]_2$ | 8 | 4 | | very weak | weak |
| Total | 24 | 16 | 20 | 14 strong | |

\* two signals only, because of alignment along [c]

alternatives, the only positive conclusion from the low temperature spectra is that at least one water molecule is reorienting reasonably rapidly at room temperature. This fact, together with a provisional allocation of curves 1 and 6 (and their symmetrically related curves) to $D_2O$ molecules (previous section), provided useful guidelines for the solution of the crystal structure.

## 4. Calculations

### (a) The approximation method

As indicated in Sec.V.2, the poor quality of the reflections from the crystal faces and their imperfect development caused some error in the optical goniometry data. In addition, the large dimensions of the specimen rendered the X-ray results unreliable to a certain degree (16), while the serious background scattering made the photographs very foggy and rather difficult to interpret. In consequence, instead of using the

available goniometric results for calculating the transformation matrix from the crystal to the laboratory frame of reference, an openly approximate method was followed.

Since the crystal offset was never higher than $3^{o}$-$4^{o}$ (rough estimate), and considering that in general a tilt affects any two related deuterons in opposing directions (Fig.V.7), it was decided to take the average of the splittings for such deuterons as the nearest approximation to the value expected for a perfect setting. This procedure simplified in a few instances the curve-deciphering, by avoiding the difficulty of having to decide between pairs of crossing and recrossing adjacent curves. A number of points thus derived are included in brackets in Appendix II.

The average splittings were then treated by the same least square analysis as for $ND_4DSO_4$ (19). Values of $A^*$, $B^*$ and $C^*$ (in gauss) were then doubled (for true line separation) and converted to KHz, after a small correction for the scale factor which allowed for the effective value of the 500 gauss range, which was used throughout. All of these data are summarised in Table 4, Appendix II. At this stage, the signs for $A^*$, $B^*$ and $C^*$ were taken as calculated directly from the pattern readings; the correct relative signs are discussed in Sec.V.4b.

(b) <u>Choice of axes; the e.f.g. tensor components</u>

Since for practical purposes the crystal is to be regarded as accurately set, further simplification can be introduced in the general expressions for A, B and C if all the curves are translated to a crystallographically meaningful azimuth. The natural choice of origin for each pattern was the direction of the intersection of one of the vertical symmetry planes, namely the nearest one to $\theta = 0^{o}$, with the plane of the magnetic field $\pi_{\overline{H}}$. These particular positions were easily and accurately

($< 0 \cdot 1^{\circ}$) found graphically by choosing a set of, say, eight reliable

curves (four symmetrical pairs) and locating their crossing points on an

expanded $\theta$ scale (4 mm/$1^{\circ}$; readings estimated to 0·25 mm). For improved

sensitivity, curves of high slope at the crossing position were chosen

wherever possible. The average values from the four readings were taken;

the crossing points were found to be at $179 \cdot 60^{\circ}$, $171 \cdot 86^{\circ}$ and $176 \cdot 80^{\circ}$ for

patterns [a], [b] and [c] respectively (Figs. V.4, 5 and 6). This purely

graphical method was preferred to the direct use of goniometric data for

reasons of accuracy and simplicity. (For pattern I - [c], the value was

also determined from the goniometer readings as a check; good agreement

between the two methods was obtained).

The equations used for the change of origin are given in Sec.IV.6b;

the new values A', B' and C' are included in Table 4, Appendix II. The

transformation matrices from the crystallographic axes (a,b,c) to this

new set of crystal-based laboratory axes (X', Y',Z') are considerably

simplified as follows:
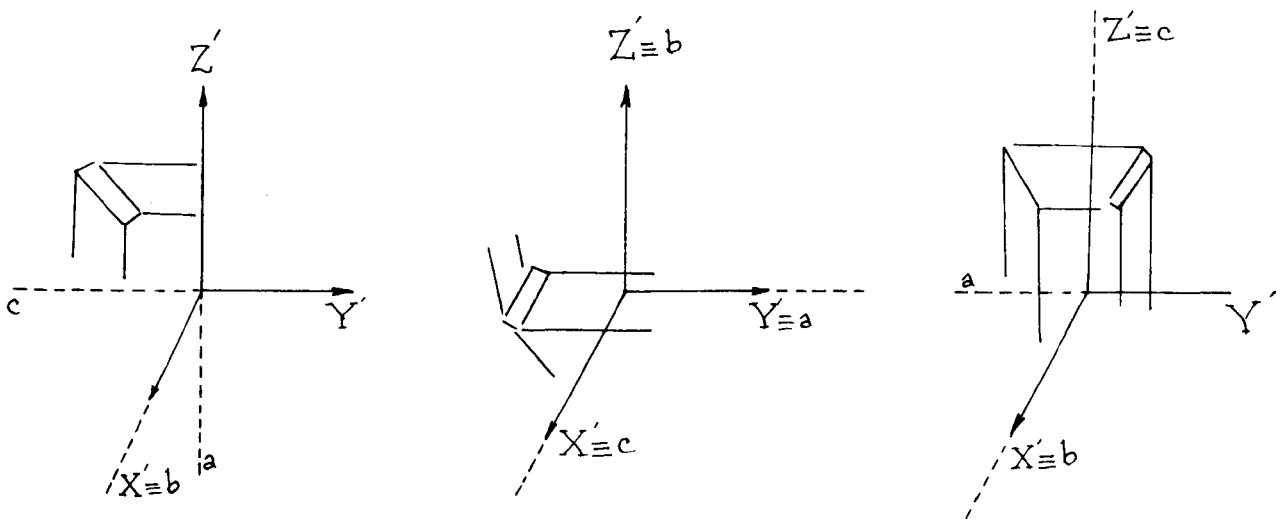


Fig.V.9

Table V.2.A

| Axis | Pat.[a] | | | Pat.[b] | | | Pat.[c] | | |
|------|---|---|---|---|---|---|---|---|---|
| | a | b | c | a | b | c | a | b | c |
| X' | 0 | 1 | 0 | 0 | 0 | 1 | 0 | 1 | 0 |
| Y' | 0 | 0 | -1 | 1 | 0 | 0 | -1 | 0 | 0 |
| Z' | -1 | 0 | 0 | 0 | 1 | 0 | 0 | 0 | 1 |

Using the above direction cosines in the general expression for A, B and C (Sec.II.2. ) we obtain:

Table V.2.B

| Const. | Pattern [a] | Pattern [b] | Pattern [c] |
|--------|-------------|-------------|-------------|
| A' | $\frac{K}{2}[\phi_{22} + \phi_{33}]$ | $\frac{K}{2}[\phi_{33} + \phi_{11}]$ | $\frac{K}{2}[\phi_{11} + \phi_{22}]$ |
| B' | $\frac{K}{2}[\phi_{22} - \phi_{33}]$ | $\frac{K}{2}[\phi_{33} - \phi_{11}]$ | $\frac{K}{2}[-\phi_{11} + \phi_{22}]$ |
| C' | $K\phi_{23}$ | $-K\phi_{13}$ | $K\phi_{12}$ |

Apart from one or two differences in sign due to the particular axis transformation involved, these expressions are virtually the same as those given by Volkoff et al. (20). Similarly, some straightforward relationships concerning the A and B constants can be extracted, e.g.

$$A'_a + A'_b + A'_c = 0$$

$$A'_a + B'_a = A'_c + B'_c$$

$$A'_b + B'_b = A'_a - B'_a$$

$$A'_b - B'_b = A'_c - B'_c$$

All these relationships (especially the first one) were very useful for establishing the relative signs of A' and B' in the three patterns. C posed more of a problem, however. Table 4, Appendix II shows clearly that in each pattern the constants A', B' and C' for symmetrically related deuterons are identical except for the sign of C'. Since the patterns have a high degree of symmetry, and at the main crossing points any two curves A'B'C', A'B'-C' are indistinguishable, some ambiguity can arise in choosing the correct sign arrangement for $C_a'$, $C_b'$, $C_c'$ (out of the eight possible). The indeterminacy can be removed if, for example:

(i) a few spectra can be recorded for the crystal set in one or more intermediate positions, so that each individual line can be followed,

(ii) a reasonably accurate knowledge of the O-D direction from other techniques enables a preliminary guess to be made of the sign of C'. Where the tensors are almost axially symmetrical ($\eta$ very small), the assumption of $\eta = 0$ will simplify the calculations, by removing the need to take into account the difference in magnitude of $q_{xx}$ and $q_{yy}$.

(iii) For the present crystal, where neither (i) nor (ii) was realised, the foolproof technique of investigating the alternative solutions and checking their feasibility is the safest procedure.

Some preliminary investigation was carried out to search for the most likely sets of signs. For this purpose, the general equations for A, B and C (Sec.II.2. ) were used in the special case where the crystal-based set of axes coincides with the principal directions of the e.f.g. tensor for a particular deuteron. All of the off-diagonal components $\emptyset_{ik}$ ($i \neq k$) should then cancel out, the tensor taking a diagonal form. The principal components may be expressed in the form (20)

$$\phi_{11} = -\frac{\phi_{zz}}{2}(1-\eta)$$

$$\phi_{22} = -\frac{\phi_{zz}}{2}(1+\eta)$$

$$\phi_{33} = \phi_{zz} = eq$$

$$\eta = \text{asymmetry parameter}$$

The resulting expressions for A,B and C in the three patterns would then be (when Table V.2.A is taken into consideration):

$$A_a = \frac{K\phi_{zz}}{4}[(1-3\alpha_{13}^2) + \eta(\alpha_{11}^2 - \alpha_{12}^2)] \tag{1}$$

$$B_a = \frac{K\phi_{zz}}{4}\{3(\alpha_{23}^2 - \alpha_{33}^2) - \eta[(\alpha_{23}^2 - \alpha_{33}^2) + 2(\alpha_{22}^2 - \alpha_{32}^2)]\} \tag{2}$$

$$C_a = \frac{K\phi_{zz}}{2}[3\alpha_{23}\alpha_{33} + \eta(-\alpha_{23}\alpha_{33} - 2\alpha_{22}\alpha_{32})] \tag{3}$$

$$A_b = \frac{K\phi_{zz}}{4}[(1-3\alpha_{23}^2) - \eta(\alpha_{21}^2 - \alpha_{22}^2)] \tag{4}$$

$$B_b = \frac{K\phi_{zz}}{4}\{3(\alpha_{33}^2 - \alpha_{13}^2) - \eta[(\alpha_{33}^2 - \alpha_{13}^2) + 2(\alpha_{32}^2 - \alpha_{12}^2)]\} \tag{5}$$

$$C_b = \frac{K\phi_{zz}}{2}[-3\alpha_{13}\alpha_{33} + \eta(\alpha_{13}\alpha_{33} + 2\alpha_{12}\alpha_{32})] \tag{6}$$

$$A_c = \frac{K\phi_{zz}}{4}[(1-3\alpha_{33}^2) - \eta(\alpha_{31}^2 - \alpha_{32}^2)] \tag{7}$$

$$B_c = \frac{K\phi_{zz}}{4}\{3(\alpha_{23}^2 - \alpha_{13}^2) - \eta[(\alpha_{23}^2 - \alpha_{13}^2) + 2(\alpha_{22}^2 - \alpha_{12}^2)]\} \tag{8}$$

$$C_c = \frac{K\phi_{zz}}{2}[3\alpha_{13}\alpha_{23} + \eta(-\alpha_{13}\alpha_{23} - 2\alpha_{12}\alpha_{22})] \tag{9}$$

where $\dfrac{K\phi_{zz}}{4} = \dfrac{Keq}{4} = \dfrac{3}{8}\dfrac{e^2qQ}{h}$

$\alpha_{iK}$ represent the direction cosines of the principal axes in the abc crystallographic set.

If the identity relationship between the OD direction and the $q_{zz}$ ($\alpha_{13}$, $\alpha_{23}$, $\alpha_{33}$) vector is taken as valid, and $\eta$ put equal to zero, the possible sign arrangements of C for four symmetrically related deuterons ($\alpha_{ik}$)

| 1 | 2 | 3 | 4 |
|---|---|---|---|
| $\alpha_{13}$ | $-\alpha_{13}$ | $-\alpha_{13}$ | $\alpha_{13}$ |
| $\alpha_{23}$ | $\alpha_{23}$ | $-\alpha_{23}$ | $-\alpha_{23}$ |
| $\alpha_{33}$ | $-\alpha_{33}$ | $\alpha_{33}$ | $-\alpha_{33}$ |

are found to be

| | | | |
|---|---|---|---|
| + | - | - | + |
| - | - | + | + |
| + | - | + | - |
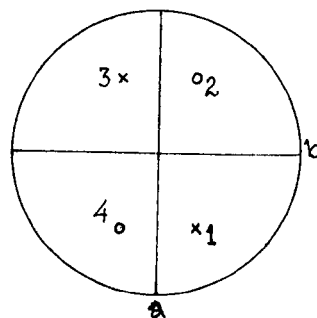


(K eq = $K\emptyset_{zz}$ was taken as positive).

All these conclusions can also be easily deduced from stereographic projections, especially by considering deuterons not far off the plane of the magnetic field $\pi_{\frac{}{H_o}}$ . In such cases it can be shown (Appendix II,3) that the location of the maximum in the rotation pattern is close to the projection of the OD vector on $\pi_{\frac{}{H_o}}$ . The positions of the curves may then be readily visualised. The above conclusions may not hold and 'forbidden' sign combinations appear for large asymmetry parameters, if any of the $\alpha_{i3}\alpha_{k3}$ products become very small, since the terms in $\eta$ may then determine the sign of C. For this reason, deuterons very close to a plane or an axis of symmetry (such as deuterons 3 and 4) have to be examined for other sign arrangements. Although not a rigid criterion for the choice of signs in a crystal of 222 symmetry, this method proved quite useful as a working hypothesis.

Table V.2 shows that six equations are available for finding the three diagonal components $\phi_{11}$, $\phi_{22}$, $\phi_{33}$ of this tensor. A seventh could be added since the tensor is traceless

$$\left( \sum_{i=1}^{3} \phi_{ii} = 0 \right)$$

This equation was only used occasionally, however; instead the experimental trace was given for each deuteron as an indication of the accuracy of the results. If all the six equations above were equal in weight as regards experimental accuracy and reliability, a least squares treatment would be justified.

The general expression for least squares applied to the system A = V is (21):

i)  $(A_t A)^{-1} A_t V = \phi$

where in this instance

$$A = \begin{bmatrix} 0 & 1 & 1 \\ 0 & 1 & -1 \\ 1 & 0 & 1 \\ -1 & 0 & 1 \\ 1 & 1 & 0 \\ -1 & 1 & 0 \end{bmatrix} \qquad V = \begin{bmatrix} 2A_a \\ 2B_a \\ 2A_b \\ 2B_b \\ 2A_c \\ 2B_c \end{bmatrix} \qquad \phi = \begin{bmatrix} K\phi_{11} \\ K\phi_{22} \\ K\phi_{33} \end{bmatrix}$$

The development of expression (i) gives:

$$K\phi_{11} = \tfrac{1}{2}(A_b - B_b + A_c - B_c)$$

$$K\phi_{22} = \tfrac{1}{2}(A_a + B_a + A_c + B_c)$$

$$K\phi_{33} = \tfrac{1}{2}(A_a - B_a + A_b + B_b)$$

If a curve in one pattern, say [c], gives less reliable values of A, B

and C, or appears from the pattern to be extensively affected by tilt,

its corresponding equations may be ignored, and from the remaining four, we

would obtain

$$K\phi_{11} = A_b - B_b$$

$$K\phi_{22} = A_a + B_a$$

$$K\phi_{33} = \tfrac{1}{2}[A_a - B_a + A_b + B_b]$$

The second pattern ([a]) is from a crystal very close to the correct

setting, while the third is the worst from this point of view. The values

of $\phi_{ii}$ shown in Table V.3 are thus optimised either from three patterns,

or sometimes from two, and in one or two cases even from $\phi_{11} = -2A_a$.

This procedure attenuates to some extent the errors introduced by the

approximation method. Unfortunately, $C_a$, $C_b$ and $C_c$ only occur in one

equation, and so they become one of the most important sources of error,

affecting particularly the $q_{xx}$ and $q_{yy}$ eigenvectors.

Since the approximation method effectively halves the number of data by

averaging all pairs of closely spaced lines, the consideration of two

rather than four symmetrically related deuterons is a more realistic view.

These have been arbitrarily chosen as the pairs related by [b]. Table 4,

Appendix II gives the final choice of signs before diagonalisation of the

interaction tensor. For deuterons 3 and 4, which are nearly aligned

along [c], two possible alternatives are included, the most likely solution

(discussed in Sec.V.5) being given first.

As an extra precaution, one of the alternative sign arrangements for

C has also been examined for each of deuterons 1, 6 and 7. The $q_{zz}$

eigenvectors were evaluated, together with the asymmetry parameter and quadrupolar constant. The results proved their early non-selection to be fully justified.

| Deuteron | $q_{zz}$ | $\dfrac{e^2qQ}{h}$ (KHz) | $\eta$ |
|:---:|:---:|:---:|:---:|
| 1 | [0·0251, −0·7944, −0·6068] | 241·1 | 0·24 |
| 6 | [0·9415, −0·1682, 0·2920] | 208·4 | 0·51 |
| 7 | [0·6317, 0·4478, 0·6104] | 152·2 | 0·85 |

(c) Calculated Results

The main calculated results for this crystal (except for molecule $[OD_2]_2$) are tabulated below.

Symmetry relationships between pairs of deuterons 1,2; 3,4; 5,6; 7 and 8 are quite evident; their eigenvectors differ from each other only in signs. These signs do not necessarily correspond to the directions chosen from a crystallographic study. With second rank tensors, the choice of the positive direction of the principal axes is not significant (20).

Numerically, the absolute values of the direction cosines are not completely identical; random experimental errors as well as the systematic errors introduced by the approximation method are responsible for this divergence. The limits of error introduced by the approximation method are difficult to assess and depend on the individual case. It can easily be shown by means of a stereographic projection or an approximate calculation, for example, that:

(i) errors should be minimal when the plane of the magnetic field intercepts the 'horizontal symmetry plane' close to or along one of the

## Table V.3
### The interaction tensor at 300°K

(All components in KHz; frame of reference (abc) as in Fig.V.9)

Deuteron 1

$$\begin{bmatrix} -160 \cdot 07 & -33 \cdot 87 & -22 \cdot 73 \\ -33 \cdot 87 & 153 \cdot 70 & 270 \cdot 85 \\ -22 \cdot 73 & 270 \cdot 85 & 8 \cdot 00 \end{bmatrix}$$

Expl. trace = 1·62 KHz

Deuteron 2

$$\begin{bmatrix} -160 \cdot 74 & 36 \cdot 24 & -21 \cdot 92 \\ 36 \cdot 24 & 154 \cdot 10 & -270 \cdot 00 \\ -21 \cdot 92 & -270 \cdot 00 & 7 \cdot 69 \end{bmatrix}$$

Expl. trace = 1·05 KHz

Deuteron 3

$$\begin{bmatrix} -121 \cdot 52 & \pm 4 \cdot 20 & 13 \cdot 93 \\ \pm 4 \cdot 20 & -128 \cdot 36 & 16 \cdot 32 \\ 13 \cdot 93 & 16 \cdot 32 & 250 \cdot 16 \end{bmatrix}$$

Expl. trace = 0·28 KHz

Deuteron 4

$$\begin{bmatrix} -120 \cdot 90 & \mp 4 \cdot 47 & 13 \cdot 71 \\ \mp 4 \cdot 47 & -129 \cdot 36 & -16 \cdot 85 \\ 13 \cdot 71 & -16 \cdot 85 & 250 \cdot 15 \end{bmatrix}$$

Expl. trace = -0·11 KHz

(top set of signs, solution α)
(bottom set of signs, solution β)

Deuteron 5

$$\begin{bmatrix} 251 \cdot 00 & 96 \cdot 18 & -142 \cdot 27 \\ 96 \cdot 18 & -134 \cdot 84 & -53 \cdot 08 \\ -142 \cdot 27 & -53 \cdot 08 & -115 \cdot 69 \end{bmatrix}$$

Expl. trace = 0·47 KHz

Deuteron 6

$$\begin{bmatrix} 251 \cdot 32 & -96 \cdot 20 & -142 \cdot 27 \\ -96 \cdot 20 & -135 \cdot 20 & 52 \cdot 26 \\ -142 \cdot 27 & 52 \cdot 26 & -116 \cdot 08 \end{bmatrix}$$

Expl. trace = 0·04 KHz

Deuteron 7

$$\begin{bmatrix} -61 \cdot 77 & -127 \cdot 94 & -73 \cdot 00 \\ -127 \cdot 94 & 110 \cdot 18 & 133 \cdot 91 \\ -73 \cdot 00 & 133 \cdot 91 & -48 \cdot 22 \end{bmatrix}$$

Expl. trace = 0·19 KHz

Deuteron 8

$$\begin{bmatrix} -62 \cdot 06 & 129 \cdot 42 & -72 \cdot 48 \\ 129 \cdot 42 & 111 \cdot 35 & -133 \cdot 06 \\ -72 \cdot 48 & -133 \cdot 06 & -48 \cdot 96 \end{bmatrix}$$

Expl. trace = 0·33 KHz

Table V.4

The Diagonalised Interaction Tensors

(abc axes defined in Fig.V.9; for the location of the atoms
in the structure see Fig.V.10)

| Deut. | | Eigenvectors | | | Eigenvalues (KHz) $K\phi_{xx}$, $K\phi_{yy}$, $K\phi_{zz}$ | Quad. const. $\dfrac{e^2 qQ}{h}$ (KHz) | Asymmetry parameter $\eta$ |
|---|---|---|---|---|---|---|---|
| | | $q_{xx}$ | $q_{yy}$ | $q_{zz}$ | | | |
| 1 | a | 0•9946 | −0•0696 | 0•0774 | −163•1 | 243•0 | 0•101 |
| | b | 0•0188 | −0•6109 | −0•7915 | −199•8 | | |
| | c | 0•1023 | 0•7886 | −0•6063 | 364•5 | | |
| 2 | a | 0•9886 | 0•1286 | 0•0800 | −163•5 | 242•7 | 0•099 |
| | b | 0•0144 | −0•6102 | 0•7921 | −199•4 | | |
| | c | 0•1496 | −0•7817 | −0•6051 | 364•0 | | |
| $3_\alpha$ | a | −0•9201 | 0•3897 | 0•0378 | −120•5 | 167•6 | 0•040 |
| | b | −0•3882 | −0•9206 | 0•0433 | −130•6 | | |
| | c | 0•0517 | 0•0244 | 0•9984 | 251•4 | | |
| $4_\alpha$ | a | 0•9340 | 0•3553 | 0•0373 | −120•0 | 167•6 | 0•046 |
| | b | −0•3536 | 0•9343 | −0•0446 | −131•6 | | |
| | c | −0•507 | 0•0282 | 0•9983 | 251•4 | | |
| $3_\beta$ | a | 0•8917 | 0•4512 | 0•0368 | −119•6 | 167•6 | 0•047 |
| | b | −0•4525 | 0•8908 | 0•0425 | −131•5 | | |
| | c | −0•0136 | −0•0546 | 0•9984 | 251•4 | | |
| $4_\beta$ | a | −0•9083 | 0•4168 | 0•0362 | −119•1 | 167•6 | 0•053 |
| | b | −0•4181 | −0•9073 | −0•0438 | −132•4 | | |
| | c | 0•0146 | −0•0547 | 0•9984 | 251•4 | | |
| 5 | a | −0•3831 | 0•1032 | 0•9179 | −143•7 | 216•8 | 0•115 |
| | b | 0•7244 | 0•6501 | 0•2293 | −181•0 | | |
| | c | −0•5731 | 0•7528 | −0•3238 | 325•2 | | |
| 6 | a | 0•3817 | 0•1044 | 0•9184 | −144•7 | 216•9 | 0•110 |
| | b | 0•7268 | −0•6477 | −0•2285 | −180•6 | | |
| | c | 0•5710 | 0•7547 | −0•3231 | 325•3 | | |
| 7 | a | 0•0054 | 0•9068 | 0•4216 | −124•6 | 170•0 | 0•022 |
| | b | 0•4977 | 0•3633 | −0•7876 | −130•3 | | |
| | c | −0•8674 | 0•2141 | −0•4493 | 255•1 | | |
| 8 | a | 0•1061 | 0•9001 | 0•4229 | −124•2 | 170•5 | 0•028 |
| | b | 0•4448 | −0•4230 | 0•7893 | −131•3 | | |
| | c | 0•8893 | 0•1042 | −0•4452 | 255•8 | | |

symmetry axes (pattern II provides a good example, favoured further by a very small tilt);

(ii) errors can be more important for deuterons whose $q_{zz}$ vector (bond direction) approaches the magnetic field rotation axis (the curves are easily recognised by their flattened-out appearance).

It is not surprising, therefore, that in pattern [b] curves 1,2,7 and 8 show such extensive effects of tilt. Fortunately C' is not very large for curves of this kind (Eqs. (3),(6),(9) in Sec.V.4b), and so its effect on $q_{zz}$, and indeed on the quadrupolar constant, is not excessive. (In (i) and (ii) above the asymmetry parameter has been assumed to be small).

Whatever the source, errors normally affect the values of $q_{xx}$ and $q_{yy}$ to a larger degree than the $q_{zz}$ values, which are generally in very good agreement. Larger errors in $q_{yy}$ and $q_{xx}$ (and characteristic roots) than in $q_{zz}$ have been found in other compounds where location of the curves became very difficult because of saturation effects (7). Unless the principal directions of the interaction tensor concerned (particularly $q_{zz}$ for $\eta \simeq 0$) make similar angles with a, b and c (e.g. deuterons 7 and 8) or at least two of these angles approach $45^o$ (e.g. deuterons 1 and 2), it is unlikely that the off diagonal elements of the tensor will be dominant in the determination of $K\phi_{zz}$ and $q_{zz}$. This empirical idea is easily confirmed from Eqs. 1-9, which show that for $\alpha_{13}^2 \simeq \alpha_{23}^2 \simeq \alpha_{33}^2 \simeq \frac{1}{3}$ the A values become very small and the C values are relatively large, while if $\alpha_{13} \simeq \alpha_{23} \simeq \frac{\sqrt{2}}{2}$, $C_c$ is very large indeed (at least of the order of magnitude of the quadrupolar constant). The conclusions for $q_{yy}$ are the reverse since basically it results from diagonalising the inverse of the original matrix.

A further contribution to the difference in errors may arise from the least squares treatment of the $\phi_{xx}$, $\phi_{yy}$ and $\phi_{zz}$ tensor components. Since these components were in most instances the largest numerically, they were the dominant factors in the first stage of diagonalisation, thus attenuating the relative errors to some extent.

The joint effect of the approximation method and of the sharp dependence of C on orientation are thus the main sources of error in the principal directions $q_{xx}$ and $q_{yy}$, but to a lesser extent for $q_{zz}$ and the quadrupolar constant. Deuterons 7 and 8 are a possible exception. The error should not be excessive, however, since the asymmetry parameter, which is very sensitive to the value of $K\phi_{11}$ and $K\phi_{22}$, is within reasonable limits for all deuterons.

Other errors committed are of smaller importance and arise from several sources. These include:

(i) the error in an individual least square study of the original curves, which is fairly low. The value is not really meaningful compared with the much larger errors resulting from the approximation method;

(ii) fluctuation of frequency, and temperature of sample;

(iii) non-linearity of sweep (Sec.III.2);

(iv) assumption of a constant drift rate for the magnetic field;

(v) calibration of the 500 gauss range. This was extrapolated from the 100 and 250 gauss ranges. For both of these, the sweep was 98•07% of the nominal value;

(vi) measurement errors on the spectra. These amounted to no more than 0•25 mm. ( 0•13 gauss) for sharp signals, but were at least 0•5 mm. (0.25 gauss) for broader and weaker resonances. A metre steel ruler was

used as the most reliable for linearity.

(vii) Errors in the location of the individual components of a superposed signal.

(viii) Interpolation errors for angles where experimental results were not available (Sec.II.2).

(ix) Imperfections from the crystal specimen (22).

The maximum difference between the absolute values of any two readings is probably a guide to the order of magnitude of the overall error.

$$q_{xx}, \quad q_{yy} \quad \text{deviations within } 7^{\circ} \ (\sim 1\%)$$

$$q_{zz} \quad \text{agreement to better than } 0.1\%.$$

A somewhat arbitrary value of 3 KHz can be given as a safe upper limit of error in the quadrupolar constant.

5. <u>Discussion</u>

The construction of a model from Osaki's X-ray data immediately reveals the role of the strontium ions as the main orienting factors in the structure. A sketch of the structure, (after Osaki), including the identified deuterons, is shown in Fig.V.10. Water molecules and formate ions cluster round the strontium ions in such a way as to complete an eight-fold co-ordination. The distances between strontium and the nearest oxygen atoms of the ligands are in the range 2.40Å to 2.66Å (1). Moreover, the strontium ions constitute the skeleton of a complex helicoidal chain parallel to [c]. Four oxygen atoms from four different formate groups (O(1), O(1'), O(3), O(3')) and two others from water molecules form the bridges. Only $H_2O(2)$ and O(2) (in C(1)O(1)O(2)) are not involved in
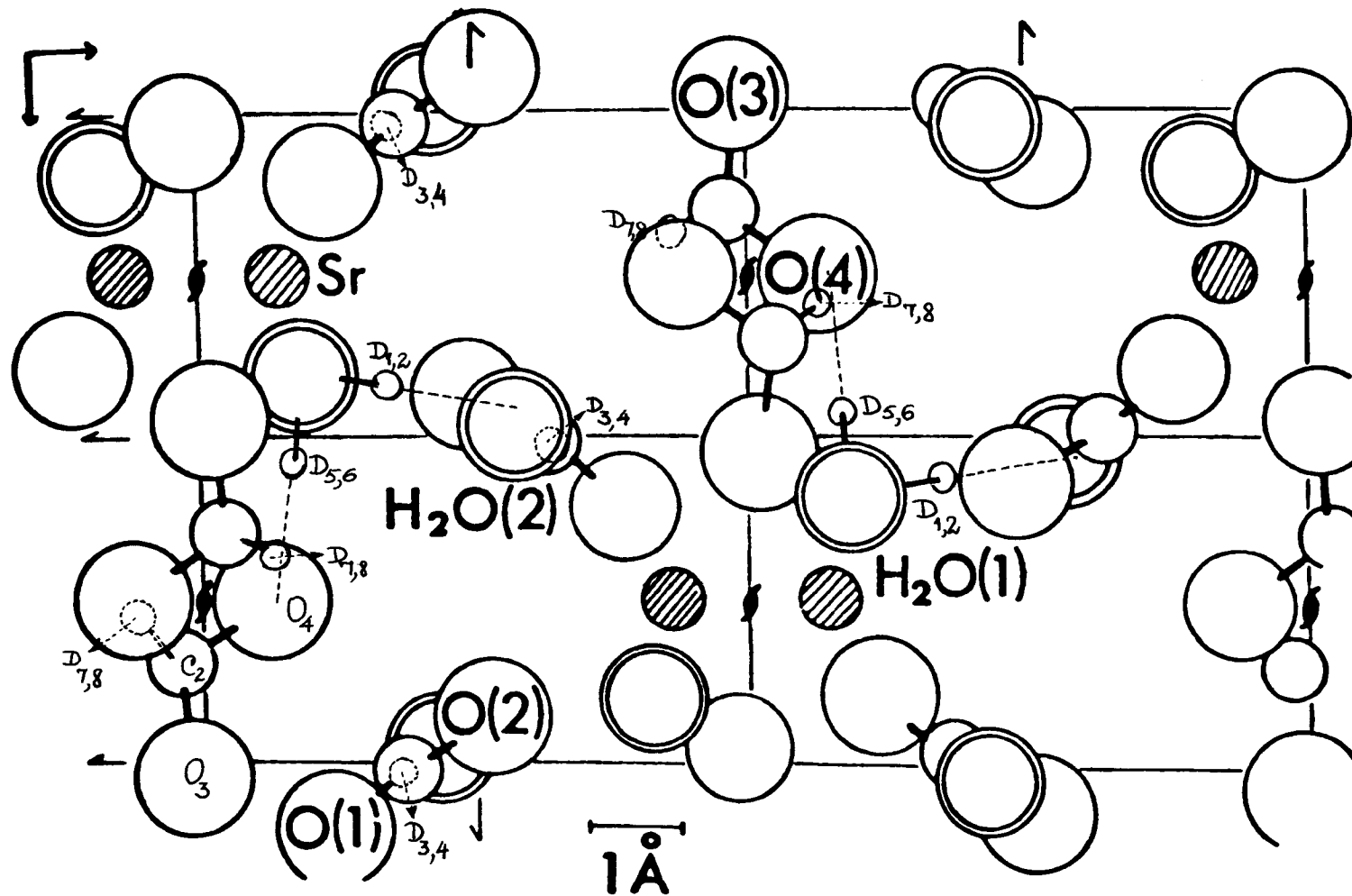
Fig.V.10.   Structure of Strontium Formate Dihydrate Viewed down [001]

bridging, although still within the co-ordination sphere of $Sr^{2+}$. Of all the oxygen atoms in the structure, O(4) seems the least subject to the influence of $Sr^{2+}$, $\sim 3.6\overset{\circ}{A}$ away. All these features give rise to a strongly-bonded structure, as is also shown by other evidence. The smaller compressibility of strontium formate dihydrate compared with the anhydrous salt, for example, shows a considerable increase in bond forces caused by H-O interaction (11).

In the present work, it can readily be deduced from the values of the quadrupolar constants and asymmetry parameters that deuterons 1,2,5 and 6 belong to stationary $D_2O$ molecules, while deuterons 3,4,7 and 8 are assigned to formate ions. It is interesting to note that deuterons 3 and 4 are aligned almost along the $[c]$ axis ($< 3.4^{\circ}$ from it). Because of the crystal structure, these lines do not show the characteristic doubling. Along the axis directions, the deuterons behave as though they were related by an additional centre of inversion, whatever the crystal position. Formate and water groups will now be discussed separately in more detail.

(a) <u>The formate ions</u>

It is clear from the tables in the previous section that both formate deuterons give rise to an almost axially symmetrical tensor ($\eta_1$ = 0.043; $\eta_2$ = 0.025). This is to be expected because of the immediate environment of these atoms. The quadrupolar constants and asymmetry parameters are given in the table below, together with the values for other C-D deuterons. It is apparent from the table that when the carbons have electronegative substituents, the quadrupolar constants are lower. The value for the formate ion is in accordance with this observation. A similar correlation between electronegativity and the magnitude of the quadrupolar constant has been given very recently (7). The constants for

Table V.5

| Compound and Physical State | $e^2qQ/h$ KHz. $\qquad$ $(\eta)$ | Ref. |
|---|---|---|
| $CD_2=CO$ vapour | $246 \pm 5$ | 23 |
| $C_6D_6$ polycrystalline | $193 \pm 3$ | 24 |
| HDCO vapour | $170.0 \pm 2.0$ $\qquad$ $(< 0.15)$ | 25 |
| $Cu(DCOO)_2.4D_2O$ single crystal | $161 \pm 2$ $\qquad$ $(0.034 \pm 0.020)$ | 5 |
| $Sr(DCOO)_2.2D_2O$ single crystal | $167.6 \pm 3$ $\qquad$ $(0.043 \pm 0.010)$ (deuteron 3) | This work |

both formate ions are in good agreement with literature values for copper(II) formate tetrahydrate (5) and formic acid (7) determined by d.m.r., and for formic acid (26) and formaldehyde (25) as found by microwave spectroscopy.

Some general geometric features are shown in Table V.6. The angle $\emptyset'_z$ is given between the C-D direction as obtained by d.m.r. $(q_{zz})$ and the calculated direction of the bisector $\bar{B}$ of the $C \overset{O_\alpha}{\underset{O_\beta}{<}}$ angle. (This would give the C-D direction for a symmetrical planar formate ion). The latter was found by considering the two main conditions of

(i) coplanarity $(\overline{CO}_\alpha \wedge \overline{CO}_\beta)/\bar{B} = 0$

(ii) equality of angles $\bar{B}/\overline{CO}_\alpha = \bar{B}/\overline{CO}_\beta$ $\therefore$ $\bar{B}/(\overline{CO}_\alpha - \overline{CO}_\beta) = 0$

A homogeneous system of two equations in $\alpha$, $\beta$ and $\gamma$ results. If $\gamma$ is taken as 1, $\alpha$ and $\beta$ can then be easily evaluated. $(\alpha \; \beta \; 1)$ is afterwards normalised and the signs selected which make $\bar{B}$ the bisector of the largest angle

$(> 180^{o})$. $\phi'_x$ is the calculated angle between $q_{xx}$ and the normal to the plane of the carboxyl group. There is a strong indication (5) that they should be close to each other (within 10 or $15^{o}$). $\phi_{\pi}$ measures the deflection of $q_{zz}$ from the $CO_{\alpha}O_{\beta}$ plane. Some data have been included in the table from copper(II) formate tetrahydrate.

<div align="center">Table V.6</div>

| Deut. | $q^{\alpha}_{zz}$, dir.cos (abc axes) | $q^{\beta}_{zz}$, dir.cos (abc axes) | bisector $C\begin{smallmatrix}O\\O\end{smallmatrix}$ (calc.) | $\phi'_z$ | $\phi'_x$ | $\phi_{\pi}$ |
|---|---|---|---|---|---|---|
| 3 $\alpha,\beta$ | -0.0378 -0.0433 -0.9984 | -0.0368 +0.0425 -0.9984 | -0.0693 -0.0368 -0.9969 | $1.8^{o}_{\alpha}$ $(4.9^{o}_{\beta})$ | $13.6^{o}_{\alpha}$ $(10.2^{o}_{\beta})$ | $1.2^{o}_{\alpha}$ |
| 4 $\alpha,\beta$ | 0.0373 -0.0446 0.9983 | 0.0362 +0.0438 0.9984 | 0.0693 -0.0368 0.9969 | $1.9^{o}_{\alpha}$ $(5^{o}_{\beta})$ | $15.7^{o}_{\alpha}$ $(12.2^{o}_{\beta})$ | $1.2^{o}_{\alpha}$ |
| 7 | 0.4216 -0.7876 -0.4493 | | 0.4009 -0.9127 -0.0790 | $22.6^{o}$ | $22.6^{o}$ | $22.5^{o}$ |
| 8 | -0.4229 -0.7893 +0.4452 | | -0.4009 -0.9127 0.0790 | $22.3^{o}$ | $24.1^{o}$ | $22.3^{o}$ |
| Cu formate Room Temp. | - | - | - | $3.7^{o}$ | $9.4^{o}$ | - |

Results from deuterons 3 and 4 are in good agreement with the general conclusions of planarity, the alignment of $q_{zz}$ with the OD direction, and $q_{yy}$ normal to the plane of $DCOO^-$. Unfortunately, neutron diffraction data are not available for the C-D direction, so that the d.m.r. data cannot be directly checked. In the following discussion the X-ray results of Osaki (1) have been taken as correct; otherwise the conclusions may not be valid. The two solutions $\alpha$ and $\beta$ for deuterons 3 and 4 are so similar that without further refinement of the data, neither can be safely eliminated. The only change between them is a difference of about 8 KHz in one of the off-diagonal tensor components. Although both $\alpha$ and $\beta$ look to be possible solutions, $\alpha$ was selected as the most probable since the $q_{zz}$ vector and the calculated C-D direction are in much closer agreement, which is always to be expected for this principal direction. The signs are also in complete concordance with this solution.

An unexpected feature of the results is the large discrepancy of $22.5^{\circ}$ between the orientations of the predicted and experimental OD vectors for deuterons 7 and 8. Although some uncertainty is to be expected because of the approximation method introduced in solving the structure, a deviation of this order of magnitude is much larger than the likely experimental error of $\pm 3^{\circ}$. The projection on the bc plane is the most affected; the angular component along [c] has a striking variation of $\sim 22^{\circ}$ in the direction of that axis. This is shown clearly in Table V.7; the experimental constants for deuteron 7 in patterns [a], [b] and [c] are compared with those calculated for a hypothetical deuteron along $\overline{B}$. In the calculations, $\dfrac{e^2 qQ}{h}$ was taken as 166 KHz (5) and the e.f.g. tensor has been assumed to be axially symmetrical. (Equations 1-9 (Sec.V.4 were used).

The third set of data is derived from the experimental values by assuming

axial symmetry (i.e. $\eta = 0$), to check the order of magnitude of the errors

thus introduced. They do not exceed 5 KHz (for C, which is always more

sensitive to approximations).

<div align="center">Table V.7</div>

| Pat. | Constants calculated from Osaki's data | | | Experimental Constants | | | Corrected expl. constants for $\eta = 0$ | | |
|------|------|------|------|------|------|------|------|------|------|
| | A | B | C | A | B | C | A | B | C |
| [a] | 32.2 | 154.4 | -26.9 | 24.5 | 79.5 | -133.1 | 28.9 | 79.3 | -131.2 |
| [b] | -93.3 | -28.9 | 11.8 | -55.2 | 6.3 | 72.5 | -54.1 | 3.6 | 70.3 |
| [c] | 61.1 | 125.5 | 136.7 | 31.0 | 87.2 | 129.4 | 25.2 | 82.9 | 124.7 |

If Osaki's results are assumed to be correct, and a safe upper limit

of error in the $\overline{q}_{zz}$ direction cosines is taken as $\pm 3^{\circ}$, it must be

concluded that this particular formate ion has a non-planar configuration.

Although outside the C(2)O(3)O(4) plane, the deuterium atom still belongs

to a plane bisecting the $C\begin{smallmatrix}\diagup O\\ \diagdown O\end{smallmatrix}$ angle:

angle$[\overline{CD},\overline{CO}(3)] \simeq$ angle$[\overline{CD},\overline{CO}(4)] = 114 \pm 1.6^{\circ}$. A very weak interaction

between this deuterium atom and the nearest oxygen from another formate

ion may perhaps be present. For this particular formate ion, one of the

oxygen atoms is closely involved with two neighbouring strontium atoms,

only $\sim 2.5\text{Å}$ away in a very favourable, almost trigonal configuration, as

shown in Fig.V.11 below.

Fig.V.11.
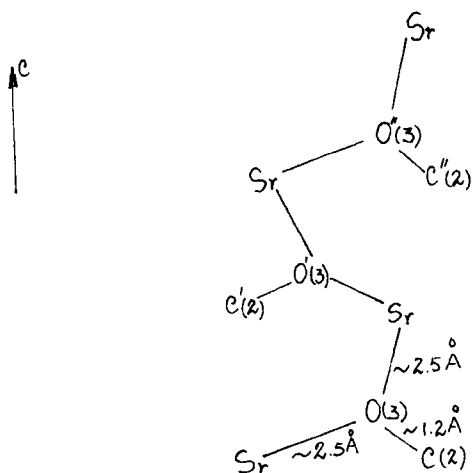


Because the formate ion has two electronegative atoms present and the strontium attracts these atoms strongly, the electrons in the C-D bond will also be pulled in the same direction. This will tend to leave a residual positive charge on the deuterium atom, which may therefore be somewhat more loosely bound to carbon. A C-D distance fractionally longer than 1.07 to 1.09Å, as generally observed for formic acid (27) and some formates (4,5) is another likely consequence. A deuterium atom in these conditions will probably be quite vulnerable to any strong influence of adjacent negative dipoles. The difficulty lies in knowing the range over which such an effect is likely to operate. Bonds of the type C-D --- O are not well-established, but have been postulated in a number of systems (28).

In Fig.V.12 the geometrical configuration of the main atoms concerned, as deduced from X-ray and d.m.r. results, is shown schematically; the C-D distance has been taken as 1.09Å. In dashed lines, an alternative set of

angles and distances is shown for a second position of D corresponding to a maximum error of $6^o$ in the $\overline{CD}$ vector determination.

## Fig.V.12.
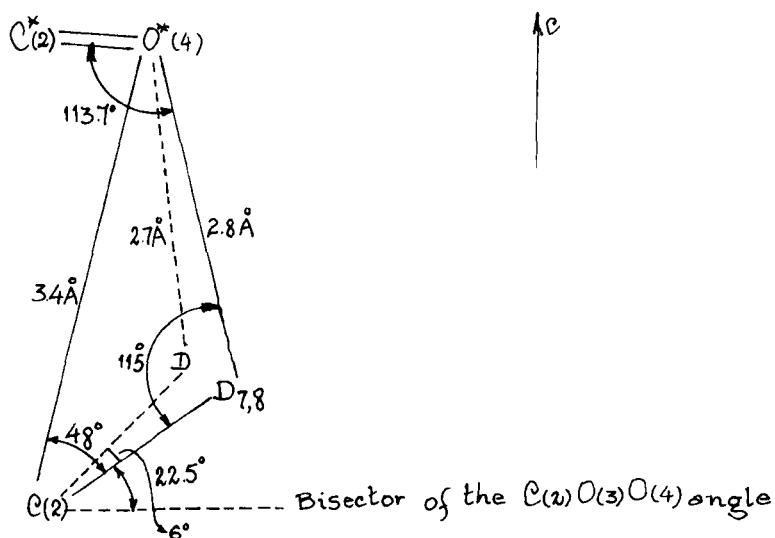


Consideration of the van der Waals distances is rather inconclusive, and possibly unfavourable. A table of van der Waals contact distances is shown below, giving a comparison between the observed and calculated bond distances for some of the known hydrogen-bonded species A-H ---- B (from ref.29). A general contraction of the A --- B and H --- B distances from the predicted values usually occurs. Although the presence of such A --- B shortening is a clear criterion for the occurrence of H-bonding, the existence of long hydrogen bonds where this effect is nil or even negative is well-known (28). Two examples are in the table; curiously, C-H --- O is one of them. O-H --- O bonds with this feature are also known.

Table V.8

| Bond type | A---B (calc.) | A---B (obs.) | H---B (calc.) | H---B (obs.) |
|-----------|---------------|--------------|---------------|--------------|
| F-H-F | 2.7 Å | 2.4 Å | 2.6 Å | 1.2 Å |
| O-H---O | 2.8 | 2.7 | 2.6 | 1.7 |
| O-H---Cl | 3.2 | 3.1 | 3.0 | 2.2 |
| N-H---Cl | 3.3 | 3.3 | 3.0 | 2.4 |
| N-H---N | 3.0 | 3.1 | 2.7 | 2.2 |
| N-H---S | 3.4 | 3.4 | 3.1 | 2.4 |
| C-H---O | 3.0 | 3.2 | 2.6 | 2.3 |

A slightly larger negative effect with the present A---B distance of 3.4Å does not therefore seem to be out of the question, since the maximum limit for A---B distances in CH---O bonds is not well established. The value of 2.8Å for the D---B distance looks embarrassingly long, however, and the possibility of an interaction between the two atoms may therefore be rather small. It is evident that at such a distance only an interaction of the weakest amplitude would arise, but it might be sufficient for an energetically stable but non-planar configuration for the formate ion to be attained.

When the non-bonding as well as the bonding electrons around O*(4) are considered, a bond angle slightly less than the trigonal value (120°) is expected, because of repulsion by the non-interacting lone pair (30). The experimental value of 113.7° for the angle between the O*(4)-D and O*(4)-C*(2) directions therefore appears very reasonable. All of these reasonings follow an essentially electrostatic interpretation of hydrogen bonding. In some systems, however, large variations of this angle are

found, between 95° and 164°, showing that other factors such as steric effects may be important. In crystalline formic acid, for example, this angle is 122°; in acetic acid, the angle is opened to 144° because of steric crowding by the methyl groups (28). Although the angular values spread considerably, statistically they are mostly concentrated inside a 120 ± 20° interval. Several of the results above implicitly assume that for either N-H---O‿C or O-H---O‿C a linear bond is formed: an accurate knowledge of the structure might in some cases give a H---O‿C angle closer to a trigonal value, however.

The angle C‹O(3) O(4) is significantly larger than C‹O(1) O(2), 127.8 and 125° respectively. This difference should be greater than experimental error, and may therefore be of structural significance. It is a tempting assumption to interpret this slight opening of the angle as a consequence of the non-planarity of the formate group. A simple electrostatic model was devised to try to predict the amount of angular variation from an ordinary planar HCOO⁻ group. (I.R. results for the anhydrous salt suggest a considerable degree of ionic character in the formate groups (31).) D.m.r. results prove that DCO(1)O(2)⁻ in the same crystal is approximately planar, while X-ray data show that the CO(1) and CO(2) distances (1.20 and 1.21Å) are virtually equivalent, and very close to the length of a typical C=O double bond (1.20Å). The CO(3) and CO(4) distances are slightly longer, 1.23 and 1.24Å respectively.

This formate ion was taken as reference, and a system of charges introduced to satisfy the following conditions:

1) complete equivalence of the two oxygen atoms,

2) the assumption that $sp^2$ hybridised orbitals at carbon are the main cause of the geometrical configuration at the ion.
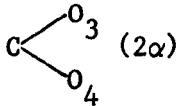
Coulombic forces proportional to the number of bonding electrons along the three directions were considered. Each of the C-O bonds was taken as containing an average of three electrons, which were treated as negative point charges localised at the same (unspecified) distance $d_o$ from C, as shown in Fig.V.13.
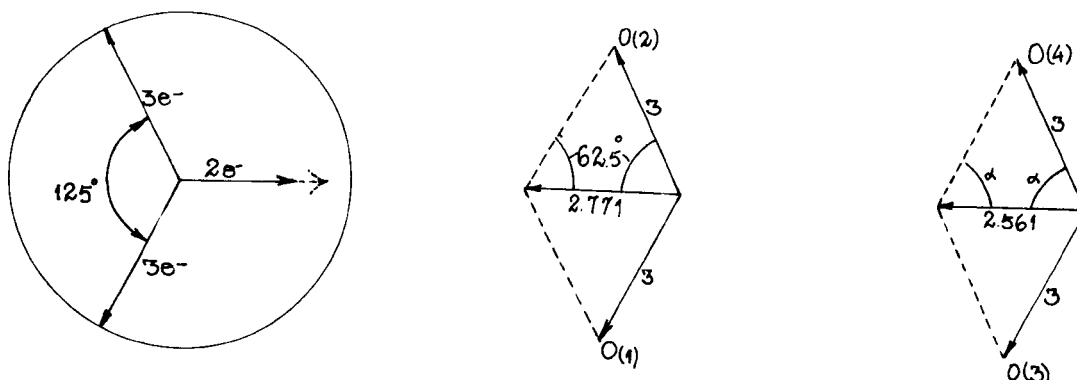


A vector $\overline{R}_o$ was found by summing vectorially the forces along CO(2) and CO(1) (experimentally $\widehat{O(1)CO}(2) = 125°$); not surprisingly, $|\overline{R}_o| = 2.771$, a natural consequence of $d_{CO} > d_{CH}$. $\overline{R}_o$ should be equal and opposite to the force allocated to direction CD. The angle $2\alpha$ (Fig.V.13) was then re-calculated for the $DCO(3)O(4)^-$ ion, by substituting for $\overline{R}_o$ its projection on a COO plane $22.4°$ away, as found from the d.m.r. results.

A second calculation was carried out with a more realistic assumption of a net overall charge of -1 attributed to the ion and two extra half charges, one for each oxygen. Involvement of all the electrons

around the oxygens was also included as another example. The results are summarised in the following table.

| No. of charges allocated to CO bond | Calc. $C\left\langle\begin{smallmatrix} O_3 \\ O_4 \end{smallmatrix}\right.$ $(2\alpha)$ | Experim. (Osaki) |
|:---:|:---:|:---:|
| 3 | $129.4^{\circ}$ | |
| 3.5 | $128.0^{\circ}$ | $127.8^{\circ}$ |
| 4 | $128.0^{\circ}$ | |

The value of $2\alpha$ is fairly insensitive to the exact number of charges allocated to the CO bonds (even five charges would still give $128.4^{\circ}$), as long as the two main hypotheses, namely complete equivalence of the CO bonds, and the magnitude of the angle between CD and the COO plane, are fulfilled. The important conclusion is that whatever the number of charges allocated to the CO directions, some opening of the OCO angle is expected for a non-planar formate ion, of the same order of magnitude as that observed experimentally for CO(3)O(4).

Two kinds of symmetrically and structurally nonequivalent formate ions are thus present in the crystal structure. Although the quadrupolar constants are often a sensitive probe of the immediate environment of deuterium atoms, the constants for D3,4 and D7,8 are not accurate enough for any meaningful structural discussion; strangely, the supposedly hydrogen-bonded deuterium has a quadrupolar constant 1.4% higher. This value of 170 KHz is obviously affected by error. Chiba (5) gives a limiting value of $166 \pm 2$ KHz for a formate ion in a perfectly static lattice, and the value for a formate hydrogen-bonded through D is expected to be lower.

There is i.r. evidence for a general fine structure of the formate lines in a number of solid anhydrous formates (32,33) and for $Sr(DCOO)_2 \cdot 2D_2O$ itself in the ranges 2000-600 $cm^{-1}$ (34) and 3500-600 $cm^{-1}$ (35). Since the $C_{2v}$ symmetry of the free formate ion precludes any degeneracy, this behaviour is attributed to a crystal field effect arising from the existence of two crystallographically independent sets of formate ions in the structures. The barium salt in particular shows fairly low (2822 and 2865 $cm^{-1}$) and rather separated (43 $cm^{-1}$) values for the C-H stretching frequency, which may indicate a possible C-H---O interaction (28). The space group of this compound is the same as for strontium formate dihydrate ($2_1 2_1 2_1$) and both structures bear definite points of similarity. From the available X-ray data (36), the group of atoms shown in Fig.V.14 would certainly have a favourable configuration for an interaction of the type postulated. The lower frequency C-H band (2820 $cm^{-1}$) is still present in aqueous solution, however, so further speculation at this stage would be premature.

Fig.V.14

(indexing of atoms as in ref.36)
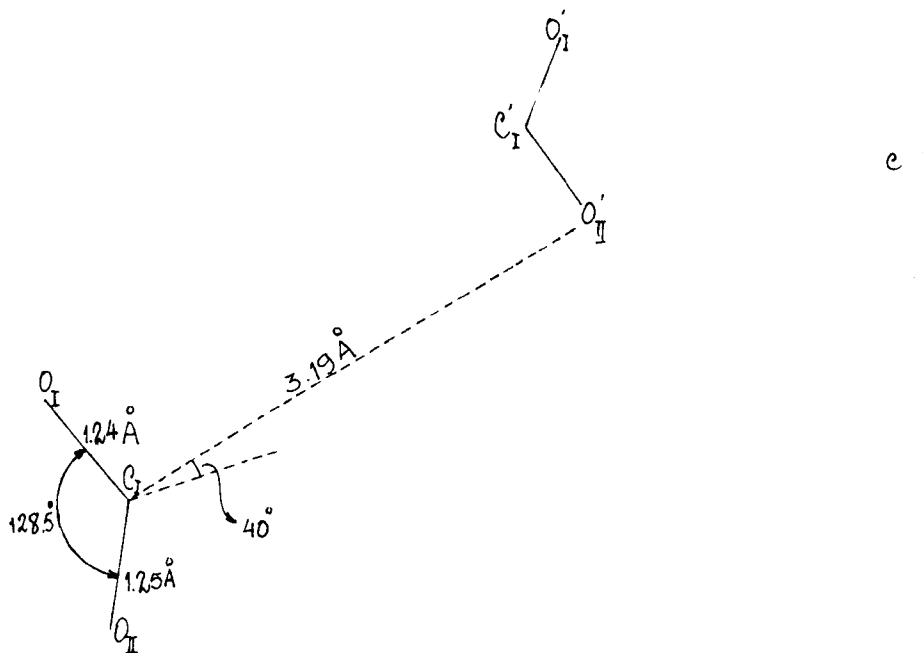
(b) <u>The $D_2O(1)$ molecule</u>

As already mentioned in Sec.V.3a, deuterons 1,2,5 and 6 belong to stationary water molecules. Their quadrupolar constants (average 242.9 KHz for 1 and 2, 216.9 KHz for 5 and 6) and asymmetry parameters (0.100 and 0.113 respectively) are well within the expected range, of which Table V.9 gives a few examples.

<div align="center">Table V.9</div>

| Compound | $e^2qQ/h$ (KHz) | $\eta$ | Ref. |
|---|---|---|---|
| $CuSO_4 \cdot 5D_2O$ | 200.2 | 0.117 | 18 |
| ($D_{83}$) | 201 | 0.12 | 37 |
| $Cu(DCOO) \cdot 4D_2O$ | 215.5 | 0.074 | 5 |
| ($D_a$) | | | |
| $Ba(ClO_3)_2 \cdot D_2O$ | 277 | | 38 |
| $(KCOO)_2 \cdot D_2O$ | 214 | 0.076 | 19 |

From the experimental value of $e^2qQ/h$, some degree of H-bonding for these $D_2O$ molecules is a strong possibility. In the absence of neutron diffraction data as the best guide for identification of $D_1$ and $D_5$ (and related deuterons) in the structure, the available X-ray co-ordinates have been used to search for all the oxygen atoms near to $D_2O(1)$ or $D_2O(2)$, and specifically within a hydrogen bonding radius (2.6-3.2Å). The corresponding O---O directions were compared with the directions of the experimental $q_{zz}$ eigenvectors. It became clear that all four deuterons could be assigned to $OH_2(1)$ molecules in Osaki's nomenclature; the oxygen atoms at the far end of the bonds were identified as $OH_2(2)$ and $O(4)$ respectively. Table V.10

gives the geometric analysis of the e.f.g. tensor eigenvectors compared with the structure as known from X-ray analysis. The meanings of the symbols employed is as follows:

$\emptyset_z'$ - angle between the 0---0 line and the $q_{zz}$ vector;

$\emptyset_y'$ - angle between the $q_{yy}$ vector and the normal to the plane defined by $q_{z_1}$ $q_{z_5}$ ;

$\theta_y$ - angle between the two $q_{yy}$ eigenvectors;

. $\theta_z$ - angle between the two $q_{zz}$ eigenvectors.

$\emptyset_z'$ has a slightly different meaning from the value of $\emptyset_z$ normally given (5), which is taken as the angle between the $q_{zz}$ eigenvector and the true OD direction. The non-availability of such data leaves $\emptyset_z'$ as its nearest substitute, which gives more of a measure of the departure of the bond from linearity. It is interesting to note that the $\theta_z$ value found from d.m.r. is not significantly different from the corresponding angle for HDO vapour as determined accurately by microwave spectroscopy (39), Fig.V.15. Since $\theta_D \simeq \theta_z$, it may be assumed that the true D-O-D angle for $D_2O(1)$ is also quite close to $\theta_B$.

Fig.V.15
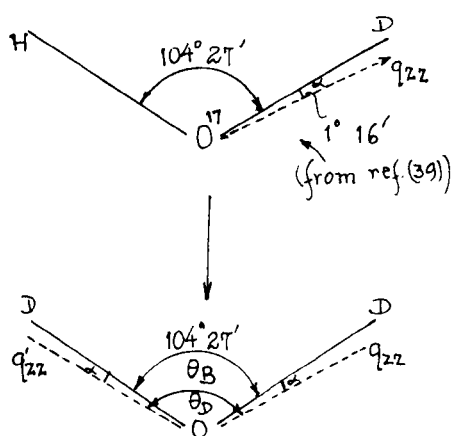


$\theta_B = 104^{\circ}\ 27'$

$\theta_D = 106^{\circ}\ 59'$

$\alpha = 1^{\circ}\ 16'$

## Table V.10

| Deut. | $q_{zz}$ dir.cos (a,b,c axis) | O(1) --- O' dir.cos | $\phi'_z$ | $\phi'_y$ | $\theta_z$ | $\theta_y$ | ident. of O'* |
|---|---|---|---|---|---|---|---|
| 1 | 0.0774<br>-0.7915<br>-0.6063 | 0.1665<br>-0.7989<br>-0.5780 | 5.3° | 3.1° | 107.9° | 3.6° | O in $D_2O(2)$ |
| 5 | 0.9179<br>0.2293<br>0.3238 | 0.9036(4)<br>0.1258<br>0.4058 | 8.2° | 3.0° | | | O(4) |
| 2 | -0.0800<br>-0.7921<br>0.6051 | -0.1665<br>-0.7989<br>0.5780 | 5.2° | 0.0° | 107.6° | 3.0° | O in $D_2O(2)$ |
| 6 | -0.9184<br>0.2285<br>-0.3231 | -0.9036(4)<br>0.1258<br>-0.4058 | 8.2° | 2.9° | | | O'(4) |

* Osaki's indexing.

The small values of $\phi_z'$, $\phi_y'$ and $\theta_y$ and the almost tetrahedral value of $\theta_z$

confirm the assignments made as reasonable. The relationship between the

principal directions of the e.f.g. tensor and the local structure of the

system can be depicted as in Fig.V.16; a $D_2O$ molecule with a non-linear

hydrogen bond has been deliberately chosen to show both $\phi_z$ and $\phi_z'$.

<u>Fig.V.16</u>

($\bar{n}$-normal to $OD_1D_2$ molecular plane)
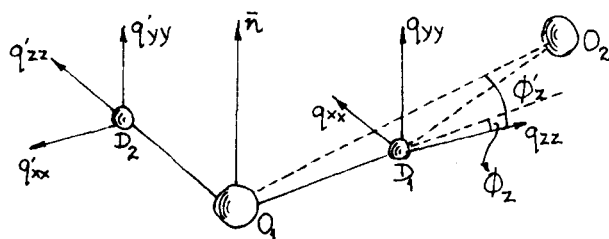


The larger limits for the deviations of $\phi_y$ and $\phi_x$ (defined as the angle

between $q_{xx}$ and the molecular plane) are not unexpected, since the $q_{xx}$ and

$q_{yy}$ directions may be more sharply influenced by the configuration of the

H-bonded system, and even by neighbouring atoms not directly involved in

H-bonding. Similar deviations have been found both in systems with

severely 'bent' H bonds, and in others with large positive charges on

metal ions, e.g. copper(II) (37,18). In many cases it is difficult to

know how meaningful the experimental deviations are, however, unless a very

careful assessment of errors has been made. In practice the $q_{zz}$ direction

cosines are normally determined with greater accuracy than their

counterparts (Sec.V.4c).

Naturally the situation is quite different for a reorientating water

molecule. While the asymmetry parameter rises to values close to 1, the

quadrupolar constant becomes about half that of a stationary molecule.

This effect can be explained by superposing the two e.f.g. tensors for a

$D_2O$ molecule in an idealised model and examining the time averaging effect introduced by a reorientation rate much faster than the quadrupolar splitting frequency (18). The $q_{xx}$ axis is nearly parallel to the bisecting axis of the molecule, while the $q_{yy}$ axis (or the $q_{zz}$ axis according to the conditions) is almost perpendicular to the molecular plane. These alternative possibilities can be predicted as a function of the value $(2\theta)$ of the D—O—D angle; there is a critical value of this angle at which the principal y and z axes switch directions ($109^{\circ}$ 28' when $\eta = 0$, $112^{\circ}$ 17' when $\eta = 0.1$).

Unless a major structural change accompanies the conversion from a static to a reorientating molecule, there is not a sharp discontinuity, but a gradual increase in the reorientation frequency with temperature. The activation energies of the process are generally in a 6-15 kcal mole$^{-1}$ range (comparable to the energy required to break two hydrogen bonds (28)). The 'fading out' of the two low-temperature lines (frequencies $\nu_1$ and $\nu_2$) (which emerge later as a single resonance (Sec.V.3b)) means that the frequency of the process $\nu_f$ lies in the particular range such that the lines are so broad as to escape detection. The conditions for detectability are therefore given by:

$$|\nu_1 - \nu_2| \gg \nu_f \quad \text{or} \quad |\nu_1 - \nu_2| \ll \nu_f$$

with, say, a linewidth of 10 gauss ($\sim$ 6.5 KHz) as a practical limit for observation.

For a detailed investigation of the kinetics of the reorientation process, $\nu_f$ can be deduced from the linewidth or, more conveniently, from S/N (17). Saturation of the deuterium signals for this compound was a good reason for not attempting a study of this kind. Although the precise value

of the potential barrier $V_o$ to reorientation about the bisecting axis in

$D_2O(1)$ was not determined, a lower limit was easily derived from the semi-

empirical relationship (18) $\dfrac{V_o}{RT_a} = 24.0$. $T_a$ represents the temperature

at which the broad absorption lines in the slow exchange limit become

observable. Since close to $30^{\circ}C$ the molecule is still stationary,

$T \simeq 300^{\circ}K < T_a$ and $v_o > 14.4$ kcal mole$^{-1}$. A very stable, approximately

tetrahedral configuration about oxygen and a strongly hydrogen bonded

system (Fig.V.17) may account for the high value of the barrier to

reorientation; in this instance sufficient energy to break two hydrogen

bonds would be required. The two oxygen lone-pair orbitals appear to be

directed towards strontium ions and this may have an additional 'locking'

effect.

<u>Fig.V.17</u>
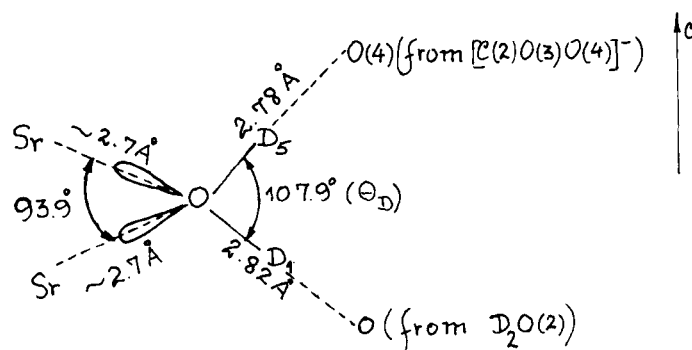


The well-known correlation between the magnitude of $\dfrac{e^2qQ}{h}$ and the O---O

distance or the H---O distance (18,40) (as given in Sec.IV.7) holds very

satisfactorily for deuterons 5 and 6 (dO---O = 2.78Å; $RO_{II}$---D $\simeq$ 1.78Å

(estimated)). For deuterons 1 and 2, however, the constants appear somewhat

high (by 20-30 KHz) for the distance involved (dO---O = 2.82Å; $RO_{II}$---D $\simeq$

1.82Å). This difference seems rather large for hydrogen bonds of virtually

the same length. Perhaps oxygen from a formate ion is more effective in forming hydrogen bonds than the oxygen of $D_2O(2)$ (Fig.V.17). Since there is some indication that this second water is reorientating reasonably rapidly (following section), a fuether weakening could result, and give rise to a higher value of the constant.

(c) The $D_2O(2)$ molecule

The weakness of the signals attributed to this molecule and the doubt about the number of signals are somewhat unexpected features. The following table lists the nearest oxygen atoms to $H_2O(2)$ and the respective $O-OH_2$ direction cosines (1). Since its presence is relevant to the immediate surroundings of this water molecule, the closest strontium ion is also included.

Table V.11

| Atom A | O---A dist. (Å) | O —— A direction cos | | |
|---|---|---|---|---|
| | | a | b | c |
| Sr | 2.72 | 0.7409 | 0.6616 | 0.1155 |
| O(3) | 3.12 | 0.1102 | 0.8714 | -0.4781 |
| O(4) | 2.67 | -0.6090 | 0.7117 | -0.3500 |
| O(1) | 3.21 | 0.3130 | 0.3941 | 0.8641 |
| O(2) | 2.80 | -0.0944 | -0.1633 | 0.9821 |
| $OH_2(1)$ | 2.82 | -0.1665 | -0.7989 | -0.5780 |

Atoms O(2) and O(4) would seem most favourable for the formation of a hydrogen-bonded structure of the type:

Fig.V.18
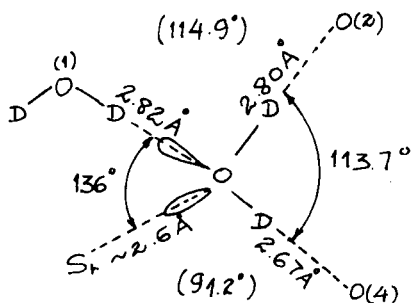


This grouping would be not only sterically favourable but possibly quite stable because of the short H bonds involved. Eight well-defined resonances would therefore be predicted (Table V.1).

Instead, a not well determined number of rather weak and broad (7 gauss in some cases) signals appeared in various field positions. A triplet structure was apparent in some of the peaks, making their exact location harder to establish. The scarcity of information available for each line made impracticable any formal least squares study. The trajectory of the curves could be broadly followed, however, and the crossing points were easily recognised. To find the approximate values of the constants, the simplified relationships given in Sec.IV.4b were used wherever possible.

Further refinement was afterwards achieved by using these preliminary values of A, B and C to calculate the splittings for experimental points of least doubtful location. The parameters were adjusted slightly by a mixture of least squares and guesswork until satisfactory agreement between the calculated and experimental values was obtained. The process was then recycled. Three sets of curves (and their

symmetrically related counterparts) were apparent in pattern [a], becoming

barely noticeable in [b] and [c], except for crossing points and odd

sections only. Another set of unidentified curves of fairly low slope

cross the [a] axis around 170 gauss in patterns [b] and [c].

The existence of sets $M_1$ and $M_3$ in pattern [a] (Fig.V.5) is certainly

beyond doubt. For this reason, a few approximate calculations were

carried out on one curve of each independent set $M_1$, $M_2$, $M_3$.

| $M_1$ | $M_2$ | $M_3$ |
|---|---|---|
| $A_a$ = 52.3 KHz | $A_a$ = -223.5 KHz | $A_a$ = -218.8 KHz |
| $B_a$ = -55.5 KHz | $B_a$ = -12.2 KHz | $B_a$ = 60.9 KHz |
| $C_a$ = -187.1 KHz | $C_a$ = -204.3 KHz | $C_a$ = -43.1 KHz |

For all curves, $A_b$, $B_b$, $A_c$ and $B_c$ were easily calculated from the equations

in Sec.V.4b. Some results are now summarised.

1. <u>Deuteron $M_1$</u>. On the assumption that $M_1$ belongs to an essentially

stationary $D_2O$ molecule, further simplifying hypotheses were axial symmetry

($\eta$ = 0) and a typical quadrupolar constant ($\frac{e^2 qQ}{h} \simeq$ 210 KHz). A $q_{zz}$

principal axis with direction cosines (0.336; 0.574; -0.747) would give good

agreement for the A and B constants (< 2.9%) and a deviation of $\simeq$ 8.3% for

C. The latter, although large, is not unexpected, given the much larger

sensitivity of C to orientation. Moreover, $\eta \simeq$ 0 is an extreme

approximation. The only positive conclusion is that the OD vector is in all

probability closer to the c-axis than any other, which suggests O(2) as a

possible bonding atom (Table V.11).

2.  <u>Deuteron $M_2$</u>.  The very high values of A and C for $M_2$ suggest a high quadrupolar constant (250 to 300 KHz) and also a rather large asymmetry parameter; the two together constitute a rather contradictory combination, which casts doubt on the very existence of this curve.  The strength of some of the signals and the regularity of their positions make this hard to believe, however.

3.  <u>Deuteron $M_3$</u>.  The constants for curve $M_3$, particularly A, are again compatible with a rather high quadrupolar constant, approaching that of free $D_2O$ or HOD (315 and 318.6 respectively; (39,25)).  By proceeding as for curve $M_1$, a preliminary set of direction cosines was found (0.94, 0.30, -0.163).  These values are in accordance with the somewhat flat appearance of the curve, which immediately suggests a deuteron approaching the normal to the magnetic field.  For deuterons in such an orientation, some improvement can be effected in the direction cosines by estimating $C_b$ and $C_c$ from patterns [b] and [c].

The maximum possible splitting for any particular deuteron in a crystal is $\frac{3}{2} \frac{e^2 qQ}{h}$, and arises when the field is exactly aligned with $q_{zz}$ (20).  If these conditions are realised only approximately (i.e. the deuteron is no more than $20^o$ to $30^o$ from the plane of the magnetic field $\pi_H$), the following relationship holds fairly closely.

$$\text{Max. of curve} = |A| \times \sqrt{B^2 + C^2} = \frac{3}{2} \frac{e^2 qQ}{h} \cos\alpha = \text{proj. } q_{zz}$$

$$\alpha = \text{angle between } q_{zz}(\alpha_{13} \; \alpha_{23} \; \alpha_{33}) \text{ and } \pi_H$$

For example, $\cos\alpha = \dfrac{\alpha_{23}^2 + \alpha_{33}^2}{\sqrt{\alpha_{23}^2 + \alpha_{33}^2}}$ for pattern [c]

This hypothesis was checked on deuterons 1, 4 and 6, and the values found

for $\cos\alpha$ were reasonable.

Deuteron 1   $\alpha$ = 4.5$^{\circ}$   Rel. Deviation = 0.4%

        4      2.5$^{\circ}$               0.17%

        6     23.0$^{\circ}$             5.8%

By using the approximate direction cosines initially found for $q_{zz}$ in

deuteron $M_3$ and assuming $e^2qQ/h \simeq 320$, $C_b$ and $C_c$ were calculated. The

complete tensor was diagonalised and the asymmetry parameter evaluated.

$$\frac{e^2qQ}{h} = 330 \pm 30 \text{ KHz}; \quad q_{zz}[0.9585; \; 0.2324; \; -0.1653]; \quad \eta \simeq 0.2$$

Although a very significant angle of 109.4$^{\circ}$ was thus determined by

the $q_{zz}$ directions for $M_1$ and $M_3$, the magnitude of the errors introduced

by all the approximations makes its numerical value uncertain. No obvious

relationship with neighbouring oxygen atoms is evident for $M_3$, not a

surprising conclusion for a supposedly "free" deuteron.

Whatever the results may be from a strictly numerical point of view,

all the data indicate that $D_2O(2)$ is a molecule which has considerably

more motional freedom than $D_2O(1)$. Through one of its deuterons $M_1$, it

still appears partially involved in H-bonding with $O(2)$ in the $C(1)O(1)O(2)$

formate ion. A barrier to reorientation of around 14.4-15 kcal mole$^{-1}$

at 300 K would still be compatible with a $D_2O$ molecule hydrogen bonded on

three sites when stationary. The lesser involvement with the strontium

ions may be a reason for the difference in the stability of the two $D_2O$

arrangements.

## Further Work

Strontium formate dihydrate presents an interesting study, especially for what could be called its degree of internal disymmetry; slight differences in their respective surroundings cause a marked difference of behaviour for both formate ions and water molecules alike. The C(2)O(3)O(4) formate ion in particular would benefit from a more precise study without resorting to the approximation method, so that its quadrupolar constant and the limits of deviation from planarity could be more accurately assessed. As already mentioned in Sec.V.5a, a d.m.r. study on $Ba(DCOO)_2$ would perhaps be an interesting complement for deciding on the viability of a C-D---O interaction. The more electropositive character of $Ba^{2+}$ compared with $Sr^{2+}$ should accentuate such effects if they exist. A neutron diffraction study of strontium formate dihydrate would complete the knowledge of this structure.

## Additional Note

A refinement of the X-ray crystal structure has very recently been reported by Galigné (41). The revised co-ordinates give very good agreement with the direction cosines determined for D7,8 as shown in the following table. The suggestion of a weak C-D---O hydrogen bond to account for the apparent non-planarity of the formate ion $[C(2)O(3)O(4)]^-$ is therefore no longer necessary, since the planarity of the formate group is now evident.

| Deut. | $q_{zz}$ dir.cos. (d.m.r.) | calc. dir. for C(2)O(3)O(4) bisector, $\overline{B}$ | $q_{zz}$ ∧ $\overline{B}$ |
|---|---|---|---|
| 7 | 0.4216 | 0.4220 | $1.5^{o}$ |
| | -0.7876 | -0.7747 | |
| | -0.4493 | -0.4709 | |
| 8 | -0.4229 | -0.4220 | $1.7^{o}$ |
| | -0.7893 | -0.7747 | |
| | 0.4452 | 0.4709 | |

# REFERENCES

## Chapter I.

1. E.M. Purcell, H.C. Torrey and R.V. Pound, Phys. Rev., 1946, 69, 37.

2. F. Bloch, W.W. Hansen and M.E. Packard, Phys. Rev., 1946, 69, 127.

3. R.V. Pound, Phys. Rev., 1950, 79, 685.

4. M.H. Cohen and F. Reif, Solid State Phys., 1957, 5, 321.

5. G.M. Volkoff, H.E. Petch and D.W.L. Smellie, Can. J. Phys., 1952, 30, 270.

6. G.M. Volkoff, Can. J. Phys., 1953, 31, 820.

7. T. Chiba, J. Chem. Phys., 1964, 41, 1352.

8. R. Blinc and D. Hadži, Nature, 1966, 212, 1307.

9. G. Soda and T. Chiba, J. Chem. Phys., 1969, 50, 439.

10. H. Narumi and T. Watanabe, Bull. Amer. Phys. Soc., 1964, 9, 11.

11. J.A.S. Smith, J. Chem. Ed., 1971, 48, 39.

12. H.D. Megaw, "Ferroelectricity in Crystals", Methuen, London, 1957.

13. R. Blinc, "Magnetic Resonance in Hydrogen-Bonded Ferroelectrics", in Advances in Magnetic Resonance, J.S. Waugh Ed., Academic Press, New York, 1968, Volume 3.

14. E.A. Uehling and J.L. Bjorkstam, Phys. Rev., 1959, 114, 961.

15. J.L. Bjorkstam, Phys. Rev., 1967, 153, 599.

16. E.O. Schlemper and W.C. Hamilton, J. Chem. Phys., 1966, 44, 4498.

17. D.E. O'Reilly and T. Tsang, J. Chem. Phys., 1967, 46, 1291.

# Chapter II.

1. S. Ketudat and R.V. Pound, J. Chem. Phys., 1956, 26, 708.

2. R.V. Pound, Phys. Rev., 1950, 79, 685.

3. C.P. Slichter, 'Principles of Magnetic Resonance', Harper and Row, New York, 1963.

4. G.M. Volkoff, H.E. Petch and D.W.L. Smellie, Can. J. Phys., 1952, 30, 270.

5. G.M. Volkoff, Can. J. Phys., 1953, 31, 820.

6. M.H. Cohen and F. Reif, Solid State Phys., 1957, 5, 321.

7. T.P. Das and E.L. Hahn, 'Nuclear Quadrupole Resonance Spectroscopy', Academic Press, New York, 1958.

8. J.O. Clifford, Ph.D. Thesis, Leeds, 1968.

9. J. Royston, Ph.D. Thesis, Warwick, 1969.

10. J.A.S. Smith, J. Chem. Ed., 1971, 48, 39.

11. H. Narumi and T. Watanabe, Bull. Amer. Phys. Soc., 1964, 9, 11.

12. J.E. Nye, 'Physical Properties of Crystals. Their Representation by Tensors and Matrices', Oxford University Press, Oxford, 1957.

13. B. Pedersen, Acta Chem. Scand., 1968, 22, 453.

14. S.J. McMinn, 'Matrices for Structural Analysis', Second Edition, Spon, London, 1966.

# Chapter III

1. E.R. Andrew, "Nuclear Magnetic Resonance", The University Press, Cambridge, 1958.

2. M. Mehring and O. Kanert, J. Sci. Instrum., 1965, 42, 449.

3. C.W. Fryer, J. Sci. Instrum., (J. Phys. E), 1969, 2, 230.

4. J. Royston, Ph.D. Thesis, Warwick, 1969.

5. H.L. Anderson, Phys. Rev., 1949, 76, 1460.

6. "Radio Designer's Handbook", F. Langford Smith, ed., Iliffe and Sons, London.

Chapter IV

1.   E.O. Schlemper and W.C. Hamilton, J. Chem. Phys., 1966, 44, 4498.

2.   D.E. O'Reilly and T. Tsang, J. Chem. Phys., 1967, 46, 1291.

3.   W.C. Hamilton, J. Chem. Phys., 1969, 50, 2275.

4.   M. Kasahara and I. Tatsuzaki, J. Phys. Soc. Jap., 1970, 29, 1392.

5.   R. Pepinsky, K. Vedam, S. Hoshino and Y. Okaya, Phys. Rev., 1958, 111,
     1508.

6.   R.J. Nelmes, Acta Cryst., 1971, B27, 272.

7.   R.J. Nelmes, 1972, submitted to Acta Cryst.

8.   R.J. Nelmes, 1972, submitted to 'Ferroelectrics'.

9.   R. Pepinsky and K. Vedam, Phys. Rev., 1960, 117, 1502.

10.  J.J. Rush and T.I. Taylor 'Study of Low Frequency Motions in Several
     Ferroelectric Salts by the Inelastic Scattering of Cold Neutrons',
     Inelastic Scattering of Neutrons, I.A.E.A., Vol. II, Vienna,
     1965, p. 333.

11.  J.W. Arthur, D.J. Lockwood and W. Taylor, Personal Communication to
     Prof. J.A.S. Smith.

12.  H.E. Buckley, 'Crystal Growth', J. Wiley, New York, 1951.

13.  'Gmelins Handbuch der Anorganischen Chemie', Vol. 23 (Ammonium),
     Verlag Chemie, Berlin, 1936.

14.  B. Pedersen, Acta Chem. Scand., 1968, 22, 453.

15.  G.M. Volkoff, Can. J. Phys., 1953, 31, 820.

16.  J.F. Nye, 'Physical Properties of Crystals. Their Representation by
     Tensors and Matrices', Oxford University Press, Oxford, 1957.

17.  S.J. McMinn, 'Matrices for Structural Analysis', Second Edition, Spon,
     London, 1966.

18.  R. Blinc and D. Hadži, Nature, 1966, 212, 1307.

19. G. Soda and T. Chiba, J. Chem. Phys., 1969, $\underline{50}$, 439.

20. T.P. Myasnikova and A.F. Yatsenko, Sov. Phys. Solid State, 1962,

    $\underline{4}$, 475.

21. P.A. Bazhulin, T.P. Myasnikova and A.V. Rakov, Sov. Phys. Solid State,

    1963, $\underline{5}$, 1299.

22. T. Chiba, J. Chem. Phys., 1962, $\underline{36}$, 1122.

23. W.C. Hamilton and J.A. Ibers, 'Hydrogen Bonding in Solids',

    Benjamin, New York, 1968.

24. T.P. Das and E.L. Hahn, 'Nuclear Quadrupole Resonance Spectroscopy',

    Academic Press, New York, 1958.

25. G.E. Bacon and R.S. Pease, Proc. Roy. Soc. A., 1955, $\underline{230}$, 359.

26. J.L. Bjorkstam, Phys. Rev., 1967, $\underline{153}$, 599.

# Chapter V

1. K. Osaki, Ann. Rep. Sci. Works, Fac. Sci., Osaka Univ., 1958, 6, 13. Struct. Reports 1958, 22, 564.

2. J.-L. Galigné, and J. Falgueirettes, Compt. Rend., 1961, 994.

3. J.R. Clark, Acta Cryst., 1964, 17, 459.

4. G. Soda and T. Chiba, J. Chem. Phys., 1968, 48, 4328.

5. G. Soda and T. Chiba, J. Phys. Soc. Japan, 1969, 26, 249.

6. F. Holtzberg, B. Post and L. Fankuchen, Acta Cryst., 1953, 6, 127.

7. G.J. Adriaenssens and J.L. Bjorkstam, J. Chem. Phys., 1972, 56, 1223.

8. I. Nitta, Bull. Inst. Phys. and Chem. Research (Tokyo), 1927, 6, 377; Chem. Abs., 1929, 23, 1541.

9. R. Kiriyama, Science (Japan)1947,17,239; Chem. Abs. 1951,45, 2278d.

10. I.W. Ashton, D.F. Houston and C.P. Saylor, Bureau of Standards J. Research, 1933, 11, 233.

11. S. Haussuehl, Phys. Status Solidi, 1963, 3, 1201.

12. R. Kiriyama, J. Chem. Soc. Jap., Pure Chem. Section, 1950, 71, 125; Chem. Abs., 1951, 45, 4534.

13. R. Kiriyama, J. Chem. Soc. Jap., Pure Chem. Section, 1949, 70, 260; Chem. Abs., 1951, 45, 2740.

14. A. Holden and P. Singer 'Crystals and Crystal Growing', Doubleday-Anchor Books, New York, 1960.

15. 'Barker Index of Crystals', M.W. Porter and R.C. Spiller, eds., Heffer, Cambridge, 1956.

16. N.F.M. Henry, H. Lipson and W.A. Wooster, 'The Interpretation of X-ray Diffraction Photographs', McMillan, London, 1953.

17. T. Chiba, J. Chem. Phys., 1963, 39, 947.

18. G. Soda and T. Chiba, J. Chem. Phys., 1969, 50, 439.

19. B. Pedersen, Acta Chem. Scand, 1968, 22, 453.

20. G.M. Volkoff, H.E. Petch and D.W.L. Smellie, Can. J. Phys., 1952, 30, 270.

21. J.F. Nye, "Physical Properties of Crystals", Clarendon Press, Oxford, 1957. Chapter IX.

22. M.H. Cohen and F. Reif, Solid State Phys., 1957, 5, 321.

23. V.W. Weiss and W.H. Flygare, J. Chem. Phys., 1966, 45, 3475.

24. J. Rowell, W. Phillips, L. Melby and M. Panar, J. Chem. Phys., 1965, 43, 3442.

25. P. Thadeus, L.C. Krisher and J.H.N. Loubser, J. Chem. Phys., 1964, 40, 257.

26. S.G. Kukolich, J. Chem. Phys., 1969, 51, 358.

27. R.G. Lerner, J.P. Friend and B.P. Dailey. J. Chem. Phys., 1955, 23, 210.

28. G.C. Pimentel and A.L. McClellan, 'The Hydrogen Bond', Freeman, San Francisco, 1960.

29. W.C. Hamilton and J.A. Ibers, 'Hydrogen Bonding in Solids', Benjamin, New York, 1968.

30. R.J. Gillespie and R.S. Nyholm, 'The Steroechemistry of Inorganic Molecules and Complex Ions', in 'Progress in Stereochemistry', W. Klyne and P.B.D. de la Mare, eds., Butterworths, London, 1958. Volume 2, p. 261.

31. J.D. Donaldson, J.F. Knifton and S.D. Ross, Spectrochim. Acta, 1964. 20, 847.

32. K.B. Harvey, B.A. Morrow and H.F. Shurvell, Can. J. Chem., 1963, 41, 1181.

33. C.J.H. Schutte and K. Buijs, Spectrochim. Acta, 1964, 20, 187.

34. A-M. Vergnoux and R. Vierne, Compt. rend., 1965, 261, 1236.

35. R. Vierne, Opt. Acta, 1963, 10, 233.

36.  T. Sugawara, M. Kakudo, Y. Saito and I. Nitta, X-sen Kondankai,

     Osaka University, 1951, <u>6</u>, 85; Struct. Reports, 1951, <u>15</u>, 382.

37.  J.O. Clifford and J.A.S. Smith, Mol. Phys., 1967, <u>13</u>, 297.

38.  T. Chiba, J. Chem. Phys., 1964, <u>41</u>, 1352.

39.  J. Verhoeven, A. Dymanus and H. Bluyssen, J. Chem. Phys., 1969, <u>50</u>, 3330.

40.  R. Blinc and D. Hadži, Nature, 1966, <u>212</u>, 1307.

41.  J.L. Galigné, Acta Cryst., 1971, <u>B27</u>, 2429.

Results for $ND_4DSO_4$

(all half splittings in gauss)

| θ | Deuteron No. | | | |
|---|---|---|---|---|
| | 1 | 2 | 3 | 4 |
| 0 | −76•9 | −76•9 | −101•7 | −101•7 |
| 10 | −38•4 | −43•9 | −100•3 | −102•9 |
| 20 | 11•0 | −3•7 | −80•2 | −91•0 |
| 30 | 66•5 | 40•5 | −40•5 | −71•0 |
| 40 | 123•0 | 85•5 | 7•5 | −44•0 |
| 50 | 167•3 | 122•0 | 60•5 | −12•0 |
| 60 | 199•3 | 147•1 | 113•0 | 19•0 |
| 70 | 215•8 | 159•2 | 160•0 | 48•2 |
| 80 | 213•0 | 155•0 | 188•6 | 69•7 |
| 90 | 189•5 | 134•3 | 213•1 | 81•7 |
| 100 | 150•1 | 101•2 | 211•5 | 82•6 |
| 110 | 100•0 | 58•5 | 191•0 | 71•4 |
| 120 | 42•5 | 13•6 | 154•5 | 51•0 |
| 130 | −10•0 | −29•0 | 104•8 | 24•4 |
| 140 | −53•6 | −64•0 | 49•0 | −7•0 |
| 150 | −86•8 | −90•3 | −4•5 | −38•2 |
| 160 | −104•5 | −102•2 | −50•5 | −69•1 |
| 170 | −100•0 | −97•7 | −84•2 | −89•6 |
| $A^*$ (gauss) | 55•989 | 28•289 | 55•089 | −9•917 |
| $B^*$ (gauss) | −133•06 | −105•62 | −156•48 | −91•365 |
| $C^*$ (gauss) | 89•816 | 76•631 | −22•663 | −18•484 |
| A (KHz) | 73•19 | 36•98 | 72•01 | −12•96 |
| B (KHz) | −173•93 | −138•07 | −204•55 | −119•43 |
| C (KHz) | 117•41 | 100•17 | −29•63 | −24•16 |

Table II

$\underline{ND}_4\underline{DSO}_4$ (Room Temperature)

Pattern II

| θ | Deuteron No. | | | |
|---|---|---|---|---|
| | 1 | 2 | 3 | 4 |
| 0 | −57·3 | 94·0 | 19·6 | 78·3 |
| 10 | −14·7 | 80·2 | 51·8 | 74·0 |
| 20 | 33·2 | 63·2 | 76·5 | 71·3 |
| 30 | 79·5 | 45·8 | 90·0 | 69·5 |
| 40 | 122·8 | 28·3 | 95·0 | 72·0 |
| 50 | 152·5 | 14·7 | 87·5 | 75·3 |
| 60 | 166·6 | 3·8 | 67·6 | 79·5 |
| 70 | 166·5 | 0·5 | 39·5 | 85·0 |
| 80 | 148·3 | 2·1 | 6·0 | 90·3 |
| 90 | 117·0 | 10·4 | −29·8 | 95·0 |
| 100 | 74·7 | 23·5 | −61·8 | 99·8 |
| 110 | 25·4 | 40·8 | −87·0 | 102·7 |
| 120 | −21·9 | 58·5 | −102·3 | 104·1 |
| 130 | −62·4 | 75·3 | −104·8 | 103·6 |
| 140 | −92·2 | 89·7 | −96·9 | 99·7 |
| 150 | −108·3 | 98·7 | −77·6 | 95·1 |
| 160 | −105·9 | 104·3 | −49·4 | 89·8 |
| 170 | −86·3 | 102·3 | −16·5 | 84·3 |
| $A^*$ (gauss) | 29·861 | 52·006 | −5·144 | 87·183 |
| $B^*$ (gauss) | −86·505 | 41·520 | 24·264 | −8·634 |
| $C^*$ (gauss) | 108·782 | −31·170 | 97·716 | −14·296 |
| A (KHz) | 39·03 | 67·98 | −6·72 | 113·97 |
| B (KHz) | −113·08 | 54·28 | 31·72 | −11·29 |
| C (KHz) | 142·20 | −40·75 | 127·73 | −18·69 |

## Table 3

$\underline{N}D_4\underline{D}\underline{S}O_4$     Pattern I'     230K

| $\theta^o$ | 1 | 1' | 2' | 3 | 3' | 4 | 4' |
|---|---|---|---|---|---|---|---|
| 0 | -73.2 | -78.5 | -84.0 | -102.0 | -102.0 | -98.0 | -101.2 |
| 10 | -35.0 | -41.4 | -58.2 | -102.0 | -96.0 | -99.0 | -99.8 |
| 20 | 14.5 | 6.5 | -27.0 | -83.0 | -69.5 | -88.0 | -89.2 |
| 30 | 68.3 | 58.0 | 6.5 | -42.4 | -29.4 | -67.8 | -70.3 |
| 40 | 120.9 | 109.0 | 39.9 | 5.5 | 17.6 | -39.9 | -45.3 |
| 50 | 167.0 | 152.5 | 71.2 | 58.3 | 71.9 | -9.2 | -17.3 |
| 60 | 198.6 | 183.0 | 90.6 | 111.2 | 123.3 | 22.2 | 11.3 |
| 70 | 211.8 | 196.3 | 103.0 | 159.5 | 166.5 | 50.3 | 37.1 |
| 80 | 207.3 | 191.2 | 103.3 | 193.7 | 195.7 | 71.7 | 55.0 |
| 90 | 184.9 | 169.3 | 88.3 | 212.5 | 209.9 | 83.6 | 64.6 |
| 100 | 146.5 | 130.8 | 64.8 | 210.5 | 203.6 | 85.0 | 65.5 |
| 110 | 96.3 | 84.0 | 34.5 | 190.7 | 179.2 | 74.8 | 54.7 |
| 120 | 42.5 | 32.5 | 0.0 | 153.8 | 138.3 | 53.5 | 35.0 |
| 130 | -9.7 | -17.3 | -38.0 | 105.3 | 89.0 | 26.0 | 10.5 |
| 140 | -56.0 | -61.8 | -71.5 | 49.8 | 34.3 | -3.8 | -17.7 |
| 150 | -87.3 | -91.0 | -91.7 | -5.7 | -15.5 | -35.7 | -47.4 |
| 160 | -101.0 | -104.0 | -101.5 | -52.2 | -59.7 | -63.6 | -73.0 |
| 170 | -97.6 | -100.3 | -99.8 | -85.0 | -91.5 | -86.1 | -91.2 |
| A* (gauss) | 55.44 | 45.49 | 1.69 | 54.36 | 53.65 | -6.888 | -17.71 |
| B* (gauss) | -129.33 | -123.61 | -86.85 | -157.45 | -155.48 | -90.54 | -82.76 |
| C* (gauss) | 89.96 | 86.54 | 55.56 | -23.33 | -8.56 | -18.39 | -13.69 |
| A (KHz) | 72.47 | 59.46 | 2.21 | 71.06 | 70.13 | -9.004 | -23.15 |
| B (KHz) | -169.07 | -161.58 | -113.5 | -205.82 | -203.24 | -118.35 | -108.19 |
| C (KHz) | 117.60 | 113.12 | 72.63 | -30.50 | -11.19 | -24.04 | -17.89 |

**Line 2 could not be fully detected in this pattern.**

## Table 4

$\underline{N}D_4\underline{D}\underline{S}O_4$     Pattern II'     230K

| $\theta^{\circ}$ | 1 | 1' | 2 | 2' | 3 | 3' | 4 | 4' |
|---|---|---|---|---|---|---|---|---|
| 0 | −58.5 | −52.1 | 91.0 | 95.4 | 20.8 | 9.0 | 75.0 | 78.0 |
| 10 | −14.5 | −3.0 | 72.3 | 87.2 | 48.3 | 44.5 | 72.0 | 73.0 |
| 20 | 28.3 | 48.5 | 47.6 | 77.7 | 76.7 | 75.1 | 71.0 | 69.0 |
| 30 | 81.9 | 98.6 | 21.5 | 70.0 | 93.7 | 91.9 | 73.0 | 68.0 |
| 40 | 119.0 | 144.5 | −1.2 | 62.3 | 100.3 | 98.3 | 75.0 | 69.0 |
| 50 | 154.2 | 175.5 | −19.7 | 57.2 | 90.1 | 90.1 | 80.0 | 72.0 |
| 60 | 168.4 | 188.8 | −31.5 | 51.4 | 72.0 | 77.3 | 85.0 | 77.0 |
| 70 | 168.5 | 184.5 | −34.4 | 49.3 | 42.2 | 52.0 | 90.8 | 84.2 |
| 80 | 147.9 | 162.9 | −31.2 | 51.7 | 10.0 | 19.0 | 95.2 | 90.3 |
| 90 | 118.3 | 127.0 | −17.9 | 56.6 | −24.7 | −17.9 | 99.7 | 95.7 |
| 100 | 78.0 | 79.5 | −1.5 | 64.7 | −59.7 | −51.1 | 102.7 | 102.7 |
| 110 | 26.0 | 27.0 | 25.7 | 74.6 | −88.5 | −75.6 | 104.3 | 106.9 |
| 120 | −17.4 | −22.7 | 47.9 | 80.5 | −102.7 | −94.7 | 103.0 | 106.5 |
| 130 | −60.4 | −66.6 | 73.3 | 89.6 | −109.2 | −102.8 | 101.0 | 107.9 |
| 140 | −90.4 | −97.6 | 90.8 | 96.4 | −102.4 | −97.0 | 97.0 | 104.0 |
| 150 | −107.0 | −111.6 | 103.0 | 100.7 | −84.0 | −84.0 | 92.5 | 99.5 |
| 160 | −108.0 | −109.2 | 107.5 | 102.0 | −50.8 | −57.8 | 85.0 | 92.0 |
| 170 | −89.8 | −88.5 | 103.3 | 100.4 | −13.4 | −26.9 | 80.0 | 84.0 |
| A*(gauss) | 30.25 | 38.08 | 35.92 | 75.98 | −4.52 | −2.81 | 87.90 | 87.76 |
| B*(gauss) | −88.50 | −89.08 | 54.49 | 18.88 | 22.61 | 13.34 | −12.29 | −9.49 |
| C*(gauss) | 107.88 | 122.49 | −46.60 | −17.57 | 101.33 | 99.94 | −10.87 | −17.78 |
| A (KHz) | 39.54 | 49.78 | 46.96 | 99.32 | −5.91 | −3.67 | 114.90 | 114.72 |
| B (KHz) | −115.69 | −116.44 | 71.23 | 24.68 | 29.56 | 17.44 | −16.06 | −12.41 |
| C (KHz) | 141.02 | 160.12 | −60.92 | −22.97 | 132.46 | 130.64 | −14.21 | −23.24 |

APPENDIX II

Results for Strontium Formate Dihydrate

(all half splittings in gauss)

## APPENDIX II

### Table 1

$Sr(DCOO)_2 \cdot 2D_2O$
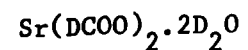
Pattern I    $300^\circ K$    $\underline{c}$ axis

| θ° | 1 | 1' | Av.1 | 2 | 2' | Av.2 | 3 and 3' | 4 and 4' | 5 | 5' | Av.5 | 6 | 6' | Av.6 | 7 | 7' | Av.7 | 8 | 8' | Av.8 |
|---|---|---|---|---|---|---|---|---|---|---|---|---|---|---|---|---|---|---|---|---|
| 0 | 129·6 | 102·2 | 115·9 | 136·1 | 108·3 | 122·2 | 99·6 | 99·6 | -100·4 | -92·5 | -96·5 | -115·2 | -108·8 | -112·0 | 67·5 | 80·1 | 73·8 | 88·7 | 105·8 | 97·3 |
| 5 | 120·8 | 93·1 | 106·9 | 137·0 | 108·6 | 122·8 | 100·0 | 100·0 | -82·3 | -74·8 | -78·5 | -121·3 | -118·8 | -120·0 | 49·5 | 62·9 | 56·2 | 103·3 | 121·3 | 112·3 |
| 10 | 106·9 | 80·8 | 93·9 | 132·4 | 106·9 | 119·7 | 99·8 | 99·2 | -60·6 | -51·6 | -56·1 | -122·7 | -122·7 | -122·7 | 30·2 | 40·9 | 35·5 | 116·3 | 132·4 | 124·3 |
| 15 | 93·3 | 65·4 | 79·3 | 122·2 | 101·3 | 111·7 | 101·3 | 97·9 | -37·5 | -26·7 | -32·1 | -122·0 | -122·0 | -122·0 | 7·7 | 19·5 | 13·6 | 127·2 | 141·8 | 134·5 |
| 20 | 77·2 | 51·3 | 64·3 | 112·4 | 91·4 | 101·9 | 101·0 | 97·0 | -11·0 | 0·0 | -5·5 | -114·4 | -114·4 | -114·4 | -11·3 | 0·0 | -5·7 | 133·0 | 149·5 | 141·3 |
| 25 | 55·8 | 31·6 | 43·7 | 97·8 | 75·9 | 86·9 | 102·0 | 97·1 | 17·9 | 31·6 | 24·7 | -101·9 | -101·9 | -101·9 | -31·6 | -21·1 | -26·3 | 132·4 | 149·0 | 140·7 |
| 30 | 34·5 | 10·5 | 22·5 | 80·4 | 60·5 | 72·3 | 101·7 | 96·2 | 46·0 | 59·4 | 52·7 | -82·3 | -86·3 | -84·3 | -47·3 | -40·1 | -43·7 | 131·8 | 147·6 | 139·7 |
| 35 | 9·0 | -10·5 | -0·7 | 63·5 | 40·5 | 49·7 | 101·0 | 94·6 | 75·5 | 87·7 | 81·6 | -59·3 | -65·7 | -62·5 | -64·7 | -59·0 | -61·9 | 124·7 | 139·8 | 132·3 |
| 40 | -13·0 | -31·0 | -22·0 | 42·5 | 21·5 | 32·0 | 101·5 | 94·5 | 101·7 | 117·7 | 109·7 | -36·5 | -39·5 | -38·0 | -79·0 | -74·0 | -76·5 | 115·4 | 131·2 | 123·3 |
| 45 | -34·0 | -50·7 | -42·3 | 20·3 | 0·0 | 10·1 | 100·7 | 93·7 | 130·1 | 144·9 | 137·5 | -14·7 | -8·0 | -11·4 | -91·0 | -87·7 | -89·3 | 103·7 | 117·1 | 110·4 |
| 50 | -56·7 | -70·4 | -63·5 | -3·8 | -19·0 | -11·4 | 101·0 | 94·0 | 154·6 | 168·4 | 161·5 | 12·0 | 20·0 | 16·0 | -101·6 | -94·0 | -97·8 | 88·9 | 101·6 | 95·3 |
| 55 | -75·1 | -85·6 | -80·3 | -28·0 | -39·0 | -33·5 | 100·4 | 93·0 | 173·6 | 187·1 | 180·3 | 43·5 | 48·1 | 45·8 | -104·5 | -100·4 | -102·5 | 72·5 | 85·6 | 79·1 |
| 60 | -92·1 | -101·1 | -96·6 | -47·2 | -57·9 | -52·5 | 100·1 | 92·8 | 191·2 | 203·3 | 197·3 | 70·0 | 78·0 | 74·0 | -104·5 | -101·0 | -102·7 | 54·0 | 64·9 | 59·5 |
| 65 | -107·9 | -114·3 | -111·1 | -67·9 | -76·2 | -72·1 | 98·3 | 93·2 | 202·7 | 214·7 | 208·7 | 99·3 | 108·9 | 104·1 | -98·3 | -98·3 | -98·3 | 34·8 | 43·5 | 39·1 |
| 70 | -118·8 | -121·0 | -119·9 | -86·0 | -92·2 | -89·1 | 96·4 | 92·7 | 208·6 | 218·8 | 213·7 | 125·5 | 133·6 | 129·5 | -92·7 | -92·7 | -92·7 | 13·6 | 21·1 | 17·3 |
| 75 | -125·8 | -125·8 | -125·8 | -102·0 | -105·8 | -103·9 | 94·6 | 92·9 | 211·1 | 220·0 | 215·5 | 150·9 | 159·0 | 154·9 | -80·7 | -83·2 | -81·9 | 0·8 | -5·5 | -2·3 |
| 80 | -126·9 | -126·9 | -126·9 | -112·9 | -114·9 | -113·9 | 94·7 | 93·1 | 207·3 | 215·0 | 211·1 | 172·9 | 180·0 | 176·5 | -68·3 | -70·7 | -69·5 | -24·7 | -19·8 | -22·3 |
| 85 | -126·1 | -126·1 | -126·1 | -123·0 | -123·0 | -123·0 | 94·7 | 94·7 | 199·7 | 206·0 | 202·9 | 190·0 | 196·1 | 193·1 | -53·5 | -55·7 | -54·6 | -42·3 | -40·2 | -41·3 |
| 90 | -121·2 | -121·2 | -121·2 | -128·0 | -128·0 | -128·0 | 95·1 | 95·1 | 185·5 | 190·0 | 187·7 | 203·6 | 208·4 | 206·0 | -36·8 | -36·8 | -36·8 | -60·6 | -58·2 | -59·4 |
| 95 | -112·7 | -112·7 | -112·7 | -128·4 | -128·4 | -128·4 | 95·3 | 95·3 | 169·0 | 172·7 | 170·9 | 211·2 | 212·3 | 211·7 | -16·2 | -19·0 | -17·6 | -74·7 | -73·3 | -74·0 |
| 100 | -102·0 | -102·0 | -102·0 | -125·7 | -125·7 | -125·7 | 94·7 | 96·5 | 150·3 | 153·5 | 151·9 | 214·5 | 214·5 | 214·5 | 5·9 | 2·8 | 4·3 | -89·2 | -87·8 | -88·5 |
| 105 | -86·0 | -86·0 | -86·0 | -119·3 | -119·3 | -119·3 | 95·0 | 98·0 | 125·5 | 125·5 | 125·5 | 213·3 | 213·3 | 213·3 | 26·2 | 23·8 | 25·0 | -95·7 | -95·7 | -95·7 |
| 110 | -66·8 | -68·3 | -67·6 | -107·5 | -107·5 | -107·5 | 94·3 | 98·5 | 94·6 | 94·6 | 94·6 | 206·0 | 206·0 | 206·0 | [45·4] | [43·8] | 44·6 | -100·0 | -100·0 | -100·0 |
| 115 | -46·6 | -48·0 | -47·3 | -92·4 | -96·0 | -94·2 | 94·0 | 99·2 | 68·0 | 68·0 | 68·0 | 193·5 | 192·2 | 192·9 | 63·0 | 66·3 | 64·7 | -101·5 | -101·5 | -101·5 |
| 120 | -24·5 | -28·0 | -26·3 | -75·5 | -81·0 | -78·3 | 93·8 | 99·5 | 37·5 | 37·5 | 37·5 | 175·7 | 173·7 | 174·7 | 81·8 | 84·8 | 83·3 | -100·0 | -100·0 | -100·0 |
| 125 | -4·0 | -8·2 | -6·1 | -58·4 | -64·6 | -61·5 | 93·7 | 100·0 | 9·0 | 9·0 | 9·0 | 156·0 | 151·3 | 153·7 | 96·5 | 102·0 | 99·3 | -94·7 | -94·7 | -94·7 |
| 130 | 19·7 | 12·1 | 15·9 | -39·6 | -48·2 | -43·9 | 93·6 | 100·4 | -18·7 | -19·7 | -19·2 | 133·5 | 126·4 | 129·9 | 110·7 | 117·1 | 113·9 | [-83·6] | [-85·6] | -84·6 |
| 135 | 32·3 | 40·8 | 36·5 | -15·5 | -25·3 | -20·4 | 94·2 | 100·9 | -43·3 | -46·6 | -44·9 | 105·5 | 98·7 | 102·1 | 121·0 | 128·7 | 124·9 | -73·6 | -73·6 | -73·6 |
| 140 | 60·4 | 51·0 | 55·7 | 10·0 | -1·0 | 4·5 | 94·9 | 101·3 | -66·6 | -70·0 | -68·3 | 70·5 | 77·5 | 74·0 | 128·9 | 138·0 | 133·5 | -60·1 | -60·1 | -60·1 |
| 145 | 79·4 | 68·2 | 73·8 | 32·3 | 19·6 | 25·9 | 95·3 | 102·1 | -87·6 | -89·0 | -88·3 | 47·0 | 40·8 | 43·9 | 133·7 | 143·8 | 138·7 | -43·5 | -40·5 | -42·0 |
| 150 | 96·7 | 83·1 | 89·9 | 55·9 | 40·6 | 48·3 | 96·7 | 102·8 | -105·0 | -105·0 | -105·0 | 18·7 | 11·7 | 15·2 | 134·6 | 145·1 | 139·9 | -24·7 | -18·7 | -21·7 |
| 155 | 110·6 | 93·8 | 102·2 | 76·1 | 56·7 | 66·4 | 96·8 | 102·9 | -115·7 | -115·7 | -115·7 | -8·7 | -15·2 | -11·9 | 130·7 | 142·8 | 136·7 | -6·5 | 2·0 | -2·3 |
| 160 | 125·2 | 102·9 | 114·1 | 94·9 | 73·2 | 84·1 | 97·6 | 102·9 | -123·0 | -121·8 | -122·4 | -34·2 | -42·8 | -38·5 | 122·3 | 136·5 | 129·4 | 14·7 | 24·7 | 19·7 |
| 165 | 133·0 | 107·7 | 120·3 | 111·4 | 86·0 | 98·7 | 98·0 | 101·9 | -124·7 | -122·5 | -123·6 | -59·0 | -66·2 | -62·6 | 112·8 | 126·7 | 119·7 | 34·4 | 46·8 | 40·6 |
| 170 | 137·1 | 109·7 | 123·4 | 124·2 | 96·4 | 110·3 | 98·3 | 100·9 | -122·8 | -118·7 | -120·7 | -80·4 | -87·5 | -83·9 | 100·9 | 115·4 | 108·1 | 54·9 | 67·2 | 61·1 |
| 175 | 136·3 | 108·0 | 122·1 | 132·3 | 103·5 | 117·9 | 99·0 | 100·3 | -113·0 | -107·3 | -110·1 | -97·3 | -103·7 | -100·5 | 85·3 | 97·7 | 91·5 | 73·0 | 86·8 | 79·9 |

## Table 2

$Sr(DCOO)_2 \cdot 2D_2O$
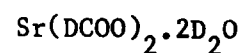
Pattern II    300°K    a axis

| θ° | 1 and 1' | 2 and 2' | 3 and 3' | 4 and 4' | 5 | 5' | Av.5 | 6 | 6' | Av.6 | 7 | 7' | Av.7 | 8 | 8' | Av.8 |
|---|---|---|---|---|---|---|---|---|---|---|---|---|---|---|---|---|
| 0 | 122·2 | 117·9 | -100·2 | -100·2 | 102·3 | 108·1 | 105·2 | 102·3 | 108·1 | 105·2 | 84·1 | 90·6 | 87·4 | 83·0 | 88·3 | 85·7 |
| 5 | 157·9 | 81·0 | -95·7 | -100·8 | 111·5 | 114·7 | 113·1 | 95·7 | 100·8 | 98·3 | 100·5 | 108·0 | 104·3 | 64·0 | 67·5 | 65·7 |
| 10 | 189·3 | 42·3 | -86·6 | -94·6 | 117·8 | 120·8 | 119·3 | 87·6 | 93·6 | 90·6 | 116·3 | 120·8 | 118·6 | 42·3 | 48·3 | 45·3 |
| 15 | 218·7 | 4·8 | -73·6 | -85·8 | 123·9 | 125·9 | 124·9 | 80·2 | 85·8 | 83·0 | 125·9 | 133·5 | 129·7 | 23·2 | 26·8 | 25·0 |
| 20 | 243·3 | -30·1 | -55·7 | -74·0 | 129·4 | 129·4 | 129·4 | 74·8 | 80·3 | 77·6 | 135·5 | 141·5 | 138·5 | 1·6 | 5·6 | 3·6 |
| 25 | 263·6 | -62·3 | -36·2 | -56·7 | 134·1 | 134·1 | 134·1 | 68·3 | 74·3 | 71·3 | 141·4 | 147·4 | 144·4 | -17·8 | -15·3 | -16·5 |
| 30 | 274·9 | -91·3 | -14·3 | -36·2 | 136·3 | 136·3 | 136·3 | 62·4 | 67·9 | 65·2 | 142·4 | 148·4 | 145·4 | -37·7 | -35·5 | -36·6 |
| 35 | 282·2 | -117·1 | 9·5 | -13·9 | 138·3 | 138·3 | 138·3 | 59·2 | 63·8 | 61·5 | 140·4 | 146·5 | 143·5 | -54·0 | -54·0 | -54·0 |
| 40 | 281·0 | -136·7 | 36·7 | 10·3 | 140·0 | 140·0 | 140·0 | 56·2 | 60·5 | 58·4 | 134·5 | 140·0 | 137·1 | -68·2 | -68·2 | -68·2 |
| 45 | 274·1 | -148·9 | 63·4 | 35·7 | 138·8 | 138·8 | 138·8 | 54·6 | 58·3 | 56·5 | 127·2 | 130·8 | 129·0 | -80·5 | -80·5 | -80·5 |
| 50 | 259·5 | -153·6 | 86·1 | 61·0 | 136·5 | 136·5 | 136·5 | 53·4 | 57·9 | 55·7 | 114·1 | 116·3 | 115·2 | -86·9 | -89·6 | -88·3 |
| 55 | 239·7 | -153·9 | 112·5 | 86·3 | 133·2 | 133·2 | 133·2 | 54·7 | 58·0 | 56·4 | 99·2 | 100·7 | 100·0 | -92·7 | -95·2 | -93·9 |
| 60 | 218·9 | -148·6 | 131·6 | 112·1 | 130·0 | 130·0 | 130·0 | 58·0 | 60·5 | 59·3 | 80·8 | 84·2 | 82·5 | -94·0 | -97·4 | -95·7 |
| 65 | 186·2 | -133·0 | 153·7 | 133·0 | 124·4 | 124·4 | 124·4 | 62·2 | 62·2 | 62·2 | 62·2 | 62·2 | 62·2 | -93·0 | -95·6 | -94·3 |
| 70 | 153·1 | -114·3 | 170·2 | 153·1 | 117·8 | 117·8 | 117·8 | 66·5 | 66·5 | 66·5 | 42·3 | 42·3 | 42·3 | [-89·7] | [-91·1] | -90·4 |
| 75 | 116·9 | -91·0 | 183·0 | 170·3 | 112·1 | 112·1 | 112·1 | 72·2 | 72·2 | 72·2 | 19·3 | 21·8 | 20·5 | -81·3 | -81·3 | -81·3 |
| 80 | 78·3 | -60·0 | 191·8 | 183·6 | 105·1 | 105·1 | 105·1 | 78·5 | 78·5 | 78·5 | 0·0 | 0·0 | 0·0 | -68·8 | -68·8 | -68·8 |
| 85 | 41·2 | -27·6 | 195·7 | 193·2 | 98·0 | 98·0 | 98·0 | 85·4 | 85·4 | 85·4 | -22·1 | -18·6 | -20·3 | -54·8 | -54·8 | -54·8 |
| 90 | 3·5 | 9·0 | 195·0 | 194·7 | 90·8 | 90·8 | 90·8 | 90·8 | 90·8 | 90·8 | -39·0 | -36·8 | -37·9 | -39·0 | -36·8 | -37·9 |
| 95 | -32·0 | 44·8 | 190·3 | 194·3 | 81·5 | 82·6 | 82·1 | 98·0 | 98·0 | 98·0 | -55·4 | -55·4 | -55·4 | -18·6 | -15·5 | -17·1 |
| 100 | -65·4 | 84·1 | 180·2 | 189·3 | 76·3 | 76·3 | 76·3 | 106·0 | 106·0 | 106·0 | -69·6 | -69·6 | -69·6 | 1·8 | 4·8 | 3·3 |
| 105 | -94·5 | 120·3 | 165·8 | 179·8 | 67·5 | 71·2 | 69·4 | 112·7 | 112·7 | 112·7 | -82·0 | -82·0 | -82·0 | 22·8 | 22·8 | 22·8 |
| 110 | -117·5 | 156·2 | 149·9 | 166·8 | 61·8 | 66·8 | 64·3 | 118·7 | 118·7 | 118·7 | -90·6 | -90·6 | -90·6 | [43·0] | [46·0] | 44·5 |
| 115 | -135·1 | 189·8 | 129·9 | 150·6 | 58·7 | 63·3 | 61·0 | 123·3 | 123·3 | 123·3 | [-94·0] | [-96·4] | -95·2 | 63·3 | 66·3 | 64·8 |
| 120 | -148·9 | 219·3 | 108·7 | 130·8 | 56·3 | 61·2 | 58·8 | 128·3 | 128·3 | 128·3 | [-96·8] | [-98·0] | -97·4 | 83·5 | 87·5 | 85·5 |
| 125 | -153·5 | 242·5 | 82·8 | 107·3 | 54·6 | 58·6 | 56·6 | 132·1 | 132·1 | 132·1 | -94·7 | -94·7 | -94·7 | 98·8 | 103·7 | 101·3 |
| 130 | -151·8 | 260·6 | 57·7 | 81·6 | 53·7 | 57·7 | 55·7 | [134·2] | [136·6] | 135·4 | -88·3 | -88·3 | -88·3 | 112·8 | 118·0 | 115·4 |
| 135 | -146·5 | 273·5 | 31·8 | 57·5 | 53·7 | 58·7 | 56·2 | 138·7 | 138·7 | 138·7 | -76·9 | -79·3 | -78·5 | 125·8 | 131·5 | 128·7 |
| 140 | -133·0 | 280·6 | 7·3 | 32·2 | 55·0 | 60·5 | 57·8 | 140·2 | 140·2 | 140·2 | -64·7 | -67·2 | -66·0 | 136·0 | 139·0 | 137·5 |
| 145 | -113·0 | 280·5 | -16·5 | 7·2 | 58·5 | 65·0 | 61·8 | 140·0 | 140·0 | 140·0 | -48·5 | -52·0 | -50·3 | 141·2 | 145·0 | 143·1 |
| 150 | -87·7 | 274·2 | -38·0 | -17·2 | 62·3 | 68·5 | 65·4 | 138·0 | 138·0 | 138·0 | -33·0 | -33·0 | -33·0 | 142·5 | 147·5 | 145·0 |
| 155 | -58·6 | 260·2 | -58·6 | -39·6 | 68·3 | 73·8 | 71·1 | 133·4 | 135·0 | 134·2 | -15·2 | -15·2 | -15·2 | 140·6 | 146·7 | 143·7 |
| 160 | -26·0 | 239·6 | -73·8 | -58·0 | 73·6 | 79·3 | 76·5 | 127·7 | 130·8 | 129·3 | 4·2 | 6·3 | 5·3 | 134·3 | 141·2 | 137·8 |
| 165 | 9·7 | 214·7 | -87·3 | -75·2 | 80·2 | 86·0 | 83·1 | 121·3 | 125·6 | 123·5 | 24·6 | 28·0 | 26·3 | 125·0 | 131·7 | 128·4 |
| 170 | 46·3 | 185·3 | -96·3 | -88·0 | 87·2 | 93·4 | 90·3 | 114·5 | 119·6 | 117·1 | 45·3 | 50·1 | 47·7 | 113·3 | 119·3 | 116·3 |
| 175 | 85·0 | 153·2 | -100·0 | -96·2 | 94·7 | 111·2 | 103·0 | 108·7 | 113·4 | 111·1 | 65·8 | 71·0 | 68·4 | 99·2 | 105·0 | 102·1 |

# Table 3

$Sr(DCOO)_2.2D_2O$
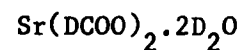
Pattern III    300°K    b axis

| θ° | 1 | 1' | Av.1 | 2 | 2' | Av.2 | 3 and 3' | 4 and 4' | 5 | 5' | Av.5 | 6 | 6' | Av.6 | 7 | 7' | Av.7 | 8 | 8' | Av.8 |
|---|---|---|---|---|---|---|---|---|---|---|---|---|---|---|---|---|---|---|---|---|
| 0 | -2·4 | -13·8 | -8·1 | 6·2 | -6·2 | 0·0 | 185·1 | 191·7 | -51·4 | -55·5 | -53·5 | -115·8 | -115·8 | -115·8 | 56·2 | 51·4 | 53·8 | 25·8 | 19·3 | 22·6 |
| 10 | 4·2 | -10·0 | -2·9 | 22·6 | 10·0 | 16·3 | 159·9 | 172·7 | 5·8 | 0·6 | 3·2 | -127·2 | -127·2 | -127·2 | 73·6 | 68·9 | 71·3 | 10·0 | 0·0 | 5·0 |
| 20 | 16·9 | 1·4 | 9·2 | 44·0 | 30·4 | 37·2 | 120·9 | 140·3 | 69·8 | 63·3 | 66·6 | -120·4 | -120·4 | -120·4 | 88·8 | 86·8 | 87·8 | -1·5 | -13·5 | -7·5 |
| 30 | 36·0 | 19·5 | 27·8 | 65·9 | 54·7 | 60·3 | 74·5 | 94·8 | 130·8 | 122·9 | 126·9 | -89·1 | -89·1 | -89·1 | 96·3 | 96·3 | 96·3 | -7·6 | -19·5 | -13·6 |
| 40 | 56·5 | 40·3 | 48·4 | 87·7 | 77·6 | 82·7 | 23·3 | 44·9 | 181·5 | 174·4 | 178·0 | -42·3 | -42·3 | -42·3 | 99·8 | 99·8 | 99·8 | -6·6 | -18·0 | -12·3 |
| 50 | 78·0 | 65·4 | 71·7 | 107·4 | 98·5 | 103·0 | -22·3 | -4·0 | 219·0 | 212·3 | 215·6 | 19·6 | 14·0 | 16·8 | 94·0 | 96·7 | 95·4 | 0·0 | -11·2 | -5·6 |
| 60 | 97·1 | 88·0 | 92·6 | 117·9 | 113·2 | 115·6 | -59·6 | -45·5 | 234·6 | 226·7 | 230·7 | 80·5 | 77·5 | 79·0 | 80·5 | 87·5 | 84·0 | 12·9 | 2·0 | 7·5 |
| 70 | 113·8 | 107·7 | 110·8 | 124·5 | 124·5 | 124·5 | -85·7 | -77·1 | 223·5 | 230·7 | 227·1 | 136·8 | 141·6 | 139·2 | 65·3 | 72·0 | 68·7 | 28·5 | 19·5 | 24·0 |
| 80 | [123·0] | [121·0] | 122·0 | 125·0 | 125·0 | 125·0 | -94·2 | -91·8 | 203·8 | 197·5 | 200·7 | 185·3 | 190·9 | 188·1 | 47·6 | 54·2 | 50·9 | 47·6 | 40·0 | 43·8 |
| 90 | 127·0 | 127·0 | 127·0 | 117·4 | 120·1 | 118·8 | -86·4 | -92·0 | 159·5 | 155·9 | 157·7 | 223·7 | 219·0 | 221·4 | 29·0 | 36·0 | 32·5 | 67·0 | 62·0 | 64·5 |
| 100 | 122·0 | 124·2 | 123·1 | 101·0 | 105·4 | 103·2 | -60·8 | -73·3 | 104·8 | 99·9 | 102·3 | 236·1 | 231·9 | 234·0 | 10·2 | 17·8 | 14·0 | 82·7 | 79·2 | 81·0 |
| 110 | 107·4 | 111·4 | 109·4 | 79·3 | 85·5 | 82·4 | -20·6 | -38·3 | 40·0 | 38·3 | 39·2 | 225·3 | 222·3 | 223·8 | -3·8 | 2·0 | -0·9 | 93·0 | 93·0 | 93·0 |
| 120 | 91·1 | 93·7 | 92·4 | 56·6 | 61·2 | 58·9 | 28·3 | 8·0 | -22·0 | -22·0 | -22·0 | 194·2 | 194·2 | 194·2 | -11·5 | -8·0 | -9·8 | 100·1 | 100·1 | 100·1 |
| 130 | 67·3 | 73·0 | 70·2 | 34·8 | 34·8 | 34·8 | 77·8 | 56·2 | -73·0 | -73·0 | -73·0 | 146·2 | 146·2 | 146·2 | -13·7 | -13·7 | -13·7 | 98·5 | 98·5 | 98·5 |
| 140 | [43·9] | [46·1] | 45·0 | 15·1 | 15·1 | 15·1 | 123·3 | 104·4 | -109·2 | -109·2 | -109·2 | 85·5 | 89·9 | 87·7 | -10·5 | -10·5 | -10·5 | 90·9 | 90·9 | 90·9 |
| 150 | 24·6 | 24·6 | 24·6 | 0·0 | -2·5 | -1·3 | 162·5 | 148·0 | -127·2 | -127·2 | -127·2 | 24·6 | 24·6 | 24·6 | 1·2 | 0·0 | 0·6 | 78·3 | 78·3 | 78·3 |
| 160 | 10·3 | 3·5 | 6·9 | -4·0 | -10·3 | -7·2 | 187·4 | 178·4 | -123·2 | -123·2 | -123·2 | -35·8 | -33·8 | -34·8 | 18·4 | 15·5 | 17·0 | 63·1 | 60·5 | 61·8 |
| 170 | 0·5 | -9.7 | -4·6 | -1·5 | -12·0 | -6·8 | 195·3 | 193·7 | -96·2 | -96·2 | -96·2 | -82·3 | -84·3 | 83·3 | 33·7 | 36·0 | 34·9 | 43·8 | 39·0 | 41·4 |

Table 4.    A,B,C, Constants

(a) All values in gauss

| Curve | 1 & 1' | 2 & 2' | 3 & 3' | 4 & 4' | 5 & 5' | 6 & 6' | 7 & 7' | 8 & 8' |
|---|---|---|---|---|---|---|---|---|
| $A_a*$ | 63.39 | 62.95 | 47.24 | 47.00 | 97.69 | 97.81 | 24.28 | 24.13 |
| $B_a*$ | 59.37 | 54.74 | -147.30 | -147.82 | 7.85 | 6.86 | 62.93 | 60.84 |
| $C_a*$ | 210.02 | -210.95 | 14.76 | -11.05 | 41.21 | -40.78 | 103.36 | -104.43 |
| $A_b*$ | 59.20 | 59.03 | 50.48 | 50.62 | 52.43 | 52.37 | 42.90 | 42.97 |
| $B_b*$ | -67.06 | -58.28 | 135.39 | 141.41 | -105.33 | -168.60 | 11.24 | -20.84 |
| $C_b*$ | 1.15 | 34.13 | -50.84 | -30.36 | 146.27 | -65.98 | 55.06 | -53.11 |
| $A_c*$ | -2.93 | -3.37 | 97.50 | 97.63 | 45.98 | 45.70 | 19.05 | 19.06 |
| $B_c*$ | 118.71 | 125.00 | 2.42 | 2.70 | -143.00 | -159.15 | 55.70 | 78.57 |
| $C_c*$ | -39.74 | 14.47 | 3.02 | -3.80 | 91.24 | -57.63 | -106.40 | 92.61 |

(b) All values in KHz

| Curve | 1 & 1' | 2 & 2' | 3 & 3' | 4 & 4' | 5 & 5' | 6 & 6' | 7 & 7' | 8 & 8' |
|---|---|---|---|---|---|---|---|---|
| $A_a$ | 81.44 | 80.87 | 60.69 | 60.38 | 125.50 | 125.66 | 31.19 | 31.00 |
| $B_a$ | 76.27 | 70.33 | -189.24 | -189.90 | 10.08 | 8.81 | 80.85 | 78.16 |
| $C_a$ | 269.81 | -271.01 | 18.96 | -14.20 | 52.94 | -52.39 | 132.79 | -134.16 |

Table 4 contd.

(b) All values in KHz

| Curve | 1 & 1' | 2 & 2' | 3 & 3' | 4 & 4' | 5 & 5' | 6 & 6' | 7 & 7' | 8 & 8' |
|---|---|---|---|---|---|---|---|---|
| $A_b$ | 76.05 | 75.84 | 64.85 | 65.03 | 67.36 | 67.28 | 55.11 | 55.20 |
| $B_b$ | -86.15 | -74.87 | 173.94 | 181.67 | -135.32 | -216.60 | 14.44 | -26.77 |
| $C_b$ | 1.48 | 43.85 | -65.31 | -39.00 | 187.91 | -84.76 | 70.74 | -68.23 |
| $A_c$ | -3.76 | -4.33 | 125.26 | 125.43 | 59.07 | 58.71 | 24.47 | 24.49 |
| $B_c$ | 152.51 | 160.59 | 3.11 | 3.47 | -183.71 | -204.47 | 71.56 | 100.94 |
| $C_c$ | -51.05 | 18.59 | 3.88 | -4.88 | 117.22 | -74.04 | -136.69 | 118.98 |

(c) Conversion to new origin and correct relative sign (KHz)

| Curve | 1 & 1' | 2 & 2' | 3 & 3' | 4 & 4' | 5 & 5' | 6 & 6' | 7 & 7' | 8 & 8' |
|---|---|---|---|---|---|---|---|---|
| $A'_a$ | 81.44 | 80.87 | 60.69 | 60.38 | -125.50 | -125.66 | 31.19 | 31.00 |
| $B'_a$ | 72.50 | 74.11 | -189.49 | -189.68 | -9.34 | -9.54 | 78.99 | 80.03 |
| $C'_a$ | 270.85 | -270.00 | 16.32 | -16.85 | -53.08 | 52.26 | 133.91 | -133.06 |
| $A'_b$ | -76.05 | -75.84 | 64.85 | 65.03 | 67.36 | 67.28 | -55.20 | -55.16 |
| $B'_b$ | 83.11 | 84.16 | 185.28 | 185.32 | -182.57 | -184.15 | 6.57 | 6.27 |
| $C'_b$ | 22.73 | 21.10 | -13.93 | -13.49 | 142.44 | 142.09 | 73.00 | 72.48 |
| $A'_c$ | -3.76 | -4.33 | -125.26 | -125.43 | 59.07 | 58.71 | 24.47 | 24.49 |
| $B'_c$ | 157.22 | 157.55 | -2.66 | -3.99 | -195.55 | -195.03 | 86.24 | 87.17 |
| $C'_c$ | -33.87 | 36.24 | 4.20 | -4.47 | 96.18 | -96.20 | -127.94 | 129.42 |

In chapter II the expression for the quadrupolar splitting has been given

$$y(\theta) = A + B\cos 2\theta + C\sin 2\theta$$

Without loss of generality, A can be taken as positive. Inspection of the first and second derivatives $\frac{dy}{d\theta}$ and $\frac{d^2 y}{d\theta^2}$ shows that the function $y(\theta)$ has a maximum when

$$\tan 2\theta = \frac{C}{B} \; ;$$

$$y - A = B\cos 2\theta + C\sin 2\theta > 0 \; .$$

A,B, C can be expressed as functions of the direction cosines $a_{ik}$ of the principal directions of the e.f.g. tensor in the fixed system of laboratory axes and its eigenvalues, which are in turn functions of $\eta$ and $q_{zz} = eq$. The expressions obtained are similar in form to equations (1)-(9) in Chapter V.

$$A = \frac{Keq}{4}\left[(1 - 3a_{33}^2) - \eta\,(a_{31}^2 - a_{32}^2)\right]$$

$$B = \frac{Keq}{4}\left\{3\,(a_{13}^2 - a_{23}^2) - \eta\left[(a_{13}^2 - a_{23}^2) + 2\,(a_{12}^2 - a_{22}^2)\right]\right\}$$

$$C = \frac{Keq}{2}\left[-3a_{13}a_{23} + \eta\,(a_{13}a_{23} + 2a_{12}a_{22})\right] \; .$$

| | $q_{xx}$ | $q_{yy}$ | $q_{zz}$ |
|---|---|---|---|
| X | $a_{11}$ | $a_{12}$ | $a_{13}$ |
| Y | $a_{21}$ | $a_{22}$ | $a_{23}$ |
| Z | $a_{31}$ | $a_{32}$ | $a_{33}$ |

A more convenient set of axes can be chosen whereby two of the angular variables $\theta_1$ and $\theta_2$ completely define the direction of the maximum component of the e.f.g. tensor. A third angular co-ordinate $\theta_0$ between $q_{xx}$ and XY plane can be defined
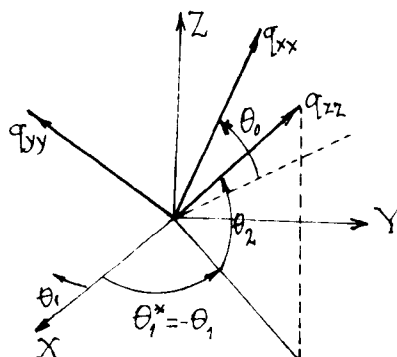
The $a_{ik}$ elements of the matrix T $(q_{xx} \; q_{yy} \; q_{zz}) \rightarrow (XYZ)$ can be easily expressed as functions of $\theta_0$, $\theta_1$, $\theta_2$:

|   | $q_{xx}$ | $q_{yy}$ | $q_{zz}$ |
|---|----------|----------|----------|
| $X$ | $\cos\theta_0 \sin\theta_1 - \sin\theta_0 \cos\theta_1 \sin\theta_2$ | $-\cos\theta_0 \cos\theta_1 \sin\theta_2 - \sin\theta_0 \sin\theta_1$ | $\cos\theta_1 \cos\theta_2$ |
| $Y$ | $\cos\theta_0 \cos\theta_1 + \sin\theta_0 \sin\theta_1 \sin\theta_2$ | $\cos\theta_0 \sin\theta_1 \sin\theta_2 - \sin\theta_0 \cos\theta_1$ | $-\sin\theta_1 \cos\theta_2$ |
| $Z$ | $\sin\theta_0 \cos\theta_2$ | $\cos\theta_0 \cos\theta_2$ | $\sin\theta_2$ |

By developing $\dfrac{C}{B} = f(\eta)$ in a Taylor series about the origin and making the necessary substitutions,

$$f(\eta) = f_{\eta=0} + \eta \, f'_{\eta=0} + \frac{\eta^2}{2!} \, f''_{\eta=0} + \cdots$$

$$f(\eta) = \tan 2\theta_1 + \frac{2}{3} \, \frac{\sin 2\theta_0 \, \sin\theta_2}{\cos^2 2\theta_1 \, \cos^2\theta_2} \, \eta + \cdots$$

General considerations for convergence of the series

$$\lim_{n \to \infty} \frac{\dfrac{\eta^n}{n!} \, f^{(n)}(0)}{\dfrac{\eta^{n-1}}{(n-1)!} \, f^{(n-1)}(0)} < 1$$

were studied, partly on an approximate basis.  The series converges rapidly if, for example,

$$2\theta_1 \le 25°$$

$$\theta_2 < 25°$$

$$|2^{nd} \text{ term}| \le 0.42 \, \underbrace{\eta \sin 2\theta_0}$$

$$\text{for } \eta = 0.15 \quad \sim 0.06$$
$$\text{for } \eta = 0.10 \quad \sim 0.04$$

$\dfrac{C}{B}$ is then $\simeq \tan\theta_1$, $\theta_1$ being by definition the projection of the $q_{zz}$ vector on the XY ($\equiv \pi_{\bar{H}}$) plane.